

Copyright © 1995, by the author(s).
All rights reserved.

Permission to make digital or hard copies of all or part of this work for personal or classroom use is granted without fee provided that copies are not made or distributed for profit or commercial advantage and that copies bear this notice and the full citation on the first page. To copy otherwise, to republish, to post on servers or to redistribute to lists, requires prior specific permission.

**VALIDITY OF THE CLASSICAL THEORY OF
SPONTANEOUS EMISSION AND THE FAST
MULTIPOLE METHOD FOR ELECTROMAGNETIC
SCATTERING**

by

Si Chuen Michael Yeung

Memorandum No. UCB/ERL M95/112

15 December 1995

COVER PAGE

**VALIDITY OF THE CLASSICAL THEORY OF
SPONTANEOUS EMISSION AND THE FAST
MULTIPOLE METHOD FOR ELECTROMAGNETIC
SCATTERING**

by

Si Chuen Michael Yeung

Memorandum No. UCB/ERL M95/112

15 December 1995

ELECTRONICS RESEARCH LABORATORY

**College of Engineering
University of California, Berkeley
94720**

Abstract

Validity of the Classical Theory of Spontaneous Emission and the Fast Multipole Method for Electromagnetic Scattering

by

Si Chuen Michael Yeung

Doctor of Philosophy in Electrical Engineering and Computer Sciences

University of California, Berkeley

Professor Andrew R. Neureuther, Chair

The interaction of the electromagnetic field with material boundaries has long been a subject of intense investigation. On the theoretical side are problems concerning the quantum-mechanical properties of the electromagnetic field near material boundaries. Such problems are of interest to physicists in the field of quantum optics near surfaces. On the practical side are problems concerning the numerical techniques used to solve the equations of classical electrodynamics in various practical situations involving boundaries. Such problems are of interest to engineers in the field of electromagnetic scattering. This thesis provides quantitative solutions to specific theoretical and practical problems in the subject of the interaction between the electromagnetic field and material boundaries.

First, the lifetime of an excited atom near a lossy dielectric surface is calculated from an exact solution of a microscopic Hamiltonian model, which includes the effects of dispersion, local field correction and near-field Coulomb interaction. Results for the total decay rate are shown to be in excellent agreement with those based on classical electromagnetic theory and to yield the well-known result for the rate of nonradiative energy transfer in the limit of very small distance from the surface. Because our calculation is based on a fully canonical quantum theory, it provides the first fundamental demonstration of the validity of the classical electromagnetic theory of the rate of spontaneous emission near a lossy dielectric surface.

Next, two new numerical techniques for three-dimensional electromagnetic scattering are proposed. The first technique is based on the physical-optics approximation

and is suitable for piecewise-linear topography. The formalism of generalized Sommerfeld integrals is used to treat the effects of intra-surface multiple scattering in the physical-optics approximation. The technique of multipole acceleration is used to reduce the CPU cost of intra-surface multiple-scattering computation to $O(N^{3/2})$, where N is the number of surface unknowns. This approximate numerical technique is suitable for use in the simulation of photoresist exposure over large, piecewise-linear 3-D topography.

The second technique is a rigorous numerical technique based on an alternative formulation of the Fast Multipole Method (FMM) and is suitable for arbitrarily shaped, perfectly conducting objects. Our FMM algorithm differs from the standard FMM algorithm in that we represent the field in the far zone due to a localized group of sources by a sum of multipole waves, rather than by a sum of plane waves. A procedure involving a combination of coordinate rotations and translation was developed to speed up the transformation of the multipole expansions. The CPU cost of our algorithm is $O(N^{5/3})$ compared to $O(N^{3/2})$ for the standard FMM algorithm. However, our algorithm is numerically stable in the long-wavelength limit whereas the standard FMM algorithm is not. This rigorous numerical technique can be extended for use in many important 3-D problems such as the modeling of optical proximity probes and on-chip interconnects.



Professor Andrew R. Neureuther
Thesis Committee Chairman

Contents

1	Introduction	1
1.1	Spontaneous Emission near a Lossy Mirror	1
1.2	Three-Dimensional Topography Scattering	4
1.2.1	The Physical-Optics Method	5
1.2.2	The Fast Multipole Method	6
1.3	Summary	7
2	Spontaneous Emission Near a Lossy Mirror	9
2.1	Introduction	9
2.2	The Microscopic Hamiltonian Model	10
2.3	Diagonalization of the Matter Part	14
2.4	Spontaneous Decay Rate	17
2.5	Green Functions for the Half-Space	28
2.6	Comparison with the Classical Theory	46
2.7	Conclusions	47
3	Three-Dimensional Topography Scattering Part I: Multipole Accelerated Physical-Optics Method	51
3.1	Introduction	51
3.2	Problem Statement	52
3.3	The Physical-Optics Approximation	55
3.4	Multiple Scattering between Surfaces	56
3.5	Multiple Scattering within a Surface	60

3.6	Sommerfeld's Solution	62
3.7	The Multipole Approximation	64
3.8	Generalized Sommerfeld Integrals	66
3.9	Multipole Acceleration	69
3.10	Numerical Evaluation of the Integrals	71
3.11	Operation Count	76
3.12	Application to Reflective Notching	78
3.13	Conclusions	81
4	Three-Dimensional Topography Scattering Part II: Fast Multipole Solution of Integral Equation	89
4.1	Introduction	89
4.2	Problem Formulation	90
4.3	GMRES	93
4.4	The FMM Algorithm	95
4.5	Operation Count	99
4.6	Use of Symmetry	100
4.7	Scattering from Plates and Cubes	103
4.8	Problems with Guided Mode Excitation	105
4.8.1	Shorted Waveguide	109
4.8.2	Horn Antenna	110
4.9	The Long-Wavelength Limit	111
4.10	Comparison with the Standard FMM	113
4.11	Conclusions	118
5	Conclusions	128
Appendix A	Expansion Coefficients for B_ω	131
Appendix B	Derivation of Eq. (2.101)	134

Appendix C	Green Function for the Matter Field	139
Appendix D	Integral of $\xi(\omega)$	150
Appendix E	Green Function for the Transverse Photons	152
Appendix F	Derivation of Eq. (2.191)	169
Appendix G	Physical-Optics Induced Fields	173
Appendix H	Rotation Matrices	180
Appendix I	Translation Coefficients	184
Appendix J	Fields of the Multipole Waves	188
Appendix K	Integration over Singularities	195
Bibliography		199

List of Figures

2.1	Perturbation series for photon Green function.	48
2.2	Lifetime of an excited atom near a gold mirror.	49
2.3	Lifetime of an excited atom near a lossless dielectric surface.	50
3.1	Multilayer piecewise-linear topography.	82
3.2	Multiple-reflection series for multiple scattering between adjacent surfaces.	82
3.3	Dipole above a lossy plane surface.	83
3.4	Transformation from distant to local coordinate system.	83
3.5	Branch cuts and integration paths in the complex λ -plane.	84
3.6	Three-dimensional Matzusawa step divided into panels.	84
3.7	Tangential magnetic field amplitude on bottom of step, for x -polarized, normally incident plane wave.	85
3.8	0.7 μm line over 0.4 μm high step.	86
3.9	0.35 μm line over 0.128 μm high step.	87
3.10	0.35 μm line over 0.2 μm high step.	88
4.1	Electromagnetic scattering from a perfectly conducting object.	121
4.2	A scattering problem with symmetry in the x - y and y - z planes.	121
4.3	Broadside RCS of perfectly conducting square plates 0.0317 λ thick.	122
4.4	Broadside RCS of perfectly conducting cubes.	123
4.5	CPU cost per iteration.	124
4.6	Storage cost for double precision.	125
4.7	Horn model.	126

4.8	A pyramidal horn antenna.	126
4.9	Radiation patterns of the horn antenna.	127
H.1	Euler angles.	183
J.1	Isoparametric mapping.	194

List of Tables

1.1	Comparison of techniques of topography scattering in two and three dimensions.	8
4.1	Computed results for RCS of perfectly conducting plates of thickness 0.0317λ	120
4.2	Computed results for RCS of perfectly conducting cubes.	120

Acknowledgements

The completion of this work would not have been possible without the help of many people. First, I would like to thank my advisors Professors Andrew Neureuther and Ken Gustafson for their guidance throughout this work. Both of them have been untiring in their efforts to act as sounding boards for my ideas. Professor Neureuther's keen sense of judgement as to whether an idea is likely to work or not has several times saved me from going on a wrong track. Furthermore, a number of key ideas used in my research were suggested by him. These included the idea of multipole acceleration used in FastCap and the recurrence relationships discussed in Appendix I. Professor Gustafson, on the other hand, has always been ready to listen and discuss with me at times when an idea seemed to have come to a dead end. His constant enthusiasm and encouragement throughout the years have been of great help to my work.

I have benefited from discussions with Professor Bill Oldham during the initial stages of my research. I have also benefited from Professor Theodore Van Duzer's course on superconductive devices. The Wiener-Hopf technique I heard of while doing a term paper for that course was eventually applied successfully to my research. I am grateful to Professor Kenneth Mei for helpful discussions and to Professors John Whinnery and Raymond Chiao for serving on my qualifying committee. In addition, I would like to pay my tribute to the late Professor Leo Falicov who had served on my qualifying committee and had been a great teacher to me.

Friends have made my graduate student life enjoyable. In particular, I would like to thank Alfred Wong, John Helmsen, Derek Lee, Robert Socha, Robert Wang and Byoung-ho Lee for discussions and help.

The financial support of SRC/SEMATECH under contract #95-MC-500 is gratefully acknowledged.

Lastly, I give my special thanks to Jeannie for her love, support and sacrifice during the first few years of my graduate study.

Chapter 1

Introduction

The interaction of the electromagnetic field with material boundaries has long been a subject of intense investigation. On the theoretical side are problems concerning the quantum-mechanical properties of the electromagnetic field near material boundaries. Such problems are of interest to physicists in the field of quantum optics near surfaces. On the practical side are problems concerning the numerical techniques used to solve the equations of classical electrodynamics in various practical situations involving boundaries. Such problems are of interest to engineers in the field of electromagnetic scattering. This thesis is aimed at providing quantitative solutions to specific theoretical and practical problems in the subject of the interaction between the electromagnetic field and material boundaries.

1.1 Spontaneous Emission near a Lossy Mirror

The effects of material boundaries on the quantum mechanical properties of atoms interacting with the electromagnetic field have been observed in many experiments. Among these are the modification of the lifetime of an excited atom near a mirror [1], the microlaser [2] and the level shifts of atoms in small cavities [3]. Such effects are investigated not only for their scientific value, but also for their potential technological application, such as the possible construction of low-threshold semiconductor lasers through controlled spontaneous emission. In Chapter 2 of this thesis, we shall be concerned with the first of the above-mentioned effects, namely, the lifetime of an

excited atom near a mirror.

Different techniques have been used by others to calculate the lifetime of excited atoms near boundaries. These techniques can be grouped into two main approaches, the classical approach and the macroscopic quantum-mechanical approach. In the classical approach, the excited atom is modeled by an oscillating classical dipole and the radiation field produced by the dipole in the presence of material boundaries is found by solving Maxwell's equations. Such an approach is suitable for both lossy and lossless materials, and it has been shown to give good agreement with experimental data for the lifetime of an excited atom near a lossy mirror [4].

In the macroscopic quantum-mechanical approach, the radiation field is expanded in a complete, orthogonal set of spatial modes and the rate of spontaneous emission is found by applying Fermi's Golden Rule. These spatial modes are solutions of the macroscopic Maxwell equations satisfying the usual boundary conditions at the material interfaces. A complete set of such spatial modes can in general be constructed when the materials involved are lossless. In that case, the macroscopic quantum-mechanical approach has been shown to give good qualitative agreement with experimental data for the spontaneous-emission characteristics of microscopic optical cavities [5]. An important situation in which a complete set of spatial modes *cannot* be constructed is the case of a *lossy* dielectric half-space. This is because, in order for the spatial modes to form a complete set, they must represent waves incident from *both* sides of the interface between the two half-spaces [6]. When one of the half-spaces is filled with a lossy material, waves incident from infinity in that material toward the interface are not well defined, since their amplitudes would have decayed to zero by the time they reached the interface. Thus, it is not possible to expand the radiation field in a lossy dielectric half-space in a complete set of spatial modes. As such, the macroscopic quantum-mechanical approach cannot be used to calculate the lifetime of an excited atom near a lossy mirror.

The above discussion indicates that, whereas the problem of the lifetime of an excited atom near a *lossless* mirror has been analyzed by both the classical and the

macroscopic quantum-mechanical approach, the case of a *lossy* mirror has up to now only been analyzed by the classical approach. Although the results of the classical theory are in good agreement with experimental data, it is desirable to have an independent check on the validity of the classical theory, by performing an analysis of the problem based on a fully canonical quantum theory.

A fully canonical quantum theory is one derived from a Lagrangian density, by imposing equal-time commutation relations between the field operators and their conjugate momenta. In the case of *lossless* materials, one can use an effective Lagrangian density whose Euler-Lagrange equations reproduce the macroscopic Maxwell equations in the materials. The constitutive relation $\mathbf{D}(\mathbf{r}, t) = \epsilon(\mathbf{r})\mathbf{E}(\mathbf{r}, t)$ in this case is local in time, thus allowing the use of the canonical quantization method. When losses are present, however, the constitutive relation becomes a convolution in time and so the canonical quantization method cannot be used. Thus, an effective Lagrangian density cannot be used to model lossy materials. Instead, a Lagrangian density based on a *microscopic* model of the loss mechanism must be used.

A microscopic model of a lossy dielectric was recently proposed by Huttner and Barnett [7]. In this model, the bare (lossless) dielectric is represented by a harmonic-oscillator field and the losses are modeled by an interaction between the bare dielectric and a reservoir field. The model including the interaction with the electromagnetic field has been shown to be exactly solvable in the case of an *infinite* lossy dielectric [7]. The resulting solution has been used in the study of spontaneous emission in an *infinite* lossy dielectric [8].

In Chapter 2 of this thesis, the microscopic model of [7] is extended to include the effects of local field correction and applied to the case of a lossy dielectric *half-space*. Although exact diagonalization of the Hamiltonian is not feasible for the half-space problem, we have nevertheless been able to obtain *exact* solutions for the Green function for the transverse photons and the Green function for the harmonic-oscillator field in the half-space. These Green functions are used in Section 2.6 to compute the lifetime of an excited atom near the dielectric surface. Numerical results

of our theory are in excellent agreement with those of classical electromagnetic theory. In particular, the decay rate of an excited atom near a lossy mirror is shown to follow an inverse-cubed law in the limit of very small distance from the surface.

1.2 Three-Dimensional Topography Scattering

As the technology of integrated-circuit fabrication evolves, lithographers are faced with the ever increasing challenge of printing smaller and smaller features over non-planar wafer topography. Topography scattering has long been a problem for optical lithographers. Such scattering gives rise to critical-dimension (CD) variations due to standing-wave effects and the redirection of light into otherwise unexposed regions of the photoresist. Computer simulation of topography-scattering effects in photolithography can be a valuable tool for predicting the complex interaction between the projected aerial image and the wafer topography.

A new class of photolithography simulators based on classical electromagnetic theory have emerged to take on the challenge of topography-scattering simulation. Several of the numerical techniques used in these simulators are listed in Table 1.1, together with their storage and CPU costs in two and three dimensions. From this table, it can be seen that, while most of the rigorous techniques work well for 2-D problems, they cannot easily be generalized to 3-D because of storage and speed limitations. For example, the waveguide, differential and integral methods all have the same storage requirement as the time-domain method in 2-D. However, in 3-D, the former three methods are all far more expensive than the time-domain method in both storage and operation count. At present, the time-domain method is the most commonly used technique for 3-D problems. However, because its storage cost scales as n^3 , where n is the number of nodes in each dimension, it is restricted to use on supercomputers for all but very small 3-D problems.

1.2.1 The Physical-Optics Method

One way to reduce the storage and CPU costs in 3-D is to use an approximate rather than a rigorous technique. Approximate techniques based on the Geometrical Theory of Diffraction [9] and the physical-optics approximation [10] have been developed for 2-D problems. The latter technique has been shown to give good results for multilayer, piecewise-linear topography in 2-D. In Chapter 3 of this thesis, we present a generalization of the physical-optics technique of [10] to 3-D.

To take into account multiple scattering between adjacent surfaces in a multilayer structure, we use an iterative scheme developed by Pai and Awada [13] for the waveguide model. This scheme allows us to treat each surface one at a time and to include the interaction between adjacent surfaces by iteration. In the treatment of multiple scattering *within* a given surface, we consider each element of the surface as a source of scattered waves illuminating every other point on the same surface. Then, we apply the physical-optics approximation to determine the fields induced by these scattered waves on the same surface. Specifically, the scattered waves incident at a given point on the surface are assumed to interact with the surface in the same way that they would interact with the *tangent plane* at that point of the surface. Thus, the problem becomes one of the reflection of the scattered waves from the tangent planes. In 3-D, the waves incident on the tangent planes are spherical rather than plane. To treat the reflection of such spherical waves from the tangent planes, it is necessary to use the formalism of generalized Sommerfeld integrals developed by Chang and Mei [12], as discussed in Section 3.8, instead of the usual Fresnel laws.

In contrast to the 2-D case, direct evaluation of the above physical-optics induced fields over the surface of the topography is impractical in 3-D, since this would require $O(N^2)$ floating-point operations, where $N \sim n^2$ is the number of unknowns on the surface. Thus, we have adopted the technique of multipole acceleration used in Rokhlin's Fast Multipole Method (FMM) [11] to speed up the evaluation of the physical-optics induced fields. This results in a CPU cost of $O(N^{3/2})$ in 3-D. Using this multipole accelerated physical-optics technique, we are able to perform reflective-notching sim-

ulation of large 3-D structures on an ordinary workstation with reasonable CPU time.

1.2.2 The Fast Multipole Method

Instead of using the technique of multipole acceleration in the context of the physical-optics approximation, as we do in Chapter 3, the Fast Multipole Method (FMM) [11] can also be used directly in the iterative solution of the integral equations of electromagnetic scattering. *Direct* solution of these integral equations, as employed in the standard Method of Moments (MOM), is impractical in 3-D (see Table 1.1). There are two key ideas in FMM that render *iterative* solution of the integral equations practical in 3-D. The first idea lies in the choice of an iterative algorithm based on the technique of approximations from Krylov subspaces. In this class of algorithms, one has to perform a matrix-vector multiplication at each iteration step. The matrix itself is not needed, but only the result of the matrix-vector multiplication, which is another vector. Hence, it is not necessary to store the matrix itself, which would require $O(N^2)$ bytes of storage in 3-D. Instead, one only has to store vectors, which require $O(N)$ bytes of storage. The second idea lies in the use of multipole acceleration to speed up the evaluation of the matrix-vector product. Thus, in FMM, both the storage and CPU costs are rendered practical in 3-D.

FMM was first developed by Rokhlin for the efficient solution of the integral equations of 2-D acoustic scattering [11]. Later, it was generalized to 2-D [14] and 3-D [15] electromagnetic scattering. In Chapter 4 of this thesis, we present a new, alternative formulation of FMM for 3-D electromagnetic scattering. Our algorithm differs from the standard FMM algorithm of [15] in that we represent the radiation field in the far zone due to the sources in a given panel by a sum of *multipole waves*, whereas in the standard FMM algorithm the same radiation field is represented by a sum of *plane waves* propagating in various directions. As a result, our FMM algorithm is numerically stable in the long-wavelength limit, whereas the standard FMM algorithm is not. However, this numerical stability is achieved at the expense of a slight increase in CPU cost, namely, $O(N^{5/3})$ for our algorithm compared to $O(N^{3/2})$ for the standard

FMM algorithm. The reason for this increase in CPU cost is that the transformation formulas for the multipole waves used in our algorithm are more complicated than those for the plane waves used in the standard FMM algorithm. Indeed, it was necessary for us to develop a three-step transformation procedure consisting of a rotation, a translation and another rotation, as discussed in Section 4.4, in order to achieve a lower than $O(N^2)$ CPU cost. Fortunately, the benchmarks discussed in Sections 4.7 and 4.10 indicate that, for problem size of a few thousand unknowns, the difference in CPU cost between our algorithm and the standard FMM algorithm is insignificant.

1.3 Summary

This thesis addresses two specific problems in the subject of the interaction of the electromagnetic field with material media. The first concerns the validity of the classical theory of the lifetime of an excited atom near a lossy mirror. In Chapter 2 of this thesis, we present a fully canonical quantum theory of the lifetime of such an excited atom and show that the results of this theory are in excellent agreement with those of the classical theory. The second problem concerns the development of numerical techniques of topography scattering useful for integrated-circuit process simulation. Two such techniques are presented in this thesis. An approximate technique based on the physical-optics method is presented in Chapter 3 and a rigorous technique based on the Fast Multipole Method is presented in Chapter 4.

There are eleven appendices in this thesis. As they contain important though often lengthy mathematical derivations and formulas, they constitute an integral part of the thesis.

Throughout this thesis, we use i and j interchangeably for the unit imaginary number $\sqrt{-1}$.

Table 1.1: Comparison of techniques of topography scattering in two and three dimensions (assuming n grid points in each dimension)

Method	Features	Storage cost ¹	CPU cost ^{1,2}	Availability
Time-domain finite difference	Absorbing boundary conditions. Massively parallel.	n^3 (n^2)	$n^3 \times \mathfrak{S}$ ($n^2 \times \mathfrak{S}$)	TEMPEST (UC Berkeley, 3-D) EMFlex (Weidlinger Associates, 3-D)
Waveguide	Rigorous. Suitable for small refractive-index changes.	n^4 (n^2)	n^6 (n^3)	METRO (Carnegie-Mellon, 2-D)
Differential	Rigorous. Suitable for smooth topography.	n^4 (n^2)	n^6 (n^3)	iPHOTO (Intel, 2-D)
Integral (Method of Moments)	Rigorous. Direct solution.	n^4 (n^2)	n^6 (n^3)	(NIST, 2-D)
Frequency-domain finite element	Periodic boundary conditions. Sparse matrix. Direct solution.	n^5 (n^3)	n^7 (n^4)	(Phillips/Signetics, 2-D)
Physical-optics + Fast Multipole	Approximate. Suitable for piecewise-linear topography.	n^2 (n)	n^3 ($n^{1.5}$)	(UC Berkeley, 3-D)
Integral + Fast Multipole	Rigorous. Iterative solution.	n^2 (n)	$n^{3.33} \times \aleph$ ($n^{1.5} \times \aleph$)	(UC Berkeley, 3-D, under development)

¹Costs for 2-D are enclosed in parentheses.

² \mathfrak{S} is the number of iterations in the time-domain method. \aleph is the number of iterations in the frequency-domain method.

Chapter 2

Spontaneous Emission Near a Lossy Mirror

2.1 Introduction

The lifetime of an excited molecule has been known for a long time to be significantly affected by a partially reflecting mirror in its vicinity [1]. Early attempts to explain the experimental results using classical electromagnetic theory [16, 17] have been quite successful. Nevertheless, the accuracy of these theoretical results has so far not been verified by calculation based on a fully canonical quantum theory. Recently, spontaneous emission by an excited atom near a lossless dielectric surface was analyzed from the viewpoint of quantization of macroscopic spatial modes [18]. However, such an approach cannot easily be extended to include the effects of losses in the dielectric. Thus, up to now, an analysis of the lifetime of an excited atom near an absorbing dielectric surface based on a fully canonical quantum theory has been lacking. In this chapter, we present one such analysis based on an exact solution of a microscopic Hamiltonian model.

After discussing the Hamiltonian formulation in Section 2.2, we diagonalize the matter part of the Hamiltonian density to obtain the dressed matter field in Section 2.3. In Section 2.4, the self-energy of an excited atom near the dielectric surface is obtained to second order of perturbation theory by considering the Green function of the excited atom to this order. The decay rate of the excited atom, which is pro-

portional to the imaginary part of the atom self-energy, is then expressed in terms of the instantaneous Coulomb interaction, the Green function for the transverse photons and the Green function for the harmonic-oscillator field. In Section 2.5, the latter two Green functions are obtained by solving the corresponding Dyson equations *exactly*. This involves a three-step procedure. First, the Green function for the harmonic-oscillator field is solved exactly by ignoring the coupling to the transverse photons. Then, the Green function for the transverse photons is solved exactly by including both the bulk and the surface contributions to the photon self-energy. Finally, the Green function for the harmonic-oscillator field is corrected by including the coupling to the transverse photons. Numerical results for the decay rate of the excited atom obtained from the above theory are compared with those obtained from the classical theory in Section 2.6.

2.2 The Microscopic Hamiltonian Model

Our microscopic model of the absorbing dielectric is the Hopfield model extended to include coupling to a continuum [7]. This model has been used in the study of spontaneous emission in an *infinite* absorbing dielectric medium [8]. Here, we apply it instead to an absorbing dielectric occupying the half-space $z < 0$.

In the absence of the excited atom, the Lagrangian density of the system consisting of the lossy dielectric half-space and the radiation field is

$$\mathcal{L} = \mathcal{L}_{\text{em}} + \mathcal{L}_{\text{mat}} + \mathcal{L}_{\text{res}} + \mathcal{L}_{\text{int}}^{\text{res}} + \mathcal{L}_{\text{int}}^{\text{em}} + \mathcal{L}_{\text{local}}. \quad (2.1)$$

The various parts of this Lagrangian density are:

1. \mathcal{L}_{em} is the Lagrangian density of the free radiation field,

$$\mathcal{L}_{\text{em}} = \frac{\epsilon_0}{2} \mathbf{E}^2 - \frac{1}{2\mu_0} \mathbf{B}^2, \quad (2.2)$$

where \mathbf{E} and \mathbf{B} are the electric and magnetic fields which are related to the vector and scalar potentials by $\mathbf{E} = -\dot{\mathbf{A}} - \nabla U$ and $\mathbf{B} = \nabla \times \mathbf{A}$.

2. \mathcal{L}_{mat} is the Lagrangian density of the bare dielectric occupying the half-space $z < 0$, modeled by a harmonic-oscillator field,

$$\mathcal{L}_{\text{mat}} = \theta(-z) \left(\frac{\rho}{2} \dot{\mathbf{X}}^2 - \frac{\rho\omega_0^2}{2} \mathbf{X}^2 \right), \quad (2.3)$$

where \mathbf{X} is the bare matter field operator.

3. \mathcal{L}_{res} is the Lagrangian density of the reservoir associated with the dielectric, modeled by a continuum of harmonic oscillators,

$$\mathcal{L}_{\text{res}} = \theta(-z) \int_0^\infty d\omega \left(\frac{\rho}{2} \dot{\mathbf{Y}}_\omega^2 - \frac{\rho\omega^2}{2} \mathbf{Y}_\omega^2 \right). \quad (2.4)$$

4. $\mathcal{L}_{\text{int}}^{\text{res}}$ is the coupling between the bare dielectric and the reservoir leading to losses in the dielectric,

$$\mathcal{L}_{\text{int}}^{\text{res}} = -\theta(-z) \int_0^\infty d\omega v(\omega) \mathbf{X} \cdot \dot{\mathbf{Y}}_\omega, \quad (2.5)$$

where $v(\omega)$ is a square-integrable function with the following properties: (i) the analytic continuation of $v(\omega)^2$ to negative frequencies is an even function and (ii) $v(\omega) \neq 0$ for all nonzero frequencies.

5. $\mathcal{L}_{\text{int}}^{\text{em}}$ is the interaction between the bare dielectric and the radiation field,

$$\mathcal{L}_{\text{int}}^{\text{em}} = e\mathbf{A} \cdot \dot{\mathbf{X}}\theta(-z) + eU \nabla \cdot [\mathbf{X}\theta(-z)]. \quad (2.6)$$

6. $\mathcal{L}_{\text{local}}$ is a term modeling the effects of local field correction,

$$\mathcal{L}_{\text{local}} = \frac{e^2}{6\epsilon_0} \mathbf{X}^2 \theta(-z). \quad (2.7)$$

For simplicity, we have omitted the dependence of the fields \mathbf{A} , U , \mathbf{X} and \mathbf{Y}_ω in the above expressions on (\mathbf{r}, t) . Also, we have attached a Heaviside unit function $\theta(\cdot)$ to each occurrence of \mathbf{X} and \mathbf{Y}_ω to indicate that the dielectric is confined to the half-space $z < 0$.

Since the time derivative of U does not appear in the above Lagrangian density, the momentum conjugate to U vanishes identically. Thus, it is impossible to quantize

U by applying the canonical quantization procedure to the above Lagrangian density. One solution to this difficulty is to treat U not as an independent field and to eliminate it from the Lagrangian density by means of its Euler-Lagrange equation of motion,

$$\begin{aligned} 0 &= \frac{\partial}{\partial x_i} \frac{\partial \mathcal{L}}{\partial (\partial U / \partial x_i)} - \frac{\partial \mathcal{L}}{\partial U} \\ &= \epsilon_0 \nabla \cdot (\dot{\mathbf{A}} + \nabla U) - e \nabla \cdot [\mathbf{X} \theta(-z)]. \end{aligned} \quad (2.8)$$

Eq. (2.8) can be simplified if we choose the Coulomb gauge, in which the vector potential is purely transverse, $\nabla \cdot \mathbf{A} = 0$. In what follows, we shall use the Coulomb gauge, so that Eq. (2.8) becomes

$$\nabla^2 U = \frac{e \nabla \cdot [\mathbf{X} \theta(-z)]}{\epsilon_0}. \quad (2.9)$$

The solution of Eq. (2.9) is the instantaneous Coulomb potential for the charge density $-e \nabla \cdot [\mathbf{X} \theta(-z)]$:

$$U(\mathbf{r}, t) = \int_{\infty} d^3 r' \frac{-e \nabla' \cdot [\mathbf{X}(\mathbf{r}', t) \theta(-z')]}{4\pi \epsilon_0 |\mathbf{r} - \mathbf{r}'|}, \quad (2.10)$$

in which the same value of time t appears on both sides of the equation.

To obtain the Hamiltonian density of the system described by Eq. (2.1), we first find the momenta conjugate to the fields \mathbf{A} , \mathbf{X} and \mathbf{Y}_ω :

$$\mathbf{P}_A = \frac{\partial \mathcal{L}}{\partial \dot{\mathbf{A}}} = \epsilon_0 (\dot{\mathbf{A}} + \nabla U). \quad (2.11)$$

$$\mathbf{P}_X = \frac{\partial \mathcal{L}}{\partial \dot{\mathbf{X}}} = \theta(-z) (\rho \dot{\mathbf{X}} + e \mathbf{A}), \quad (2.12)$$

$$\mathbf{P}_\omega = \frac{\delta \mathcal{L}}{\delta \dot{\mathbf{Y}}_\omega} = \theta(-z) [\rho \dot{\mathbf{Y}}_\omega - v(\omega) \mathbf{X}], \quad (2.13)$$

The Hamiltonian density is then obtained from

$$\mathcal{H} = \mathbf{P}_A \cdot \dot{\mathbf{A}} + \mathbf{P}_X \cdot \dot{\mathbf{X}} + \int_0^\infty d\omega \mathbf{P}_\omega \cdot \dot{\mathbf{Y}}_\omega - \mathcal{L}. \quad (2.14)$$

Substituting Eqs. (2.1) to (2.7) and (2.12) to (2.11) into Eq. (2.14), we obtain

$$\begin{aligned} \mathcal{H} &= \frac{\epsilon_0}{2} (\dot{\mathbf{A}})^2 + \frac{1}{2\mu_0} (\nabla \times \mathbf{A})^2 \\ &+ \theta(-z) \left(\frac{\rho}{2} \dot{\mathbf{X}}^2 + \frac{\rho \omega_0^2}{2} \mathbf{X}^2 \right) + \theta(-z) \int_0^\infty d\omega \left(\frac{\rho}{2} \dot{\mathbf{Y}}_\omega^2 + \frac{\rho \omega^2}{2} \mathbf{Y}_\omega^2 \right) \\ &- e U \nabla \cdot [\mathbf{X} \theta(-z)] - \frac{\epsilon_0}{2} (\nabla U)^2 - \frac{e^2}{6\epsilon_0} \mathbf{X}^2 \theta(-z), \end{aligned} \quad (2.15)$$

We now use Eqs. (2.12) and (2.13) to eliminate the velocities $\dot{\mathbf{X}}$ and $\dot{\mathbf{Y}}_\omega$ from Eq. (2.15). After rearranging terms, we obtain

$$\mathcal{H} = \mathcal{H}_{\text{em}}^A + \mathcal{H}_{\text{mat}} + \mathcal{H}_{\text{res}} + \mathcal{H}_{\text{int}}^{\text{res}} + \mathcal{H}_{\text{int}}^A + \mathcal{H}_{\text{int}}^U, \quad (2.16)$$

where

$$\mathcal{H}_{\text{em}}^A = \frac{\epsilon_0}{2}(\dot{\mathbf{A}})^2 + \frac{1}{2\mu_0}(\nabla \times \mathbf{A})^2, \quad (2.17)$$

$$\mathcal{H}_{\text{mat}} = \theta(-z) \left(\frac{1}{2\rho} \mathbf{P}_X^2 + \frac{\rho\tilde{\omega}_0^2}{2} \mathbf{X}^2 \right), \quad (2.18)$$

$$\mathcal{H}_{\text{res}} = \theta(-z) \int_0^\infty d\omega \left(\frac{1}{2\rho} \mathbf{P}_\omega^2 + \frac{\rho\omega^2}{2} \mathbf{Y}_\omega^2 \right), \quad (2.19)$$

$$\mathcal{H}_{\text{int}}^{\text{res}} = \theta(-z) \int_0^\infty d\omega \frac{v(\omega)}{\rho} \mathbf{X} \cdot \mathbf{P}_\omega, \quad (2.20)$$

$$\mathcal{H}_{\text{int}}^A = \theta(-z) \left(-\frac{e}{\rho} \mathbf{A} \cdot \mathbf{P}_X + \frac{e^2}{2\rho} \mathbf{A}^2 \right), \quad (2.21)$$

$$\mathcal{H}_{\text{int}}^U = -eU \nabla \cdot [\mathbf{X}\theta(-z)] - \frac{\epsilon_0}{2}(\nabla U)^2 - \frac{e^2}{6\epsilon_0} \mathbf{X}^2 \theta(-z), \quad (2.22)$$

and $\tilde{\omega}_0^2 = \omega_0^2 + \int_0^\infty d\omega \frac{v(\omega)^2}{\rho^2} \mathbf{X}^2$ is the renormalized resonance frequency of the dielectric.

The Hamiltonian of the system is obtained by integrating the Hamiltonian density \mathcal{H} over all space. For the Coulomb interaction $\mathcal{H}_{\text{int}}^U$, we can substitute Eq. (2.10). After integration by parts, we obtain the part of the Hamiltonian corresponding to $\mathcal{H}_{\text{int}}^U$,

$$H_{\text{int}}^U(t) = \frac{1}{2} \int_{z<0} \int_{z'<0} d^3r d^3r' X_i(\mathbf{r}, t) X_j(\mathbf{r}', t) F_{ij}(\mathbf{r} - \mathbf{r}'), \quad (2.23)$$

where

$$F_{ij}(\mathbf{r} - \mathbf{r}') \stackrel{\text{def}}{=} \frac{e^2}{\epsilon_0} \left[\frac{1}{4\pi} \frac{\partial^2}{\partial x_i \partial x_j} \left(\frac{1}{|\mathbf{r} - \mathbf{r}'|} \right) - \frac{1}{3} \delta_{ij} \delta(\mathbf{r} - \mathbf{r}') \right]. \quad (2.24)$$

The fields are quantized in the usual way by imposing equal-time commutation relations between the field operators \mathbf{A} , \mathbf{X} and \mathbf{Y}_ω and their conjugate momenta Eqs. (2.11) to (2.13):

$$[A_i(\mathbf{r}, t), \dot{A}_j(\mathbf{r}', t)] = \frac{i\hbar}{\epsilon_0} \delta_{ij} \delta(\mathbf{r} - \mathbf{r}'), \quad (2.25)$$

$$[X_i(\mathbf{r}, t), P_{X,j}(\mathbf{r}', t)] = i\hbar \delta_{ij} \delta(\mathbf{r} - \mathbf{r}'), \quad (2.26)$$

$$[Y_{\omega,i}(\mathbf{r}, t), P_{\omega',j}(\mathbf{r}', t)] = i\hbar \delta_{ij} \delta(\omega - \omega') \delta(\mathbf{r} - \mathbf{r}'), \quad (2.27)$$

where we have used the fact that \mathbf{A} commutes with ∇U .

2.3 Diagonalization of the Matter Part

Ideally, one would like to diagonalize the Hamiltonian $H = \int_{\infty} d^3r \mathcal{H}$ by means of a canonical transformation from the field operators \mathbf{A} , \mathbf{X} and \mathbf{Y}_{ω} to some other set of operators. This proved to be too ambitious a task. Instead, we seek an exact solution of the our Hamiltonian model using diagrammatic perturbation theory.

We first diagonalize the Hamiltonian density of the subsystem consisting of the bare matter field, the reservoir and the coupling between the two,

$$\mathcal{H}_{\text{mat}}^{(0)} = \mathcal{H}_{\text{mat}} + \mathcal{H}_{\text{res}} + \mathcal{H}_{\text{int}}^{\text{res}}. \quad (2.28)$$

Our approach follows closely that of Huttner et al. [7]. Whereas the latter authors performed the diagonalization in reciprocal space, as is appropriate for an *infinite* dielectric medium, we perform the diagonalization in real space instead, since we are dealing with a dielectric *half-space*. The annihilation operators $\mathbf{b}(\mathbf{r}, t)$ and $\mathbf{b}_{\omega}(\mathbf{r}, t)$ for the bare matter and reservoir fields are defined in terms of \mathbf{X} , \mathbf{Y}_{ω} and their conjugate momenta by

$$\mathbf{b} = \sqrt{\frac{\rho\bar{\omega}_0}{2\hbar}} \left(\mathbf{X} + i \frac{\mathbf{P}_X}{\rho\bar{\omega}_0} \right), \quad (2.29)$$

$$\mathbf{b}_{\omega} = \sqrt{\frac{\rho\omega}{2\hbar}} \left(-i\mathbf{Y}_{\omega} + \frac{\mathbf{P}_{\omega}}{\rho\omega} \right), \quad (2.30)$$

where, for simplicity, we have omitted the dependence of the operators on (\mathbf{r}, t) . Eqs. (2.29) and (2.30) may be inverted, using the fact that \mathbf{X} , \mathbf{Y}_{ω} and their conjugate momenta are Hermitian,

$$\mathbf{X} = \sqrt{\frac{\hbar}{2\rho\bar{\omega}_0}} (\mathbf{b}^{\dagger} + \mathbf{b}), \quad (2.31)$$

$$\mathbf{P}_X = i\sqrt{\frac{\hbar\rho\bar{\omega}_0}{2}} (\mathbf{b}^{\dagger} - \mathbf{b}), \quad (2.32)$$

$$\mathbf{Y}_{\omega} = -i\sqrt{\frac{\hbar}{2\rho\omega}} (\mathbf{b}_{\omega}^{\dagger} - \mathbf{b}_{\omega}), \quad (2.33)$$

$$\mathbf{P}_{\omega} = \sqrt{\frac{\hbar\rho\omega}{2}} (\mathbf{b}_{\omega}^{\dagger} + \mathbf{b}_{\omega}), \quad (2.34)$$

Using Eqs. (2.29), (2.30), (2.26) and (2.27) we readily obtain

$$[b_i(\mathbf{r}, t), b_j^\dagger(\mathbf{r}', t)] = \delta_{ij}\delta(\mathbf{r} - \mathbf{r}'), \quad (2.35)$$

$$[b_{\omega,i}(\mathbf{r}, t), b_{\omega',j}^\dagger(\mathbf{r}', t)] = \delta_{ij}\delta(\omega - \omega')\delta(\mathbf{r} - \mathbf{r}'), \quad (2.36)$$

while all other commutators between \mathbf{b} , \mathbf{b}_ω and their Hermitian adjoints vanish. Eqs. (2.35) and (2.36) show that \mathbf{b} and \mathbf{b}_ω are the annihilation operators for the bare matter and reservoir fields, respectively.

Substituting Eqs. (2.31) to (2.34) into Eq. (2.28) and using Eqs. (2.18) to (2.20), we obtain

$$\begin{aligned} \mathcal{H}_{\text{mat}}^{(0)} = & \theta(-z) \left[\hbar\tilde{\omega}_0 \mathbf{b}^\dagger \cdot \mathbf{b} + \int_0^\infty d\omega \hbar\omega \mathbf{b}_\omega^\dagger \cdot \mathbf{b}_\omega \right. \\ & \left. + \frac{\hbar}{2} \int_0^\infty d\omega V(\omega) (\mathbf{b}^\dagger + \mathbf{b}) \cdot (\mathbf{b}_\omega^\dagger + \mathbf{b}_\omega) \right], \end{aligned} \quad (2.37)$$

where $V(\omega) = \frac{v(\omega)}{\rho} \sqrt{\omega/\tilde{\omega}_0}$ and we have omitted an infinite zero-point energy term.

Next, we diagonalize the Hamiltonian density Eq. (2.37) by defining the annihilation operator $\mathbf{B}_\omega(\mathbf{r}, t)$ for the dressed matter field,

$$\mathbf{B}_\omega = \alpha_0(\omega)\mathbf{b} + \beta_0(\omega)\mathbf{b}^\dagger + \int_0^\infty d\omega' [\alpha_1(\omega, \omega')\mathbf{b}_{\omega'} + \beta_1(\omega, \omega')\mathbf{b}_{\omega'}^\dagger], \quad (2.38)$$

the dependence of the operators on (\mathbf{r}, t) being understood. The coefficients $\alpha_0(\omega)$, $\beta_0(\omega)$, $\alpha_1(\omega, \omega')$ and $\beta_1(\omega, \omega')$ are to be chosen so that $\mathcal{H}_{\text{mat}}^{(0)}$ is diagonalized,

$$\mathcal{H}_{\text{mat}}^{(0)}(\mathbf{r}, t) = \theta(-z) \int_0^\infty d\omega \hbar\omega \mathbf{B}_\omega^\dagger(\mathbf{r}, t) \cdot \mathbf{B}_\omega(\mathbf{r}, t), \quad (2.39)$$

and furthermore that the transformation Eq. (2.38) is canonical,

$$[B_{\omega,i}(\mathbf{r}, t), B_{\omega',j}^\dagger(\mathbf{r}', t)] = \delta_{ij}\delta(\omega - \omega')\delta(\mathbf{r} - \mathbf{r}'). \quad (2.40)$$

Eqs. (2.39) and (2.40) together imply that

$$[\mathbf{B}_\omega(\mathbf{r}, t), \mathcal{H}_{\text{mat}}^{(0)}(\mathbf{r}', t)] = \hbar\omega \mathbf{B}_\omega(\mathbf{r}, t)\delta(\mathbf{r} - \mathbf{r}')\theta(-z). \quad (2.41)$$

Eqs. (2.37) and (2.38) are substituted into Eq. (2.41) and the commutation bracket on the LHS of the resulting equation evaluated with the help of Eqs. (2.35) and

(2.36). Then, by equating the coefficients of \mathbf{b} , \mathbf{b}^\dagger , \mathbf{b}_ω and $\mathbf{b}_\omega^\dagger$ on the two sides of the equation, we obtain the following set of relations among the coefficients:

$$\alpha_0(\omega)(\omega - \bar{\omega}_0) = \frac{1}{2} \int_0^\infty d\omega' [\alpha_1(\omega, \omega')V(\omega') - \beta_1(\omega, \omega')V(\omega')], \quad (2.42)$$

$$\beta_0(\omega)(\omega + \bar{\omega}_0) = \frac{1}{2} \int_0^\infty d\omega' [\alpha_1(\omega, \omega')V(\omega') - \beta_1(\omega, \omega')V(\omega')], \quad (2.43)$$

$$\alpha_1(\omega, \omega')(\omega - \omega') = \frac{1}{2} [\alpha_0(\omega) - \beta_0(\omega)]V(\omega'), \quad (2.44)$$

$$\beta_1(\omega, \omega')(\omega + \omega') = \frac{1}{2} [\alpha_0(\omega) - \beta_0(\omega)]V(\omega'). \quad (2.45)$$

These relations, together with the commutation relation Eq. (2.40), allow us to solve for the coefficients $\alpha_0(\omega)$, $\beta_0(\omega)$, $\alpha_1(\omega, \omega')$ and $\beta_1(\omega, \omega')$, as shown in Appendix A.

Assuming that the set of dressed operators \mathbf{B}_ω and $\mathbf{B}_\omega^\dagger$, $0 < \omega < \infty$, is complete, it should be possible to invert Eq. (2.38) to obtain \mathbf{b} and \mathbf{b}_ω as functions of the dressed operators. Writing \mathbf{b} as

$$\mathbf{b} = \int_0^\infty d\omega' [r(\omega')\mathbf{B}_{\omega'} + s(\omega')\mathbf{B}_{\omega'}^\dagger], \quad (2.46)$$

we can determine the coefficients $r(\omega)$ and $s(\omega)$ by evaluating the commutators of both sides of Eq. (2.46) with \mathbf{B}_ω and $\mathbf{B}_\omega^\dagger$. Using Eqs. (2.35), (2.36), (2.38) and (2.40), we find $r(\omega) = \alpha_0^*(\omega)$ and $s(\omega) = -\beta_0(\omega)$. Hence,

$$\mathbf{b} = \int_0^\infty d\omega' [\alpha_0^*(\omega)\mathbf{B}_\omega - \beta_0(\omega)\mathbf{B}_\omega^\dagger]. \quad (2.47)$$

Similarly, we obtain

$$\mathbf{b}_\omega = \int_0^\infty d\omega' [\alpha_1^*(\omega', \omega)\mathbf{B}_{\omega'} - \beta_1(\omega', \omega)\mathbf{B}_{\omega'}^\dagger]. \quad (2.48)$$

The results Eqs. (2.47) and (2.48) are consistent with the commutation relations Eqs. (2.35) and (2.36) if and only if $V^2(\omega)$ satisfies the inequality

$$\int_0^\infty d\omega \frac{V^2(\omega)}{\omega} < \bar{\omega}_0. \quad (2.49)$$

The proof of this statement can be found in [7].

Substituting Eq. (2.47) into Eqs. (2.31) and (2.32), we can express the bare matter field operator and its conjugate momentum in terms of the dressed operators,

$$\mathbf{X} = \sqrt{\frac{\hbar}{2\rho\tilde{\omega}_0}} \int_0^\infty d\omega [h(\omega)\mathbf{B}_\omega^\dagger + \text{h.c.}], \quad (2.50)$$

$$\mathbf{P}_X = \sqrt{\frac{\hbar\rho\tilde{\omega}_0}{2}} \int_0^\infty d\omega [g(\omega)\mathbf{B}_\omega^\dagger + \text{h.c.}], \quad (2.51)$$

where

$$h(\omega) = \alpha_0(\omega) - \beta_0(\omega), \quad (2.52)$$

$$g(\omega) = i[\alpha_0(\omega) + \beta_0(\omega)], \quad (2.53)$$

and h.c. denotes the Hermitian conjugate of the immediately preceding term.

2.4 Spontaneous Decay Rate

Up to now, we have only considered the system consisting of the lossy dielectric half-space and the radiation field with which it interacts, as described by the Hamiltonian density \mathcal{H} defined by Eqs. (2.16) to (2.22). When an excited atom is introduced into the system, there is an additional interaction Hamiltonian of the form

$$H_a = \int_\infty d^3r (-\mathbf{j}_a \cdot \mathbf{A} + \rho_a U), \quad (2.54)$$

where \mathbf{j}_a and ρ_a are the current and charge densities of the atom. For simplicity, we assume the atom to be made up of a single electron of mass m and charge e in orbit around a fixed nucleus of charge $-e$ at a point \mathbf{r}_a on the *air* side of the dielectric surface, $z_a > 0$. Then the current and charge densities of the atom are given by

$$\begin{aligned} \mathbf{j}_a(\mathbf{r}, t) &= -\frac{i\hbar e}{2m} \left\{ \psi^\dagger(\mathbf{r}, t) \nabla \psi(\mathbf{r}, t) - [\nabla \psi^\dagger(\mathbf{r}, t)] \psi(\mathbf{r}, t) \right\} \\ &\quad - \frac{e^2}{2m} \mathbf{A}(\mathbf{r}, t) \psi^\dagger(\mathbf{r}, t) \psi(\mathbf{r}, t), \end{aligned} \quad (2.55)$$

$$\rho_a(\mathbf{r}, t) = e\psi^\dagger(\mathbf{r}, t)\psi(\mathbf{r}, t) - e\delta(\mathbf{r} - \mathbf{r}_a), \quad (2.56)$$

where $\psi(\mathbf{r}, t)$ is the field operator of the electron. For a two-level atom, $\psi(\mathbf{r}, t)$ may be expanded in annihilation operators $c_0(t)$ and $c_1(t)$ for the ground and excited states,

respectively,

$$\psi(\mathbf{r}, t) = c_0(t)u_0(\mathbf{r}) + c_1(t)u_1(\mathbf{r}), \quad (2.57)$$

where $u_0(\mathbf{r})$ and $u_1(\mathbf{r})$ are the ground and excited state wave functions of the atom, respectively, which are assumed to have opposite parities. The annihilation operators $c_0(t)$ and $c_1(t)$ obey the equal-time *anti*-commutation relation,

$$\{c_i(t), c_j^\dagger(t)\} = \delta_{ij}. \quad (2.58)$$

The integral over \mathbf{r} in Eq. (2.54) can be performed if we make the dipole approximation for the atom. This means that the atomic wave functions $u_0(\mathbf{r})$ and $u_1(\mathbf{r})$ are assumed to be localized to within a small neighborhood of the nucleus at \mathbf{r}_a . In that case, the vector potential appearing in Eqs. (2.54) and (2.55) may be replaced by its value at \mathbf{r}_a . Using Eqs. (2.55) and (2.57), the first term in Eq. (2.54), responsible for the radiative decay of the excited atom, can be evaluated:

$$\begin{aligned} H_a^r(t) &\stackrel{\text{def}}{=} - \int_{\infty} d^3r \mathbf{j}_a \cdot \mathbf{A} \\ &= -\frac{e}{m} [c_0^\dagger(t)c_1(t)\mathbf{A}(\mathbf{r}_a, t) \cdot \mathbf{p}_{01} + c_1^\dagger(t)c_0(t)\mathbf{A}(\mathbf{r}_a, t) \cdot \mathbf{p}_{10}] \\ &\quad + \frac{e^2}{2m} \mathbf{A}^2(\mathbf{r}_a, t) [c_0^\dagger(t)c_0(t) + c_1^\dagger(t)c_1(t)], \end{aligned} \quad (2.59)$$

where $\mathbf{p}_{01} = \mathbf{p}_{10}^*$ is the matrix element of the operator $(-i\hbar\nabla)$ between the ground and excited state wave functions.

For the second term in Eq. (2.54), we first expand the instantaneous Coulomb potential $U(\mathbf{r}, t)$ given by Eq. (2.10) about \mathbf{r}_a ,

$$U(\mathbf{r}, t) = \int_{\infty} d^3r' \frac{-e\nabla' \cdot [\mathbf{X}(\mathbf{r}', t)\theta(-z')]}{4\pi\epsilon_0} \left[\frac{1}{|\mathbf{r}_a - \mathbf{r}'|} + (x_j - x_{aj}) \frac{\partial}{\partial x_{aj}} \frac{1}{|\mathbf{r}_a - \mathbf{r}'|} \right]. \quad (2.60)$$

Using Eqs. (2.60), (2.56) and (2.57), the second term in Eq. (2.54), responsible for the nonradiative decay of the excited atom, can be evaluated,

$$\begin{aligned} H_a^{\text{nr}}(t) &\stackrel{\text{def}}{=} \int_{\infty} d^3r \rho_a U \\ &= [c_0^\dagger(t)c_1(t)r_{01,j} + c_1^\dagger(t)c_0(t)r_{10,j}] \int_{\infty} d^3r' \frac{-e^2\nabla' \cdot [\mathbf{X}(\mathbf{r}', t)\theta(-z')]}{4\pi\epsilon_0} \frac{\partial}{\partial x_{aj}} \frac{1}{|\mathbf{r}_a - \mathbf{r}'|}, \end{aligned} \quad (2.61)$$

where $r_{01} = r_{10}^*$ is the matrix element of $(\mathbf{r} - \mathbf{r}_a)$ between the ground and excited state wave functions. Using the relationship $p_{01} = -im\omega_a r_{01}$, where ω_a is the atomic transition frequency, and performing an integration by parts, Eq. (2.61) becomes

$$H_a^{\text{nr}}(t) = \frac{ie^2 [c_0^\dagger(t)c_1(t)p_{01,j} - c_1^\dagger(t)c_0(t)p_{10,j}]}{4\pi\epsilon_0 m\omega_a} \int_{z' < 0} d^3r' X_i(\mathbf{r}', t) \frac{\partial^2}{\partial x_{aj} \partial x_i'} \frac{1}{|\mathbf{r}_a - \mathbf{r}'|}. \quad (2.62)$$

The radiative and nonradiative perturbation Hamiltonians, Eqs. (2.59) and (2.62), may now be used to compute the total decay rate of the excited atom in first-order perturbation theory. This may be accomplished by applying Fermi's Golden Rule and then expressing the resulting decay rate in terms of Green functions by means of the fluctuation-dissipation theorem. This was the approach taken by Barnett et al. [8] in their treatment of the *radiative* decay rate of an excited atom in an *infinite* homogeneous dielectric medium. Instead, we shall obtain the total decay rate of the excited atom directly in terms of Green functions by considering the self-energy of the excited atom due to the perturbations Eqs. (2.59) and (2.62).

The self-energy of the excited atom enters into the computation of the Green function of the atom by diagrammatic perturbation technique. This Green function is defined by

$$g(\mathbf{r}_1, \mathbf{r}_2; t_1 - t_2) = -\frac{i}{\hbar} \langle T[\psi^{(a)}(\mathbf{r}_1, t_1) \psi^{(a)\dagger}(\mathbf{r}_2, t_2)] \rangle^{(a)}, \quad (2.63)$$

where the superscript (a) denotes exact quantities in the combined system of the half-space dielectric and the excited atom. Also, the angle brackets denote averaging over the exact ground state of this combined system and T denotes time ordering. Using Eq. (2.57), we see that the Green function is a sum of terms involving $-\frac{i}{\hbar} \langle T[c_1^{(a)}(t_1) c_1^{(a)\dagger}(t_2)] \rangle$ and $-\frac{i}{\hbar} \langle T[c_0^{(a)}(t_1) c_0^{(a)\dagger}(t_2)] \rangle$. Since we are only interested in the self-energy of the *excited* state, we consider the term involving the excited-state operators,

$$g(t_1 - t_2) = -\frac{i}{\hbar} \langle T[c_1^{(a)}(t_1) c_1^{(a)\dagger}(t_2)] \rangle^{(a)}, \quad (2.64)$$

where we have omitted the dependence on \mathbf{r}_1 and \mathbf{r}_2 which is irrelevant to the following discussion. Since $c_1^{(a)}(t_1)$ in Eq. (2.64) is an exact operator for the combined system in the Heisenberg picture, its time dependence is in general unknown. Hence, Eq. (2.64) must be evaluated by diagrammatic perturbation technique. The general result of the diagrammatic technique is:

$$g(t_1 - t_2) = -\frac{i}{\hbar} \langle T[c_1(t_1)S(\infty, -\infty)c_1^\dagger(t_2)] \rangle_{\text{conn}}, \quad (2.65)$$

where quantities without the superscript (a) are unperturbed quantities, that is, those associated with the Hamiltonian density \mathcal{H} of Eq. (2.16) without the perturbation H_a . Also, $S(\infty, -\infty)$ is an infinite series of operators,

$$S(\infty, -\infty) = 1 + \sum_{n=1}^{\infty} \frac{1}{n!} \left(\frac{-i}{\hbar}\right)^n \int_{-\infty}^{\infty} \dots \int_{-\infty}^{\infty} dt_1 \dots dt_n T[H_a(t_1) \dots H_a(t_n)], \quad (2.66)$$

and the symbol ‘conn’ in Eq. (2.65) indicates that only *connected* diagrams are to be included in the calculation. The derivation of the fundamental result Eq. (2.65) can be found in most textbooks on many-body physics [19, 20].

Substituting Eq. (2.66) into Eq. (2.65), we see that the Green function can be written as an infinite series, $g(t_1 - t_2) = g^{(0)}(t_1 - t_2) + g^{(1)}(t_1 - t_2) + g^{(2)}(t_1 - t_2) + \dots$, where the n th term of this series corresponds to the n th term of the series in Eq. (2.66).

Since $c_0(t)$ and $c_1(t)$ in Eq. (2.65) are unperturbed operators, their time dependence is simple-harmonic,

$$c_0(t) = c_0 e^{-i\omega_0 t}, \quad (2.67)$$

$$c_1(t) = c_1 e^{-i\omega_1 t}, \quad (2.68)$$

where ω_0 and ω_1 are the energies of the ground and excited states of the atom, respectively, divided by \hbar . Using Eq. (2.68), we can compute the zeroth-order, or unperturbed, Green function,

$$\begin{aligned} g^{(0)}(t_1 - t_2) &= -\frac{i}{\hbar} \langle T[c_1(t_1)c_1^\dagger(t_2)] \rangle \\ &= -\frac{i}{\hbar} e^{-i\omega_1(t_1 - t_2)} \theta(t_1 - t_2), \end{aligned} \quad (2.69)$$

where we have used Eq. (2.58) and the fact that c_1 acting on the unperturbed ground state gives zero. It is more useful to consider the Fourier transform with respect to time of the Green function:

$$\begin{aligned}
g^{(0)}(\omega) &= \int_{-\infty}^{\infty} d(t_1 - t_2) e^{i\omega(t_1 - t_2)} g^{(0)}(t_1 - t_2) \\
&= -\frac{i}{\hbar} \int_0^{\infty} d(t_1 - t_2) e^{i(\omega - \omega_1)(t_1 - t_2)} \\
&= \frac{1}{\hbar\omega - \hbar\omega_1 + i\epsilon}.
\end{aligned} \tag{2.70}$$

Next, we compute the first-order correction to the Green function,

$$g^{(1)}(t_1 - t_2) = \left(-\frac{i}{\hbar}\right)^2 \int_{-\infty}^{\infty} dt_3 \langle T[c_1(t_1) H_a(t_3) c_1^\dagger(t_2)] \rangle_{\text{conn}}, \tag{2.71}$$

by substituting the $n = 1$ term in Eq. (2.66) into Eq. (2.65). In order to have a non-vanishing expectation value, there must be the same number of annihilation and creation operators for the ground or excited state in the time-ordered product in Eq. (2.71). Upon examination of Eqs. (2.59) and (2.62), we find that the only term in $H_a(t_3)$ which contributes to the expectation value in Eq. (2.71) is the term proportional to A^2 in Eq. (2.59). Furthermore, the term $c_0^\dagger(t) c_0(t)$ in Eq. (2.59) does not contribute, since we can commute the operator $c_0(t)$ to the right of all other operators in the time-ordered product in Eq. (2.71) to annihilate the ground state. Hence, we are left with

$$g^{(1)}(t_1 - t_2) = -\frac{e^2}{2m\hbar^2} \int_{-\infty}^{\infty} dt_3 \langle T[c_1(t_1) A^2(\mathbf{r}_a, t_3) c_1^\dagger(t_3) c_1(t_3) c_1^\dagger(t_2)] \rangle_{\text{conn}}. \tag{2.72}$$

We can now apply Wick's Theorem to evaluate the time-ordered product in Eq. (2.72). This theorem says that the expectation value in the ground state of a time-ordered product of operators is equal to the sum of all possible products of expectation values of the time-ordered products of pairs of the operators [19, 20]. Since only connected diagrams are counted, we see that there is only one possible pairing of the operators in Eq. (2.72),

$$\begin{aligned}
g^{(1)}(t_1 - t_2) &= -\frac{e^2}{2m\hbar^2} \int_{-\infty}^{\infty} dt_3 \langle T[c_1(t_1) c_1^\dagger(t_3)] \rangle \langle T[A(\mathbf{r}_a, t_3) \cdot A(\mathbf{r}_a, t_3)] \rangle \\
&\quad \times \langle T[c_1(t_3) c_1^\dagger(t_2)] \rangle.
\end{aligned} \tag{2.73}$$

Using Eq. (2.69), we find that the integrand in Eq. (2.73) is non-zero only when $t_1 > t_3 > t_2$. Then, introducing the transverse photon Green function for the dielectric half-space

$$\mathcal{D}_{ij}(\mathbf{r}_1, \mathbf{r}_2; t_1 - t_2) \stackrel{\text{def}}{=} -\frac{i}{\hbar} \langle \mathbb{T}[A_i(\mathbf{r}_1, t_1)A_j(\mathbf{r}_2, t_2)] \rangle, \quad (2.74)$$

we may rewrite Eq. (2.73) as

$$\begin{aligned} g^{(1)}(t_1 - t_2) &= -\frac{ie^2}{2m\hbar} \int_{t_2}^{t_1} dt_3 \mathcal{D}_{ii}(\mathbf{r}_a, \mathbf{r}_a; t_3 - t_2) e^{-i\omega_1(t_1 - t_3 + t_3 - t_2)} \theta(t_1 - t_2) \\ &= -\frac{ie^2}{2m\hbar} \mathcal{D}_{ii}(\mathbf{r}_a, \mathbf{r}_a; 0) e^{-i\omega_1(t_1 - t_2)} (t_1 - t_2) \theta(t_1 - t_2). \end{aligned} \quad (2.75)$$

Taking the Fourier transform with respect to $(t_1 - t_2)$, we obtain

$$\begin{aligned} g^{(1)}(\omega) &= -\frac{ie^2}{2m\hbar} \mathcal{D}_{ii}(\mathbf{r}_a, \mathbf{r}_a; 0) \int_0^\infty d(t_1 - t_2) e^{i(\omega - \omega_1)(t_1 - t_2)} (t_1 - t_2) \\ &= -\frac{ie^2}{2m\hbar} \mathcal{D}_{ii}(\mathbf{r}_a, \mathbf{r}_a; 0) \left(-i \frac{\partial}{\partial \omega} \right) \left(\frac{i}{\omega - \omega_1 + i\epsilon} \right) \\ &= \frac{1}{\hbar\omega - \hbar\omega_1 + i\epsilon} \Sigma^{(1)} \frac{1}{\hbar\omega - \hbar\omega_1 + i\epsilon}, \end{aligned} \quad (2.76)$$

where

$$\Sigma^{(1)} = \frac{i\hbar e^2}{2m} \mathcal{D}_{ii}(\mathbf{r}_a, \mathbf{r}_a; 0), \quad (2.77)$$

is the self-energy of the excited atom due to the term proportional to \mathbf{A}^2 in Eq. (2.59). The reason why this is called the self-energy is as follows. Suppose the \mathbf{A}^2 terms in Eq. (2.59) were the only perturbation. Then, when we include the higher-order terms of Eq. (2.66) in Eq. (2.65), we would obtain

$$\begin{aligned} g(\omega) &= \frac{1}{\hbar\omega - \hbar\omega_1 + i\epsilon} + \frac{1}{\hbar\omega - \hbar\omega_1 + i\epsilon} \Sigma^{(1)} \frac{1}{\hbar\omega - \hbar\omega_1 + i\epsilon} \\ &\quad + \frac{1}{\hbar\omega - \hbar\omega_1 + i\epsilon} \Sigma^{(1)} \frac{1}{\hbar\omega - \hbar\omega_1 + i\epsilon} \Sigma^{(1)} \frac{1}{\hbar\omega - \hbar\omega_1 + i\epsilon} + \dots \\ &= \frac{1}{\hbar\omega - [\hbar\omega_1 + \Sigma^{(1)}] + i\epsilon}. \end{aligned} \quad (2.78)$$

Here, $\Sigma^{(1)}$ appears as a correction to the energy $\hbar\omega_1$ of the excited state. Hence the term self-energy.

It should be noted that $\Sigma^{(1)}$ given by Eq. (2.77) is purely real. Substituting Eq. (2.74) into Eq. (2.77), we obtain

$$\begin{aligned}\Sigma^{(1)} &= \frac{e^2}{2m} \langle T[A_i(\mathbf{r}_a, t_3)A_i(\mathbf{r}_a, t_3)] \rangle \\ &= \frac{e^2}{2m} \langle \mathbf{A}^2(\mathbf{r}_a, t_3) \rangle ,\end{aligned}\quad (2.79)$$

which is purely real since \mathbf{A} is Hermitian. Thus, $\Sigma^{(1)}$ contributes only to a level-shift of the excited state, but not to its lifetime. Hence, for the purpose of computing the lifetime of the excited atom, we may neglect $\Sigma^{(1)}$.

Next, we consider the second-order contribution to the atom Green function. This is obtained by substituting the $n = 2$ term in Eq. (2.66) into Eq. (2.65),

$$g^{(2)}(t_1 - t_2) = \frac{1}{2!} \left(\frac{-i}{\hbar} \right)^3 \int_{-\infty}^{\infty} dt_3 \int_{-\infty}^{\infty} dt_4 \langle T[c_1(t_1)H_a(t_3)H_a(t_4)c_1^\dagger(t_2)] \rangle_{\text{conn}} .\quad (2.80)$$

When Eqs. (2.54), (2.59) and (2.62) are substituted into Eq. (2.80) and the product of the two Hamiltonians expanded, we find that there are terms proportional to e^2 , e^3 and e^4 . It will be seen below that one of the factors of e in H_a^{nr} given by Eq. (2.62) is absorbed in the definition of the dielectric function [cf. Eq. (2.121)], which is of order unity. Hence, H_a^{nr} should be counted as a term of order e rather than e^2 . Now, since we are only interested in the decay rate of the excited atom to the same approximation as in Fermi's Golden Rule, we retain only the terms proportional to e^2 in Eq. (2.80). This amounts to omitting the \mathbf{A}^2 term in Eq. (2.59). Thus, we are left with four terms contributing to the self-energy of the excited atom to order e^2 : one due to H_a^{r} acting twice, one to H_a^{nr} acting twice, and the two cross terms. We consider each of these cases separately.

Consider first the effect of H_a^{r} acting twice. Substituting the first term in Eq. (2.59) into Eq. (2.80), we obtain

$$\begin{aligned}g_{\text{AA}}^{(2)}(t_1 - t_2) &= -\frac{1}{2!} \left(\frac{e}{m\hbar} \right)^2 \int_{-\infty}^{\infty} dt_3 \int_{-\infty}^{\infty} dt_4 \mathcal{D}_{ij}(\mathbf{r}_a, \mathbf{r}_a; t_3 - t_4) \\ &\times \langle T \{ c_1(t_1) [c_0^\dagger(t_3)c_1(t_3)p_{01,i} + \text{h.c.}] [c_0^\dagger(t_4)c_1(t_4)p_{01,j} + \text{h.c.}] c_1^\dagger(t_2) \} \rangle_{\text{conn}} ,\end{aligned}\quad (2.81)$$

where we have paired the two A operators to form the photon Green function \mathcal{D}_{ij} , since these two operators must be paired together to give a non-vanishing result. When the time-ordered product in Eq. (2.81) is expanded using Wick's Theorem, we find that there are two equal pairings of the operators which together cancel the factor $(1/2!)$,

$$g_{AA}^{(2)}(t_1 - t_2) = - \left(\frac{e}{m\hbar} \right)^2 \int_{-\infty}^{\infty} dt_3 \int_{-\infty}^{\infty} dt_4 \mathcal{D}_{ij}(\mathbf{r}_a, \mathbf{r}_a; t_3 - t_4) p_{10,i} p_{01,j} \times \langle T[c_1(t_1) c_1^\dagger(t_3)] \rangle \langle T[c_0(t_3) c_0^\dagger(t_4)] \rangle \langle T[c_1(t_4) c_1^\dagger(t_2)] \rangle. \quad (2.82)$$

Using Eq. (2.69), Eq. (2.82) becomes

$$g_{AA}^{(2)}(t_1 - t_2) = - \left(\frac{e}{m\hbar} \right)^2 p_{10,i} p_{01,j} \int_{-\infty}^{\infty} dt_3 \int_{-\infty}^{\infty} dt_4 e^{-i\omega_1(t_1-t_3)} \theta(t_1 - t_3) \times \mathcal{D}_{ij}(\mathbf{r}_a, \mathbf{r}_a; t_3 - t_4) e^{-i\omega_0(t_3-t_4)} \theta(t_3 - t_4) e^{-i\omega_1(t_4-t_2)} \theta(t_4 - t_2). \quad (2.83)$$

The integrals over t_3 and t_4 in Eq. (2.83) are the convolutions of the functions $e^{-i\omega_1 t} \theta(t)$, $\mathcal{D}_{ij}(\mathbf{r}_a, \mathbf{r}_a; t) e^{-i\omega_0 t} \theta(t)$ and $e^{-i\omega_1 t} \theta(t)$. Upon taking the Fourier transform of Eq. (2.83) with respect to $t_1 - t_2$, these convolutions become the product of the Fourier transforms of the individual terms:

$$g_{AA}^{(2)}(\omega) = \frac{1}{\hbar\omega - \hbar\omega_1 + i\epsilon} \left(\frac{e^2 p_{10,i} p_{01,j}}{m^2} \int_0^{\infty} d\tau \mathcal{D}_{ij}(\mathbf{r}_a, \mathbf{r}_a; \tau) e^{i(\omega - \omega_0)\tau} \right) \frac{1}{\hbar\omega - \hbar\omega_1 + i\epsilon} = \frac{1}{\hbar\omega - \hbar\omega_1 + i\epsilon} \Sigma_{AA}^{(2)}(\omega) \frac{1}{\hbar\omega - \hbar\omega_1 + i\epsilon}, \quad (2.84)$$

which allows us to identify the contribution to the self-energy of the excited atom to order e^2 due to the first term in Eq. (2.59) acting twice as

$$\Sigma_{AA}^{(2)}(\omega) = \left(\frac{e}{m} \right)^2 p_{10,i} p_{01,j} \int_0^{\infty} d\tau \mathcal{D}_{ij}(\mathbf{r}_a, \mathbf{r}_a; \tau) e^{i(\omega - \omega_0)\tau}. \quad (2.85)$$

Next, we consider the contribution to the self-energy of the excited atom due to H_a^{nr} acting twice. Substituting Eq. (2.62) into Eq. (2.80), we obtain

$$g_{UU}^{(2)}(t_1 - t_2) = \frac{1}{2!} \left(\frac{-i}{\hbar} \right)^3 \left(\frac{ie^2}{4\pi\epsilon_0 m\omega_a} \right)^2 \int_{-\infty}^{\infty} dt_3 \int_{-\infty}^{\infty} dt_4 \int_{z' < 0} d^3 r' \int_{z'' < 0} d^3 r'' \times \left(\frac{\partial^2}{\partial x_{\alpha j} \partial x'_i} \frac{1}{|\mathbf{r}_a - \mathbf{r}'|} \right) \left(\frac{\partial^2}{\partial x_{\alpha n} \partial x''_l} \frac{1}{|\mathbf{r}_a - \mathbf{r}''|} \right) \langle T[X_i(\mathbf{r}', t_3) X_l(\mathbf{r}'', t_4)] \rangle \times \langle T \{ c_1(t_1) [p_{01,j} c_0^\dagger(t_3) c_1(t_3) - \text{h.c.}] [p_{01,n} c_0^\dagger(t_4) c_1(t_4) - \text{h.c.}] c_1^\dagger(t_2) \} \rangle_{\text{conn}}, \quad (2.86)$$

where we have paired the two \mathbf{X} operators, since these two operators must be paired together to give a non-vanishing result. When the time-ordered product in Eq. (2.86) is expanded using Wick's Theorem, we find that there two equal pairings of the operators which together cancel the factor $(1/2!)$. Then, introducing the Green function for the matter field \mathbf{X}

$$\mathcal{G}_{ij}(\mathbf{r}_1, \mathbf{r}_2; t_1 - t_2) \stackrel{\text{def}}{=} -\frac{i}{\hbar} \langle \text{T}[X_i(\mathbf{r}_1, t_1)X_j(\mathbf{r}_2, t_2)] \rangle, \quad (2.87)$$

Eq. (2.86) becomes

$$\begin{aligned} g_{UU}^{(2)}(t_1 - t_2) &= \left(\frac{-i}{\hbar}\right)^2 \left(\frac{e^2}{4\pi\epsilon_0 m\omega_a}\right)^2 \int_{-\infty}^{\infty} dt_3 \int_{-\infty}^{\infty} dt_4 \int_{z' < 0} d^3 r' \int_{z'' < 0} d^3 r'' p_{10,j} p_{01,n} \\ &\times \left(\frac{\partial^2}{\partial x_{aj} \partial x'_i} \frac{1}{|\mathbf{r}_a - \mathbf{r}'|}\right) \mathcal{G}_{ii}(\mathbf{r}', \mathbf{r}''; t_3 - t_4) \left(\frac{\partial^2}{\partial x_{an} \partial x''_l} \frac{1}{|\mathbf{r}_a - \mathbf{r}''|}\right) \\ &\times \langle \text{T}[c_1(t_1)c_1^\dagger(t_3)] \rangle \langle \text{T}[c_0(t_3)c_0^\dagger(t_4)] \rangle \langle \text{T}[c_1(t_4)c_1^\dagger(t_2)] \rangle. \end{aligned} \quad (2.88)$$

Following the steps leading from Eq. (2.82) through (2.83) to (2.84), we can substitute Eq. (2.69) into Eq. (2.88) and then take the Fourier transform with respect to $(t_1 - t_2)$. The result is

$$g_{UU}^{(2)}(\omega) = \frac{1}{\hbar\omega - \hbar\omega_1 + i\epsilon} \Sigma_{UU}^{(2)}(\omega) \frac{1}{\hbar\omega - \hbar\omega_1 + i\epsilon}, \quad (2.89)$$

where

$$\begin{aligned} \Sigma_{UU}^{(2)}(\omega) &= \left(\frac{e^2}{4\pi\epsilon_0 m\omega_a}\right)^2 p_{10,j} p_{01,n} \int_0^\infty d\tau e^{i(\omega - \omega_0)\tau} \int_{z' < 0} d^3 r' \int_{z'' < 0} d^3 r'' \\ &\times \left(\frac{\partial^2}{\partial x_{aj} \partial x'_i} \frac{1}{|\mathbf{r}_a - \mathbf{r}'|}\right) \mathcal{G}_{ii}(\mathbf{r}', \mathbf{r}''; \tau) \left(\frac{\partial^2}{\partial x_{an} \partial x''_l} \frac{1}{|\mathbf{r}_a - \mathbf{r}''|}\right). \end{aligned} \quad (2.90)$$

In terms of the function F_{ij} defined by Eq. (2.24), we can rewrite Eq. (2.90) as

$$\begin{aligned} \Sigma_{UU}^{(2)}(\omega) &= \left(\frac{1}{m\omega_a}\right)^2 p_{10,j} p_{01,n} \int_{z' < 0} d^3 r' \int_{z'' < 0} d^3 r'' \int_0^\infty d\tau e^{i(\omega - \omega_0)\tau} \\ &\times F_{ji}(\mathbf{r}_a - \mathbf{r}') \mathcal{G}_{ii}(\mathbf{r}', \mathbf{r}''; \tau) F_{in}(\mathbf{r}'' - \mathbf{r}_a), \end{aligned} \quad (2.91)$$

since $\delta(\mathbf{r}_a - \mathbf{r}')$ and $\delta(\mathbf{r}'' - \mathbf{r}_a)$ are zero for $z_a > 0$ and $z', z'' < 0$.

Lastly, we consider the contribution to the self-energy of the excited atom due to H_a^r and H_a^{nr} each acting once. Whether we take $H_a(t_3)$ in Eq. (2.80) to be H_a^r

and $H_a(t_4)$ to be H_a^{nr} or vice versa, we get the same result. Hence these two choices together cancel the factor (1/2!), and we obtain

$$g_{\text{AU}}^{(2)}(t_1 - t_2) = \left(\frac{-i}{\hbar}\right)^3 \left(\frac{-ie^3}{4\pi\epsilon_0 m^2 \omega_a}\right) \int_{-\infty}^{\infty} dt_3 \int_{-\infty}^{\infty} dt_4 \int_{z' < 0} d^3 r' \int_{z'' < 0} d^3 r'' \\ \times \left(\frac{\partial^2}{\partial x_{aj} \partial x'_l} \frac{1}{|\mathbf{r}_a - \mathbf{r}'|}\right) \langle \text{T}[A_i(\mathbf{r}_a, t_3) X_l(\mathbf{r}', t_4)] \rangle \\ \times \left\langle \text{T} \left\{ c_1(t_1) [p_{01,i} c_0^\dagger(t_3) c_1(t_3) + \text{h.c.}] [p_{01,j} c_0^\dagger(t_4) c_1(t_4) - \text{h.c.}] c_1^\dagger(t_2) \right\} \right\rangle_{\text{conn}}, \quad (2.92)$$

where we have paired the **A** and **X** operators, since these two operators must be paired together to give a non-vanishing result. When the time-ordered product in Eq. (2.92) is expanded using Wick's Theorem, there are two non-vanishing pairings of the operators,

$$g_{\text{AU}}^{(2)}(t_1 - t_2) = \left(\frac{-i}{\hbar}\right)^3 \left(\frac{-ie^3}{4\pi\epsilon_0 m^2 \omega_a}\right) \int_{-\infty}^{\infty} dt_3 \int_{-\infty}^{\infty} dt_4 \int_{z' < 0} d^3 r' \int_{z'' < 0} d^3 r'' \\ \times \left(\frac{\partial^2}{\partial x_{aj} \partial x'_l} \frac{1}{|\mathbf{r}_a - \mathbf{r}'|}\right) \langle \text{T}[A_i(\mathbf{r}_a, t_3) X_l(\mathbf{r}', t_4)] \rangle \\ \times \left\{ p_{10,i} p_{01,j} \langle \text{T}[c_1(t_1) c_1^\dagger(t_3)] \rangle \langle \text{T}[c_0(t_3) c_0^\dagger(t_4)] \rangle \langle \text{T}[c_1(t_4) c_1^\dagger(t_2)] \rangle \right. \\ \left. - p_{01,i} p_{10,j} \langle \text{T}[c_1(t_1) c_1^\dagger(t_4)] \rangle \langle \text{T}[c_0(t_4) c_0^\dagger(t_3)] \rangle \langle \text{T}[c_1(t_3) c_1^\dagger(t_2)] \rangle \right\}. \quad (2.93)$$

Again, following the steps leading from Eq. (2.82) through (2.83) to (2.84), we can substitute Eq. (2.69) into Eq. (2.93) and then take the Fourier transform with respect to $(t_1 - t_2)$. The result is

$$g_{\text{AU}}^{(2)}(\omega) = \frac{1}{\hbar\omega - \hbar\omega_1 + i\epsilon} \Sigma_{\text{AU}}^{(2)}(\omega) \frac{1}{\hbar\omega - \hbar\omega_1 + i\epsilon}, \quad (2.94)$$

where

$$\Sigma_{\text{AU}}^{(2)}(\omega) = -\frac{e}{m^2 \hbar \omega_a} \int_0^{\infty} d\tau e^{i(\omega - \omega_0)\tau} \int_{z' < 0} d^3 r' \int_{z'' < 0} d^3 r'' F_{jl}(\mathbf{r}_a - \mathbf{r}') \\ \times \left\{ p_{10,i} p_{01,j} \langle \text{T}[A_i(\mathbf{r}_a, \tau) X_l(\mathbf{r}', 0)] \rangle - p_{01,i} p_{10,j} \langle \text{T}[A_i(\mathbf{r}_a, 0) X_l(\mathbf{r}', \tau)] \rangle \right\}, \quad (2.95)$$

where we have used Eq. (2.24).

The spontaneous decay rate of the excited atom is proportional to the imaginary part of its self-energy in the excited state,

$$W_{\text{spont}} = -2 \text{Im} \left. \frac{\Sigma(\omega)}{\hbar} \right|_{\omega=\omega_1}, \quad (2.96)$$

where the self-energy $\Sigma(\omega)$ of the atom in the excited state is given to order e^2 by

$$\Sigma(\omega) = \Sigma^{(1)}(\omega) + \Sigma_{AA}^{(2)}(\omega) + \Sigma_{UU}^{(2)}(\omega) + \Sigma_{AU}^{(2)}(\omega). \quad (2.97)$$

We now assume that the transition dipole moment of the atom is parallel to one of the coordinate axes, say, the j -axis. Its decay rate in free-space is given by

$$W_{\text{spont}}^{(0)} = \frac{\omega_a}{3\pi\hbar\epsilon_0 c^3} \left(\frac{e}{m}\right)^2 p_{10,[j]} p_{01,[j]}, \quad (2.98)$$

where the brackets around the index j means that this index is *not* summed. Then, normalizing the decay rate Eq. (2.96) near the dielectric surface to this free-space value and using Eqs. (2.85), (2.91) and (2.95), we obtain

$$\begin{aligned} \frac{W_{\text{spont},j}}{W_{\text{spont}}^{(0)}} &= -\frac{6\pi c^3 \epsilon_0}{\omega_a} \text{Im} \int_0^\infty d\tau e^{i\omega\tau} \left[\mathcal{D}_{[j][j]}(\mathbf{r}_a, \mathbf{r}_a; \tau) \right. \\ &\quad + \frac{1}{e^2 \omega_a^2} \int_{z<0} \int_{z'<0} d^3r d^3r' F_{[j]m}(\mathbf{r}_a - \mathbf{r}) \mathcal{G}_{mn}(\mathbf{r}, \mathbf{r}'; \tau) F_{n[j]}(\mathbf{r}' - \mathbf{r}_a) \\ &\quad \left. + \frac{1}{e\omega_a} \int_{z'<0} d^3r' F_{[j]m}(\mathbf{r}_a - \mathbf{r}') \mathcal{C}_{m[j]}(\mathbf{r}', \mathbf{r}_a; \tau) \right] \Big|_{\omega=\omega_a}, \quad (2.99) \end{aligned}$$

where

$$C_{ij}(\mathbf{r}_1, \mathbf{r}_2; \tau) \stackrel{\text{def}}{=} \frac{1}{\hbar} \langle T[X_i(\mathbf{r}_1, \tau) A_j(\mathbf{r}_2, 0) - X_i(\mathbf{r}_1, 0) A_j(\mathbf{r}_2, \tau)] \rangle. \quad (2.100)$$

The integration over τ in Eq. (2.99) can be performed explicitly by making use of the analytic properties of the Green functions. This is discussed in Appendix B, where it is shown that Eq. (2.99) reduces to

$$\begin{aligned} \frac{W_{\text{spont},j}}{W_{\text{spont}}^{(0)}} &= -\frac{6\pi c^3 \epsilon_0}{\omega_a} \text{Im} \left[\mathcal{D}_{[j][j]}^\omega(\mathbf{r}_a, \mathbf{r}_a) \right. \\ &\quad + \frac{1}{e^2 \omega_a^2} \int_{z<0} \int_{z'<0} d^3r d^3r' F_{[j]m}(\mathbf{r}_a - \mathbf{r}) \mathcal{G}_{mn}^\omega(\mathbf{r}, \mathbf{r}') F_{n[j]}(\mathbf{r}' - \mathbf{r}_a) \\ &\quad \left. + \frac{1}{e\omega_a} \int_{z'<0} d^3r' F_{[j]m}(\mathbf{r}_a - \mathbf{r}') \mathcal{C}_{m[j]}^\omega(\mathbf{r}', \mathbf{r}_a) \right] \Big|_{\omega=\omega_a}, \quad (2.101) \end{aligned}$$

where the superscript $^\omega$ denotes Fourier transform with respect to τ .

Eq. (2.101) shows that the spontaneous decay rate of the excited atom near the dielectric surface is given, to the same order of approximation as in Fermi's Golden

Rule, in terms of the Fourier transforms with respect to $(t_1 - t_2)$ of the photon Green function Eq. (2.74), the matter Green function Eq. (2.87) and the function $C_{ij}(\mathbf{r}_1, \mathbf{r}_2; t_1 - t_2)$ defined by Eq. (2.100). The latter three functions are defined with respect to the Hamiltonian density \mathcal{H} for the dielectric half-space defined by Eqs. (2.16) to (2.22), without the perturbation \mathcal{H}_a due to the excited atom. In contrast to the atom Green function Eq. (2.63), the functions $\mathcal{D}_{ij}^\omega, \mathcal{G}_{ij}^\omega$ and \mathcal{C}_{ij}^ω *cannot* be approximated by the first few terms of their perturbation expansions, since the cumulative effect of the electrons in the dielectric can be large. Instead, these functions are obtained as exact solutions of the Dyson equations which they satisfy. This is discussed in the next section.

2.5 Green Functions for the Half-Space

The Hamiltonian density \mathcal{H} for the dielectric half-space can be rewritten according to Eqs. (2.16) and (2.28) as

$$\mathcal{H} = \mathcal{H}_{\text{em}}^A + \mathcal{H}_{\text{mat}}^{(0)} + \mathcal{H}_{\text{int}}^U + \mathcal{H}_{\text{int}}^A. \quad (2.102)$$

To obtain the exact Green functions for this Hamiltonian density, we first separate the latter into an unperturbed part,

$$\mathcal{H}_0 = \mathcal{H}_{\text{em}}^A + \mathcal{H}_{\text{mat}}^{(0)} + \mathcal{H}_{\text{int}}^U, \quad (2.103)$$

and a perturbation $\mathcal{H}_{\text{int}}^A$. First, we consider the photon Green function in the subsystem described by the Hamiltonian density of Eq. (2.103),

$$\mathcal{D}_{ij}^{(0)}(\mathbf{r}_1, \mathbf{r}_2; t_1 - t_2) = -\frac{i}{\hbar} \langle \text{T}[A_i^{(0)}(\mathbf{r}_1, t_1) A_j^{(0)}(\mathbf{r}_2, t_2)] \rangle^{(0)}, \quad (2.104)$$

where the superscript (0) denotes quantities associated with the Hamiltonian density \mathcal{H}_0 . From Eqs. (2.17), (2.37), (2.22) and (2.10), we see that, in the subsystem described by \mathcal{H}_0 , the transverse radiation field $\mathbf{A}^{(0)}$ is completely decoupled from the matter field \mathbf{X} and the instantaneous Coulomb potential U . Hence, in this subsystem,

$\mathbf{A}^{(0)}$ is just the free-space radiation field, which can be expanded in a complete set of transverse, monochromatic plane waves,

$$\mathbf{A}^{(0)}(\mathbf{r}, t) = \int \frac{d^3k}{(2\pi)^{3/2}} \sqrt{\frac{\hbar}{2\epsilon_0\omega_k}} \sum_{\lambda=1,2} [a_\lambda(\mathbf{k})\mathbf{e}_\lambda(\mathbf{k})e^{i(\mathbf{k}\cdot\mathbf{r}-\omega_k t)} + \text{h.c.}] , \quad (2.105)$$

where $\omega_k = |\mathbf{k}|c$ and h.c. denotes the Hermitian conjugate of the immediately preceding term. Also, $\mathbf{e}_\lambda(\mathbf{k})$, $\lambda = 1, 2$, are unit vectors such that $[\mathbf{e}_1(\mathbf{k}), \mathbf{e}_2(\mathbf{k}), \frac{\mathbf{k}}{|\mathbf{k}|}]$ form an orthonormal right-handed triad. Eq. (2.105) can be inverted to give

$$a_\lambda(\mathbf{k}) = \sqrt{\frac{\epsilon_0\omega_k}{2\hbar}} \int \frac{d^3r}{(2\pi)^{3/2}} \mathbf{e}_\lambda(\mathbf{k}) \cdot \left[\mathbf{A}^{(0)}(\mathbf{r}, t) + \frac{i}{\omega_k} \dot{\mathbf{A}}^{(0)}(\mathbf{r}, t) \right] e^{-i(\mathbf{k}\cdot\mathbf{r}-\omega_k t)} , \quad (2.106)$$

Using Eqs. (2.106) and (2.25), we readily obtain

$$[a_\lambda(\mathbf{k}), a_{\lambda'}^\dagger(\mathbf{k}')] = \delta_{\lambda,\lambda'} \delta(\mathbf{k} - \mathbf{k}') , \quad (2.107)$$

while the commutator between $a_\lambda(\mathbf{k})$ and $a_{\lambda'}(\mathbf{k}')$, or between $a_\lambda^\dagger(\mathbf{k})$ and $a_{\lambda'}^\dagger(\mathbf{k}')$, vanishes. Eq. (2.107) shows that $a_\lambda^\dagger(\mathbf{k})$ and $a_\lambda(\mathbf{k})$ are the creation and annihilation operators of a transverse photon of wavevector \mathbf{k} and polarization λ . It should be noted that the expansion Eq. (2.105) would not be possible if we had included the term $\mathcal{H}_{\text{int}}^A$ as in Eq. (2.102), since then the time dependence of the annihilation operators $a_\lambda(\mathbf{k}, t)$ would not be simple-harmonic.

The free-space photon Green function can be computed by substituting Eq. (2.105) into Eq. (2.104),

$$\begin{aligned} \mathcal{D}_{ij}^{(0)}(\mathbf{r}_1, \mathbf{r}_2; t_1 - t_2) &= -i \int \frac{d^3k}{(2\pi)^{3/2}} \int \frac{d^3k'}{(2\pi)^{3/2}} \frac{1}{2\epsilon_0\sqrt{\omega_k\omega_{k'}}} \sum_{\lambda=1,2} \sum_{\lambda'=1,2} \\ &\quad \times \left\langle \text{T} \left\{ [a_\lambda(\mathbf{k})e_{\lambda,i}(\mathbf{k})e^{i(\mathbf{k}\cdot\mathbf{r}_1-\omega_k t_1)} + \text{h.c.}] [a_{\lambda'}(\mathbf{k}')e_{\lambda',j}(\mathbf{k}')e^{i(\mathbf{k}'\cdot\mathbf{r}_2-\omega_{k'} t_2)} + \text{h.c.}] \right\} \right\rangle^{(0)} \\ &= -i \int \frac{d^3k}{(2\pi)^3} \frac{1}{2\epsilon_0\omega_k} \sum_{\lambda=1,2} e_{\lambda,i}(\mathbf{k})e_{\lambda,j}(\mathbf{k}) \times \begin{cases} e^{i\mathbf{k}\cdot(\mathbf{r}_1-\mathbf{r}_2)-i\omega_k(t_1-t_2)} , & t_1 > t_2 , \\ e^{-i\mathbf{k}\cdot(\mathbf{r}_1-\mathbf{r}_2)+i\omega_k(t_1-t_2)} , & t_1 < t_2 . \end{cases} \quad (2.108) \end{aligned}$$

From the completeness of the triad $[\mathbf{e}_1(\mathbf{k}), \mathbf{e}_2(\mathbf{k}), \frac{\mathbf{k}}{|\mathbf{k}|}]$ for each \mathbf{k} , we have

$$\sum_{\lambda=1,2} e_{\lambda,i}(\mathbf{k})e_{\lambda,j}(\mathbf{k}) + \frac{k_i k_j}{k^2} = \delta_{ij} . \quad (2.109)$$

Substituting Eq. (2.109) into Eq. (2.108), we obtain

$$\mathcal{D}_{ij}^{(0)}(\mathbf{r}_1, \mathbf{r}_2; t_1 - t_2) = -i \int \frac{d^3k}{(2\pi)^3} \frac{\left(\delta_{ij} - \frac{k_i k_j}{k^2}\right)}{2\epsilon_0 \omega_k} \begin{cases} e^{i\mathbf{k}\cdot(\mathbf{r}_1 - \mathbf{r}_2) - i\omega_k(t_1 - t_2)}, & t_1 > t_2, \\ e^{-i\mathbf{k}\cdot(\mathbf{r}_1 - \mathbf{r}_2) + i\omega_k(t_1 - t_2)}, & t_1 < t_2. \end{cases} \quad (2.110)$$

Eq. (2.110) can be written in a more compact form,

$$\mathcal{D}_{ij}^{(0)}(\mathbf{r}_1, \mathbf{r}_2; t_1 - t_2) = \frac{1}{\epsilon_0} \int \frac{d^3k}{(2\pi)^3} \int \frac{d\omega}{2\pi} \frac{\left(\delta_{ij} - \frac{k_i k_j}{k^2}\right)}{\omega^2 - k^2 c^2 + i\epsilon} e^{i\mathbf{k}\cdot(\mathbf{r}_1 - \mathbf{r}_2) - i\omega(t_1 - t_2)}, \quad (2.111)$$

as can be verified by contour integration in the complex ω -plane. From Eq. (2.111), we immediately obtain the Fourier transform of $\mathcal{D}_{ij}^{(0)}$ with respect to $(t_1 - t_2)$,

$$\mathcal{D}_{ij}^{(0)\omega}(\mathbf{r}_1, \mathbf{r}_2) = \frac{1}{\epsilon_0} \int \frac{d^3k}{(2\pi)^3} \frac{\left(\delta_{ij} - \frac{k_i k_j}{k^2}\right)}{\omega^2 - k^2 c^2 + i\epsilon} e^{i\mathbf{k}\cdot(\mathbf{r}_1 - \mathbf{r}_2)}. \quad (2.112)$$

Next, we consider the Green function for the matter field \mathbf{X} for the unperturbed Hamiltonian density of Eq. (2.103). To do so, it is necessary to partition \mathcal{H}_0 further into a part without the Coulomb interaction,

$$\mathcal{H}_{00} = \mathcal{H}_{\text{em}}^A + \mathcal{H}_{\text{mat}}^{(0)}, \quad (2.113)$$

and the Coulomb interaction term $\mathcal{H}_{\text{int}}^U$. We first obtain the Green function for \mathbf{X} in the subsystem described by \mathcal{H}_{00} ,

$$\mathcal{G}_{ij}^{(00)}(\mathbf{r}_1, \mathbf{r}_2; t_1 - t_2) = -\frac{i}{\hbar} \langle \text{T}[X_i^{(00)}(\mathbf{r}_1, t_1) X_j^{(00)}(\mathbf{r}_2, t_2)] \rangle^{(00)}, \quad (2.114)$$

where the superscript (00) denotes quantities associated with the Hamiltonian density Eq. (2.113). For this purpose, the first term in Eq. (2.113) has no effect, since there is no coupling between the radiation field and matter in this subsystem. Next, since the term $\mathcal{H}_{\text{mat}}^{(0)}$ given by Eq. (2.39) is diagonal in the dressed matter operators, the time dependence of the latter operators in this subsystem is simple-harmonic. Hence, substituting Eq. (2.50) into Eq. (2.114) and using the commutation relation Eq. (2.40),

we obtain

$$\begin{aligned}
\mathcal{G}_{ij}^{(00)}(\mathbf{r}_1, \mathbf{r}_2; t_1 - t_2) &= -\frac{i}{2\rho\tilde{\omega}_0} \int_0^\infty d\omega \int_0^\infty d\omega' \\
&\quad \times \left\langle \text{T} \left\{ [h(\omega)B_{\omega,i}^\dagger(\mathbf{r}_1)e^{i\omega t_1} + \text{h.c.}] [h(\omega')B_{\omega',j}^\dagger(\mathbf{r}_2)e^{i\omega' t_2} + \text{h.c.}] \right\} \right\rangle^{(00)} \\
&= -\frac{i}{2\rho\tilde{\omega}_0} \delta_{ij} \delta(\mathbf{r}_1 - \mathbf{r}_2) \int_0^\infty d\omega' |h(\omega')|^2 \begin{cases} e^{-i\omega'(t_1-t_2)}, & t_1 > t_2, \\ e^{i\omega'(t_1-t_2)}, & t_1 < t_2. \end{cases} \quad (2.115)
\end{aligned}$$

Taking the Fourier transform with respect to $(t_1 - t_2)$, we obtain

$$\mathcal{G}_{ij}^{(00)\omega}(\mathbf{r}_1, \mathbf{r}_2) = -\frac{i}{2\rho\tilde{\omega}_0} \delta_{ij} \delta(\mathbf{r}_1 - \mathbf{r}_2) \int_0^\infty d\omega' |h(\omega')|^2 \left[\frac{i}{\omega - \omega' + i\epsilon} - \frac{i}{\omega + \omega' - i\epsilon} \right]. \quad (2.116)$$

Using Eqs. (2.52), (A.11) and (A.13), we obtain

$$|h(\omega')|^2 = \frac{\tilde{\omega}_0}{\omega'} \xi(\omega'), \quad (2.117)$$

where

$$\xi(\omega') \stackrel{\text{def}}{=} \frac{\tilde{\omega}_0 \omega' V^2(\omega')}{|\omega'^2 - \tilde{\omega}_0^2 z(\omega')|^2}. \quad (2.118)$$

Eq. (2.118) shows that $\xi(\omega)$ is an even function of ω , since $V^2(\omega)$ is odd and $z(-\omega) = z^*(\omega)$. Furthermore, $\xi(\omega)$ is analytic on the real ω axis. This follows from the fact that the denominator on the RHS of Eq. (2.118) is non-zero on the real ω' axis [7].

The integral over ω' in Eq. (2.116) can be rewritten as

$$\begin{aligned}
J(\omega) &\stackrel{\text{def}}{=} \int_0^\infty d\omega' |h(\omega')|^2 \left[\frac{1}{\omega - \omega' + i\epsilon} - \frac{1}{\omega + \omega' - i\epsilon} \right] \\
&= \int_0^\infty d\omega' \frac{\tilde{\omega}_0}{\omega'} \xi(\omega') \frac{2\omega'}{\omega^2 - (\omega' - i\epsilon)^2} \\
&= \frac{\tilde{\omega}_0}{\omega} \int_0^\infty d\omega' \xi(\omega') \frac{2\omega}{\omega^2 - (\omega' - i\epsilon)^2} \\
&= \frac{\tilde{\omega}_0}{\omega} \int_0^\infty d\omega' \xi(\omega') \left[\frac{1}{\omega - \omega' + i\epsilon} + \frac{1}{\omega + \omega' - i\epsilon} \right]. \quad (2.119)
\end{aligned}$$

Using the fact that $\xi(\omega)$ is an even function of ω , the principal parts of the two terms inside the brackets in Eq. (2.119) can be combined,

$$\begin{aligned}
J(\omega) &= \frac{\tilde{\omega}_0}{\omega} \left\{ \text{P} \int_{-\infty}^\infty d\omega' \frac{\xi(\omega')}{\omega - \omega'} - i\pi \int_0^\infty d\omega' \xi(\omega') [\delta(\omega - \omega') - \delta(\omega + \omega')] \right\} \\
&= \frac{\tilde{\omega}_0}{\omega} \left[\text{P} \int_{-\infty}^\infty d\omega' \frac{\xi(\omega')}{\omega - \omega'} - i\pi \xi(\omega) \theta(\omega) + i\pi \xi(-\omega) \theta(-\omega) \right]. \quad (2.120)
\end{aligned}$$

Following Huttner et al. [7], we define the dielectric function of the dielectric as

$$\begin{aligned}\epsilon(\omega) &= 1 - \frac{e^2}{2\rho\epsilon_0\omega} \int_{-\infty}^{\infty} d\omega' \frac{\xi(\omega')}{\omega - \omega' + i\epsilon} \\ &= 1 - \frac{e^2}{2\rho\epsilon_0\omega} \left[\text{P} \int_{-\infty}^{\infty} d\omega' \frac{\xi(\omega')}{\omega - \omega'} - i\pi\xi(\omega) \right].\end{aligned}\quad (2.121)$$

This function satisfies the Kramers-Krönig relations, since the first form of the function given in Eq. (2.121) shows that $\epsilon(\omega)$ is analytic in the upper half of the complex plane. Comparing the quantities inside the brackets in Eqs. (2.120) and (2.121) and using the fact that $\xi(\omega)$ is an even function, we see that, when $\omega > 0$, the two quantities in brackets are identical, whereas when $\omega < 0$, they are complex conjugates of each other. Then, using the fact that $\epsilon(-\omega) = \epsilon^*(\omega)$, we conclude that

$$J(\omega) = -\frac{2\rho\epsilon_0\tilde{\omega}_0}{e^2} [\epsilon(|\omega|) - 1]. \quad (2.122)$$

Substituting Eq. (2.122) into Eq. (2.116), we obtain

$$\mathcal{G}_{ij}^{(00)\omega}(\mathbf{r}_1, \mathbf{r}_2) = -\frac{\epsilon_0[\epsilon(|\omega|) - 1]}{e^2} \delta_{ij} \delta(\mathbf{r}_1 - \mathbf{r}_2). \quad (2.123)$$

When the Coulomb interaction Eq. (2.23) is added, the matter Green function $\mathcal{G}_{ij}^{(0)}$ can be expressed in terms of quantities without the Coulomb interaction using the general result of the diagrammatic technique,

$$\mathcal{G}_{ij}^{(0)}(\mathbf{r}_1, \mathbf{r}_2; t_1 - t_2) = -\frac{i}{\hbar} \langle \text{T}[X_i^{(00)}(\mathbf{r}_1, t_1) S^U(\infty, -\infty) X_j^{(00)}(\mathbf{r}_2, t_2)] \rangle_{\text{conn}}^{(00)}, \quad (2.124)$$

where

$$S^U(\infty, -\infty) = 1 + \sum_{n=1}^{\infty} \frac{1}{n!} \left(\frac{-i}{\hbar} \right)^n \int_{-\infty}^{\infty} \dots \int_{-\infty}^{\infty} dt_1 \dots dt_n \text{T}[H_{\text{int}}^{(00)U}(t_1) \dots H_{\text{int}}^{(00)U}(t_n)]. \quad (2.125)$$

Substituting Eq. (2.125) into Eq. (2.124) and using Eq. (2.23), we obtain an infinite series

$$\begin{aligned}\mathcal{G}_{ij}^{(0)}(\mathbf{r}_1, \mathbf{r}_2; t_1 - t_2) &= \mathcal{G}_{ij}^{(00)}(\mathbf{r}_1, \mathbf{r}_2; t_1 - t_2) + \frac{1}{2} \left(\frac{-i}{\hbar} \right)^2 \int_{-\infty}^{\infty} dt_3 \int_{z' < 0} d^3 r' \int_{z'' < 0} d^3 r'' \\ &\quad \times F_{lm}(\mathbf{r}' - \mathbf{r}'') \langle \text{T}[X_i^{(00)}(\mathbf{r}_1, t_1) X_l^{(00)}(\mathbf{r}', t_3) X_m^{(00)}(\mathbf{r}'', t_3) X_j^{(00)}(\mathbf{r}_2, t_2)] \rangle_{\text{conn}}^{(00)} + \dots\end{aligned}\quad (2.126)$$

Expanding the time-ordered product in the second term on the RHS of Eq. (2.126) by means of Wick's Theorem, we find two equal pairings of the operators which together cancel the factor (1/2),

$$\begin{aligned} \mathcal{G}_{ij}^{(0)}(\mathbf{r}_1, \mathbf{r}_2; t_1 - t_2) &= \mathcal{G}_{ij}^{(00)}(\mathbf{r}_1, \mathbf{r}_2; t_1 - t_2) + \left(\frac{-i}{\hbar}\right)^2 \int_{-\infty}^{\infty} dt_3 \int_{z' < 0} d^3 r' \int_{z'' < 0} d^3 r'' \\ &\times \langle T[X_i^{(00)}(\mathbf{r}_1, t_1) X_l^{(00)}(\mathbf{r}', t_3)] \rangle^{(00)} F_{lm}(\mathbf{r}' - \mathbf{r}'') \langle T[X_m^{(00)}(\mathbf{r}'', t_3) X_j^{(00)}(\mathbf{r}_2, t_2)] \rangle^{(00)} + \dots \end{aligned} \quad (2.127)$$

Using Eq. (2.114), this may be rewritten as

$$\begin{aligned} \mathcal{G}_{ij}^{(0)}(\mathbf{r}_1, \mathbf{r}_2; t_1 - t_2) &= \mathcal{G}_{ij}^{(00)}(\mathbf{r}_1, \mathbf{r}_2; t_1 - t_2) + \int_{-\infty}^{\infty} dt_3 \int_{z' < 0} d^3 r' \int_{z'' < 0} d^3 r'' \\ &\times \mathcal{G}_{il}^{(00)}(\mathbf{r}_1, \mathbf{r}'; t_1 - t_3) F_{lm}(\mathbf{r}' - \mathbf{r}'') \mathcal{G}_{mj}^{(00)}(\mathbf{r}'', \mathbf{r}_2; t_3 - t_2) + \dots \end{aligned} \quad (2.128)$$

Taking the Fourier transform of Eq. (2.128) with respect to $(t_1 - t_2)$, we obtain

$$\begin{aligned} \mathcal{G}_{ij}^{(0)\omega}(\mathbf{r}_1, \mathbf{r}_2) &= \mathcal{G}_{ij}^{(00)\omega}(\mathbf{r}_1, \mathbf{r}_2) \\ &+ \int_{z' < 0} d^3 r' \int_{z'' < 0} d^3 r'' \mathcal{G}_{il}^{(00)\omega}(\mathbf{r}_1, \mathbf{r}') F_{lm}(\mathbf{r}' - \mathbf{r}'') \mathcal{G}_{mj}^{(00)\omega}(\mathbf{r}'', \mathbf{r}_2) + \dots \end{aligned} \quad (2.129)$$

The infinite series in Eq. (2.129) can be summed to give a closed-form integral equation for $\mathcal{G}_{ij}^{(0)\omega}$,

$$\begin{aligned} \mathcal{G}_{ij}^{(0)\omega}(\mathbf{r}_1, \mathbf{r}_2) &= \mathcal{G}_{ij}^{(00)\omega}(\mathbf{r}_1, \mathbf{r}_2) \\ &+ \int_{z' < 0} d^3 r' \int_{z'' < 0} d^3 r'' \mathcal{G}_{il}^{(00)\omega}(\mathbf{r}_1, \mathbf{r}') F_{lm}(\mathbf{r}' - \mathbf{r}'') \mathcal{G}_{mj}^{(0)\omega}(\mathbf{r}'', \mathbf{r}_2), \end{aligned} \quad (2.130)$$

as can be seen by repeatedly substituting $\mathcal{G}_{ij}^{(0)\omega}$ given by the RHS of Eq. (2.130) into the RHS of the same equation. Using Eq. (2.123), we obtain

$$\mathcal{G}_{ij}^{(0)\omega}(\mathbf{r}_1, \mathbf{r}_2) = -\frac{\epsilon_0[\epsilon(|\omega|) - 1]}{e^2} \left[\delta_{ij} \delta(\mathbf{r}_1 - \mathbf{r}_2) + \int_{z_3 < 0} d^3 r_3 F_{im}(\mathbf{r}_1 - \mathbf{r}_3) \mathcal{G}_{mj}^{(0)\omega}(\mathbf{r}_3, \mathbf{r}_2) \right]. \quad (2.131)$$

Eq. (2.131) is the Dyson equation for the matter Green function $\mathcal{G}_{ij}^{(0)\omega}$ for the system described by the Hamiltonian density of Eq. (2.103). This equation can be solved exactly for $\mathcal{G}_{ij}^{(0)\omega}$ using an extension of the Wiener-Hopf technique, as discussed

in Appendix C. The solution is

$$\begin{aligned} \mathcal{G}_{ij}^{(0)\omega}(\mathbf{r}_1, \mathbf{r}_2) &= -\frac{\epsilon_0[\epsilon_L(|\omega|) - 1]}{e^2} \delta_{ij} \delta(\mathbf{r}_1 - \mathbf{r}_2) + \frac{\epsilon_0[\epsilon_L(|\omega|) - 1]^2}{4\pi\epsilon_L(|\omega|)e^2} \\ &\times \left[\frac{\partial^2}{\partial x_{1i} \partial x_{2j}} \left(\frac{1}{|\mathbf{r}_1 - \mathbf{r}_2|} \right) + \frac{\epsilon_L(|\omega|) - 1}{\epsilon_L(|\omega|) + 1} \frac{\partial^2}{\partial x_{1i} \partial x_{2j}} \left(\frac{1}{|\mathbf{r}_1 - \bar{\mathbf{r}}_2|} \right) \right], \end{aligned} \quad (2.132)$$

where $\bar{\mathbf{r}}_2$ is the image of \mathbf{r}_2 in the plane $z = 0$ and

$$\epsilon_L(|\omega|) = 1 + \frac{\epsilon(|\omega|) - 1}{1 - \frac{1}{3}[\epsilon(|\omega|) - 1]} \quad (2.133)$$

is the dielectric function including local field effects. It is straightforward to check, using the integrals described in Appendix F, that $\mathcal{G}_{ij}^{(0)\omega}(\mathbf{r}_1, \mathbf{r}_2)$ given by Eq. (2.132) with $\epsilon_L(|\omega|)$ given by Eq. (2.133) does indeed satisfy the Dyson equation Eq. (2.131).

So far, we have obtained the Green functions for photons and matter, Eqs. (2.112) and (2.132), for the system described by the Hamiltonian density \mathcal{H}_0 of Eq. (2.103). Next, we calculate the Green functions for the complete Hamiltonian density \mathcal{H} given by Eq. (2.102). First, we consider the photon Green function Eq. (2.74) which, by the diagrammatic technique, can be written as

$$\mathcal{D}_{ij}(\mathbf{r}_1, \mathbf{r}_2; t_1 - t_2) = -\frac{i}{\hbar} \langle T[A_i^{(0)}(\mathbf{r}_1, t_1) S^A(\infty, -\infty) A_j^{(0)}(\mathbf{r}_2, t_2)] \rangle_{\text{conn}}^{(0)}, \quad (2.134)$$

where

$$S^A(\infty, -\infty) = 1 + \sum_{n=1}^{\infty} \frac{1}{n!} \left(\frac{-i}{\hbar} \right)^n \int_{-\infty}^{\infty} \dots \int_{-\infty}^{\infty} dt_1 \dots dt_n T[H_{\text{int}}^{(0)A}(t_1) \dots H_{\text{int}}^{(0)A}(t_n)]. \quad (2.135)$$

Here, $H_{\text{int}}^{(0)A}(t)$ is the Hamiltonian corresponding to the Hamiltonian density $\mathcal{H}_{\text{int}}^A(\mathbf{r}, t)$ of Eq. (2.21),

$$H_{\text{int}}^{(0)A}(t) = \int_{z < 0} d^3r \left[-\frac{e}{\rho} \mathbf{A}^{(0)}(\mathbf{r}, t) \cdot \mathbf{P}_X^{(0)}(\mathbf{r}, t) + \frac{e^2}{2\rho} \mathbf{A}^{(0)}(\mathbf{r}, t) \cdot \mathbf{A}^{(0)}(\mathbf{r}, t) \right]. \quad (2.136)$$

As we have mentioned, \mathcal{D}_{ij} cannot be approximated by the first few terms of its perturbation expansion. Instead, the entire infinite series in Eq. (2.135) must be substituted into Eq. (2.134). However, we shall see shortly that the resulting infinite

series of terms in \mathcal{D}_{ij} can be summed *exactly* to give a closed-form Dyson equation for the photon Green function.

The zeroth-order term in Eq. (2.135) gives just the free-space photon Green function $\mathcal{D}_{ij}^{(0)}$ of Eq. (2.104), whose Fourier transform is given by Eq. (2.112).

The $n = 1$ term in Eq. (2.135) gives a first-order correction to the free-space photon Green function. Since there must be an even number of \mathbf{A} operators in the time-ordered product to give a non-vanishing expectation value, we see that only the second term in Eq. (2.136) contributes in this order,

$$\begin{aligned} \mathcal{D}_{ij}^{(1)}(\mathbf{r}_1, \mathbf{r}_2; t_1 - t_2) &= \frac{e^2}{2\rho} \left(\frac{-i}{\hbar}\right)^2 \int_{-\infty}^{\infty} dt_3 \int_{z_3 < 0} d^3 r_3 \langle \mathbb{T}[A_i^{(0)}(\mathbf{r}_1, t_1) A_m^{(0)}(\mathbf{r}_3, t_3) \\ &\quad \times A_m^{(0)}(\mathbf{r}_3, t_3) A_j^{(0)}(\mathbf{r}_2, t_2)] \rangle_{\text{conn}}^{(0)}. \end{aligned} \quad (2.137)$$

Expanding the time-ordered product in Eq. (2.137) by Wick's Theorem, we find two equal pairings of the operators which cancel the factor (1/2),

$$\mathcal{D}_{ij}^{(1)}(\mathbf{r}_1, \mathbf{r}_2; t_1 - t_2) = \frac{e^2}{\rho} \int_{-\infty}^{\infty} dt_3 \int_{z_3 < 0} d^3 r_3 \mathcal{D}_{im}^{(0)}(\mathbf{r}_1, \mathbf{r}_3; t_1 - t_3) \mathcal{D}_{mj}^{(0)}(\mathbf{r}_3, \mathbf{r}_2; t_3 - t_2), \quad (2.138)$$

where we have used Eq. (2.104). Taking the Fourier transform with respect to $(t_1 - t_2)$, we obtain

$$\mathcal{D}_{ij}^{(1)\omega}(\mathbf{r}_1, \mathbf{r}_2) = \frac{e^2}{\rho} \int_{z_3 < 0} d^3 r_3 \mathcal{D}_{im}^{(0)\omega}(\mathbf{r}_1, \mathbf{r}_3) \mathcal{D}_{mj}^{(0)\omega}(\mathbf{r}_3, \mathbf{r}_2). \quad (2.139)$$

Next, we consider the contribution from the $n = 2$ term in Eq. (2.135),

$$\begin{aligned} \mathcal{D}_{ij}^{(2)}(\mathbf{r}_1, \mathbf{r}_2; t_1 - t_2) &= \frac{1}{2!} \left(\frac{-i}{\hbar}\right)^3 \int_{-\infty}^{\infty} dt_3 \int_{-\infty}^{\infty} dt_4 \langle \mathbb{T}[A_i^{(0)}(\mathbf{r}_1, t_1) H_{\text{int}}^{(0)\mathbf{A}}(t_3) H_{\text{int}}^{(0)\mathbf{A}}(t_4) \\ &\quad \times A_j^{(0)}(\mathbf{r}_2, t_2)] \rangle_{\text{conn}}^{(0)}. \end{aligned} \quad (2.140)$$

When Eq. (2.136) is substituted into Eq. (2.140) and the product of the two Hamiltonians expanded, there are a total of four terms: one due to the first term in Eq. (2.136) acting twice, one to the second term in Eq. (2.136) acting twice, and the two cross terms. The latter cross terms contribute nothing, since they each contain an odd number of \mathbf{A} operators.

Consider first the contribution due to the first term in Eq. (2.136) acting twice,

$$\begin{aligned} \mathcal{D}_{ij}^{(2)}(\mathbf{r}_1, \mathbf{r}_2; t_1 - t_2) &= \frac{1}{2!} \left(\frac{-i}{\hbar}\right)^3 \left(\frac{-e}{\rho}\right)^2 \int_{-\infty}^{\infty} dt_3 \int_{-\infty}^{\infty} dt_4 \int_{z_3 < 0} d^3 r_3 \int_{z_4 < 0} d^3 r_4 \\ &\times \langle T[A_i^{(0)}(\mathbf{r}_1, t_1) \mathbf{A}^{(0)}(\mathbf{r}_3, t_3) \cdot \mathbf{P}_X^{(0)}(\mathbf{r}_3, t_3) \mathbf{A}^{(0)}(\mathbf{r}_4, t_4) \cdot \mathbf{P}_X^{(0)}(\mathbf{r}_4, t_4) A_j^{(0)}(\mathbf{r}_2, t_2)] \rangle_{\text{conn}}^{(0)}. \end{aligned} \quad (2.141)$$

Expanding the time-ordered product in Eq. (2.141) using Wick's Theorem, we find two equal pairings of the operators which together cancel the factor $(1/2!)$. Using the definition Eq. (2.104), we obtain

$$\begin{aligned} \mathcal{D}_{ij}^{(2)}(\mathbf{r}_1, \mathbf{r}_2; t_1 - t_2) &= \left(\frac{-e}{\rho}\right)^2 \int_{-\infty}^{\infty} dt_3 \int_{-\infty}^{\infty} dt_4 \int_{z_3 < 0} d^3 r_3 \int_{z_4 < 0} d^3 r_4 \\ &\times \mathcal{D}_{il}^{(0)}(\mathbf{r}_1, \mathbf{r}_3; t_1 - t_3) \mathcal{Q}_{lm}^{(0)}(\mathbf{r}_3, \mathbf{r}_4; t_3 - t_4) \mathcal{D}_{mj}^{(0)}(\mathbf{r}_4, \mathbf{r}_2; t_4 - t_2), \end{aligned} \quad (2.142)$$

where

$$\mathcal{Q}_{ij}^{(0)}(\mathbf{r}_1, \mathbf{r}_2; t_1 - t_2) \stackrel{\text{def}}{=} -\frac{i}{\hbar} \langle T[P_{X,i}^{(0)}(\mathbf{r}_1, t_1) P_{X,j}^{(0)}(\mathbf{r}_2, t_2)] \rangle^{(0)}, \quad (2.143)$$

is the Green function for the operator \mathbf{P}_X in the subsystem described by \mathcal{H}_0 of Eq. (2.103). The Fourier transform of Eq. (2.142) with respect to $(t_1 - t_2)$ is

$$\mathcal{D}_{ij}^{(2)\omega}(\mathbf{r}_1, \mathbf{r}_2) = \left(\frac{-e}{\rho}\right)^2 \int_{z_3 < 0} d^3 r_3 \int_{z_4 < 0} d^3 r_4 \mathcal{D}_{il}^{(0)\omega}(\mathbf{r}_1, \mathbf{r}_3) \mathcal{Q}_{lm}^{(0)\omega}(\mathbf{r}_3, \mathbf{r}_4) \mathcal{D}_{mj}^{(0)\omega}(\mathbf{r}_4, \mathbf{r}_2), \quad (2.144)$$

where $\mathcal{Q}_{im}^{(0)\omega}$ is the Fourier transform of $\mathcal{Q}_{ij}^{(0)}$. To compute this quantity, we follow the same procedure as used in computing $\mathcal{G}_{ij}^{(0)}$, by partitioning \mathcal{H}_0 into a sum of \mathcal{H}_{00} and $\mathcal{H}_{\text{int}}^U$, where \mathcal{H}_{00} is given by Eq. (2.113). The Green function for \mathbf{P}_X in the system described by \mathcal{H}_{00} is given by an expression similar to Eq. (2.114) but with X replaced by P_X . Comparing Eqs. (2.50) and (2.51), we see that P_X is obtained from X by replacing $h(\omega)$ by $\rho\tilde{\omega}_0 g(\omega)$. Hence, following the steps leading from Eq. (2.114) to Eq. (2.116), we obtain for $\mathcal{Q}_{ij}^{(00)\omega}$ a result similar to Eq. (2.116) but with $h(\omega)$ replaced by $\rho\tilde{\omega}_0 g(\omega)$,

$$\mathcal{Q}_{ij}^{(00)\omega}(\mathbf{r}_1, \mathbf{r}_2) = -\frac{i\rho\tilde{\omega}_0}{2} \delta_{ij} \delta(\mathbf{r}_1 - \mathbf{r}_2) \int_0^{\infty} d\omega' |g(\omega')|^2 \left[\frac{i}{\omega - \omega' + i\epsilon} - \frac{i}{\omega + \omega' - i\epsilon} \right]. \quad (2.145)$$

Using Eqs. (2.53), (A.11) and (A.13), we obtain

$$|g(\omega')|^2 = \frac{\omega'}{\tilde{\omega}_0} \xi(\omega'), \quad (2.146)$$

where $\xi(\omega')$ is given by Eq. (2.118). The integral over ω' in Eq. (2.145) can be rewritten as

$$\begin{aligned} K(\omega) &\stackrel{\text{def}}{=} \int_0^\infty d\omega' |g(\omega')|^2 \left[\frac{1}{\omega - \omega' + i\epsilon} - \frac{1}{\omega + \omega' - i\epsilon} \right] \\ &= \int_0^\infty d\omega' \frac{\xi(\omega')}{\tilde{\omega}_0} \left[\frac{\omega}{\omega - \omega' + i\epsilon} - 1 + \frac{\omega}{\omega + \omega' - i\epsilon} - 1 \right] \\ &= -\frac{2}{\tilde{\omega}_0} \int_0^\infty d\omega' \xi(\omega') + \left(\frac{\omega}{\tilde{\omega}_0} \right)^2 J(\omega), \end{aligned} \quad (2.147)$$

where we have used Eq. (2.119). Now, it is shown in Appendix D that

$$\int_0^\infty d\omega' \xi(\omega') = 1. \quad (2.148)$$

Substituting Eq. (2.147) into Eq. (2.145) and using Eq. (2.122), we obtain

$$\mathcal{Q}_{ij}^{(00)\omega}(\mathbf{r}_1, \mathbf{r}_2) = -\rho \delta_{ij} \delta(\mathbf{r}_1 - \mathbf{r}_2) \left\{ 1 + \frac{\rho \epsilon_0 \omega^2}{e^2} [\epsilon(|\omega|) - 1] \right\}. \quad (2.149)$$

When the Coulomb interaction Eq. (2.23) is added, the Green function for \mathbf{P}_X is given by an infinite series similar to Eq. (2.124),

$$\mathcal{Q}_{ij}^{(0)}(\mathbf{r}_1, \mathbf{r}_2; t_1 - t_2) = -\frac{i}{\hbar} \langle \mathbb{T} [P_{X,i}^{(00)}(\mathbf{r}_1, t_1) S^U(\infty, -\infty) P_{X,j}^{(00)}(\mathbf{r}_2, t_2)] \rangle_{\text{conn}}^{(00)}, \quad (2.150)$$

where $S^U(\infty, -\infty)$ is given by Eq. (2.125). When the latter equation is substituted into Eq. (2.150), we obtain an infinite series similar to Eq. (2.127),

$$\begin{aligned} \mathcal{Q}_{ij}^{(0)}(\mathbf{r}_1, \mathbf{r}_2; t_1 - t_2) &= \mathcal{Q}_{ij}^{(00)}(\mathbf{r}_1, \mathbf{r}_2; t_1 - t_2) + \left(\frac{-i}{\hbar} \right)^2 \int_{-\infty}^\infty dt_3 \int_{z' < 0} d^3 r' \int_{z'' < 0} d^3 r'' \\ &\quad \times \langle \mathbb{T} [P_{X,i}^{(00)}(\mathbf{r}_1, t_1) X_l^{(00)}(\mathbf{r}', t_3)] \rangle^{(00)} F_{lm}(\mathbf{r}' - \mathbf{r}'') \langle \mathbb{T} [X_m^{(00)}(\mathbf{r}'', t_3) P_{X,j}^{(00)}(\mathbf{r}_2, t_2)] \rangle^{(00)} \\ &\quad + \dots \end{aligned} \quad (2.151)$$

We now have to compute the quantities $\langle \mathbb{T} [P_{X,i}^{(00)} X_j^{(00)}] \rangle^{(00)}$ and $\langle \mathbb{T} [X_i^{(00)} P_{X,j}^{(00)}] \rangle^{(00)}$.

Using Eqs. (2.50) and (2.51), we obtain

$$\begin{aligned} -\frac{i}{\hbar} \langle \mathbb{T} [P_{X,i}^{(00)}(\mathbf{r}_1, t_1) X_j^{(00)}(\mathbf{r}_2, t_2)] \rangle^{(00)} &= -\frac{i}{2} \int_0^\infty d\omega \int_0^\infty d\omega' \\ &\quad \times \langle \mathbb{T} \{ [g(\omega) B_{\omega,i}^\dagger(\mathbf{r}_1) e^{i\omega t_1} + \text{h.c.}] [h(\omega') B_{\omega',j}^\dagger(\mathbf{r}_2) e^{i\omega' t_2} + \text{h.c.}] \} \rangle^{(00)} \\ &= -\frac{i}{2} \delta_{ij} \delta(\mathbf{r}_1 - \mathbf{r}_2) \int_0^\infty d\omega' \begin{cases} g^*(\omega') h(\omega') e^{-i\omega'(t_1 - t_2)}, & t_1 > t_2, \\ g(\omega') h^*(\omega') e^{i\omega'(t_1 - t_2)}, & t_1 < t_2. \end{cases} \end{aligned} \quad (2.152)$$

Taking the Fourier transform with respect to $(t_1 - t_2)$, we obtain

$$-\frac{i}{\hbar} \langle \mathbb{T}[P_{X,i}^{(00)}(\mathbf{r}_1, t_1) X_j^{(00)}(\mathbf{r}_2, t_2)] \rangle^{(00)} \Big|^\omega = \frac{1}{2} \delta_{ij} \delta(\mathbf{r}_1 - \mathbf{r}_2) \int_0^\infty d\omega' \\ \times \left[\frac{g^*(\omega') h(\omega')}{\omega - \omega' + i\epsilon} - \frac{g(\omega') h^*(\omega')}{\omega + \omega' - i\epsilon} \right]. \quad (2.153)$$

Using Eqs. (2.52) and (2.53), we calculate

$$g^*(\omega') h(\omega') = -i[\alpha_0^*(\omega') + \beta_0^*(\omega')][\alpha_0(\omega') - \beta_0(\omega')] \\ = -i \left\{ |\alpha_0(\omega')|^2 - |\beta_0(\omega')|^2 + 2i \operatorname{Im} [\alpha_0(\omega') \beta_0^*(\omega')] \right\}. \quad (2.154)$$

From Eqs. (A.11) and (A.13), we see that $[\alpha_0(\omega') \beta_0^*(\omega')]$ is purely real. Hence,

$$g^*(\omega') h(\omega') = -i [|\alpha_0(\omega')|^2 - |\beta_0(\omega')|^2] \\ = -i \xi(\omega'), \quad (2.155)$$

where we have used Eq. (2.118). Substituting Eq. (2.155) into Eq. (2.153), we obtain

$$-\frac{i}{\hbar} \langle \mathbb{T}[P_{X,i}^{(00)}(\mathbf{r}_1, t_1) X_j^{(00)}(\mathbf{r}_2, t_2)] \rangle^{(00)} \Big|^\omega = -\frac{i}{2} \delta_{ij} \delta(\mathbf{r}_1 - \mathbf{r}_2) \int_0^\infty d\omega' \xi(\omega') \\ \times \left[\frac{1}{\omega - \omega' + i\epsilon} + \frac{1}{\omega + \omega' - i\epsilon} \right] \\ = \frac{i\rho\epsilon_0\omega[\epsilon(|\omega|) - 1]}{e^2} \delta_{ij} \delta(\mathbf{r}_1 - \mathbf{r}_2) \\ = -i\rho\omega \mathcal{G}_{ij}^{(00)\omega}(\mathbf{r}_1, \mathbf{r}_2), \quad (2.156)$$

where we have used Eqs. (2.119), (2.122) and (2.123).

For $\langle \mathbb{T}[X_i^{(00)} P_{X,j}^{(00)}] \rangle^{(00)}$, we obtain an expression similar to Eq. (2.153) but with $g(\omega')$ and $h(\omega')$ interchanged. According to Eq. (2.155), this amounts to an extra minus sign. Hence,

$$-\frac{i}{\hbar} \langle \mathbb{T}[X_i^{(00)}(\mathbf{r}_1, t_1) P_{X,j}^{(00)}(\mathbf{r}_2, t_2)] \rangle^{(00)} \Big|^\omega = i\rho\omega \mathcal{G}_{ij}^{(00)\omega}(\mathbf{r}_1, \mathbf{r}_2). \quad (2.157)$$

We now take the Fourier transform of Eq. (2.151) with respect to $(t_1 - t_2)$ and then use Eqs. (2.156) and (2.157),

$$\begin{aligned}
\mathcal{Q}_{ij}^{(0)\omega}(\mathbf{r}_1, \mathbf{r}_2) &= \mathcal{Q}_{ij}^{(00)\omega}(\mathbf{r}_1, \mathbf{r}_2) + \left(\frac{-i}{\hbar}\right)^2 \int_{z' < 0} d^3 r' \int_{z'' < 0} d^3 r'' F_{lm}(\mathbf{r}' - \mathbf{r}'') \\
&\quad \times \langle \mathcal{T}[P_{X,i}^{(00)}(\mathbf{r}_1, t_1) X_l^{(00)}(\mathbf{r}', t_3)] \rangle^{(00)\omega} \langle \mathcal{T}[X_m^{(00)}(\mathbf{r}'', t_3) P_{X,j}^{(00)}(\mathbf{r}_2, t_2)] \rangle^{(00)\omega} + \dots \\
&= \mathcal{Q}_{ij}^{(00)\omega}(\mathbf{r}_1, \mathbf{r}_2) \\
&\quad + \rho^2 \omega^2 \int_{z' < 0} d^3 r' \int_{z'' < 0} d^3 r'' \mathcal{G}_{il}^{(00)\omega}(\mathbf{r}_1, \mathbf{r}') F_{lm}(\mathbf{r}' - \mathbf{r}'') \mathcal{G}_{mj}^{(00)\omega}(\mathbf{r}'', \mathbf{r}_2) + \dots \quad (2.158)
\end{aligned}$$

Comparing Eqs. (2.129) and (2.158), we see that the infinite series in the two equations, represented by the second and higher-order terms on the RHS of each of the two equations, are identical except for a factor $\rho^2 \omega^2$. This holds because each term of the series in Eq. (2.158) differs from the corresponding term of the series in Eq. (2.129) only in replacing, in the latter series, a factor $\mathcal{G}_{il}^{(00)\omega}$ by $(-i/\hbar) \langle \mathcal{T}[P_{X,i}^{(00)} X_l^{(00)}] \rangle^{(00)\omega}$ and a factor $\mathcal{G}_{mj}^{(00)\omega}$ by $(-i/\hbar) \langle \mathcal{T}[P_{X,m}^{(00)} X_j^{(00)}] \rangle^{(00)\omega}$. According to Eqs. (2.156) and (2.157), this amounts to multiplication by a factor $(-i\rho\omega)(i\rho\omega) = \rho^2 \omega^2$. Hence, we conclude

$$\mathcal{Q}_{ij}^{(0)\omega}(\mathbf{r}_1, \mathbf{r}_2) - \mathcal{Q}_{ij}^{(00)\omega}(\mathbf{r}_1, \mathbf{r}_2) = \rho^2 \omega^2 [\mathcal{G}_{ij}^{(0)\omega}(\mathbf{r}_1, \mathbf{r}_2) - \mathcal{G}_{ij}^{(00)\omega}(\mathbf{r}_1, \mathbf{r}_2)]. \quad (2.159)$$

Substituting Eqs. (2.123) and (2.149) into Eq. (2.159), we obtain

$$\mathcal{Q}_{ij}^{(0)\omega}(\mathbf{r}_1, \mathbf{r}_2) = -\rho \delta_{ij} \delta(\mathbf{r}_1 - \mathbf{r}_2) + \rho^2 \omega^2 \mathcal{G}_{ij}^{(0)\omega}(\mathbf{r}_1, \mathbf{r}_2), \quad (2.160)$$

where $\mathcal{G}_{ij}^{(0)\omega}$ is given by Eq. (2.132). Eq. (2.160) is used in Eq. (2.144) to give $\mathcal{D}_{ij}^{(2)\omega}$.

We still have to consider the contribution from the second term in Eq. (2.136) acting twice, as well as the contributions of the higher order terms in Eq. (2.135). These contributions can be taken into account by using diagrammatic analysis.

The perturbation series Eq. (2.134) can be represented by an infinite series of diagrams as shown in Fig. 2.1. Here, the complete photon Green function is represented by a heavy dashed line and the free-space photon Green function by a thin dashed line. The contribution Eq. (2.139) due to the second term in Eq. (2.136) acting once is represented by the second diagram on the RHS of Fig. 2.1a, the contribution Eq. (2.144) due to the first term in Eq. (2.136) acting twice by the third diagram, the

contribution due to the second term in Eq. (2.136) acting twice by the fourth diagram, etc. It can be seen that any one of the higher-order diagrams in Fig. 2.1a is constructed from just two types of building blocks, known as self-energy parts, represented by a cross and a vertical dumbbell, which correspond to the second term in Eq. (2.136) acting once and the first term in Eq. (2.136) acting twice, respectively. We can separate the higher-order diagrams into two groups: those containing a self-energy part of the first type at the bottom and those containing a self-energy part of the second type at the bottom, as shown in Fig. 2.1b. The infinite series connected to either one of these factors consists of all possible diagrams constructed from an arbitrary number of self-energy parts of either type strung together in any order by free-space photon Green functions. Such a series is just the complete photon Green function. Hence we obtain the equivalent representation shown in Fig. 2.1c. This means that the higher-order diagrams are all included in just two diagrams obtained from the second and third diagrams on the RHS of Fig. 2.1a by replacing the thin dotted lines at the top of the latter diagrams by heavy dotted lines. Mathematically, the complete photon Green function is given by the sum of the free-space photon Green function and the two terms derived from Eqs. (2.139) and (2.144) by replacing the factor $\mathcal{D}_{mj}^{(0)\omega}$ in these equations by \mathcal{D}_{mj}^ω ,

$$\begin{aligned} \mathcal{D}_{ij}^\omega(\mathbf{r}_1, \mathbf{r}_2) &= \mathcal{D}_{ij}^{(0)\omega}(\mathbf{r}_1 - \mathbf{r}_2) + \frac{e^2}{\rho} \int_{z_3 < 0} d^3 r_3 \mathcal{D}_{im}^{(0)\omega}(\mathbf{r}_1 - \mathbf{r}_3) \mathcal{D}_{mj}^\omega(\mathbf{r}_3, \mathbf{r}_2) \\ &+ \left(\frac{-e}{\rho}\right)^2 \int_{z_3 < 0} d^3 r_3 \int_{z_4 < 0} d^3 r_4 \mathcal{D}_{il}^{(0)\omega}(\mathbf{r}_1 - \mathbf{r}_3) \mathcal{Q}_{lm}^{(0)\omega}(\mathbf{r}_3, \mathbf{r}_4) \mathcal{D}_{mj}^\omega(\mathbf{r}_4, \mathbf{r}_2). \end{aligned} \quad (2.161)$$

Substituting Eq. (2.160) into Eq. (2.161), we obtain

$$\begin{aligned} \mathcal{D}_{ij}^\omega(\mathbf{r}_1, \mathbf{r}_2) &= \mathcal{D}_{ij}^{(0)\omega}(\mathbf{r}_1 - \mathbf{r}_2) \\ &+ e^2 \omega^2 \int_{z_3 < 0} d^3 r_3 \int_{z_4 < 0} d^3 r_4 \mathcal{D}_{il}^{(0)\omega}(\mathbf{r}_1 - \mathbf{r}_3) \mathcal{G}_{lm}^{(0)\omega}(\mathbf{r}_3, \mathbf{r}_4) \mathcal{D}_{mj}^\omega(\mathbf{r}_4, \mathbf{r}_2). \end{aligned} \quad (2.162)$$

We may now substitute Eq. (2.132) into Eq. (2.162). For the second term in Eq. (2.132), we perform integration by parts twice and make use of the transversality of the photon Green function,

$$\frac{\partial}{\partial x_i} \mathcal{D}_{ij}^\omega(\mathbf{r}, \mathbf{r}') = \frac{\partial}{\partial x'_j} \mathcal{D}_{ij}^\omega(\mathbf{r}, \mathbf{r}') = 0. \quad (2.163)$$

The result is

$$\begin{aligned} \mathcal{D}_{ij}^\omega(\mathbf{r}_1, \mathbf{r}_2) &= \mathcal{D}_{ij}^{(0)\omega}(\mathbf{r}_1 - \mathbf{r}_2) - \omega^2 \epsilon_0 [\epsilon_L(|\omega|) - 1] \int_{z_3 < 0} d^3 r_3 \mathcal{D}_{im}^{(0)\omega}(\mathbf{r}_1 - \mathbf{r}_3) \mathcal{D}_{mj}^\omega(\mathbf{r}_3, \mathbf{r}_2) \\ &+ \frac{\omega^2 \epsilon_0 [\epsilon_L(|\omega|) - 1]^2}{2\pi [\epsilon_L(|\omega|) + 1]} \iint d^2 s_3 d^2 s_4 \mathcal{D}_{iz}^{(0)\omega}(\mathbf{r}_1 - \mathbf{s}_3) \frac{1}{|\mathbf{s}_3 - \mathbf{s}_4|} \mathcal{D}_{zj}^\omega(\mathbf{s}_4, \mathbf{r}_2), \end{aligned} \quad (2.164)$$

where \mathbf{s}_3 and \mathbf{s}_4 are integration points on the plane $z = 0$.

Eq. (2.164) is the *exact* Dyson equation for the transverse photon Green function for the complete Hamiltonian density \mathcal{H} of Eq. (2.16). This equation can be solved exactly for \mathcal{D}_{ij}^ω using an extension of the Wiener-Hopf technique, as discussed in Appendix E.

Before continuing to calculate the other functions \mathcal{G}_{ij}^ω and \mathcal{C}_{ij}^ω needed in Eq. (2.101), it is instructive to consider the photon Green function for an *infinite* dielectric medium. In that case, the Dyson equation Eq. (2.164) is modified to read

$$\mathcal{D}_{ij}^\omega(\mathbf{r}_1, \mathbf{r}_2) = \mathcal{D}_{ij}^{(0)\omega}(\mathbf{r}_1 - \mathbf{r}_2) - \omega^2 \epsilon_0 [\epsilon_L(|\omega|) - 1] \int_{\infty} d^3 r_3 \mathcal{D}_{im}^{(0)\omega}(\mathbf{r}_1 - \mathbf{r}_3) \mathcal{D}_{mj}^\omega(\mathbf{r}_3, \mathbf{r}_2), \quad (2.165)$$

where the integral over \mathbf{r}_3 extends over all of space and the surface term in Eq. (2.164) is absent. Eq. (2.165) is easily solved by taking the Fourier transform with respect to $(\mathbf{r}_1 - \mathbf{r}_2)$,

$$\mathcal{D}_{ij}^\omega(\mathbf{k}) = \left(\frac{1}{\epsilon_0} \right) \frac{\left(\delta_{ij} - \frac{k_i k_j}{k^2} \right)}{\omega^2 - k^2 c^2 + i\epsilon} - \omega^2 [\epsilon_L(|\omega|) - 1] \frac{\left(\delta_{im} - \frac{k_i k_m}{k^2} \right)}{\omega^2 - k^2 c^2 + i\epsilon} \mathcal{D}_{mj}^\omega(\mathbf{k}). \quad (2.166)$$

To solve Eq. (2.166), we assume a solution of the form

$$\mathcal{D}_{ij}^\omega(\mathbf{k}) = A \delta_{ij} + B \frac{k_i k_j}{k^2}. \quad (2.167)$$

Substituting Eq. (2.167) into Eq. (2.166) and using the fact that $\left(\delta_{im} - \frac{k_i k_m}{k^2} \right) k_m = 0$, we obtain

$$A \delta_{ij} + B \frac{k_i k_j}{k^2} = \left(\frac{1}{\epsilon_0} \right) \frac{\left(\delta_{ij} - \frac{k_i k_j}{k^2} \right)}{\omega^2 - k^2 c^2 + i\epsilon} \{1 - A \epsilon_0 \omega^2 [\epsilon_L(|\omega|) - 1]\}. \quad (2.168)$$

Equating the coefficients of δ_{ij} and $\frac{k_i k_j}{k^2}$ on both sides of Eq. (2.168), we obtain

$$A = \left(\frac{1}{\epsilon_0} \right) \frac{1}{\omega^2 + \omega^2 [\epsilon_L(|\omega|) - 1] - k^2 c^2 + i\epsilon} \quad (2.169)$$

$$B = -A. \quad (2.170)$$

Hence, for an infinite dielectric medium,

$$\mathcal{D}_{ij}^\omega(\mathbf{k}) = \left(\frac{1}{\epsilon_0}\right) \frac{\left(\delta_{ij} - \frac{k_i k_j}{k^2}\right)}{\omega^2 \epsilon_L(|\omega|) - k^2 c^2 + i\epsilon}. \quad (2.171)$$

The dispersion relationship for the photons is given by the singularity of the photon Green function,

$$k^2 = \frac{\omega^2}{c^2} \epsilon_L(|\omega|), \quad (2.172)$$

which shows that $\epsilon_L(\cdot)$ is indeed the dielectric function of the medium.

Next, we calculate the matter Green function \mathcal{G}_{ij}^ω for the complete Hamiltonian density \mathcal{H} . This is given according to the diagrammatic technique by

$$\mathcal{G}_{ij}(\mathbf{r}_1, \mathbf{r}_2; t_1 - t_2) = -\frac{i}{\hbar} \langle \text{T}[X_i^{(0)}(\mathbf{r}_1, t_1) S^A(\infty, -\infty) X_j^{(0)}(\mathbf{r}_2, t_2)] \rangle_{\text{conn}}^{(0)}, \quad (2.173)$$

where $S^A(\infty, -\infty)$ is given by Eq. (2.135). The zeroth-order term in Eq. (2.173) is $\mathcal{G}_{ij}^{(0)}$ whose Fourier transform is given by Eq. (2.132). The $n = 1$ term is

$$\mathcal{G}_{ij}^{(1)}(\mathbf{r}_1, \mathbf{r}_2; t_1 - t_2) = \left(-\frac{i}{\hbar}\right)^2 \int_{-\infty}^{\infty} dt_3 \langle \text{T}[X_i^{(0)}(\mathbf{r}_1, t_1) H_{\text{int}}^{(0)A}(t_3) X_j^{(0)}(\mathbf{r}_2, t_2)] \rangle_{\text{conn}}^{(0)}. \quad (2.174)$$

The first term in Eq. (2.136) does not contribute, since it has an odd number of \mathbf{A} operator. Substituting the second term in Eq. (2.136) into Eq. (2.174), we obtain

$$\begin{aligned} \mathcal{G}_{ij}^{(1)}(\mathbf{r}_1, \mathbf{r}_2; t_1 - t_2) &= \left(-\frac{i}{\hbar}\right)^2 \left(\frac{e^2}{2\rho}\right) \int_{-\infty}^{\infty} dt_3 \int_{z_3 < 0} d^3 r_3 \\ &\times \langle \text{T}[X_i^{(0)}(\mathbf{r}_1, t_1) \mathbf{A}^{(0)}(\mathbf{r}_3, t_3) \cdot \mathbf{A}^{(0)}(\mathbf{r}_3, t_3) X_j^{(0)}(\mathbf{r}_2, t_2)] \rangle_{\text{conn}}^{(0)}. \end{aligned} \quad (2.175)$$

When the time-ordered product in Eq. (2.175) is expanded using Wick's Theorem, the two \mathbf{A} operators must be paired together and so must the two X operators, since, in the subsystem described by the Hamiltonian density \mathcal{H}_0 of Eq. (2.103), there is no coupling between the transverse radiation field \mathbf{A} and \mathbf{X} . But this results in a *disconnected* diagram, which we do not count. Hence,

$$\mathcal{G}_{ij}^{(1)}(\mathbf{r}_1, \mathbf{r}_2; t_1 - t_2) = 0. \quad (2.176)$$

Next, consider the contribution from the n th term in Eq. (2.173), where $n \geq 2$,

$$\mathcal{G}_{ij}^{(n)}(\mathbf{r}_1, \mathbf{r}_2; t_1 - t_2) = \frac{1}{n!} \left(-\frac{i}{\hbar}\right)^{n+1} \int_{-\infty}^{\infty} \dots \int_{-\infty}^{\infty} dt'_1 \dots dt'_n \langle \mathbb{T}[X_i^{(0)}(\mathbf{r}_1, t_1) \times H_{\text{int}}^{(0)\text{A}}(t'_1) \dots H_{\text{int}}^{(0)\text{A}}(t'_n) X_j^{(0)}(\mathbf{r}_2, t_2)] \rangle_{\text{conn}}^{(0)}. \quad (2.177)$$

The $X_i^{(0)}$ or $X_j^{(0)}$ operator in Eq. (2.177) cannot be paired with an $\text{A}^{(0)}$ operator in the expansion of the time-ordered product using Wick's Theorem. Hence, $X_i^{(0)}$ must be paired with a $\text{P}_X^{(0)}$ operator from one of the Hamiltonian factors $H_{\text{int}}^{(0)\text{A}}$, and $X_j^{(0)}$ must be paired with a $\text{P}_X^{(0)}$ operator from another Hamiltonian factor. There are altogether $n(n-1)$ distinct, ordered *pairs* of these Hamiltonian factors, all of which contribute equally. Hence, we need only consider one particular pair of Hamiltonian factors, namely, $H_{\text{int}}^{(0)\text{A}}(t'_{n-1})$, and $H_{\text{int}}^{(0)\text{A}}(t'_n)$ and multiply the result by $n(n-1)$. Using Eq. (2.136) we obtain

$$\begin{aligned} \mathcal{G}_{ij}^{(n)}(\mathbf{r}_1, \mathbf{r}_2; t_1 - t_2) &= \frac{n(n-1)}{n!} \left(-\frac{i}{\hbar}\right)^{n+1} \left(\frac{-e}{\rho}\right)^2 \int_{-\infty}^{\infty} \dots \int_{-\infty}^{\infty} dt'_1 \dots dt'_n \\ &\times \int_{z_{n-1} < 0} d^3 r_{n-1} \int_{z_n < 0} d^3 r_n \langle \mathbb{T}[X_i^{(0)}(\mathbf{r}_1, t_1) P_{X,i}^{(0)}(\mathbf{r}_{n-1}, t'_{n-1})] \rangle^{(0)} \langle \mathbb{T}[A_i^{(0)}(\mathbf{r}_{n-1}, t'_{n-1}) \\ &\times H_{\text{int}}^{(0)\text{A}}(t'_1) \dots H_{\text{int}}^{(0)\text{A}}(t'_{n-2}) A_m^{(0)}(\mathbf{r}_n, t'_n)] \rangle_{\text{conn}}^{(0)} \langle \mathbb{T}[P_{X,m}^{(0)}(\mathbf{r}_n, t'_n) X_j^{(0)}(\mathbf{r}_2, t_2)] \rangle^{(0)} \\ &= \left(-\frac{i}{\hbar}\right)^2 \left(\frac{-e}{\rho}\right)^2 \int_{-\infty}^{\infty} dt'_{n-1} \int_{-\infty}^{\infty} dt'_n \int_{z_{n-1} < 0} d^3 r_{n-1} \int_{z_n < 0} d^3 r_n \\ &\times \langle \mathbb{T}[X_i^{(0)}(\mathbf{r}_1, t_1) P_{X,i}^{(0)}(\mathbf{r}_{n-1}, t'_{n-1})] \rangle^{(0)} \mathcal{D}_{lm}^{(n-2)}(\mathbf{r}_{n-1}, \mathbf{r}_n; t'_{n-1} - t'_n) \\ &\times \langle \mathbb{T}[P_{X,m}^{(0)}(\mathbf{r}_n, t'_n) X_j^{(0)}(\mathbf{r}_2, t_2)] \rangle^{(0)}, \end{aligned} \quad (2.178)$$

where $\mathcal{D}_{ij}^{(n-2)}$ is the $(n-2)$ th term of the perturbation series given by Eq. (2.134).

When Eq. (2.178) is summed from $n = 2$ to ∞ , the summation of the $\mathcal{D}_{ij}^{(n-2)}$ factor simply gives the complete photon Green function \mathcal{D}_{ij} . Hence, summing $\mathcal{G}_{ij}^{(n)}$ from $n = 0$ to ∞ , taking into account Eq. (2.176) and going over to frequency space, we obtain

$$\begin{aligned} \mathcal{G}_{ij}^{\omega}(\mathbf{r}_1, \mathbf{r}_2) &= \mathcal{G}_{ij}^{(0)\omega}(\mathbf{r}_1, \mathbf{r}_2) + \left(-\frac{i}{\hbar}\right)^2 \left(\frac{-e}{\rho}\right)^2 \int_{z_3 < 0} d^3 r_3 \int_{z_4 < 0} d^3 r_4 \\ &\times \langle \mathbb{T}[X_i^{(0)}(\mathbf{r}_1, t_1) P_{X,i}^{(0)}(\mathbf{r}_3, t_3)] \rangle^{(0)} \Big| \mathcal{D}_{lm}^{\omega}(\mathbf{r}_3, \mathbf{r}_4) \\ &\times \langle \mathbb{T}[P_{X,m}^{(0)}(\mathbf{r}_4, t_4) X_j^{(0)}(\mathbf{r}_2, t_2)] \rangle^{(0)} \Big|^{\omega}. \end{aligned} \quad (2.179)$$

We now have to compute the quantities $\langle T[P_{X,i}^{(0)}X_j^{(0)}] \rangle^{(0)}$ and $\langle T[X_i^{(0)}P_{X,j}^{(0)}] \rangle^{(0)}$. These are obtained in terms of the quantities $\langle T[P_{X,i}^{(00)}X_j^{(00)}] \rangle^{(00)}$ and $\langle T[X_i^{(00)}P_{X,j}^{(00)}] \rangle^{(00)}$ by the diagrammatic technique with the Coulomb interaction $H_{\text{int}}^{(00)U}$ as perturbation,

$$-\frac{i}{\hbar} \langle T[P_{X,i}^{(0)}(\mathbf{r}_1, t_1)X_j^{(0)}(\mathbf{r}_2, t_2)] \rangle^{(0)} = -\frac{i}{\hbar} \langle T[P_{X,i}^{(00)}(\mathbf{r}_1, t_1)S^U(\infty, -\infty) \times X_j^{(00)}(\mathbf{r}_2, t_2)] \rangle_{\text{conn}}^{(00)}, \quad (2.180)$$

where $S^U(\infty, -\infty)$ is given by Eq. (2.125). Comparing the two infinite series Eqs. (2.124) and (2.180), we see that each term of the latter series differs from the corresponding term of the former series only in replacing, in the former series, a factor $(-i/\hbar) \langle T[X_i^{(00)}X_l^{(00)}] \rangle^{(00)}$ by $(-i/\hbar) \langle T[P_{X,i}^{(00)}X_l^{(00)}] \rangle^{(00)}$. Thus, after taking the Fourier transform of the series Eq. (2.180) with respect to $(t_1 - t_2)$, we obtain a series that differs only from that in Eq. (2.129) by replacing, in each term of the latter series, a factor $\mathcal{G}_{il}^{(00)\omega}$ by $(-i/\hbar) \langle T[P_{X,i}^{(00)}X_l^{(00)}] \rangle^{(00)}|^\omega$. By Eq. (2.156), this amounts to multiplying each term of the series in Eq. (2.129) by $-i\rho\omega$. Thus, we conclude

$$-\frac{i}{\hbar} \langle T[P_{X,i}^{(0)}(\mathbf{r}_1, t_1)X_j^{(0)}(\mathbf{r}_2, t_2)] \rangle^{(0)}|^\omega = -i\rho\omega \mathcal{G}_{ij}^{(0)\omega}(\mathbf{r}_1, \mathbf{r}_2). \quad (2.181)$$

Similarly, using Eq. (2.157),

$$-\frac{i}{\hbar} \langle T[X_i^{(0)}(\mathbf{r}_1, t_1)P_{X,j}^{(0)}(\mathbf{r}_2, t_2)] \rangle^{(0)}|^\omega = i\rho\omega \mathcal{G}_{ij}^{(0)\omega}(\mathbf{r}_1, \mathbf{r}_2). \quad (2.182)$$

Substituting Eqs. (2.181) and (2.182) into Eq. (2.179), we obtain

$$\mathcal{G}_{ij}^\omega(\mathbf{r}_1, \mathbf{r}_2) = \mathcal{G}_{ij}^{(0)\omega}(\mathbf{r}_1, \mathbf{r}_2) + e^2\omega^2 \int_{z_3 < 0} d^3r_3 \int_{z_4 < 0} d^3r_4 \times \mathcal{G}_{il}^{(0)\omega}(\mathbf{r}_1, \mathbf{r}_3) \mathcal{D}_{lm}^\omega(\mathbf{r}_3, \mathbf{r}_4) \mathcal{G}_{mj}^{(0)\omega}(\mathbf{r}_3, \mathbf{r}_2). \quad (2.183)$$

Eq. (2.183) is an explicit expression for the complete matter Green function \mathcal{G}_{ij}^ω , since $\mathcal{G}_{ij}^{(0)\omega}$ is known from Eq. (2.132) and the complete photon Green function \mathcal{D}_{ij}^ω is known from Appendix E.

Lastly, we calculate the function \mathcal{C}_{ij} given by Eq. (2.100). We consider each of the two terms in the latter equation separately. By the diagrammatic technique, we have

$$\frac{1}{\hbar} \langle T[X_i(\mathbf{r}_1, \tau)A_j(\mathbf{r}_2, 0)] \rangle = \frac{1}{\hbar} \langle T[X_i^{(0)}(\mathbf{r}_1, \tau)S^A(\infty, -\infty)A_j(\mathbf{r}_2, 0)] \rangle^{(0)}, \quad (2.184)$$

where $S^A(\infty, -\infty)$ is given by Eq. (2.135). The zeroth-order term of the series Eq. (2.184) vanishes, since in the subsystem described by \mathcal{H}_0 of Eq. (2.103) there is no coupling between \mathbf{A} and \mathbf{X} . Hence, consider the n th term in Eq. (2.184), where $n \geq 1$,

$$\frac{1}{\hbar} \langle \mathcal{T}[X_i(\mathbf{r}_1, \tau) A_j(\mathbf{r}_2, 0)] \rangle^{(n)} = \frac{1}{\hbar n!} \left(-\frac{i}{\hbar} \right)^n \int_{-\infty}^{\infty} \dots \int_{-\infty}^{\infty} dt'_1 \dots dt'_n \langle \mathcal{T}[X_i^{(0)}(\mathbf{r}_1, \tau) \times H_{\text{int}}^{(0)A}(t'_1) \dots H_{\text{int}}^{(0)A}(t'_n) A_j^{(0)}(\mathbf{r}_2, 0)] \rangle_{\text{conn}}^{(0)}. \quad (2.185)$$

Following the steps leading from Eq. (2.177) to (2.178), we see that $X_i^{(0)}$ must be paired with a $P_X^{(0)}$ operator from one of the n Hamiltonian factors. Choosing $H_{\text{int}}^{(0)A}(t'_n)$ to pair with $X_i^{(0)}$ and multiplying the result by n , we obtain

$$\begin{aligned} \frac{1}{\hbar} \langle \mathcal{T}[X_i(\mathbf{r}_1, \tau) A_j(\mathbf{r}_2, 0)] \rangle^{(n)} &= - \left(\frac{e}{\hbar \rho} \right) \frac{n}{n!} \left(-\frac{i}{\hbar} \right)^n \int_{z_n < 0} d^3 r_n \\ &\quad \times \int_{-\infty}^{\infty} \dots \int_{-\infty}^{\infty} dt'_1 \dots dt'_n \langle \mathcal{T}[X_i^{(0)}(\mathbf{r}_1, \tau) P_{X,i}^{(0)}(\mathbf{r}_n, t'_n)] \rangle^{(0)} \\ &\quad \times \langle \mathcal{T}[A_i^{(0)}(\mathbf{r}_n, t'_n) \times H_{\text{int}}^{(0)A}(t'_1) \dots H_{\text{int}}^{(0)A}(t'_{n-1}) A_j^{(0)}(\mathbf{r}_2, 0)] \rangle_{\text{conn}}^{(0)} \\ &= - \left(\frac{e}{\hbar \rho} \right) \int_{-\infty}^{\infty} dt'_n \int_{z_n < 0} d^3 r_n \langle \mathcal{T}[X_i^{(0)}(\mathbf{r}_1, \tau) P_{X,i}^{(0)}(\mathbf{r}_n, t'_n)] \rangle^{(0)} \mathcal{D}_{ij}^{(n-1)}(\mathbf{r}_n, \mathbf{r}_2; t'_n), \end{aligned} \quad (2.186)$$

where $\mathcal{D}_{ij}^{(n-1)}$ is the $(n-1)$ th term of the series in Eq. (2.134). When Eq. (2.186) is summed from $n = 1$ to ∞ , the summation over the $\mathcal{D}_{ij}^{(n-1)}$ factor simply gives the complete photon Green function \mathcal{D}_{ij} . Then, taking the Fourier transform with respect to τ and using Eq. (2.182), we obtain

$$\frac{1}{\hbar} \langle \mathcal{T}[X_i(\mathbf{r}_1, \tau) A_j(\mathbf{r}_2, 0)] \rangle |^\omega = e\omega \int_{z_3 < 0} d^3 r_3 \mathcal{G}_{il}^{(0)\omega}(\mathbf{r}_1, \mathbf{r}_3) \mathcal{D}_{ij}^\omega(\mathbf{r}_3, \mathbf{r}_2). \quad (2.187)$$

Similarly, we obtain

$$\begin{aligned} \frac{1}{\hbar} \langle \mathcal{T}[X_i(\mathbf{r}_1, 0) A_j(\mathbf{r}_2, \tau)] \rangle |^\omega &= \frac{1}{\hbar} \langle \mathcal{T}[X_i(\mathbf{r}_1, \tau) A_j(\mathbf{r}_2, 0)] \rangle |^{-\omega} \\ &= e(-\omega) \int_{z_3 < 0} d^3 r_3 \mathcal{G}_{il}^{(0)-\omega}(\mathbf{r}_1, \mathbf{r}_3) \mathcal{D}_{ij}^{-\omega}(\mathbf{r}_3, \mathbf{r}_2). \end{aligned} \quad (2.188)$$

It can be seen from Eq. (2.132) and Appendix E that the Green functions $\mathcal{G}_{ij}^{(0)\omega}$ and \mathcal{D}_{ij}^ω are even functions of ω , since ω enters into these Green functions only in the form

$|\omega|$ or ω^2 . Hence, the RHS of Eq. (2.188) is equal and opposite to the RHS of Eq. (2.187). Taking into account the minus sign between the two terms in Eq. (2.100), we see that Eqs. (2.187) and (2.188) contribute equally to the Fourier transform with respect to τ of Eq. (2.100). Thus,

$$C_{ij}^\omega(\mathbf{r}_1, \mathbf{r}_2) = 2e\omega \int_{z_3 < 0} d^3r_3 \mathcal{G}_{il}^{(0)\omega}(\mathbf{r}_1, \mathbf{r}_3) \mathcal{D}_{lj}^\omega(\mathbf{r}_3, \mathbf{r}_2). \quad (2.189)$$

We now have all the quantities we need, namely, \mathcal{D}_{ij}^ω , \mathcal{G}_{ij}^ω and C_{ij}^ω , to compute the spontaneous decay rate of the excited atom using Eq. (2.101).

2.6 Comparison with the Classical Theory

Results for the total decay rate calculated from Eq. (2.101) using the exact functions \mathcal{D}_{ij}^ω , \mathcal{G}_{ij}^ω and C_{ij}^ω are in excellent agreement with those of classical electromagnetic theory [16]. These are shown in Fig. 2.2 for a gold mirror with refractive index $n = 0.505 + 3.66i$. The total decay rate contains a nonradiative component due to energy transfer from the excited atom to the absorbing mirror via the near-field Coulomb interaction. The contribution due to the instantaneous Coulomb interaction U alone may be obtained from Eq. (2.101) by setting \mathcal{D}_{ij}^ω equal to zero,

$$\frac{W_{\text{spont},j}^U}{W_{\text{spont}}^{(0)}} = -\frac{6\pi c^3 \epsilon_0}{\omega_a} \text{Im} \frac{1}{e^2 \omega_a^2} \int_{z < 0} \int_{z' < 0} d^3r d^3r' F_{[j]m}(\mathbf{r}_a - \mathbf{r}) \mathcal{G}_{mn}^{(0)\omega_a}(\mathbf{r}, \mathbf{r}') F_{n[j]}(\mathbf{r}' - \mathbf{r}_a). \quad (2.190)$$

In Appendix F, the integrals over \mathbf{r} and \mathbf{r}' are evaluated to give

$$\begin{aligned} & \int_{z < 0} \int_{z' < 0} d^3r d^3r' F_{[j]m}(\mathbf{r}_a - \mathbf{r}) \mathcal{G}_{mn}^{(0)\omega_a}(\mathbf{r}, \mathbf{r}') F_{n[j]}(\mathbf{r}' - \mathbf{r}_a) \\ &= -\frac{e^2}{4\pi\epsilon_0} \left[\frac{\epsilon_L(\omega_a) - 1}{\epsilon_L(\omega_a) + 1} \right] \left[\frac{\partial^2}{\partial x_{a[j]} \partial x_{b[j]}} \left(\frac{1}{|\mathbf{r}_a - \mathbf{r}_b|} \right) \right] \Big|_{\mathbf{r}_b = \bar{\mathbf{r}}_a}, \end{aligned} \quad (2.191)$$

where $\bar{\mathbf{r}}_a$ is the image of \mathbf{r}_a in the plane $z = 0$. Substituting Eq. (2.191) into Eq. (2.190) and evaluating the partial derivatives, we obtain

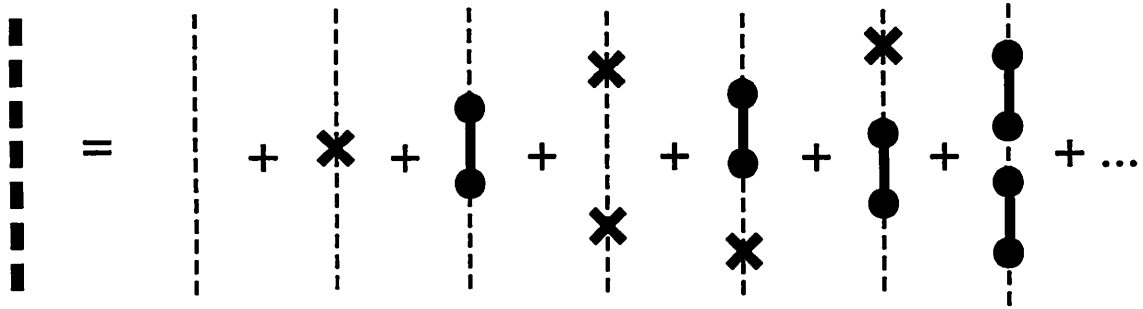
$$\frac{W_{\text{spont},j}^U}{W_{\text{spont}}^{(0)}} = \frac{3\theta_j}{8\omega_a^3 z_a^3} \text{Im} \left[\frac{-1}{\epsilon_L(\omega_a) + 1} \right], \quad (2.192)$$

where $\theta_j = 2$ for $j = z$ and $\theta_j = 1$ for $j = x$ or y . Eq. (2.192) agrees with the classical result [16] for the rate of nonradiative energy transfer in the limit $z_a \rightarrow 0$. At distances z_a greater than a fraction of a wavelength, however, Eq. (2.192) differs considerably from the classical result, suggesting that the latter includes partially the effects of the transverse photons.

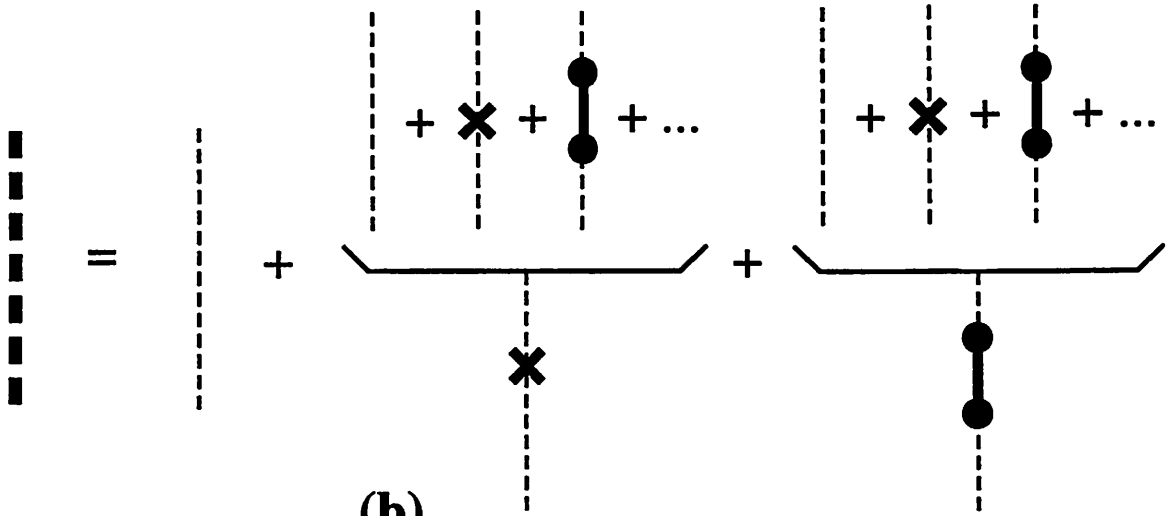
Nonradiative decay is absent for a perfect dielectric. In this case, our results for the decay rate W_j are in excellent agreement not only with the results of classical electromagnetic theory, but also with those based on quantization of macroscopic spatial modes [18]. These are shown in Fig. 2.3 for a dielectric half-space with refractive index $n = 3$.

2.7 Conclusions

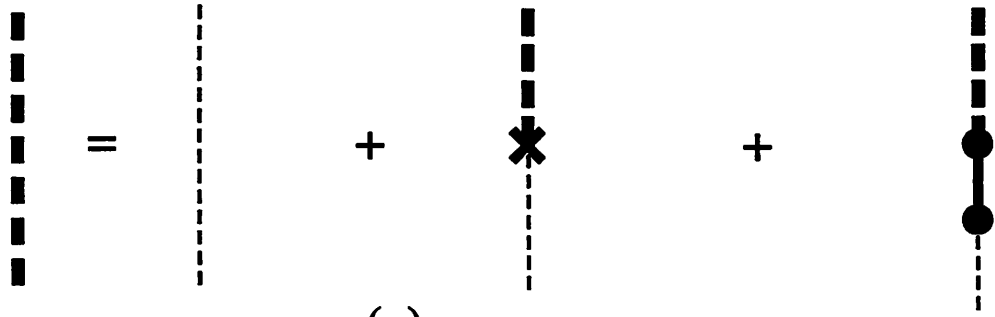
In this chapter, we have presented an exact solution of a microscopic Hamiltonian model of an absorbing dielectric half-space and used it to calculate the spontaneous emission rate to order e^2 of an excited atom near the surface. Because our calculation is based on a fully canonical quantization scheme, it provides a fundamental demonstration of the validity of the classical electromagnetic theory of the rate of spontaneous emission near an absorbing dielectric surface. This serves to increase our confidence in the results of recent work on spontaneous lifetime based on classical electromagnetic theory [21]. Also, the exact photon Green function for the half-space given in Appendix E can be used to treat other quantum mechanical interaction phenomena between charged particles and the electromagnetic field near an absorbing plane surface, such as the level shift of an electron undergoing cyclotron motion near such a surface [22]. In the above discussion, we have only considered the case for which the excited atom is on the air side of the surface. However, our approach can be extended to treat the other case also.



(a)



(b)



(c)

Figure 2.1: Perturbation series for photon Green function. A heavy dashed line represents the complete photon Green function. A light dashed line represents the free-space photon Green function. A cross represents an interaction vertex due to the $\mathbf{A}\cdot\mathbf{A}$ term in Eq. (2.136) acting once. A vertical dumbbell consists of two interaction vertices due to the $\mathbf{A}\cdot\mathbf{P}$ term in Eq. (2.136) acting twice.

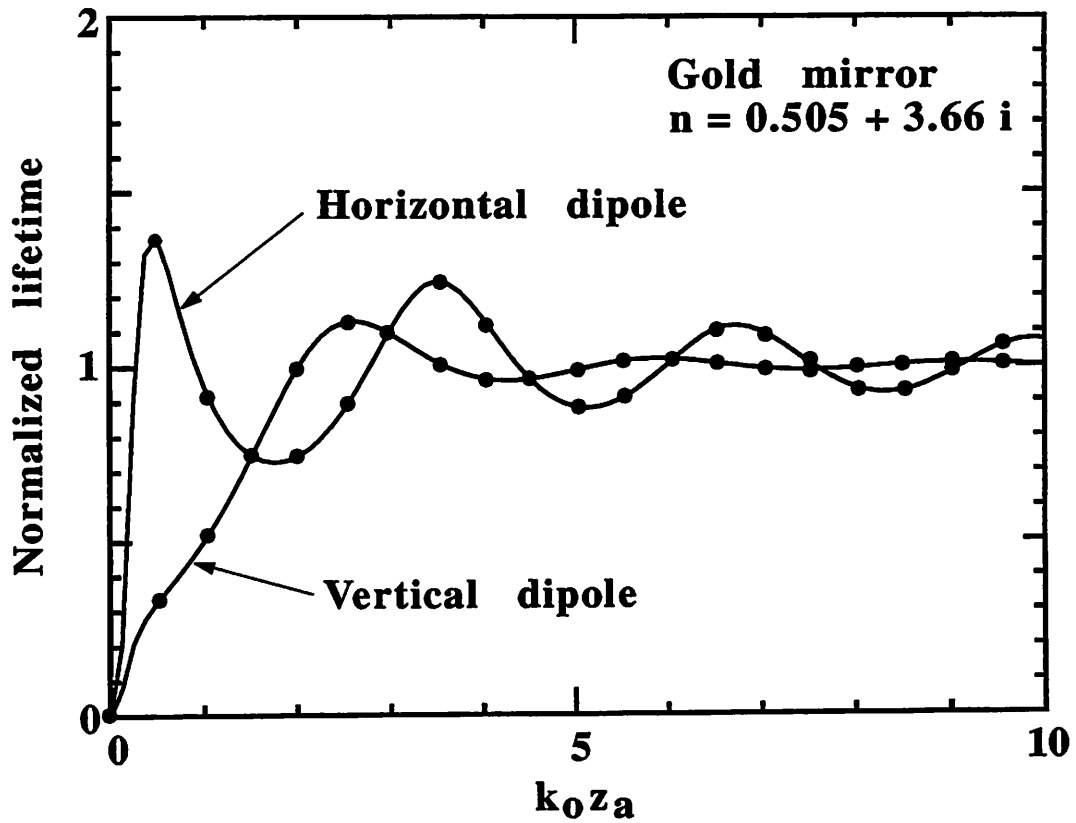


Figure 2.2: Lifetime of an excited atom near a gold mirror. Solid lines are the results of classical electromagnetic theory. Dots are the results of our quantum theory. k_0 is the wavevector in air. z_a is the distance of the atom above the mirror.

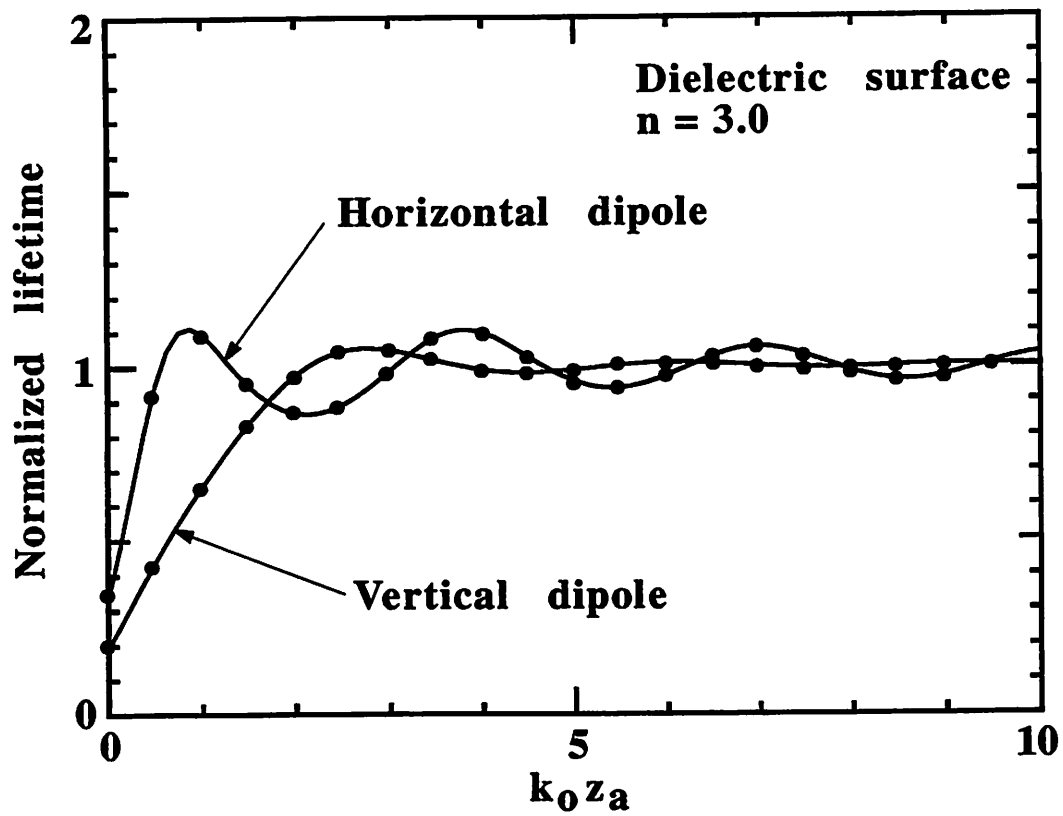


Figure 2.3: Lifetime of an excited atom near a lossless dielectric surface. Solid lines are the results of the spatial-mode quantization theory. Dots are the results of our quantum theory.

Chapter 3

Three-Dimensional Topography Scattering Part I: Multipole Accelerated Physical-Optics Method

3.1 Introduction

In the past few years, electromagnetic simulation of photolithography has received much attention. This is because, as the design rule of integrated circuits shrinks, it becomes necessary to control CD variations due to topography scattering and other effects within tighter and tighter limits. Accurate simulation of topography scattering using electromagnetic theory can be a valuable tool for predicting CD variations over wafer topography. A related problem arises in mask design. As the aspect ratio of the mask topography increases, due to design-rule shrinkage or to the use of phase-shifting-mask structures, electromagnetic-diffraction effects in mask transmission become increasingly more important and thus need to be simulated accurately.

Various rigorous techniques of computational electromagnetics have been applied successfully to topography scattering problems in 2-D. These include the time-domain finite-difference [24, 25, 26, 27], waveguide [28], differential [29], finite-element [30, 31] and spectral-element [32] methods. Already in 2-D, such techniques are very CPU and memory intensive. Their extensions to 3-D would certainly be much more so. In an attempt to reduce the CPU cost of topography-scattering simulation, approxi-

mate techniques based on the Geometrical Theory of Diffraction (GTD) [9] and the physical-optics approximation [10] have been developed for 2-D problems. In this chapter, we discuss an extension of the physical-optics approach in [10] to 3-D topography scattering. The resulting technique is suitable for piecewise-linear topography and allows reflective-notching simulation of large 3-D structures to be performed on an ordinary workstation with reasonable CPU time.

We begin the discussion of our multipole accelerated physical-optics technique with a review of the diffraction integrals of electromagnetic theory in Section 3.2 and an outline of the physical-optics approximation in Section 3.3. To simplify the treatment of multilayer structures, we use an iterative scheme developed by Pai and Awada [13] to take into account multiple scattering between adjacent surfaces in the structure. This is discussed in Section 3.4, where the special case of a pair of non-interlacing adjacent surfaces is discussed in detail. The problem of multiple scattering within a given surface is discussed in Section 3.5, while the problem of the reflection of multiply scattered *dipole* waves from the tangent planes on the same surface is discussed in Section 3.6. Next, the multipole approximation is introduced in Section 3.7 to speed up the computation of the multiply scattered waves. The discussion for dipole waves in Section 3.6 is then generalized to the case of *multipole* waves in Section 3.8. The technique of multipole acceleration is discussed in Section 3.9, while the approximation methods used to evaluate the resulting integrals are discussed in Section 3.10. In Section 3.11, the operation count of our algorithm is estimated. Then, the results of 3-D reflective-notching simulation are presented in Section 3.12.

3.2 Problem Statement

Fig. 3.1 shows the type of topography of interest in photolithography simulation. It consists of a number of homogeneous media of permittivity ϵ_i separated by surfaces S_i . The structure is assumed to be periodic in the horizontal (x and y) directions with periods d_x and d_y . A set of plane waves representing an aerial image is incident on the uppermost, photoresist surface. The incident field on a horizontal reference

plane above the photoresist surface is in the form of a superposition of a finite number of spatial harmonics $e^{j(\alpha_m x + \beta_n y)}$, where

$$\alpha_m = k_x^{(0)} + \frac{2\pi m}{d_x}, \quad (3.1)$$

$$\beta_n = k_y^{(0)} + \frac{2\pi n}{d_y}. \quad (3.2)$$

Here, m and n are integers and $k_x^{(0)}$ and $k_y^{(0)}$ are components of the incident wavevector of the $(0, 0)$ -th harmonic. Our goal is to simulate the intensity distribution within the photoresist layer.

According to the Kirchhoff-Huygens principle [33], the electric and magnetic fields at any point \mathbf{r} within a *homogeneous* volume can be computed from the values of the tangential field components over a surface completely enclosing the volume,

$$\mathbf{E}(\mathbf{r}) = \frac{1}{4\pi} \int_S \left[-j\omega\mu(\mathbf{n}' \times \mathbf{H}')\psi - \frac{j}{\omega\epsilon_1}(\mathbf{n}' \times \mathbf{H}') \cdot \nabla'(\nabla'\psi) - (\mathbf{n}' \times \mathbf{E}') \times \nabla'\psi \right] dS', \quad (3.3)$$

$$\mathbf{H}(\mathbf{r}) = \frac{1}{4\pi} \int_S \left[j\omega\epsilon_1(\mathbf{n}' \times \mathbf{E}')\psi + \frac{j}{\omega\mu}(\mathbf{n}' \times \mathbf{E}') \cdot \nabla'(\nabla'\psi) - (\mathbf{n}' \times \mathbf{H}') \times \nabla'\psi \right] dS', \quad (3.4)$$

where S is the enclosing surface, ϵ_1 and μ are the permittivity and permeability of the enclosed volume V , and ψ is the Green function for the Helmholtz equation in V ,

$$\psi = \frac{e^{jk_1|\mathbf{r}-\mathbf{r}'|}}{|\mathbf{r}-\mathbf{r}'|}, \quad (3.5)$$

k_1 being the wavevector in V . Also, in Eqs. (3.3) and (3.4), \mathbf{n}' is the *outward* unit normal at a point \mathbf{r}' on S , a prime on \mathbf{E} or \mathbf{H} indicates that the corresponding quantity is to be evaluated at \mathbf{r}' , and our time convention is $e^{-j\omega t}$.

Eqs. (3.3) and (3.4) are equivalent to the standard form of the Kirchhoff-Huygens principle [34],

$$\mathbf{E}(\mathbf{r}) = \frac{1}{4\pi} \int_S [-j\omega\mu(\mathbf{n}' \times \mathbf{H}')\psi - (\mathbf{n}' \cdot \mathbf{E}')\nabla'\psi - (\mathbf{n}' \times \mathbf{E}') \times \nabla'\psi] dS', \quad (3.6)$$

$$\mathbf{H}(\mathbf{r}) = \frac{1}{4\pi} \int_S [j\omega\epsilon_1(\mathbf{n}' \times \mathbf{E}')\psi - (\mathbf{n}' \cdot \mathbf{H}')\nabla'\psi - (\mathbf{n}' \times \mathbf{H}') \times \nabla'\psi] dS'. \quad (3.7)$$

This can be seen by performing an integration by parts on the second term on the RHS of each of Eqs. (3.6) and (3.7). For example, using the Maxwell's equation $-j\omega\epsilon_1\mathbf{E} = \nabla \times \mathbf{H}$, the i th component of the second term on the RHS of Eq. (3.6) becomes

$$\begin{aligned} \frac{1}{4\pi} \int_S -(\mathbf{n}' \cdot \mathbf{E}') \frac{\partial \psi}{\partial x'_i} dS' &= \frac{1}{4\pi} \int_S -\frac{j}{\omega\epsilon_1} [\mathbf{n}' \cdot (\nabla' \times \mathbf{H}')] \frac{\partial \psi}{\partial x'_i} dS' \\ &= \frac{1}{4\pi} \int_S -\frac{j}{\omega\epsilon_1} \mathbf{n}' \cdot \left[\nabla' \times \left(\mathbf{H}' \frac{\partial \psi}{\partial x'_i} \right) + \mathbf{H}' \times \left(\nabla' \frac{\partial \psi}{\partial x'_i} \right) \right] dS'. \end{aligned} \quad (3.8)$$

Using Stokes' Theorem, the first term on the RHS of Eq. (3.8) is transformed into a line integral along the boundary of S , which is zero since S is closed. Hence, Eq. (3.8) becomes

$$\begin{aligned} \frac{1}{4\pi} \int_S -(\mathbf{n}' \cdot \mathbf{E}') \frac{\partial \psi}{\partial x'_i} dS' &= \frac{1}{4\pi} \int_S -\frac{j}{\omega\epsilon_1} \mathbf{n}' \cdot \left[\mathbf{H}' \times \left(\nabla' \frac{\partial \psi}{\partial x'_i} \right) \right] dS' \\ &= \frac{1}{4\pi} \int_S -\frac{j}{\omega\epsilon_1} (\mathbf{n}' \times \mathbf{H}') \cdot \nabla' \frac{\partial \psi}{\partial x'_i} dS', \end{aligned} \quad (3.9)$$

which is the same as the i th component of the second term on the RHS of Eq. (3.3). Similarly, the second terms on the RHS of Eqs. (3.7) and (3.4) can be shown to be equivalent.

There is an advantage to using the *amended* form Eqs. (3.3) and (3.4), rather than the standard form Eqs. (3.6) and (3.7), in that the former has a simple interpretation in terms of vector potentials. If we regard the tangential fields $(\mathbf{n}' \times \mathbf{E}')$ and $(-\mathbf{n}' \times \mathbf{H}')$ on S as equivalent to magnetic and electric surface current densities, respectively, then the magnetic and electric vector potentials $\mathbf{A}_m(\mathbf{r})$ and $\mathbf{A}_e(\mathbf{r})$ at any point \mathbf{r} within V due to these equivalent sources on S are

$$\mathbf{A}_m(\mathbf{r}) = \frac{1}{4\pi} \int_S -(\mathbf{n}' \times \mathbf{E}') \psi dS', \quad (3.10)$$

$$\mathbf{A}_e(\mathbf{r}) = \frac{1}{4\pi} \int_S -(\mathbf{n}' \times \mathbf{H}') \psi dS'. \quad (3.11)$$

The electric and magnetic fields are then given by

$$\mathbf{E}(\mathbf{r}) = \nabla \times \mathbf{A}_m + \frac{j}{\omega\epsilon_1} \nabla \times \nabla \times \mathbf{A}_e, \quad (3.12)$$

$$\mathbf{H}(\mathbf{r}) = \nabla \times \mathbf{A}_e - \frac{j}{\omega\mu} \nabla \times \nabla \times \mathbf{A}_m. \quad (3.13)$$

When Eqs. (3.10) and (3.11) are substituted into Eqs. (3.12) and the ∇ operators allowed to act on ψ with the substitution $\nabla = -\nabla'$, we obtain

$$\mathbf{E}(\mathbf{r}) = \frac{1}{4\pi} \int_S \left\{ -(\mathbf{n}' \times \mathbf{E}') \times \nabla' \psi - \frac{j}{\omega \epsilon_1} [(\mathbf{n}' \times \mathbf{H}') \cdot \nabla' (\nabla' \psi) - (\mathbf{n}' \times \mathbf{H}') \nabla'^2 \psi] \right\} dS'. \quad (3.14)$$

Eq. (3.14) is seen to be the same as Eq. (3.3) when we use the fact that $\nabla'^2 \psi = -k_1^2 \psi = -(\omega^2 \mu \epsilon_1) \psi$ when $\mathbf{r} \neq \mathbf{r}'$. Similarly, Eq. (3.13) can be shown to be equivalent to Eq. (3.4).

From the above discussions, it is clear that the main problem in topography-scattering simulation is to determine the values of the tangential fields on the surface $S = S_1 + S_2$ enclosing the photoresist region whose permittivity is ϵ_1 (see Fig. 3.1). The rigorous approach would be to set up integral equations for the tangential fields on S_1 and S_2 , using outgoing-wave boundary conditions in the region above S_1 (air) and the region below S_2 (substrate). In this chapter, however, we use instead an approximate approach based on the physical-optics approximation.

3.3 The Physical-Optics Approximation

The basic idea of the physical-optics approximation is that the tangential fields at each point on the surface of a scatterer may be approximated by those that would be present on the tangent plane at that point, i.e., by the sum of the incident and reflected fields on the tangent plane. A condition of validity of this approximation is that the local radius of curvature r_c of the surface be large compared with the wavelength λ of light in the incidence medium. In the simplest implementation of the physical-optics approximation, multiple scattering between opposing elements of the same surface is ignored. We shall refer to this as the zeroth-order physical-optics approximation. The condition of validity of this zeroth-order approximation is $r_c \cos \theta \gg \lambda/4\pi$, where θ is the local angle of incidence [35]. This is satisfied for gently undulating topography in which the surface slope is everywhere small, so that $\cos \theta \approx 1$, and no sharp edges are present, so that $r_c \gg \lambda$. A number of structures of interest in photolithography

simulation are of this type, e.g., bird's beaks and planarizing dielectric layers. In order to extend the class of topography to which the physical-optics approximation is applicable to include piecewise-linear topography with large surface slopes, it is necessary to go beyond the zeroth-order approximation by including the effects of multiple scattering within each surface.

3.4 Multiple Scattering between Surfaces

In a multilayer structure such as the one shown in Fig. 3.1, multiple scattering between adjacent surfaces such as S_1 and S_2 can give rise to important standing-wave effects. When doing topography-scattering calculations, it is convenient to treat each surface one at a time and to include the effects of neighboring surfaces by iteration. A suitable iterative scheme for this purpose is the one-way multiple-reflection-series method developed by Pai and Awada [13] to improve the numerical stability of the waveguide model. In this scheme, the field throughout the multilayer structure is represented by a series of multiply reflected waves,

$$\mathbf{E}(\mathbf{r}) = \mathbf{E}_0^{(-)}(\mathbf{r}) + \mathbf{E}_1^{(+)}(\mathbf{r}) + \mathbf{E}_2^{(-)}(\mathbf{r}) + \dots, \quad (3.15)$$

where the subscript on each term on the RHS indicates the number of reflections undergone by the corresponding wave, and the superscript indicates whether the wave is downgoing ($-$) or upgoing ($+$). This is illustrated in Fig. 3.2. The zeroth-reflection wave $\mathbf{E}_0^{(-)}(\mathbf{r})$ is obtained by propagating the incident wave down through the entire structure, using the transmitted field generated at each surface as incident field for the surface below. The one-reflection wave $\mathbf{E}_1^{(+)}(\mathbf{r})$ is obtained by propagating the reflected fields generated at the various surfaces during the preceding downgoing step up through the entire structure. The two-reflection wave $\mathbf{E}_2^{(-)}(\mathbf{r})$ is obtained by propagating the reflected fields generated at the various surfaces during the preceding upgoing step down through the structure, and so on.

The propagation of each of the above multiply reflected waves from one surface to the next can be treated by diffraction theory. The interaction of the waves with each

surface can then be treated either approximately by the physical-optics method, or rigorously by the integral method (Method of Moments).

Consider the propagation of waves from a surface S_i to an adjacent surface S_j in a multilayer structure such as the one shown in Fig. 3.1. The permittivity of the intervening medium is assumed to be ϵ_1 . The fields incident on S_j due to the tangential fields on S_i are given by expressions similar to Eqs. (3.3) and (3.4), except that the integrations are now restricted to the surface S_i . Each surface element $\delta S'$ on S_i , centered at \mathbf{r}' , contributes an amount $\delta \mathbf{E}(\mathbf{r})$ to the electric field incident at a point \mathbf{r} on S_j given by

$$\delta \mathbf{E}(\mathbf{r}) = \frac{1}{4\pi} \left[-j\omega\mu(\mathbf{n}' \times \mathbf{H}')\psi - \frac{j}{\omega\epsilon_1}(\mathbf{n}' \times \mathbf{H}') \cdot \nabla'(\nabla'\psi) - (\mathbf{n}' \times \mathbf{E}') \times \nabla'\psi \right] \delta S'. \quad (3.16)$$

From the form of the Green function ψ given by Eq. (3.5), we see that Eq. (3.16) represents a spherical wave originating from the source point \mathbf{r}' on S_i . We are then faced with the problem of how to treat the interaction of such spherical waves from S_i with the adjacent surface S_j .

In the physical-optics approximation, we assume that the spherical waves represented by Eq. (3.16) interact with the tangent plane at each point of S_j independently of the rest of S_j . Because these waves are spherical, the treatment of their reflection from the tangent planes on S_j is based on Sommerfeld's solution, which is much more complicated than the Fresnel laws for plane waves. We defer discussion of Sommerfeld's solution to Section 3.6. For the present, we note that a considerable simplification occurs when the adjacent surfaces S_i and S_j under consideration do not interlace, i.e., the lowest point of the upper surface is higher than the highest point of the lower surface. In that case, it is possible to draw a horizontal reference plane S_{ref} between S_i and S_j which does not intersect either surface. The spherical waves from S_i can then be decomposed into a sum of plane waves. To do so, we first evaluate the fields on the reference plane S_{ref} using Eqs. (3.3) and (3.4) but with the integrations restricted to S_i . By Floquet's theorem, the fields on the reference plane S_{ref} may be

written as a sum of spatial harmonics,

$$\mathbf{E}(x, y) = \sum_{m,n} [A_{mn} \mathbf{e}_{mn}^{(s)} + B_{mn} \mathbf{e}_{mn}^{(p)}] e^{j(\alpha_m x + \beta_n y)}, \quad (3.17)$$

$$\sqrt{\frac{\mu}{\epsilon_1}} \mathbf{H}(x, y) = \sum_{m,n} [A_{mn} \mathbf{h}_{mn}^{(s)} + B_{mn} \mathbf{h}_{mn}^{(p)}] e^{j(\alpha_m x + \beta_n y)}, \quad (3.18)$$

where α_m and β_n are given by Eqs. (3.1) and (3.2). Also, in Eqs. (3.17) and (3.18), $\mathbf{e}_{mn}^{[s(p)]}$ and $\mathbf{h}_{mn}^{[s(p)]}$ are unit vectors of the (m, n) -th harmonic for s (p) polarization. The form of these polarization vectors depends on whether they represent upgoing or downgoing spatial harmonics. When S_i is above S_j , only downgoing spatial harmonics are present on the intervening reference plane S_{ref} , and conversely when S_i is below S_j . For upgoing spatial harmonics,

$$\mathbf{e}_{mn}^{(s+)} = \frac{-\beta_n \mathbf{x} + \alpha_m \mathbf{y}}{\sqrt{\alpha_m^2 + \beta_n^2}}, \quad (3.19)$$

$$\mathbf{h}_{mn}^{(s+)} = \frac{-\alpha_m \gamma_{mn} \mathbf{x} - \beta_n \gamma_{mn} \mathbf{y} + (\alpha_m^2 + \beta_n^2) \mathbf{z}}{k_1 \sqrt{\alpha_m^2 + \beta_n^2}}, \quad (3.20)$$

$$\mathbf{e}_{mn}^{(p+)} = -\mathbf{h}_{mn}^{(s+)}, \quad (3.21)$$

$$\mathbf{h}_{mn}^{(p+)} = \mathbf{e}_{mn}^{(s+)}, \quad (3.22)$$

where

$$\gamma_{mn} = \begin{cases} \sqrt{k_1^2 - \alpha_m^2 - \beta_n^2} \\ j\sqrt{\alpha_m^2 + \beta_n^2 - k_1^2} \end{cases}, \quad \text{Im } \gamma_{mn} \geq 0, \quad (3.23)$$

and \mathbf{x}, \mathbf{y} and \mathbf{z} are the Cartesian unit vectors with \mathbf{z} pointing upwards. For downgoing spatial harmonics,

$$\mathbf{e}_{mn}^{(s-)} = \mathbf{e}_{mn}^{(s+)}, \quad (3.24)$$

$$\mathbf{h}_{mn}^{(s-)} = \frac{\alpha_m \gamma_{mn} \mathbf{x} + \beta_n \gamma_{mn} \mathbf{y} + (\alpha_m^2 + \beta_n^2) \mathbf{z}}{k_1 \sqrt{\alpha_m^2 + \beta_n^2}}, \quad (3.25)$$

$$\mathbf{e}_{mn}^{(p-)} = -\mathbf{h}_{mn}^{(s-)}, \quad (3.26)$$

$$\mathbf{h}_{mn}^{(p-)} = \mathbf{e}_{mn}^{(s-)}. \quad (3.27)$$

With the help of these polarization vectors, we can invert Eqs. (3.17) and (3.18) to find the coefficients A_{mn} and B_{mn} ,

$$A_{mn}^{(\pm)} = \frac{\pm k_1}{2d_x d_y \gamma_{mn}} \int_0^{d_x} \int_0^{d_y} \left[\mathbf{E}(x, y) \times \mathbf{h}_{mn}^{(s\pm)} - \sqrt{\frac{\mu}{\epsilon_1}} \mathbf{H}(x, y) \times \mathbf{e}_{mn}^{(s\pm)} \right] \cdot \mathbf{z} \times e^{-j(\alpha_m x + \beta_n y)} dx dy, \quad (3.28)$$

$$B_{mn}^{(\pm)} = \frac{\pm k_1}{2d_x d_y \gamma_{mn}} \int_0^{d_x} \int_0^{d_y} \left[\mathbf{E}(x, y) \times \mathbf{h}_{mn}^{(p\pm)} - \sqrt{\frac{\mu}{\epsilon_1}} \mathbf{H}(x, y) \times \mathbf{e}_{mn}^{(p\pm)} \right] \cdot \mathbf{z} \times e^{-j(\alpha_m x + \beta_n y)} dx dy, \quad (3.29)$$

where the superscript (\pm) indicates an upgoing or downgoing spatial harmonic.

Knowing the expansion coefficients on the reference plane S_{ref} , the fields incident on S_j are easily obtained,

$$\mathbf{E}(\mathbf{r}) = \sum_{m,n} \left[A_{mn}^{(\pm)} \mathbf{e}_{mn}^{(s\pm)} + B_{mn}^{(\pm)} \mathbf{e}_{mn}^{(p\pm)} \right] e^{j(\alpha_m x + \beta_n y \pm \gamma_{mn} z)}, \quad (3.30)$$

$$\sqrt{\frac{\mu}{\epsilon_1}} \mathbf{H}(\mathbf{r}) = \sum_{m,n} \left[A_{mn}^{(\pm)} \mathbf{h}_{mn}^{(s\pm)} + B_{mn}^{(\pm)} \mathbf{h}_{mn}^{(p\pm)} \right] e^{j(\alpha_m x + \beta_n y \pm \gamma_{mn} z)}, \quad (3.31)$$

where z is measured from the reference plane. The interaction of the spatial harmonics contained in Eqs. (3.30) and (3.31) with S_j can now be treated readily within the physical-optics approximation, by applying the Fresnel laws of optics.

Specifically, consider the interaction of the (m, n) -th spatial harmonic contained in Eqs. (3.30) and (3.31) with the tangent plane \mathcal{P} at a particular point \mathbf{r} on S_j . In general, \mathcal{P} is not horizontal. Let the normal to \mathcal{P} point in a direction described by polar coordinates $(\tilde{\theta}, \tilde{\phi})$ with respect to the *global* coordinate system shown in Fig. 3.1. Then, we can define a *local* coordinate system (x'', y'', z'') in which the z'' axis is normal to \mathcal{P} by the following coordinate transformation:

$$\begin{pmatrix} x'' \\ y'' \\ z'' \end{pmatrix} = \begin{pmatrix} \cos \tilde{\theta} \cos \tilde{\phi} & \cos \tilde{\theta} \sin \tilde{\phi} & -\sin \tilde{\theta} \\ -\sin \tilde{\phi} & \cos \tilde{\phi} & 0 \\ \sin \tilde{\theta} \cos \tilde{\phi} & \sin \tilde{\theta} \sin \tilde{\phi} & \cos \tilde{\theta} \end{pmatrix} \begin{pmatrix} x \\ y \\ z \end{pmatrix}. \quad (3.32)$$

The wavevector $(\alpha_m, \beta_n, \pm \gamma_{mn})$ of the (m, n) -th spatial harmonic is similarly transformed into components $(\alpha''_m, \beta''_n, \gamma''_{mn})$ with respect to the local coordinate system,

$$\begin{pmatrix} \alpha''_m \\ \beta''_n \\ \gamma''_{mn} \end{pmatrix} = \begin{pmatrix} \cos \tilde{\theta} \cos \tilde{\phi} & \cos \tilde{\theta} \sin \tilde{\phi} & -\sin \tilde{\theta} \\ -\sin \tilde{\phi} & \cos \tilde{\phi} & 0 \\ \sin \tilde{\theta} \cos \tilde{\phi} & \sin \tilde{\theta} \sin \tilde{\phi} & \cos \tilde{\theta} \end{pmatrix} \begin{pmatrix} \alpha_m \\ \beta_n \\ \pm \gamma_{mn} \end{pmatrix}. \quad (3.33)$$

Next, we construct polarization vectors $\mathbf{e}_{mn}^{[s(p)]''}$ and $\mathbf{h}_{mn}^{[s(p)]''}$ associated with the direction of incidence $(\alpha''_m, \beta''_n, \gamma''_{mn})$ in the local system, using Eqs. (3.19) to (3.22) with $(\alpha_m, \beta_n, \gamma_{mn})$ replaced by $(\alpha''_m, \beta''_n, \gamma''_{mn})$. With the help of these polarization vectors, we can resolve the amplitudes of the (m, n) -th spatial harmonic in Eqs. (3.30) and (3.31) into components A'' and B'' along the directions of these vectors,

$$\left[A_{mn}^{(\pm)} \mathbf{e}_{mn}^{(s\pm)} + B_{mn}^{(\pm)} \mathbf{e}_{mn}^{(p\pm)} \right] = A'' \mathbf{e}_{mn}^{(s)''} + B'' \mathbf{e}_{mn}^{(p)''}, \quad (3.34)$$

$$\left[A_{mn}^{(\pm)} \mathbf{h}_{mn}^{(s\pm)} + B_{mn}^{(\pm)} \mathbf{h}_{mn}^{(p\pm)} \right] = A'' \mathbf{h}_{mn}^{(s)''} + B'' \mathbf{h}_{mn}^{(p)''}, \quad (3.35)$$

where

$$A'' = \frac{1}{2C} \left\{ \left[A_{mn}^{(\pm)} \mathbf{e}_{mn}^{(s\pm)} + B_{mn}^{(\pm)} \mathbf{e}_{mn}^{(p\pm)} \right] \times \mathbf{h}_{mn}^{(s)''} - \left[A_{mn}^{(\pm)} \mathbf{h}_{mn}^{(s\pm)} + B_{mn}^{(\pm)} \mathbf{h}_{mn}^{(p\pm)} \right] \times \mathbf{e}_{mn}^{(s)''} \right\} \cdot \mathbf{z}'', \quad (3.36)$$

and B'' is obtained from Eq. (3.36) by replacing $\mathbf{h}_{mn}^{(s)''}$ and $\mathbf{e}_{mn}^{(s)''}$ by $\mathbf{h}_{mn}^{(p)''}$ and $\mathbf{e}_{mn}^{(p)''}$, respectively. Also, in Eq. (3.36), $C = [\mathbf{e}_{mn}^{(s)''} \times \mathbf{h}_{mn}^{(s)''}] \cdot \mathbf{z}''$. This way, the (m, n) -th spatial harmonic incident on the tangent plane \mathcal{P} is resolved into an s -polarized incident plane wave with amplitude A'' and a p -polarized incident plane wave with amplitude B'' . The reflected waves can now be found by applying the laws of optics. In particular, the amplitude of the reflected s -polarized wave is equal to A'' times the Fresnel reflection coefficient for s -polarization, and similarly for the reflected p -polarized wave.

Having thus found a way to deal with multiple scattering between adjacent surfaces iteratively, we can now concentrate on the multiple scattering taking place within each surface.

3.5 Multiple Scattering within a Surface

This type of multiple scattering is important in topography with large surface slopes, or in which the inclined surfaces are closely spaced. The crudest way to take into account multiple scattering within a surface is to use geometrical optics to trace the rays reflected multiple times within the surface. However, this technique neglects near-field diffraction and thus leads to unphysical discontinuities in the reflected fields

at the geometrical-optics shadow boundaries [10]. Bischoff et al. [9] overcame this difficulty in the 2-D case by the addition of an edge diffracted field in accordance with the rules of GTD. We, however, use a different technique to take into account near-field diffraction, namely, by considering each element dS' of the surface S_j under consideration as a source of spherical waves illuminating every other point on the same surface. Thus, the tangential fields $(\mathbf{n}' \times \mathbf{E}')$ and $(-\mathbf{n}' \times \mathbf{H}')$ induced by some incident field on an element dS' at \mathbf{r}' may be regarded as dipole sources producing *magnetic* and *electric* vector potentials $d\mathbf{A}_m(\mathbf{r})$ and $d\mathbf{A}_e(\mathbf{r})$, respectively,

$$d\mathbf{A}_m(\mathbf{r}) = -(\mathbf{n}' \times \mathbf{E}') \frac{e^{jk_1|\mathbf{r}-\mathbf{r}'|}}{4\pi|\mathbf{r}-\mathbf{r}'|} dS', \quad (3.37)$$

$$d\mathbf{A}_e(\mathbf{r}) = -(\mathbf{n}' \times \mathbf{H}') \frac{e^{jk_1|\mathbf{r}-\mathbf{r}'|}}{4\pi|\mathbf{r}-\mathbf{r}'|} dS'. \quad (3.38)$$

Our terminology for the vector potentials follows that of Stratton [36]. Strictly speaking, there are two such sets of vector potentials to consider, one for the medium above S_j and the other for the medium below S_j . These correspond to the reflected and transmitted waves produced by the incident wave. Both sets of vector potentials have the form of Eqs. (3.37) and (3.38), provided that \mathbf{n}' is interpreted as the unit surface normal pointing *out of* the medium under consideration and the appropriate wavevector k_1 for that medium is used.

We now have to consider the interaction of the spherical waves scattered by each surface element dS' of S_j with all other parts of the same surface. In general, the source element dS' at a given point \mathbf{r}' on S_j may or may not be directly visible from the field point \mathbf{r} on the same surface. In our physical-optics technique, we ignore the interaction between any pair of points which do not lie on each other's direct line-of-sight, or when the source point lies *on* the tangent plane of the field point. The latter condition means that, as a result of discretization of the surface S_j , we only consider source elements dS' lying at some finite distance d away from the tangent plane at the field point. In general, the direct line-of-sight between a pair of interacting points may lie in the medium above or below S_j . In each case, we must use the set of vector potentials Eqs. (3.37) and (3.38) appropriate to that medium, as mentioned in the

last paragraph. It frequently happens in photolithography simulation that one of the media on the two sides of S_j , for example, silicon, is highly lossy. In such case, it is a good approximation to neglect the interaction between any pair of points on S_j whose direct line-of-sight lies in the highly lossy medium. This is because the waves Eqs. (3.37) and (3.38) scattered into the latter medium are expected to be heavily attenuated in that medium before they could interact with the same surface again.

3.6 Sommerfeld's Solution

In the physical-optics approximation, we have to consider the reflection of spherical waves of the form Eqs. (3.37) and (3.38), due to each surface element dS' on S_j , from the tangent plane at every other point on S_j . The spherical waves represented by Eqs. (3.37) and (3.38) are the simplest of a type of waves known as multipole waves. The problem of the reflection of such simplest, or dipole waves, from a lossy plane surface was first solved by Sommerfeld [37]. The geometry of the problem is shown in Fig. 3.3, in which a point dipole is situated a distance d from a lossy plane surface representing the tangent plane at the field point \mathbf{r} on S_j . Without loss of generality, we assume $d > 0$. The permittivities of the media above and below the plane surface are ϵ_1 and ϵ_2 , respectively, while the permeability everywhere is μ . It is convenient to resolve the dipole direction, $(\mathbf{n}' \times \mathbf{E}')$ or $(\mathbf{n}' \times \mathbf{H}')$, into a linearly polarized *vertical* direction and left- and right-hand circularly polarized *horizontal* directions with respect to the lossy plane surface. We separately consider the cases when the dipole is of the magnetic [Eq. (3.37)] or electric [Eq. (3.38)] type, and when it is polarized vertically or horizontally.

For a unit, vertically polarized dipole source of the *magnetic* type, the incident and reflected vector potentials are given by

$$\begin{aligned} \mathbf{A}_m^{(z)\text{inc}}(\mathbf{r}) &= \mathbf{z}_2 \frac{e^{jk_1|\mathbf{r}-\mathbf{r}'|}}{jk_1|\mathbf{r}-\mathbf{r}'|} \\ &= \mathbf{z}_2 \int_0^\infty J_0(\lambda\rho_2) e^{j\sqrt{k_1^2-\lambda^2}|z_2|} \frac{\lambda d \lambda}{k_1 \sqrt{k_1^2-\lambda^2}}, \end{aligned} \quad (3.39)$$

$$\mathbf{A}_m^{(z)\text{refl}}(\mathbf{r}) = \mathbf{z}_2 \int_0^\infty R_s(\lambda) J_0(\lambda \rho_2) e^{j\sqrt{k_1^2 - \lambda^2}(2d+z_2)} \frac{\lambda d \lambda}{k_1 \sqrt{k_1^2 - \lambda^2}}, \quad (3.40)$$

where (ρ_2, ϕ_2, z_2) are cylindrical polar coordinates of the field point \mathbf{r} with respect to a coordinate system centered at the dipole, as shown in Fig. 3.3. Also, $R_s(\lambda)$ is the Fresnel reflection coefficient for an s -polarized incident plane wave at an angle of incidence $\theta = \sin^{-1}(\lambda/k_1)$,

$$R_s(\lambda) = \frac{\sqrt{k_1^2 - \lambda^2} - \sqrt{k_2^2 - \lambda^2}}{\sqrt{k_1^2 - \lambda^2} + \sqrt{k_2^2 - \lambda^2}}, \quad (3.41)$$

where k_1 and k_2 are wavevectors in the media above and below the lossy plane surface, respectively. The branches of the quantities $\sqrt{k_1^2 - \lambda^2}$ and $\sqrt{k_2^2 - \lambda^2}$ in Eqs. (3.39) to (3.41) are chosen so that

$$\mu_1 = -j\sqrt{k_1^2 - \lambda^2}, \quad \text{Re } \mu_1 \geq 0, \quad (3.42)$$

$$\mu_2 = -j\sqrt{k_2^2 - \lambda^2}, \quad \text{Re } \mu_2 \geq 0. \quad (3.43)$$

For a unit dipole source of the magnetic type circularly polarized in the horizontal direction, the incident and reflected vector potentials are given by

$$\begin{aligned} \mathbf{A}_m^{(\pm)\text{inc}}(\mathbf{r}) &= (\mathbf{x}_2 \pm j\mathbf{y}_2) \frac{e^{jk_1|\mathbf{r}-\mathbf{r}'|}}{jk_1|\mathbf{r}-\mathbf{r}'|} \\ &= (\mathbf{x}_2 \pm j\mathbf{y}_2) \int_0^\infty J_0(\lambda \rho_2) e^{j\sqrt{k_1^2 - \lambda^2}|z_2|} \frac{\lambda d \lambda}{k_1 \sqrt{k_1^2 - \lambda^2}}, \end{aligned} \quad (3.44)$$

$$\begin{aligned} \mathbf{A}_m^{(\pm)\text{refl}}(\mathbf{r}) &= (\mathbf{x}_2 \pm j\mathbf{y}_2) \int_0^\infty R_p(\lambda) J_0(\lambda \rho_2) e^{j\sqrt{k_1^2 - \lambda^2}(2d+z_2)} \frac{\lambda d \lambda}{k_1 \sqrt{k_1^2 - \lambda^2}} \\ &\quad + j\mathbf{z}_2 e^{\pm j\phi_2} \int_0^\infty [R_s(\lambda) + R_p(\lambda)] J_1(\lambda \rho_2) e^{j\sqrt{k_1^2 - \lambda^2}(2d+z_2)} \frac{d \lambda}{k_1}, \end{aligned} \quad (3.45)$$

where $R_p(\lambda)$ is the Fresnel reflection coefficient for a p -polarized incident plane wave at an angle of incidence $\theta = \sin^{-1}(\lambda/k_1)$,

$$R_p(\lambda) = \frac{\epsilon_2 \sqrt{k_1^2 - \lambda^2} - \epsilon_1 \sqrt{k_2^2 - \lambda^2}}{\epsilon_2 \sqrt{k_1^2 - \lambda^2} + \epsilon_1 \sqrt{k_2^2 - \lambda^2}}. \quad (3.46)$$

Corresponding expressions for the incident and reflected vector potentials for a unit dipole source of the *electric* type polarized vertically or horizontally are obtained from Eqs. (3.39), (3.40), (3.44) and (3.45) by interchanging $R_s(\lambda)$ and $R_p(\lambda)$.

The first-order vector potentials induced at \mathbf{r} on S_j by the surface element dS' are obtained by adding the incident and reflected vector potentials, Eqs. (3.39) and (3.40), or (3.44) and (3.45), appropriately weighed by the dipole amplitudes $-(\mathbf{n}' \times \mathbf{E}') \frac{dS'}{4\pi}$ and $-(\mathbf{n}' \times \mathbf{H}') \frac{dS'}{4\pi}$. The corresponding first-order induced fields are computed from Eqs. (3.12) and (3.13). These must be repeated for each source point $\mathbf{r}' \neq \mathbf{r}$ on S_j and the results added together to give the *total* first-order induced fields at \mathbf{r} . In principle, this procedure can be applied repeatedly to a given surface S_j to obtain physical-optics approximations to the successively higher order multiply scattered waves within the same surface. In the photolithography simulation problems we have studied, in which the inclined faces of the topography were sufficiently far apart, the effects of waves reflected more than twice from the same surface were found to be quite negligible.

If this procedure were used, the operation count per multiple-scattering calculation would be proportional to N^2 , where N is the number of surface elements on S_j . This would be prohibitively expensive for large 3-D problems. Instead, we use the multipole approximation to speed up the computation of the first-order induced fields.

3.7 The Multipole Approximation

Instead of treating the surface elements dS' on S_j as independent sources of radiation, it is more efficient, for the purpose of computing the multiply scattered fields, to group the N surface elements, or nodes, on S_j into P panels, each of which contains roughly the same number, $\approx N/P$, of nodes. For a piecewise-linear surface S_j , the panels can be chosen to be planar. The radiation field produced in the far zone by the magnetic current sources in a panel q consisting of the portion ΔS_q of S_j may be approximated by that of a collection of M multipoles located at the center of that panel,

$$\begin{aligned} \Delta \mathbf{A}_m^q(\mathbf{r}) &= \int_{\Delta S_q} -(\mathbf{n}' \times \mathbf{E}') \frac{e^{jk_1|\mathbf{r}-\mathbf{r}'|}}{4\pi|\mathbf{r}-\mathbf{r}'|} dS' \\ &\approx \sum_{l=0}^L \sum_{m=-l}^l \mathbf{a}_{lm}^q h_l^{(1)}(k_1 r) P_l^m(\cos \theta) e^{jm\phi}, \end{aligned} \quad (3.47)$$

where $\Delta \mathbf{A}_m^q$ is the magnetic vector potential produced by the sources in panel q and \mathbf{a}_{lm}^q are the corresponding multipole coefficients with respect to a coordinate system K_q centered at that panel,

$$\mathbf{a}_{lm}^q = \int_{\Delta S_q} -(\mathbf{n}' \times \mathbf{E}') \frac{jk_1(2l+1)(l-m)!}{4\pi(l+m)!} j_l(k_1 r') P_l^m(\cos \theta') e^{-jm\phi'} dS'. \quad (3.48)$$

In Eqs. (3.47) and (3.48), (r, θ, ϕ) and (r', θ', ϕ') are spherical polar coordinates of the points \mathbf{r} and \mathbf{r}' , respectively, relative to the distant coordinate system K_q . These equations follow from the series expansion for the Green function,

$$\frac{e^{jk_1|\mathbf{r}-\mathbf{r}'|}}{4\pi|\mathbf{r}-\mathbf{r}'|} = \sum_{l=0}^{\infty} \sum_{m=-l}^l \frac{jk_1(2l+1)(l-m)!}{4\pi(l+m)!} j_l(k_1 r') h_l^{(1)}(k_1 r) P_l^m(\cos \theta') P_l^m(\cos \theta) \times e^{-jm(\phi'-\phi)}, \quad (3.49)$$

where we have assumed that $r > r'$. Similarly, for the electric vector potential produced by panel q , we have

$$\Delta \mathbf{A}_e^q(\mathbf{r}) = \sum_{l=0}^L \sum_{m=-l}^l \mathbf{b}_{lm}^q h_l^{(1)}(k_1 r) P_l^m(\cos \theta) e^{jm\phi}, \quad (3.50)$$

where \mathbf{b}_{lm}^q are the electric multipole coefficients of panel q with respect to the coordinate system K_q ,

$$\mathbf{b}_{lm}^q = \int_{\Delta S_q} -(\mathbf{n}' \times \mathbf{H}') \frac{jk_1(2l+1)(l-m)!}{4\pi(l+m)!} j_l(k_1 r') P_l^m(\cos \theta') e^{-jm\phi'} dS'. \quad (3.51)$$

The multipole expansions Eqs. (3.47) and (3.50) converge rapidly when the field point \mathbf{r} is more than a wavelength away from the smallest sphere enclosing all the elements of the panel q . As a rule of thumb, the number of multipole coefficients $M = \sum_{l=0}^L (2l+1) = (L+1)^2$ needed to represent the field due to a panel q in the far zone accurately is on the order of the number of nodes in that panel, $M \approx N/P$. This assumes a fixed discretization rate on the order of 2π nodes per wavelength. Depending on the accuracy desired, fewer multipole coefficients than this may be used to reduce computation time. For sources in the panel p containing the field point \mathbf{r}

itself, or in the panels adjacent to panel p , the multipole approximation cannot be used. Instead, the individual contributions from the sources in these neighboring panels, Eqs. (3.37) and (3.38), must be used directly.

We may now use the physical-optics approximation to treat the interaction of the waves scattered from the distant panels, Eqs. (3.47) and (3.50), with the tangent plane at any point \mathbf{r} on S_j . Since the waves represented by Eqs. (3.47) and (3.50) are multipole waves of arbitrary orders, we need to generalize our earlier treatment of the reflection of dipole waves from a lossy plane surface to the case of higher-order multipole waves.

3.8 Generalized Sommerfeld Integrals

The problem of the reflection of a general multipole wave from a lossy plane surface was first solved by Chang and Mei [12, 38]. The geometry of the problem is the same as in Fig. 3.3, except that the point dipole is replaced by a collection of M point multipoles. The basic idea of Chang and Mei's approach is to express the incident multipole wave as a superposition of cylindrical waves propagating in various directions,

$$h_l^{(1)}(k_1 r) P_l^m(\cos \theta) e^{jm\phi} = e^{jm\phi} \int_0^\infty f_{m,l}(\lambda) J_m(\lambda \rho) e^{j\sqrt{k_1^2 - \lambda^2}|z|} d\lambda. \quad (3.52)$$

Chang and Mei gave a closed-form expression for $f_{m,m}(\lambda)$,

$$f_{m,m}(\lambda) = \left(\frac{\lambda}{k_1}\right)^{m+1} \frac{P_m^m(0)}{\sqrt{k_1^2 - \lambda^2}}, \quad (3.53)$$

and derived a recurrence relationship for computing $f_{m,l}(\lambda)$ for $l > m$,

$$\frac{(l-m+1)}{(2l+1)} f_{m,l+1}(\lambda) = -j\sqrt{1-\lambda^2/k_1^2} f_{m,l}(\lambda) + \frac{(l+m)}{(2l+1)} f_{m,l-1}(\lambda). \quad (3.54)$$

Actually, the coefficients $f_{m,l}(\lambda)$ are proportional to the associated Legendre polynomials $P_l^m(x)$. This can be seen from the following textbook relationships for the associated Legendre polynomials,

$$P_m^m(x) = (\sqrt{1-x^2})^m P_m^m(0), \quad (3.55)$$

$$\frac{(l-m+1)}{(2l+1)} P_{l+1}^m(x) = x P_l^m(x) - \frac{(l+m)}{(2l+1)} P_{l-1}^m(x). \quad (3.56)$$

If we let $x = \sqrt{1 - \lambda^2/k_1^2}$, Eqs. (3.55) and (3.56) may be rewritten as

$$P_m^m(x) = \left(\frac{\lambda}{k_1}\right)^m P_m^m(0), \quad (3.57)$$

$$\frac{(l-m+1)}{(2l+1)} \left[\frac{P_{l+1}^m(x)}{j^{l+1-m}} \right] = -j \sqrt{1 - \lambda^2/k_1^2} \left[\frac{P_l^m(x)}{j^{l-m}} \right] + \frac{(l+m)}{(2l+1)} \left[\frac{P_{l-1}^m(x)}{j^{l-1-m}} \right]. \quad (3.58)$$

Comparing Eq. (3.53) with Eq. (3.57) and Eq. (3.54) with Eq. (3.58), we find that the quantities $f_{m,l}(\lambda)$ and $[P_l^m(x)/j^{l-m}]$ are proportional to each other, and the proportionality constant is $(\lambda/k_1)/\sqrt{k_1^2 - \lambda^2}$. Hence,

$$f_{m,l}(\lambda) = j^{m-l} P_l^m \left(\sqrt{1 - \lambda^2/k_1^2} \right) \frac{\lambda}{k_1 \sqrt{k_1^2 - \lambda^2}}. \quad (3.59)$$

Eq. (3.59) is correct only when $\cos \theta > 0$ in Eq. (3.52). When $\cos \theta < 0$, the argument of the associated Legendre polynomial in Eq. (3.59) should have a minus sign.

An integral representation equivalent to Eq. (3.52) with $f_{m,l}(\lambda)$ given by Eq. (3.59) was known as early as 1954 [44]. In this sense, Chang and Mei rediscovered the result more than twenty years later.

We may now describe the reflection of the multipole waves from the lossy plane surface. The results are similar to those for the dipole waves discussed previously. For a unit, vertically polarized multipole source of the *magnetic* type, the incident and reflected vector potentials are given by

$$\mathbf{A}_m^{(z)\text{inc}}(\mathbf{r}) = \mathbf{z}_2 e^{jm\phi_2} \int_0^\infty f_{m,l}(\lambda) J_m(\lambda\rho_2) e^{j\sqrt{k_1^2 - \lambda^2}|z_2|} d\lambda, \quad (3.60)$$

$$\mathbf{A}_m^{(z)\text{refl}}(\mathbf{r}) = \mathbf{z}_2 e^{jm\phi_2} \int_0^\infty R_s(\lambda) f_{m,l}(\lambda) J_m(\lambda\rho_2) e^{j\sqrt{k_1^2 - \lambda^2}(2d+z_2)} d\lambda, \quad (3.61)$$

where (r_2, θ_2, ϕ_2) and (ρ_2, ϕ_2, z_2) are the spherical and cylindrical polar coordinates, respectively, of the field point \mathbf{r} with respect to a coordinate system centered at the multipole source, as shown in Fig. 3.3, and $R_s(\lambda)$ is given by Eq. (3.41).

For a unit multipole source of the magnetic type circularly polarized in the horizontal direction, the incident and reflected vector potentials are given by

$$\mathbf{A}_m^{(\pm)\text{inc}}(\mathbf{r}) = (\mathbf{x}_2 \pm j\mathbf{y}_2) e^{jm\phi_2} \int_0^\infty f_{m,l}(\lambda) J_m(\lambda\rho_2) e^{j\sqrt{k_1^2 - \lambda^2}|z_2|} d\lambda, \quad (3.62)$$

$$\begin{aligned} \mathbf{A}_m^{(\pm)\text{refl}}(\mathbf{r}) = & (\mathbf{x}_2 \pm j\mathbf{y}_2) e^{jm\phi_2} \int_0^\infty R_p(\lambda) f_{m,l}(\lambda) J_m(\lambda\rho_2) e^{j\sqrt{k_1^2 - \lambda^2}(2d+z_2)} d\lambda \\ & \pm jz_2 e^{j(m\pm 1)\phi_2} \int_0^\infty [R_s(\lambda) + R_p(\lambda)] f_{m,l}(\lambda) J_{m\pm 1}(\lambda\rho_2) e^{j\sqrt{k_1^2 - \lambda^2}(2d+z_2)} \\ & \times \sqrt{k_1^2 - \lambda^2} \frac{d\lambda}{\lambda}, \end{aligned} \quad (3.63)$$

where $R_p(\lambda)$ is given by Eq. (3.46).

Corresponding expressions for the incident and reflected vector potentials for a unit multipole source of the *electric* type polarized vertically or horizontally are obtained from Eqs. (3.60) to (3.63) by interchanging $R_s(\lambda)$ and $R_p(\lambda)$.

The first-order vector potentials induced at \mathbf{r} on S_j by the distant panel q are obtained adding the incident and reflected vector potentials, Eqs. (3.60) and (3.61), or (3.62) and (3.63), appropriately weighed by the multipole coefficients \mathbf{a}_{lm}^q and \mathbf{b}_{lm}^q , and summing over the multipole indices (l, m) . The corresponding first-order induced fields are computed from Eqs. (3.12) and (3.13). These must be repeated for each distant panel q and the results added together. To these we must add the direct contributions from the neighboring panels using Sommerfeld's results for the individual dipole sources discussed in Section 3.6. If this procedure were used to compute the distant-panel contributions to the first-order induced fields at the N nodes of S_j , the operation count would be proportional to $NMP \approx N(N/P)P = N^2$, since each node would require the evaluation of M multipole terms for each of approximately P distant panels. This would again be prohibitively expensive for large 3-D problems. Instead, we compute the distant-panel contributions using the technique of multipole acceleration.

3.9 Multipole Acceleration

The Fast Multipole Method (FMM) was developed by Rokhlin for the rapid iterative solution of the integral equations arising in acoustic [11] and electromagnetic [14] scattering. The technique can be adapted for use in our case to accelerate the computation of the distant-panel contributions to the physical-optics induced fields discussed in the last section. The key idea of FMM is that, for each pair of sufficiently separated panels p and q , the fields on panel p due to the M multipoles centered at panel q can be approximated by the first M terms of a multipole expansion about a *local* coordinate system K_p centered at panel p , instead of the first M terms of a multipole expansion about the *distant* coordinate system K_q .

Consider the total magnetic vector potential induced on panel p by vertically polarized magnetic multipoles in the distant panel q . This is obtained by adding the incident and reflected vector potentials, Eqs. (3.60) and (3.61), appropriately weighed by the z_2 -components $(a_{lm}^q)_z$ of the multipole coefficients and summing over the multipole indices (l, m) ,

$$\mathbf{A}^{(z)q}(\mathbf{r}) = \mathbf{z}_2 \sum_{l,m} (a_{lm}^q)_z e^{jm\phi_2} \int_0^\infty \left[e^{-j\sqrt{k_1^2 - \lambda^2} z_2} + R_s(\lambda) e^{j\sqrt{k_1^2 - \lambda^2} (2d+z_2)} \right] f_{m,l}(\lambda) \times J_m(\lambda\rho_2) d\lambda, \quad (3.64)$$

where (ρ_2, z_2, ϕ_2) are cylindrical polar coordinates of the field point \mathbf{r} on panel p with respect to the distant coordinate system K_q , and we have used the fact that $z_2 < 0$ in the geometry of Fig. 3.3. In order to transform Eq. (3.64) into a multipole expansion about the local coordinate system K_p , we first rewrite this equation using the integral representation of the Bessel function,

$$J_m(\lambda\rho_2) = \frac{1}{2\pi} \int_0^{2\pi} d\beta e^{j\lambda\rho_2 \cos\beta + jm(\beta - \frac{\pi}{2})}. \quad (3.65)$$

Substituting Eq. (3.65) into Eq. (3.64) and changing the variable of integration β into $(\beta + \phi_2)$, we obtain

$$\mathbf{A}^{(z)q}(\mathbf{r}) = \mathbf{z}_2 \sum_{l,m} (a_{lm}^q)_z \frac{1}{2\pi} \int_0^{2\pi} d\beta \int_0^\infty d\lambda \left[e^{-j\sqrt{k_1^2 - \lambda^2} z_2} + R_s(\lambda) e^{j\sqrt{k_1^2 - \lambda^2} (2d+z_2)} \right] \times f_{m,l}(\lambda) e^{j\lambda\rho_2 \cos(\beta - \phi_2) + jm(\beta - \frac{\pi}{2})}. \quad (3.66)$$

Assume for the moment that the axes of K_q are parallel to those of K_p and that the origin of K_q has the coordinates (ρ_q, z_q, ϕ_q) with respect to coordinate system K_p , as shown in Fig. 3.4. From this figure and Fig. 3.3, it can be seen that the coordinates of the field point \mathbf{r} in the two coordinate systems are related by

$$z_2 = z_1 - z_q, \quad (3.67)$$

$$\rho_2 \cos(\beta - \phi_2) = \rho_1 \cos(\beta - \phi_1) - \rho_q \cos(\beta - \phi_q), \quad (3.68)$$

where (ρ_1, z_1, ϕ_1) are the coordinates of the field point \mathbf{r} with respect to the local system K_p . Substituting Eqs. (3.67) to (3.68) into Eq. (3.66) and rearranging terms, we obtain the desired *local* expansion for the total vector potential due to vertically polarized magnetic multipoles in panel q ,

$$\begin{aligned} \mathbf{A}^{(z)q}(\mathbf{r}) = z_1 \frac{1}{2\pi} \int_0^{2\pi} d\beta \int_0^\infty d\lambda e^{j\lambda\rho_1 \cos(\beta-\phi_1)} \left[e^{-j\sqrt{k_1^2-\lambda^2}z_1} + R_s(\lambda) e^{j\sqrt{k_1^2-\lambda^2}z_1} \right] \\ \times G_q(\lambda, \beta, \rho_q, z_q, \phi_q), \end{aligned} \quad (3.69)$$

where

$$G_q(\lambda, \beta, \rho_q, z_q, \phi_q) = \sum_{l,m} (a_{lm}^q)_{zfm,l}(\lambda) e^{-j\lambda\rho_q \cos(\beta-\phi_q) + jm(\beta-\frac{\pi}{2})} e^{j\sqrt{k_1^2-\lambda^2}z_q}, \quad (3.70)$$

and we have used the fact that $z_q = d$. Note that the quantity G_q is independent of the coordinates (ρ_1, z_1, ϕ_1) of the field point. Hence, in summing the contributions from all the distant panels q , we can carry out the summation over q in Eq. (3.69) prior to evaluating the integrals over β and λ for the different field points (ρ_1, z_1, ϕ_1) on panel p . This results in substantial saving in computation time for large 3-D problems, as will be shown in a later section.

It should be noted that the integral over λ in Eq. (3.69) is convergent when $z_1 < d$. This is due to the factor $e^{j\sqrt{k_1^2-\lambda^2}z_q}$ in Eq. (3.70). From Eq. (3.42) this factor can be rewritten as $e^{-\mu_1 z_q} = e^{-\mu_1 d}$, which approaches $e^{-\lambda d}$ as $\lambda \rightarrow \infty$, since $\text{Re } \mu_1 \geq 0$.

In general, the axes of the coordinate system K_p are *not* parallel to those of K_q . The reason is that the expressions Eqs. (3.61) and (3.63) for the physical-optics reflected waves are valid only in a coordinate system in which the z -axis is normal to

the tangent plane under consideration. Hence, K_p and K_q are generally chosen so that their z -axes are normal to their respective panels p and q , which, however, may be arbitrarily oriented. The multipole coefficients $\mathbf{a}_{lm}^{(q)}$ and $\mathbf{b}_{lm}^{(q)}$ appearing in the *distant* expansions Eqs. (3.47) and (3.50) with respect to K_q must first be transformed into multipole coefficients with respect to the local coordinate system K_p before they may be used in Eq. (3.70). Suppose (α, β, γ) are Euler angles characterizing the rotation of the axes of K_q into those of K_p . Then, the magnetic multipole coefficients $\tilde{\mathbf{a}}_{lm}^q$ of panel q with respect to the local system K_p are obtained from the magnetic multipole coefficients \mathbf{a}_{lm}^q with respect to the distant system K_q by

$$\tilde{\mathbf{a}}_{lm}^q = \sum_{m'=-l}^l (-1)^{m-m'} \sqrt{\frac{(l-m)!(l+m')!}{(l+m)!(l-m')!}} \mathcal{D}_{mm'}^{(l)}(\alpha, \beta, \gamma) \mathbf{a}_{lm'}^q, \quad (3.71)$$

where $\mathcal{D}_{mm'}^{(l)}(\alpha, \beta, \gamma)$ are matrix elements of the irreducible representations of the rotation group [40]. A similar transformation holds for the electric multipole coefficients \mathbf{b}_{lm}^q . The computation of the matrix elements $\mathcal{D}_{mm'}^{(l)}$ by means of recurrence relationship is discussed in Appendix H.

3.10 Numerical Evaluation of the Integrals

The integrand in Eq. (3.69) contains the functions $R_s(\lambda)$ and $f_{m,l}(\lambda)$ which, according to Eqs. (3.41) and (3.59), depend on quantities $\sqrt{k_1^2 - \lambda^2}$ and $\sqrt{k_2^2 - \lambda^2}$ which have branch cuts in the complex λ -plane. Following Chang [38], we choose these branch cuts to be vertical, as shown in Fig. 3.5. From this figure, it is clear that when k_1 is real or has a very small imaginary part, the path of integration along the positive real axis will pass very close to the branch point at $\lambda = k_1$. Since $f_{m,l}(\lambda)$ given by Eq. (3.59) contains the denominator $\sqrt{k_1^2 - \lambda^2}$, the integrand in Eq. (3.69) will be large and rapidly changing near $\lambda = k_1$. Chang [38] avoided this difficulty by deforming the path of integration to go around the branch point at a sufficiently large distance. This, however, means increasing the total length of the integration path and hence the amount of computation labor. We instead chose to avoid the singularity by changing

the variable of integration from λ to μ_1 , where, as in Eq. (3.42),

$$\mu_1 = -j\sqrt{k_1^2 - \lambda^2}, \text{ Re } \mu \geq 0.$$

In the complex μ_1 -plane, there is no longer any singularity at $\lambda = k_1$, since the offending denominator $\sqrt{k_1^2 - \lambda^2}$ is transformed away,

$$\frac{\lambda d\lambda}{\sqrt{k_1^2 - \lambda^2}} = -jd\mu_1. \quad (3.72)$$

Next, we discuss the integration over β in Eq. (3.69). Since the quantity G_q given by Eq. (3.70) contains the phase factor $e^{-j\lambda\rho_q \cos(\beta-\phi_q)+jm\beta}$, in order to sample the phase of G_q correctly, the discretization of the range $[0, 2\pi]$ of the β integration should be no coarser than $\Delta\beta \leq \min[\frac{2\pi}{2\lambda\rho_q}, \frac{2\pi}{2m}]$. Since ρ_q is the horizontal distance between a pair of sufficiently separately panels, it can be equal to many wavelengths for large 3-D problems. Hence, over the range of values of λ for which the integrand of Eq. (3.69) is significant, the quantity $1/(\lambda\rho_q)$ can be very small. This would necessitate the use of a very fine grid for the β integration. In order to avoid this problem, we employ the technique of asymptotic integration for the β integration for large values of λ .

When $\lambda\rho_q$ is greater than some parameter Λ_0 to be discussed later, the integral over β in Eq. (3.69) may be approximated by its asymptotic value,

$$\begin{aligned} \frac{1}{2\pi} \int_0^{2\pi} d\beta e^{j\lambda\rho_1 \cos(\beta-\phi_1) - j\lambda\rho_q \cos(\beta-\phi_q) + jm(\beta-\frac{\pi}{2})} \\ \approx \sqrt{\frac{1}{2\pi\lambda\rho_q}} \left[e^{j\lambda\rho_1 \cos(\phi_q-\phi_1) - j(\lambda\rho_q - \frac{\pi}{4}) + jm(\phi_q - \frac{\pi}{2})} \right. \\ \left. + e^{-j\lambda\rho_1 \cos(\phi_q-\phi_1) + j(\lambda\rho_q - \frac{\pi}{4}) + jm(\phi_q + \frac{\pi}{2})} \right]. \quad (3.73) \end{aligned}$$

To show this, we call the phase of the integrand on the LHS of Eq. (3.73) $\Psi(\beta)$ and expand it about its stationary point,

$$\Psi(\beta) = \Psi(\beta_0) + \frac{1}{2} \left. \frac{d^2\Psi(\beta)}{d\beta^2} \right|_{\beta=\beta_0} (\beta - \beta_0)^2 + \dots, \quad (3.74)$$

where β_0 is a stationary point determined by

$$0 = \left. \frac{d\Psi(\beta)}{d\beta} \right|_{\beta=\beta_0} = -\lambda\rho_1 \sin(\beta_0 - \phi_1) + \lambda\rho_q \sin(\beta_0 - \phi_q) + m. \quad (3.75)$$

In the limit $\lambda\rho_q \gg 1$, Eq. (3.75) may be approximated by the simpler condition $0 = \lambda\rho_q \sin(\beta_0 - \phi_q)$. This has two solutions, $\beta_0 = \phi_q$ or $\beta_0 = \phi_q + \pi$, each of which contributes a term to the integral on the LHS of Eq. (3.73). For $\beta_0 = \phi_q$, Eq. (3.74) gives

$$\Psi(\beta) \approx \lambda\rho_1 \cos(\phi_q - \phi_1) - \lambda\rho_q + m \left(\phi_q - \frac{\pi}{2} \right) + \frac{\lambda\rho_q}{2} (\beta - \phi_q)^2, \quad (3.76)$$

while for $\beta_0 = \phi_q + \pi$, we have

$$\Psi(\beta) \approx -\lambda\rho_1 \cos(\phi_q - \phi_1) + \lambda\rho_q + m \left(\phi_q + \frac{\pi}{2} \right) - \frac{\lambda\rho_q}{2} (\beta - \phi_q - \pi)^2. \quad (3.77)$$

Hence, the integral on the LHS of Eq. (3.73) becomes

$$\begin{aligned} & \frac{1}{2\pi} \int_0^{2\pi} d\beta e^{j\lambda\rho_1 \cos(\beta - \phi_1) - j\lambda\rho_q \cos(\beta - \phi_q) + jm(\beta - \frac{\pi}{2})} \\ & \approx \frac{1}{2\pi} \int_0^{2\pi} d\beta \left[e^{j\lambda\rho_1 \cos(\phi_q - \phi_1) - j\lambda\rho_q + jm(\phi_q - \frac{\pi}{2}) + j\frac{\lambda\rho_q}{2} (\beta - \phi_q)^2} \right. \\ & \quad \left. + e^{-j\lambda\rho_1 \cos(\phi_q - \phi_1) + j\lambda\rho_q + jm(\phi_q + \frac{\pi}{2}) - j\frac{\lambda\rho_q}{2} (\beta - \phi_q - \pi)^2} \right]. \quad (3.78) \end{aligned}$$

The integration over β in Eq. (3.78) may be performed in the limit $\lambda\rho_q \gg 1$,

$$\int_0^{2\pi} d\beta e^{\pm j\frac{\lambda\rho_q}{2} (\beta - \phi_q)^2} \approx e^{\pm j\frac{\pi}{4}} \sqrt{\frac{2\pi}{\lambda\rho_q}}. \quad (3.79)$$

Substituting Eq. (3.79) into Eq. (3.78) then gives Eq. (3.73).

We now discuss the choice of the parameter Λ_0 . From the discussion following Eq. (3.75), it is clear that our result for the asymptotic integration, Eq. (3.73), is valid when $\Lambda_0 \gg \max[1, m]$ and $\rho_q \gg \rho_1$. The latter condition is valid when panels p and q are well separated, which is usually the case, since ρ_q must be at least a few times ρ_1 in order for the multipole approximation to be usable. Next, in the photolithography simulation problems we have studied using the present technique, the maximum multipole order used was usually 5 or smaller. Hence, the condition $\Lambda_0 \gg m$ is satisfied when $\Lambda_0 \approx 50$. In practice, a value of $\Lambda_0 = 40$ was found to be adequate.

In Eq. (3.73), we seem to have lost the advantage of FMM in being able to carry out the summation over the distant-panel index q before evaluating the integral over

λ for different field points (ρ_1, z_1, ϕ_1) . This is because the terms on the RHS of Eq. (3.73) contain the factor $e^{\pm j\lambda\rho_1 \cos(\phi_q - \phi_1)}$, which *cannot* be factorized into a product of two terms one of which depends only on (ρ_1, z_1, ϕ_1) and the other of which depends only on (ρ_q, z_q, ϕ_q) . The solution to this difficulty is to discretize the range $[0, 2\pi]$ into a number $n \geq 2L$ of intervals, where L is the maximum multipole order used. Then one defines quantities $J_1^{(z)}(\lambda, i)$ and $J_2^{(z)}(\lambda, i)$, $i = 1$ to n , as follows,

$$J_1^{(z)}(\lambda, i) = \sum_q'' \sqrt{\frac{1}{2\pi\lambda\rho_q}} e^{-j(\lambda\rho_q - \frac{\pi}{4}) + j\sqrt{k_1^2 - \lambda^2}d} \sum_{l,m} (a_{lm}^q)_z f_{m,l}(\lambda) e^{jm(\theta_i - \frac{\pi}{2})}, \quad (3.80)$$

$$J_2^{(z)}(\lambda, i) = \sum_q'' \sqrt{\frac{1}{2\pi\lambda\rho_q}} e^{j(\lambda\rho_q - \frac{\pi}{4}) + j\sqrt{k_1^2 - \lambda^2}d} \sum_{l,m} (a_{lm}^q)_z f_{m,l}(\lambda) e^{jm(\theta_i + \frac{\pi}{2})}, \quad (3.81)$$

where $\theta_i = \frac{2\pi(i-0.5)}{n}$ is the center of the i th interval and the double prime on the summation over q means that only those distant panels q are included whose coordinates (ρ_q, z_q, ϕ_q) with respect to the local panel p satisfy the following two conditions: (1) $\lambda\rho_q > \Lambda_0$, and (2) $\frac{2\pi(i-1)}{n} \leq \phi_q < \frac{2\pi i}{n}$. The first condition means that we use the technique of asymptotic integration for the β integration whenever the product $\lambda\rho_q$ exceeds the parameter Λ_0 . The second condition means that we sort the ϕ_q coordinates of the distant panels q into n bins of width $\frac{2\pi}{n}$ centered at $\theta_i, i = 1$ to n . Subsequent summation over the index i then takes the place of the β integration.

The quantities $J_1^{(z)}(\lambda, i)$ and $J_2^{(z)}(\lambda, i)$, $i = 1$ to n , account for the contribution to the λ integration at each point λ from those distant panels q for which $\lambda\rho_q > \Lambda_0$. There can also be combinations of values of λ and ρ_q for which $\lambda\rho_q \leq \Lambda_0$. For such combinations of λ and ρ_q , we accumulate the summation over q in another quantity $I^{(z)}(\lambda, \beta)$,

$$I^{(z)}(\lambda, \beta) = \frac{1}{2\pi} \sum_q' e^{-j\lambda\rho_q \cos(\beta - \phi_q) + j\sqrt{k_1^2 - \lambda^2}d} \sum_{l,m} (a_{lm}^q)_z f_{m,l}(\lambda) e^{jm(\beta - \frac{\pi}{2})}, \quad (3.82)$$

where the prime on the summation over q means that only those distant panels q are included for which $\lambda\rho_q \leq \Lambda_0$. Since there is a minimum $\rho_q = \rho_q^{\min}$ for which the multipole approximation is valid, $I(\lambda, \beta)$ is non-vanishing only for $\lambda \leq \Lambda_0/\rho_q^{\min} = \lambda_0$.

The total contribution from the vertically polarized magnetic multipoles in all the distant panels to the local expansion for the vector potential is obtained by summing

Eq. (3.69) over the distant-panel index q ,

$$\begin{aligned}
\mathbf{A}^{(z)}(\mathbf{r}) &= \sum_q \mathbf{A}^{(z)q}(\mathbf{r}) \\
&= \mathbf{z}_1 \int_0^{\lambda_0} d\lambda \left[e^{-j\sqrt{k_1^2 - \lambda^2} z_1} + R_s(\lambda) e^{j\sqrt{k_1^2 - \lambda^2} z_1} \right] \int_0^{2\pi} d\beta e^{j\lambda \rho_1 \cos(\beta - \phi_1)} I^{(z)}(\lambda, \beta) \\
&\quad + \mathbf{z}_1 \int_0^\infty d\lambda \left[e^{-j\sqrt{k_1^2 - \lambda^2} z_1} + R_s(\lambda) e^{j\sqrt{k_1^2 - \lambda^2} z_1} \right] \sum_{i=1}^n \left[e^{j\lambda \rho_1 \cos(\theta_i - \phi_1)} J_1^{(z)}(\lambda, i) \right. \\
&\quad \left. + e^{-j\lambda \rho_1 \cos(\theta_i - \phi_1)} J_2^{(z)}(\lambda, i) \right]. \quad (3.83)
\end{aligned}$$

The first λ integral in Eq. (3.83) has finite limits, since $I^{(z)}(\lambda, \beta)$ is non-zero only for $\lambda \leq \lambda_0$. The second λ integral in Eq. (3.83) has an infinite limit. To accelerate convergence of this integral, the path of integration is deformed in the complex λ -plane as shown in Fig. 3.5. The term containing $J_1^{(z)}(\lambda, i)$ in Eq. (3.83) is integrated along the path $\Gamma_a + \Gamma_c$, since along Γ_c , the $e^{-j\lambda \rho_q}$ factor in $J_1^{(z)}(\lambda, i)$ is exponentially decaying. Similarly, the term containing $J_2^{(z)}(\lambda, i)$ is integrated along the path $\Gamma_a + \Gamma_b$, since along Γ_b , the $e^{j\lambda \rho_q}$ factor in $J_2^{(z)}(\lambda, i)$ is exponentially decaying. Writing the total contribution from the vertically polarized magnetic multipoles in all the distant panels to the vector potential in the form

$$\mathbf{A}^{(z)}(\mathbf{r}) = \mathbf{z}_1 A^{(z)}(\mathbf{r}), \quad (3.84)$$

we obtain the final result

$$\begin{aligned}
A^{(z)}(\mathbf{r}) &= \int_{\Gamma_a} d\lambda \left[e^{-j\sqrt{k_1^2 - \lambda^2} z_1} + R_s(\lambda) e^{j\sqrt{k_1^2 - \lambda^2} z_1} \right] \int_0^{2\pi} d\beta e^{j\lambda \rho_1 \cos(\beta - \phi_1)} I^{(z)}(\lambda, \beta) \\
&\quad + \int_{\Gamma_a + \Gamma_c} d\lambda \left[e^{-j\sqrt{k_1^2 - \lambda^2} z_1} + R_s(\lambda) e^{j\sqrt{k_1^2 - \lambda^2} z_1} \right] \sum_{i=1}^n e^{j\lambda \rho_1 \cos(\theta_i - \phi_1)} J_1^{(z)}(\lambda, i) \\
&\quad + \int_{\Gamma_a + \Gamma_b} d\lambda \left[e^{-j\sqrt{k_1^2 - \lambda^2} z_1} + R_s(\lambda) e^{j\sqrt{k_1^2 - \lambda^2} z_1} \right] \sum_{i=1}^n e^{-j\lambda \rho_1 \cos(\theta_i - \phi_1)} J_2^{(z)}(\lambda, i). \quad (3.85)
\end{aligned}$$

A similar result is obtained for the total magnetic vector potential induced on panel p by *horizontally polarized* magnetic multipoles in all the distant panels, starting from Eqs. (3.62) and (3.63). We write this total magnetic vector potential as

$$\mathbf{A}^{(\pm)}(\mathbf{r}) = (\mathbf{e}_{\rho_1} \pm j\mathbf{e}_{\phi_1}) A_{\text{hor}}^{(\pm)}(\mathbf{r}) \pm j\mathbf{z}_1 A_{\text{ver}}^{(\pm)}(\mathbf{r}), \quad (3.86)$$

where the cylindrical unit vectors \mathbf{e}_{ρ_1} and \mathbf{e}_{ϕ_1} are related to the Cartesian unit vectors \mathbf{x}_1 and \mathbf{y}_1 by

$$(\mathbf{x}_1 \pm j\mathbf{y}_1) = (\mathbf{e}_{\rho_1} \pm j\mathbf{e}_{\phi_1})e^{\pm j\phi_1}. \quad (3.87)$$

The horizontal component $A_{\text{hor}}^{(\pm)}(\mathbf{r})$ is then given by

$$\begin{aligned} A_{\text{hor}}^{(\pm)}(\mathbf{r}) = & e^{\pm j\phi_1} \int_{\Gamma_a} d\lambda \left[e^{-j\sqrt{k_1^2 - \lambda^2} z_1} + R_p(\lambda) e^{j\sqrt{k_1^2 - \lambda^2} z_1} \right] \int_0^{2\pi} d\beta e^{j\lambda\rho_1 \cos(\beta - \phi_1)} I^{(\pm)}(\lambda, \beta) \\ & + e^{\pm j\phi_1} \int_{\Gamma_a + \Gamma_c} d\lambda \left[e^{-j\sqrt{k_1^2 - \lambda^2} z_1} + R_p(\lambda) e^{j\sqrt{k_1^2 - \lambda^2} z_1} \right] \sum_{i=1}^n e^{j\lambda\rho_1 \cos(\theta_i - \phi_1)} J_1^{(\pm)}(\lambda, i) \\ & + e^{\pm j\phi_1} \int_{\Gamma_a + \Gamma_b} d\lambda \left[e^{-j\sqrt{k_1^2 - \lambda^2} z_1} + R_p(\lambda) e^{j\sqrt{k_1^2 - \lambda^2} z_1} \right] \sum_{i=1}^n e^{-j\lambda\rho_1 \cos(\theta_i - \phi_1)} J_2^{(\pm)}(\lambda, i), \end{aligned} \quad (3.88)$$

where $I^{(\pm)}(\lambda, \beta)$, $J_1^{(\pm)}(\lambda, i)$ and $J_2^{(\pm)}(\lambda, i)$ are obtained from Eqs. (3.80) to (3.82) by replacing the multipole component $(a_{lm}^q)_z$ in these equations by the component $\frac{1}{2} [(a_{lm}^q)_x \mp j(a_{lm}^q)_y]$. Similarly, the vertical component $A_{\text{ver}}^{(\pm)}(\mathbf{r})$ is given by

$$\begin{aligned} A_{\text{ver}}^{(\pm)}(\mathbf{r}) = & \int_{\Gamma_a} d\lambda S(\lambda) \frac{\sqrt{k_1^2 - \lambda^2}}{\lambda} e^{j\sqrt{k_1^2 - \lambda^2} z_1} \int_0^{2\pi} d\beta e^{j\lambda\rho_1 \cos(\beta - \phi_1)} e^{\pm j(\beta - \frac{\pi}{2})} I^{(\pm)}(\lambda, \beta) \\ & + \int_{\Gamma_a + \Gamma_c} d\lambda S(\lambda) \frac{\sqrt{k_1^2 - \lambda^2}}{\lambda} e^{j\sqrt{k_1^2 - \lambda^2} z_1} \sum_{i=1}^n e^{j\lambda\rho_1 \cos(\theta_i - \phi_1)} e^{\pm j(\theta_i - \frac{\pi}{2})} J_1^{(\pm)}(\lambda, i) \\ & + \int_{\Gamma_a + \Gamma_b} d\lambda S(\lambda) \frac{\sqrt{k_1^2 - \lambda^2}}{\lambda} e^{j\sqrt{k_1^2 - \lambda^2} z_1} \sum_{i=1}^n e^{-j\lambda\rho_1 \cos(\theta_i - \phi_1)} e^{\pm j(\theta_i + \frac{\pi}{2})} J_2^{(\pm)}(\lambda, i), \end{aligned} \quad (3.89)$$

where $S(\lambda) = R_s(\lambda) + R_p(\lambda)$.

What we actually need are the tangential fields rather than the vector potentials. The former can be computed from the latter by Eqs. (3.12) and (3.13). The resulting expressions for the tangential fields are given in full in Appendix G.

3.11 Operation Count

The number of floating-point operations required for each computation of multiple scattering within a surface, using the multipole accelerated physical-optics technique discussed above, can be estimated as follows:

Step 1: The $2M$ multipole coefficients for each of the P panels are computed using Eqs. (3.48) and (3.51). Since there are on the average N/P nodes per panel, each

evaluation of the integral in Eq. (3.48) or (3.51) requires $O(N/P)$ operations. Hence, the total operation count for this step is $c_1 M(N/P)P = c_1 MN$ for some constant c_1 .

Step 2: For each pair of sufficiently separated panels, the multipole coefficients with respect to the local system are computed from those with respect to the distant system using Eq. (3.71). For each l , the quantities $\tilde{\mathbf{a}}_{lm}^q$ may be regarded as a column vector of length $(2l+1)$. Hence, the matrix-vector multiplication represented by Eq. (3.71) requires $O[(2l+1)^2]$ operations. To do this for all l from 0 to L therefore requires $O[\sum_{l=0}^L (2l+1)^2] \sim O(L^3) \sim O(M^{3/2})$ operations. Since there are approximately P^2 pairs of sufficiently separated panels, the total operation count for this step is $c_2 M^{3/2} P^2$ for some constant c_2 .

Step 3: For each panel, the quantities $J_1^{[z(\pm)]}(\lambda, i)$, $J_2^{[z(\pm)]}(\lambda, i)$ and $I^{[z(\pm)]}(\lambda, \beta)$ are computed using Eqs. (3.80) to (3.82) and similar equations for the (\pm) quantities. The summation over (l, m) in these equations is an $O(M)$ process, while the summation over q is an $O(P)$ process, since there are approximately P distant panels for each of the P panels. Hence, the total operation count for this step is $c_3 MP^2$ for some constant c_3 . Notice that $c_3 \gg 1$, since the quantities $J_1^{[z(\pm)]}(\lambda, i)$, etc. must be computed for each λ, i and β .

Step 4: For each panel, the distant-panel contributions to the tangential fields given by Eqs. (G.9) to (G.12), (G.20) to (G.23) and (G.28) to (G.31), are evaluated at each of the N/P nodes of that panel. The total operation count for this step is $c_4(N/P)P = c_4 N$. Again, $c_4 \gg 1$, since each of these field expressions involves an integration over λ and an integration over β or a summation over i .

Step 5: For each panel, the neighboring-panel contributions to the tangential fields are evaluated at each of the N/P nodes of that panel, as discussed in Section G.2 of Appendix G. For each node, we have to add the contributions from all $\approx N/P$ nodes in the neighboring panels. The total operation count for this step is $c_5(N/P)^2 P = c_5 N^2/P$ for some constant c_5 . Again, $c_5 \gg 1$, since the contribution from each neighboring node involves integrations over λ and β .

Adding the operation counts for the above five steps, the total operation count T

for computing the first-order physical-optics induced fields on S is estimated to be

$$\begin{aligned} T &= c_1 MN + c_2 M^{3/2} P^2 + c_3 MP^2 + c_4 N + c_5 \frac{N^2}{P} \\ &\approx (c_1 + c_5) \frac{N^2}{P} + c_2 N^{3/2} \sqrt{P} + c_3 NP + c_4 N , \end{aligned} \quad (3.90)$$

where we have used the fact that $M \approx N/P$. In practice, the most time consuming steps in our algorithm are those involving generalized Sommerfeld integrals, namely, Steps 3 to 5. This was found to be the case for all the photolithography simulation problems we have studied, with N as large as tens of thousands. Counting only Steps 3 to 5, we obtain a simpler estimate for T ,

$$T \approx c_5 \frac{N^2}{P} + c_3 NP + c_4 N . \quad (3.91)$$

Minimizing this expression with respect to P , we obtain for the optimum operation count of our algorithm

$$T_{\text{opt}} \approx 2\sqrt{c_3 c_5} N^{3/2} + c_4 N . \quad (3.92)$$

On the other hand, if multipole acceleration were not used, the operation count would be $c_5 N^2$, which would be significantly greater than T_{opt} for large N .

3.12 Application to Reflective Notching

As we do not have a Method-of-Moments (MOM) computer code capable of handling 3-D *dielectric* substrates, we tested our physical-optics results by comparison with the results of a 2-D MOM code. The test structure was a 0.4- μm deep cavity in silicon with sloping sidewalls, as shown in Fig. 3.6. For simplicity, we refer to such a structure as a 3-D Matzusawa step. In this example, the medium above the step was air. From the 2-D MOM results for the tangential magnetic fields $H_{\text{TE}}(y)$ and $H_{\text{TM}}(x)$ in TE and TM polarizations, we extrapolated the results to 3-D using the heuristic formula

$$H(x, y) = \frac{1}{2} H_{\text{TM}}(x) H_{\text{TE}}(y) . \quad (3.93)$$

Eq. (3.93) is expected to be a reasonable estimate of the correct fields not too close to the edges and corners of the topography. The extrapolated results are shown in Fig. 3.7a, while the physical-optics results for a normally incident plane wave polarized in the x -direction are shown in Fig. 3.7b. Induced fields up to the first order were included in the physical-optics calculation. It is seen from these figures that the physical-optics results are in reasonable agreement with the extrapolated results based on Eq. (3.93).

Next, we applied our multipole accelerated physical-optics technique to reflective-notching simulation, using 3-D Matzusawa steps with different slope angles. The calculations were done on an IBM RS/6000 Model 530 workstation with 64 megabytes of storage. In all cases, the upper surface of the photoresist was taken to be planar and its refractive index was assumed to be constant at $n = 1.70 + 0.01j$. The incident light was assumed to be coherent but with the intensity distribution of a partially coherent aerial image, and the wavelength was $0.365\mu\text{m}$. Also, to take into account multiple scattering between the topography and the upper photoresist surface, a total of eight terms in the one-way multiple-reflection series were used, which corresponded to four successive reflections of the scattered light from the photoresist surface back onto the substrate.

Our first example is a $0.7\mu\text{m}$ photoresist line going over the $0.4\mu\text{m}$ high step of Fig. 3.6. The surface of this topography was divided into 613 panels containing a total of 22,753 nodes. Physical-optics induced fields up to the first order were included in the intra-surface multiple-scattering calculation, which took a total of 17 hours. The simulator SAMPLE was used to develop a series of 2-D cross sections of the exposed photoresist and the resulting 2-D profiles were assembled to produce a 3-D photoresist profile. The results for x - and y -polarized incident light are shown separately in Figs. 3.8a and 3.8b. In the former case, the foot of photoresist line at the bottom of the step shows noticeable undercutting. This was caused by light reflected twice from the substrate, first from sidewall A and then from the bottom of the step, as depicted in the ray diagram shown in Fig. 3.8c. In the y -polarized result of Fig. 3.8b, this

undercutting is less noticeable. This was because the angle of incidence on sidewall A , $\theta_{\text{inc}} = 58^\circ$, was near the Brewster angle for this inclined surface, $\theta_{\text{Brewster}} = 74.6^\circ$. Instead, the photoresist sidewall in Fig. 3.8b shows pronounced standing wave effects along its length. This was because the light incident on sidewalls C and D was s -polarized and thus strongly reflected. Furthermore, the resulting reflected light traveling parallel to the photoresist sidewall had the same polarization as the incident light and thus interfered strongly with the latter. One should expect to find a similar region of strong standing waves, too, in Fig. 3.8a, but rotated by 90 degrees about the z -axis. Indeed, the remnants of such a region of strong interference are visible in Fig. 3.8a in the form of ripples on the top of the photoresist line near its middle.

Our next example is a $0.35 \mu\text{m}$ photoresist line going over a $0.128\text{-}\mu\text{m}$ high step with a slope angle of 22.8° . The 19,820 nodes on the surface of this topography were divided into 542 panels. Only the zeroth-order physical-optics induced fields were included in the calculation, which took only 1.2 hours. The simulated photoresist profile for unpolarized incident light is shown in Fig. 3.9a. The most prominent features in this figure are the two notches at the top of the photoresist line near the middle. These notches can also be understood with the help of ray diagrams. Fig. 3.9b shows the bundles of rays reflected from sidewalls A and B intersecting the upper photoresist surface in two trapezoidal areas u and v . Fig. 3.9c shows the bundles of rays reflected from sidewalls C and D intersecting the upper photoresist surface in four trapezoidal areas p to s . A $0.35\text{-}\mu\text{m}$ wide region representing the volume occupied by the photoresist line is devoid of incident light. From Figs. 3.9b and 3.9c, we see that the six trapezoidal areas overlap in four small regions on the upper surface of the photoresist, two on each side of the photoresist line near its middle. It is expected that the photoresist initially developed most rapidly downwards through these overlap regions of increased exposure dose. This, together with the subsequent undercutting caused by the light reflected from sidewalls A and B , gave rise to the notches seen in Fig. 3.9a.

Our last example is a $0.35 \mu\text{m}$ photoresist line going over a $0.2\text{-}\mu\text{m}$ high step with

a slope angle of 32.0° . There were 20,490 nodes on the surface of this topography divided into 544 panels. Again, only the zeroth-order physical-optics induced fields were included in the calculation, which took 1.7 hours. The simulated photoresist profile for unpolarized incident light is shown in Fig. 3.10a. This time, the lower half of the photoresist profile facing the topography sidewalls *A* and *B* shows a small amount of notching. With the help of the ray diagram shown in Fig. 3.10b, we can understand this notching as being caused by the light reflected from sidewalls *A* and *B* of the topography. This effect was enhanced by the light reflected from sidewalls *C* and *D*, which happened to overlap the light reflected from sidewalls *A* and *B* near the notched parts of the photoresist profile.

3.13 Conclusions

In this chapter, we have discussed a three-dimensional topography-scattering technique based on the physical-optics approximation suitable for piecewise-linear topography. It makes use of the Fast Multipole idea to accelerate the computation of multiple scattering within a surface. Its storage and CPU costs scale as N and $N^{3/2}$, respectively, where N is the number of nodes on the surface of the topography. This allows reflective-notching simulation of large ($N \approx 20,000$) 3-D structures to be done on an ordinary workstation with reasonable CPU time (< 20 hours). The technique was tested on 3-D cavities in silicon with sloping sidewalls having different slope angles. The simulated reflective-notching effects were found to be in qualitative agreement with a ray-optics model. Although the Fast Multipole algorithm discussed in this chapter was used in the context of the physical-optics approximation, it can be extended for use in a rigorous integral-equation approach suitable for arbitrary topography. This is discussed in the next chapter.

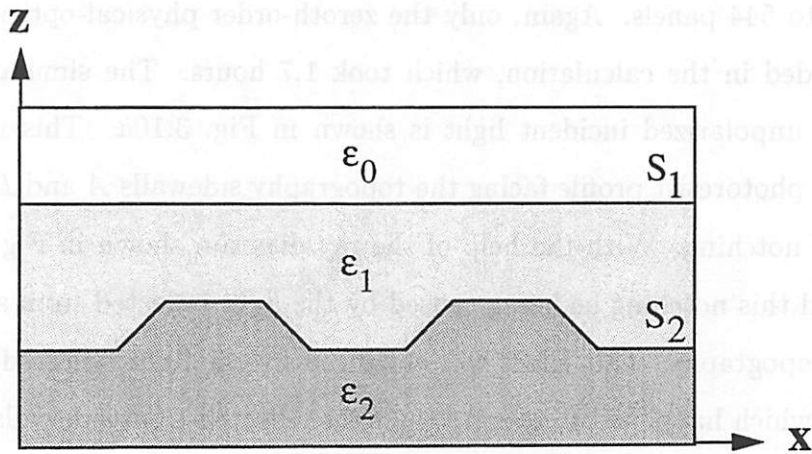


Figure 3.1: Multilayer piecewise-linear topography.

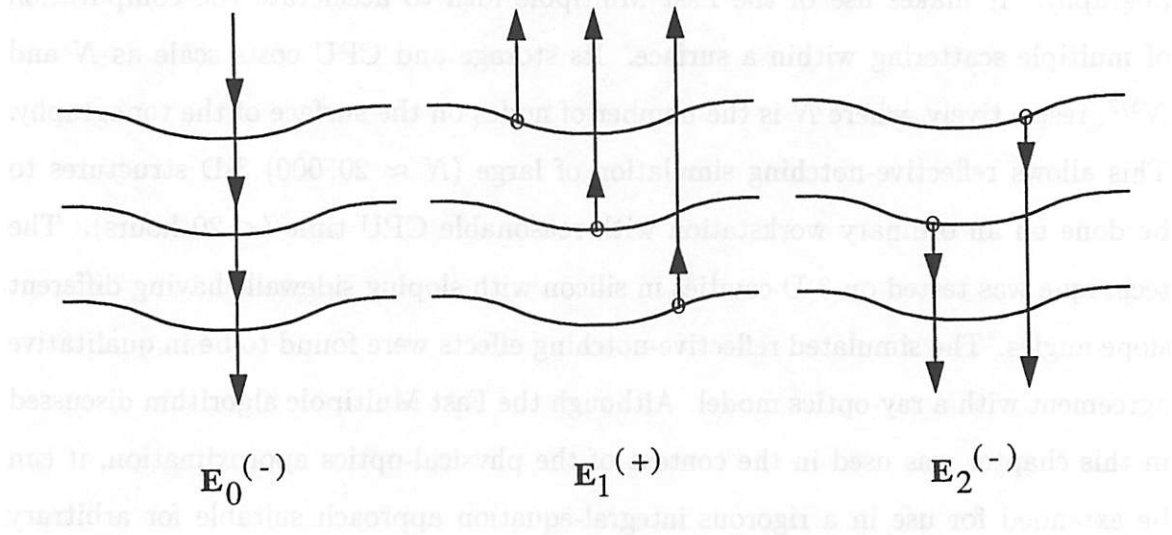


Figure 3.2: Multiple-reflection series for multiple scattering between adjacent surfaces. $\mathbf{E}_0^{(-)}$ is the incident field for $\mathbf{E}_1^{(+)}$, and $\mathbf{E}_1^{(+)}$ is the incident field for $\mathbf{E}_2^{(-)}$, etc.

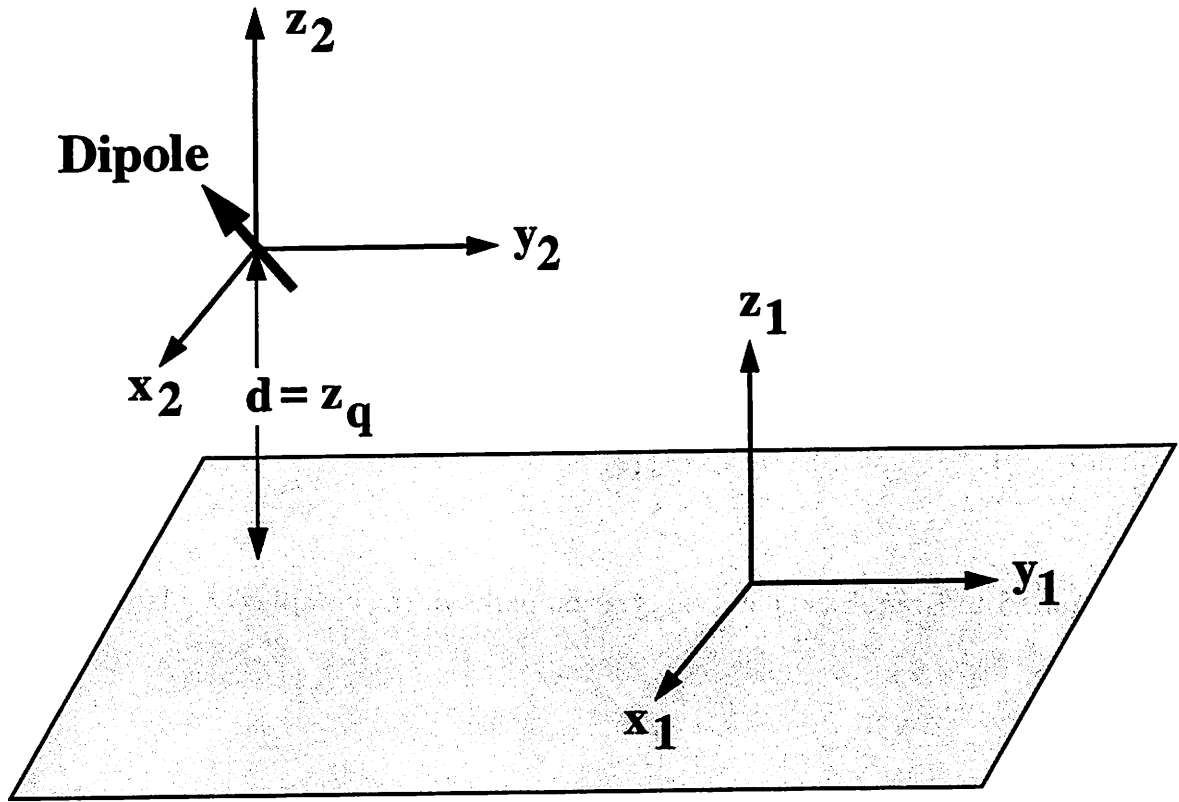


Figure 3.3: Dipole above a lossy plane surface.

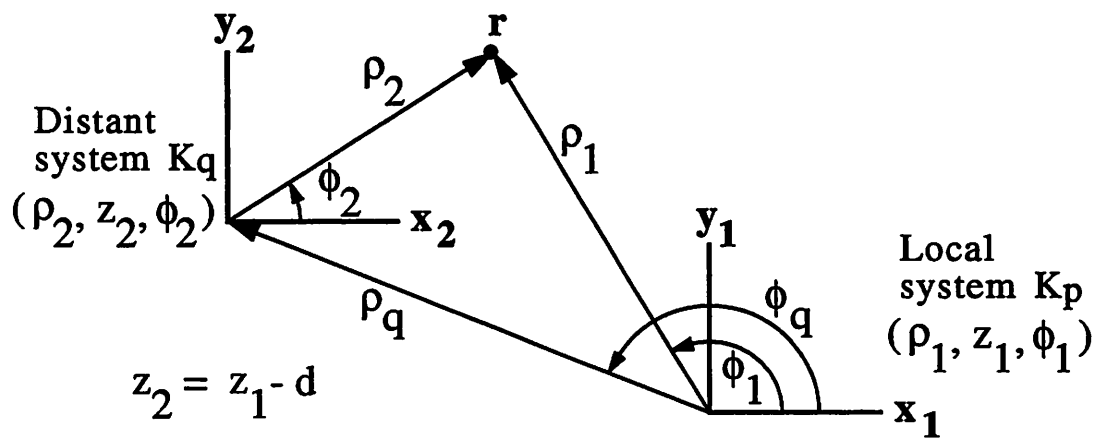


Figure 3.4: Transformation from distant to local coordinate system.

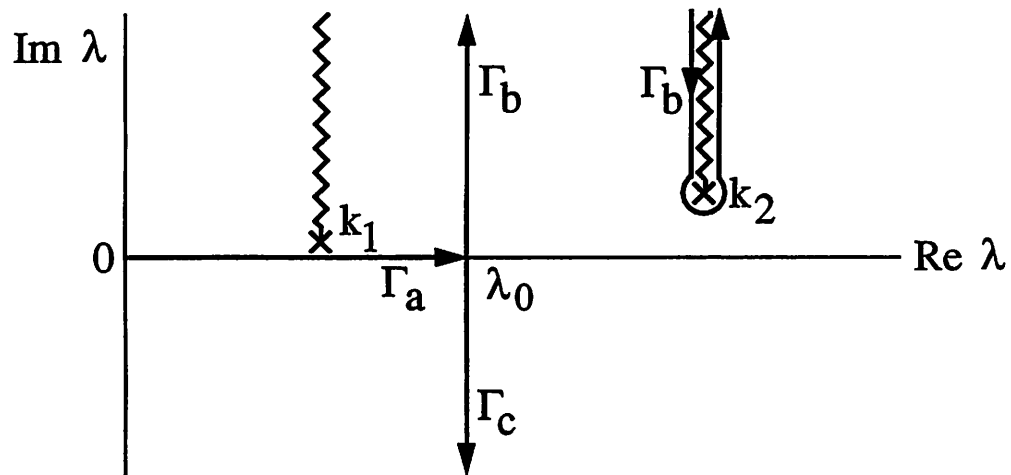


Figure 3.5: Branch cuts and integration paths in the complex λ -plane.

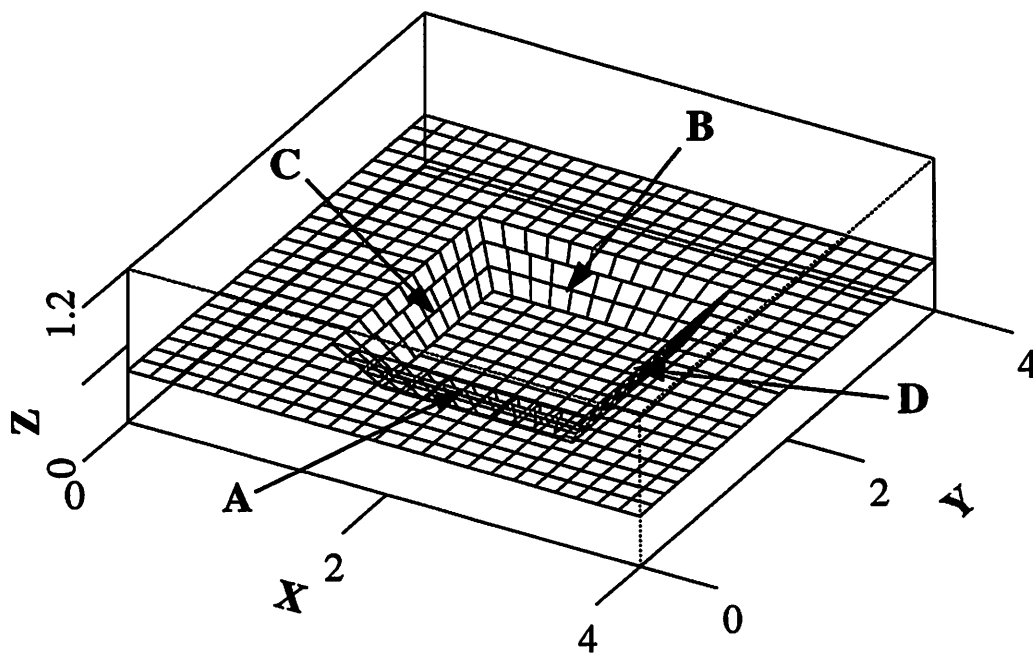


Figure 3.6: Three-dimensional Matzusawa step divided into panels. Wavelength = $0.365 \mu\text{m}$. Substrate refractive index = $6.18 + 2.45j$.

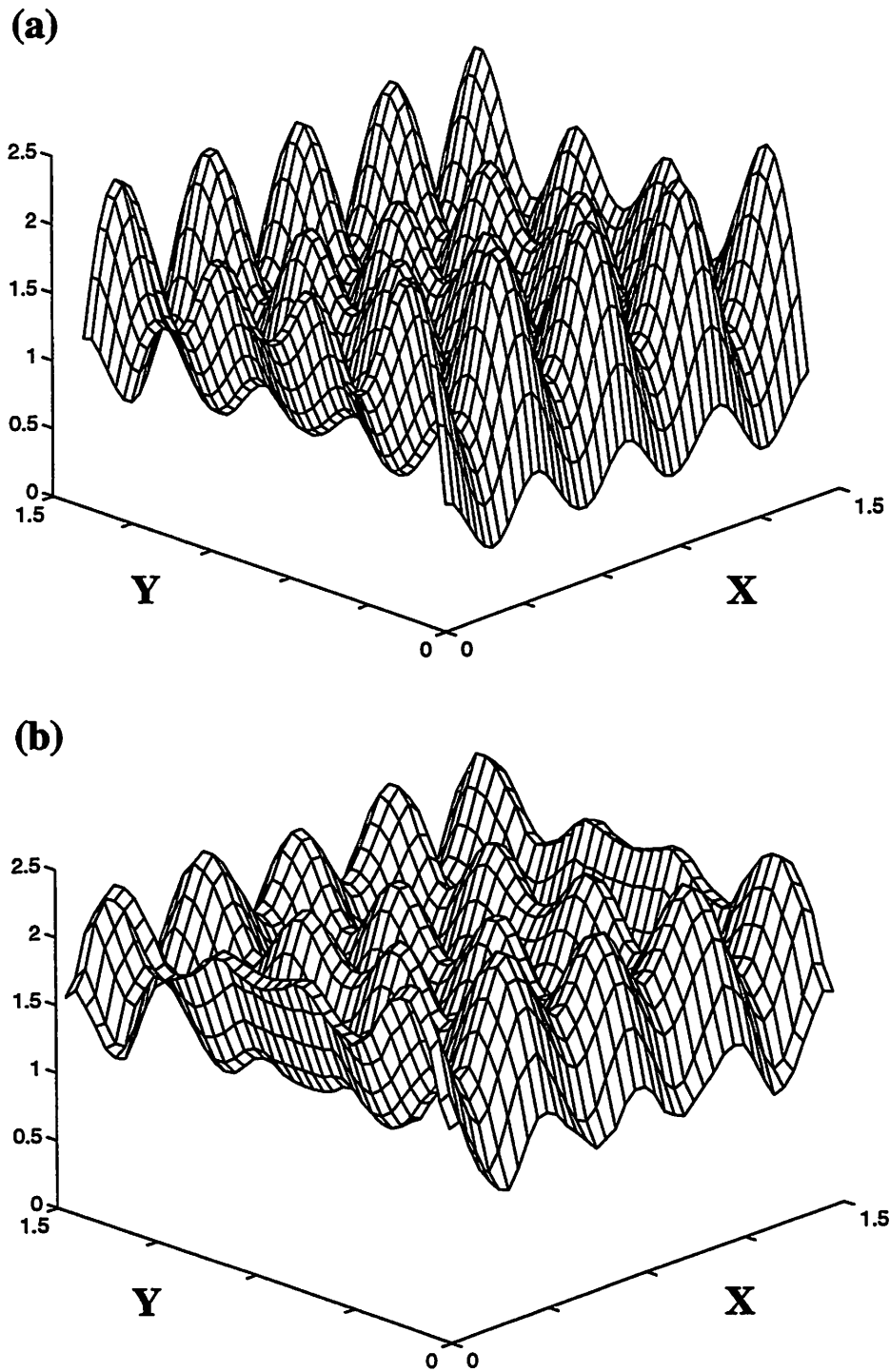


Figure 3.7: Tangential magnetic field amplitude on bottom of step, for x -polarized, normally incident plane wave. (a) 2-D MOM results extrapolated to 3-D using Eq. (3.93). (b) Physical-optics results including zero- and first-order induced fields.

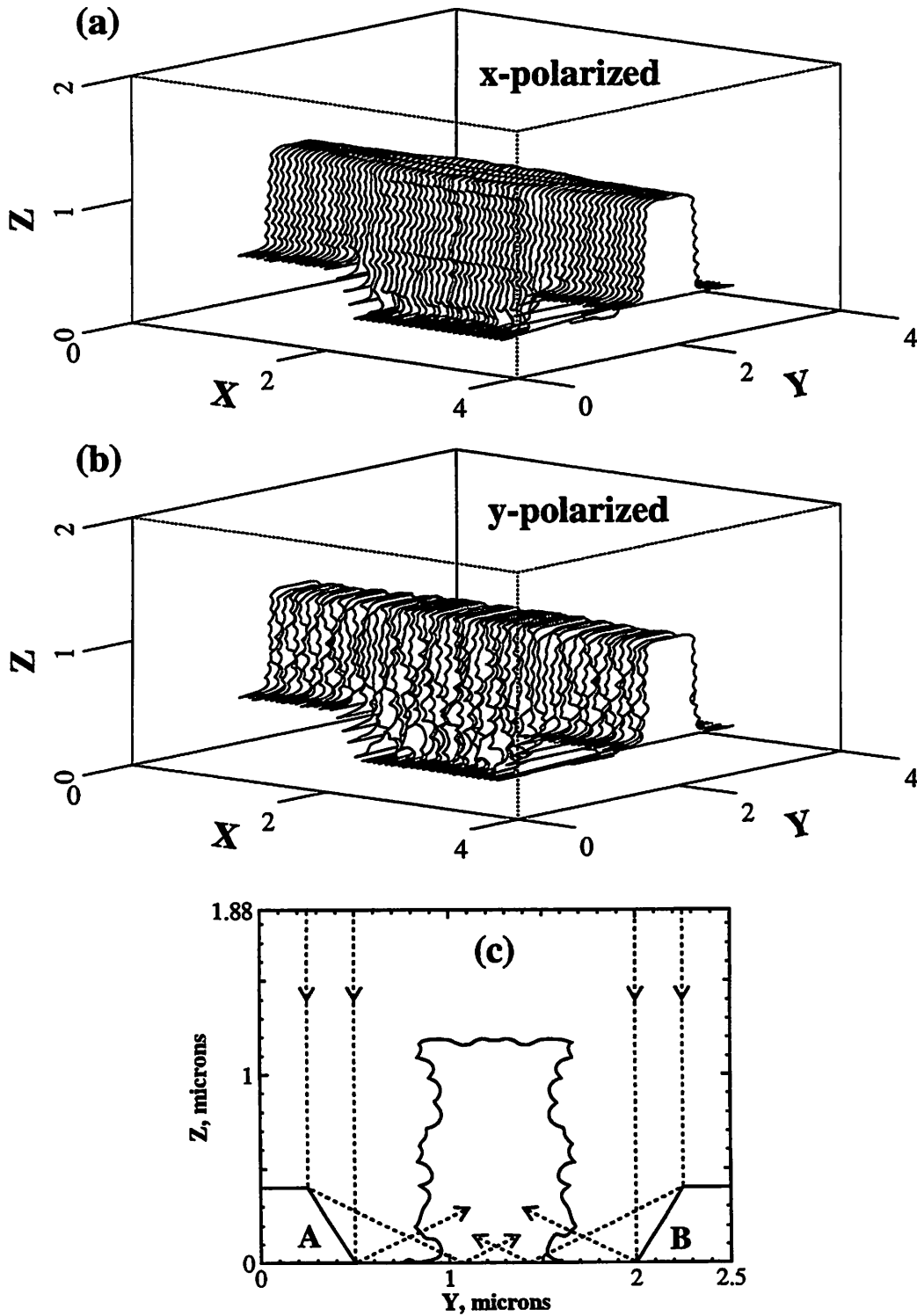


Figure 3.8: $0.7 \mu\text{m}$ line over $0.4 \mu\text{m}$ high step. Dose = 120 mJ cm^{-2} . Develop time = 60 s. (a) x-polarized incident light. (b) y-polarized incident light. (c) Doubly reflected rays from sidewalls A and B causing undercutting.

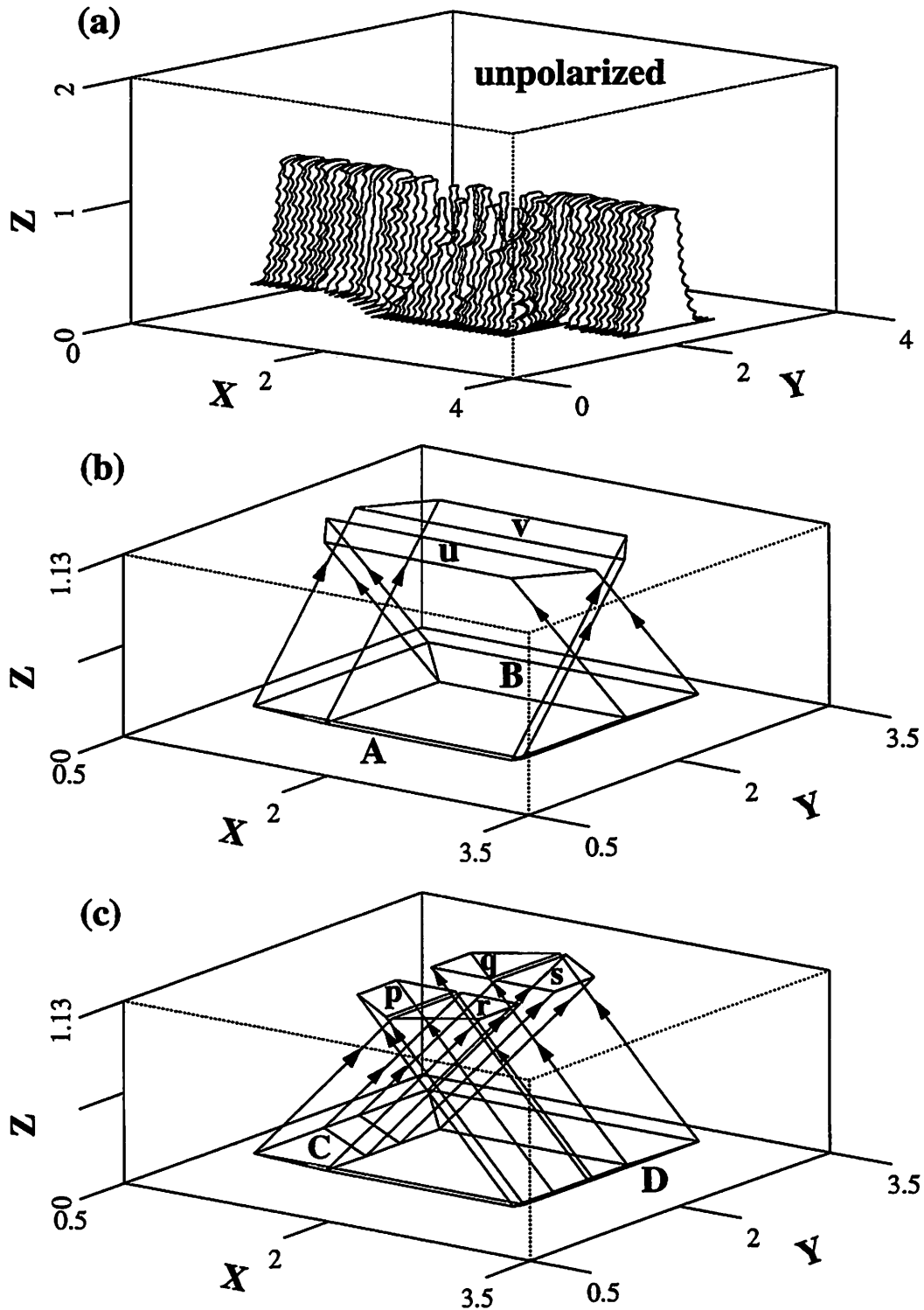


Figure 3.9: (a) $0.35 \mu\text{m}$ line over $0.128 \mu\text{m}$ high step. Dose = 100 mJ cm^{-2} . Develop time = 60 s. (b) Beams reflected from sidewalls A and B intersecting the resist surface at u and v. (c) Beams reflected from sidewalls C and D intersecting the resist surface at p, q, r and s.

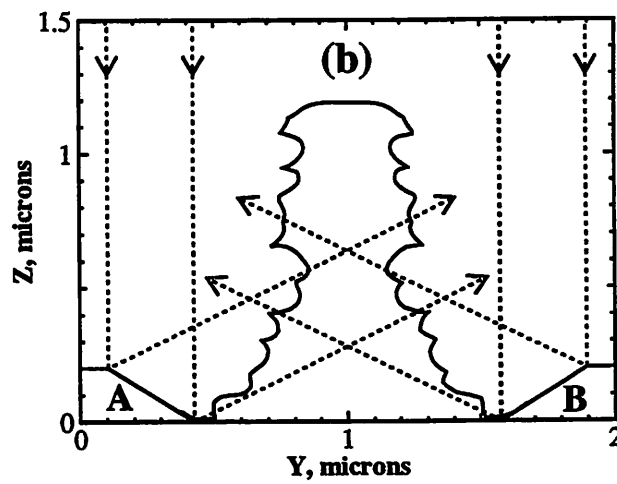
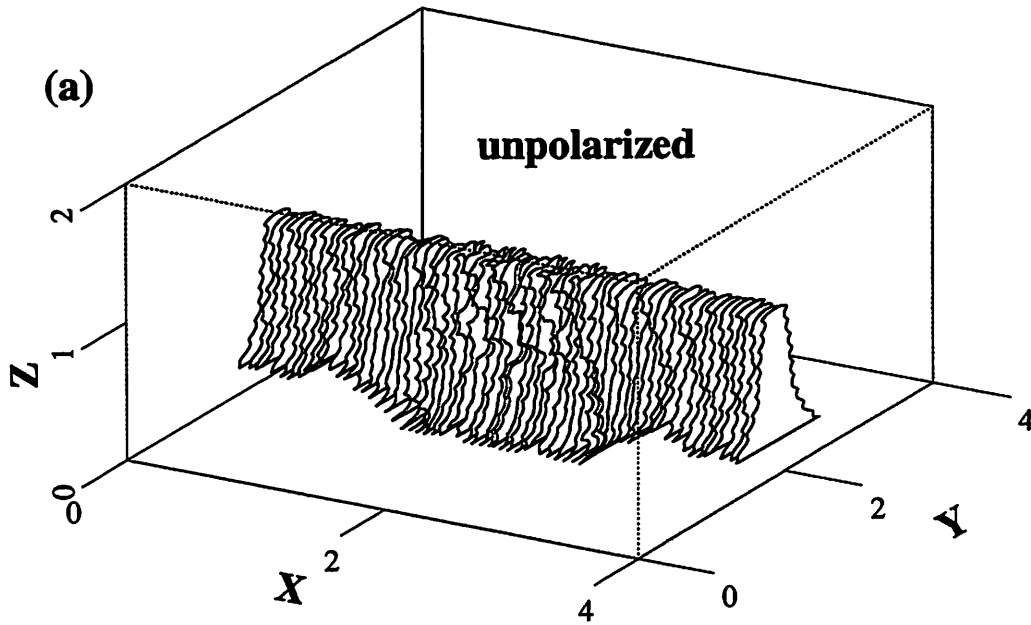


Figure 3.10: (a) $0.35 \mu\text{m}$ line over $0.2 \mu\text{m}$ high step. Dose = 95 mJ cm^{-2} . Develop time = 55 s. (b) Singly reflected rays from topography sidewalls A and B causing dents on resist sidewalls.

Chapter 4

Three-Dimensional Topography Scattering Part II: Fast Multipole Solution of Integral Equation

4.1 Introduction

The physical-optics technique discussed in the Chapter 3 is suitable only for piecewise-linear topography consisting of planar fragments whose dimensions are at least a wavelength in each direction. This assures the validity of the tangent-plane approximation used in the treatment of the interaction of the incident and multiply scattered waves with the topography. Also, the number of sharp edges per period should be small. This renders negligible the contributions to the *integrated* field distribution throughout the photoresist due to non-physical-optics edge currents. In order to handle curved topography in which the local radii of curvature are of the order of a wavelength or smaller, or piecewise-linear topography containing a large number of sharp edges per period, one has to go beyond the physical-optics approximation and use a rigorous technique based on an integral formulation of the scattering problem.

An integral formulation of the scattering problem can be based on either the electric-field integral equation (EFIE) or the magnetic-field integral equation (MFIE). The kernel of EFIE is more singular than that of MFIE and so requires more sophisticated integration technique and choice of basis functions. For simplicity, therefore, we use the MFIE in this chapter. Direct solution of the MFIE using the standard

Method of Moments is not practical in 3-D, as Table 1.1 shows. Thus, it is necessary to use the Fast Multipole Method (FMM) developed by Rokhlin [11] to accelerate the solution of the MFIE.

We begin the discussion of our FMM algorithm with a derivation of the MFIE for perfectly conducting objects in Section 4.2 and an outline of the GMRES iteration algorithm in Section 4.3. The FMM algorithm is then discussed in Section 4.4. The novelty of our algorithm lies in the use of a three-step distant-to-local transformation procedure consisting of a rotation, a translation and another rotation. This leads to an $O(N^{5/3})$ algorithm as discussed in Section 4.5. When a problem has reflection symmetry in some coordinate plane, the symmetry can be exploited to reduce the number of unknowns. This is discussed in Section 4.6 for reflection symmetry in two of the coordinate planes. Numerical results and performance benchmarks for scattering from perfectly conducting plates and cubes are discussed in Section 4.7. In Section 4.8, boundary conditions appropriate to problems with guided mode excitation are formulated. These are applied to the problems of a shorted waveguide section and a pyramidal horn antenna. Our FMM algorithm is shown to reduce correctly to the electrostatics results in the long-wavelength limit in Section 4.9. Then, in Section 4.10, the standard FMM algorithm is reviewed and the question of numerical instability in the long-wavelength limit is discussed.

4.2 Problem Formulation

The scattering problem is illustrated in Fig. 4.1. The region outside the perfectly conducting body is bounded by the surface S_{obj} of the body and the surface S_{∞} at infinity. The magnetic field $\mathbf{H}(\mathbf{r})$ in this region is given by Eq. (3.4) with $S = S_{\text{obj}} + S_{\infty}$. The integral over S_{∞} simply gives the incident magnetic field $\mathbf{H}_{\text{inc}}(\mathbf{r})$. In the remaining integral over S_{obj} , the terms containing $(\mathbf{n}' \times \mathbf{E}')$ are absent since the tangential electric field on the surface of a perfect conductor vanishes. By letting the field point \mathbf{r} approach the surface of the body from the outside and taking the cross product of the outward surface normal \mathbf{n} at \mathbf{r} with both sides of the resulting

equation, we obtain the MFIE,

$$\mathbf{n} \times \mathbf{H}(\mathbf{r}) = \mathbf{n} \times \mathbf{H}_{\text{inc}}(\mathbf{r}) - \frac{1}{4\pi} \mathbf{n} \times \int_{S_{\text{obj}}} (\mathbf{n}' \times \mathbf{H}') \times \nabla' \psi dS', \quad (4.1)$$

where $\psi = \frac{e^{jk|\mathbf{r}-\mathbf{r}'|}}{|\mathbf{r}-\mathbf{r}'|}$ is the Green function in the external medium with wavevector k .

The integral over S_{obj} in Eq. (4.1) includes the field point \mathbf{r} on this surface where ψ is singular. Hence, the integration over an infinitesimal area centered at \mathbf{r} must be done analytically. To do this, we choose a local coordinate system with origin just below \mathbf{r} and z -axis coinciding with the normal \mathbf{n} pointing into the body, as shown in the insert of Fig. 4.1. As \mathbf{r}' approaches \mathbf{r} , \mathbf{n}' approaches $\mathbf{n} = \mathbf{z}$. Therefore, $\mathbf{n} \times [(\mathbf{n}' \times \mathbf{H}') \times \nabla' \psi]$ approaches $\mathbf{z} \times [(\mathbf{z} \times \mathbf{H}') \times \nabla' \psi] = (\mathbf{z} \times \mathbf{H}')(\partial\psi/\partial z')$. We can write the z -derivative of ψ as

$$\begin{aligned} \frac{\partial\psi}{\partial z'} &= \frac{\partial}{\partial z'} \left[\frac{e^{ik\sqrt{(x-x')^2+(y-y')^2+(z-z')^2}}}{\sqrt{(x-x')^2+(y-y')^2+(z-z')^2}} \right] \\ &= \frac{e^{ik\sqrt{(x-x')^2+(y-y')^2+(z-z')^2}}}{(x-x')^2+(y-y')^2+(z-z')^2} \left[-ik(z-z') \right. \\ &\quad \left. + \frac{z-z'}{\sqrt{(x-x')^2+(y-y')^2+(z-z')^2}} \right]. \end{aligned} \quad (4.2)$$

In the limit as \mathbf{r}' approaches \mathbf{r} , the second term inside the brackets in Eq. (4.2) dominates over the first term. Hence, setting the exponential factor equal to unity in this limit and multiplying both sides of Eq. (4.2) by dS' , we obtain

$$\begin{aligned} \frac{\partial\psi}{\partial z'} dS' &\approx \frac{z-z'}{[(x-x')^2+(y-y')^2+(z-z')^2]^{3/2}} dS' \\ &= -d\Omega', \end{aligned} \quad (4.3)$$

where $d\Omega'$ is the solid angle subtended by the element of area dS' at the field point \mathbf{r} . In the limit as \mathbf{r}' approaches \mathbf{r} , dS' becomes essentially a half-plane as seen from \mathbf{r} , and so $d\Omega' = 2\pi$. Hence, the contribution from the infinitesimal area dS' centered at $\mathbf{r}' = \mathbf{r}$ to the integral in Eq. (4.1) is

$$\begin{aligned} \lim_{\mathbf{r}' \rightarrow \mathbf{r}} -\frac{1}{4\pi} \mathbf{n} \times [(\mathbf{n}' \times \mathbf{H}') \times \nabla' \psi] dS' &= -\frac{1}{4\pi} \mathbf{n} \times \mathbf{H}(\mathbf{r}) \frac{\partial\psi}{\partial z'} dS' \\ &= \frac{1}{2} \mathbf{n} \times \mathbf{H}(\mathbf{r}). \end{aligned} \quad (4.4)$$

Hence, Eq. (4.1) becomes

$$\frac{1}{2}\mathbf{n} \times \mathbf{H}(\mathbf{r}) = \mathbf{n} \times \mathbf{H}_{\text{inc}}(\mathbf{r}) - \frac{1}{4\pi}\mathbf{n} \times \int'_{S_{\text{obj}}} (\mathbf{n}' \times \mathbf{H}') \times \nabla' \psi dS', \quad (4.5)$$

where the prime on the integral sign means that the singular point of the integrand is omitted. For a perfect conductor, the tangential magnetic field is related to the surface current density $\mathbf{J}(\mathbf{r})$ by

$$\mathbf{J}(\mathbf{r}) = -\mathbf{n} \times \mathbf{H}(\mathbf{r}), \quad (4.6)$$

since \mathbf{n} points *into* the conductor in our convention. Using the fact that $\nabla' \psi = -\nabla \psi$, we may rewrite Eq. (4.5) as

$$\frac{1}{2}\mathbf{J}(\mathbf{r}) = \mathbf{J}^{\text{inc}}(\mathbf{r}) - \mathbf{n} \times \left[\nabla \times \int'_{S_{\text{obj}}} \mathbf{J}(\mathbf{r}') \frac{e^{jk|\mathbf{r}-\mathbf{r}'|}}{4\pi|\mathbf{r}-\mathbf{r}'|} dS' \right], \quad (4.7)$$

where $\mathbf{J}^{\text{inc}}(\mathbf{r}) = -\mathbf{n} \times \mathbf{H}_{\text{inc}}(\mathbf{r})$. Eq. (4.7) is the integral equation that we wish to solve for $\mathbf{J}(\mathbf{r})$.

The simplest way to solve Eq. (4.7) is to divide S_{obj} into N surface elements over each of which the surface current density is assumed to be constant with unknown amplitudes $\mathbf{J}(\mathbf{r}_m)$ for the m th surface element. By enforcing the integral equation to be satisfied at the center of each surface element, or node, a system of $2N$ linear algebraic equations for the $2N$ unknowns $J_\mu(\mathbf{r}_m)$ is obtained, where $\mu = 1$ or 2 is a label for two orthogonal directions within the tangent plane at \mathbf{r}_m ,

$$\frac{1}{2}J_\mu(\mathbf{r}_m) + \sum'_{n=1}^N \sum_{\nu=1}^2 B_{\mu m, \nu n} J_\nu(\mathbf{r}_n) = J_\mu^{\text{inc}}(\mathbf{r}_m), \quad (4.8)$$

for some matrix $B_{\mu m, \nu n}$, which is dense. Also, the prime on the summation sign in Eq. (4.8) means that the term $n = m$ is omitted. For small problems in which N is a thousand or less, the system of equations (4.8) can be solved directly by Gaussian elimination, which requires $O(N^3)$ operations. For larger problems, it is usually more efficient to solve Eq. (4.8) iteratively. Now, the matrix $B_{\mu m, \nu n}$ in this equation is complex and non-symmetric. Although it can be transformed into a real matrix by separately writing the real and imaginary parts of Eq. (4.8), the non-symmetry

nevertheless remains. The reason for the non-symmetry can be seen by examining the following form of the matrix elements,

$$B_{\mu m, \nu n} = \mathbf{e}_\mu \cdot \left[\mathbf{n} \times \left(\nabla \psi \times \mathbf{e}'_\nu \frac{dS'}{4\pi} \right) \right] \Big|_{\mathbf{r}=\mathbf{r}_m, \mathbf{r}'=\mathbf{r}_n}, \quad (4.9)$$

where \mathbf{e}_μ and \mathbf{e}'_ν are unit vectors on the tangent planes at \mathbf{r}_m and \mathbf{r}_n , respectively. Since the surface of the body is arbitrary, there is in general no relationship between the tangent vectors \mathbf{e}_μ and \mathbf{e}'_ν , or the surface normals \mathbf{n} and \mathbf{n}' , at different points \mathbf{r}_m and \mathbf{r}_n on the surface. Hence, the matrix $B_{\mu m, \nu n}$ is in general non-symmetric. As a result, the conjugate gradient method cannot be used for the iterative solution of the system Eq. (4.8). One possibility is to convert Eq. (4.8) into a symmetric system by multiplying both sides of the equation by the transpose of the matrix $\left(\frac{1}{2} \delta_{\mu, \nu} \delta_{m, n} + B_{\mu m, \nu n} \right)$. The resulting *normal equation* can then be solved by the conjugate gradient method. The disadvantage of this method is that the condition number of the original matrix is squared. The alternative is to use an algorithm suitable for general, non-symmetric matrices, such as the generalized minimum residual, GMRES, algorithm [42].

4.3 GMRES

Eq. (4.8) can be written in the more general form

$$\mathcal{A} \mathbf{y} = \mathbf{b}, \quad (4.10)$$

where \mathcal{A} is a $2N \times 2N$ matrix, \mathbf{y} is a column vector of unknowns and \mathbf{b} is a known column vector. Given an initial guess solution \mathbf{y}_0 , for example, $\mathbf{y}_0 = \mathbf{0}$, we compute the initial *residual* $\mathbf{r}_0 = \mathbf{b} - \mathcal{A} \mathbf{y}_0$ and use this to construct Krylov subspaces of increasing dimensionality. Specifically, at the j th iteration step, we construct a j -dimensional Krylov subspace \mathcal{K}^j consisting of all linear combinations of the j column vectors $\mathbf{r}_0, \mathcal{A} \mathbf{r}_0, \mathcal{A}^2 \mathbf{r}_0, \dots, \mathcal{A}^{j-1} \mathbf{r}_0$, that is,

$$\mathcal{K}^j = \text{Span} \{ \mathbf{r}_0, \mathcal{A} \mathbf{r}_0, \mathcal{A}^2 \mathbf{r}_0, \dots, \mathcal{A}^{j-1} \mathbf{r}_0 \}. \quad (4.11)$$

The j th iterate \mathbf{y}_j is chosen to be that vector in \mathcal{K}^j which minimizes the norm of the residual $\mathbf{r}_j = \mathbf{b} - \mathcal{A}\mathbf{y}_j$,

$$\mathbf{y}_j \in \mathcal{K}^j \text{ such that } \|\mathbf{b} - \mathcal{A}\mathbf{y}_j\|_2 \leq \|\mathbf{b} - \mathcal{A}\mathbf{x}\|_2 \quad \forall \mathbf{x} \in \mathcal{K}^j. \quad (4.12)$$

The iteration continues until the norm of the residual becomes less than a desired fraction of the norm of \mathbf{b} .

It is assumed in the above discussion that the vectors $\mathbf{r}_0, \mathcal{A}\mathbf{r}_0, \mathcal{A}^2\mathbf{r}_0, \dots$ are linearly independent. This is generally true, although as j increases, the sequence of vectors become increasingly parallel to each other. As such, they are not a good basis for \mathcal{K}^j . In actual implementation of GMRES, an orthonormal basis for \mathcal{K}^j is constructed at each iteration step j , by applying the Gram-Schmidt orthogonalization procedure to the vectors $\mathbf{r}_0, \mathcal{A}\mathbf{r}_0, \mathcal{A}^2\mathbf{r}_0, \dots, \mathcal{A}^{j-1}\mathbf{r}_0$. To avoid possible numerical instability in the Gram-Schmidt procedure, the Arnoldi algorithm is used to ensure mutually orthogonality of the resulting basis vectors $\{\mathbf{q}_1, \mathbf{q}_2, \dots, \mathbf{q}_j\}$ for \mathcal{K}^j .

As the iteration number increases, one has to store an increasing number of the basis vectors \mathbf{q}_i in the computer. For large 3-D problems, where N can be of the order of tens of thousands, this could impose a limit on the number of iterations allowed before memory capacity is exceeded on a small computer. When the latter does occur, one is forced to *restart* the GMRES algorithm, using the most recent iterate \mathbf{y}_j as the initial guess and rebuilding the Krylov subspaces from scratch. In discarding the old Krylov subspaces, one also throws away important information required for convergence. Thus, restarting GMRES due to memory limitations usually results in a drastic decrease in the rate of convergence. Because of this, we have chosen to run all our examples on workstations with sufficient memory to avoid restarting.

GMRES is one of several iterative algorithms based on the idea of approximations from Krylov subspaces. Others in this class of algorithms include conjugate gradient (CG) for symmetric matrices and bi-conjugate gradient (BiCG) for non-symmetric matrices. These and other related algorithms are available in the public domain [43]. For this reason, we do not go into the details of implementation here.

From the above discussion, it is clear that at each iteration step one has to perform a matrix-vector multiplication involving the matrix \mathcal{A} . This is usually the most time consuming part of the algorithm. Ordinary matrix-vector multiplication requires $O(N^2)$ operations, which becomes prohibitively expensive for large 3-D problems. This operation count can be reduced to $O(N^{5/3})$ by using the Fast Multipole algorithm discussed in the next section.

4.4 The FMM Algorithm

The Fast Multipole Method (FMM) discussed below is similar to that of Chapter 3 in that local, rather than distant, multipole expansions are used to compute distant-panel contributions to the scattered field. However, in the present discussion, there is no need to use the formalism of generalized Sommerfeld integrals given in Section 3.8, since we do *not* use the physical-optics approximation here. Instead, we are here concerned with the rapid evaluation of the matrix-vector product represented by the second term on the LHS of Eq. (4.8). From the discussion leading from Eq. (4.7) to Eq. (4.8), it is clear that the matrix-vector product under discussion represents the tangential magnetic field scattered to a node m from all other nodes $n \neq m$. To compute this scattered field efficiently, we again use the multipole approximation discussed in Section 3.7, by grouping the N elements of S_{obj} into P panels, each of which contains roughly the same number ($\approx N/P$) of nodes. For a perfect conductor, there are only *electric* current sources, $-\mathbf{n} \times \mathbf{H}(\mathbf{r})$, on the surface. The electric vector potential produced in the far zone by the electric current sources in a panel q is approximated by a truncated multipole expansion as given by Eq. (3.50), which we reproduce here for convenience,

$$\Delta \mathbf{A}_e^q(\mathbf{r}) = \sum_{l=0}^L \sum_{m=-l}^l \mathbf{b}_{lm}^q h_l^{(1)}(kr) P_l^m(\cos \theta) e^{jm\phi}, \quad (4.13)$$

where \mathbf{b}_{lm}^q are the electric multipole coefficients of panel q with respect to a coordinate system K_q centered at that panel,

$$\mathbf{b}_{lm}^q = \int_{\text{Panel } q} \mathbf{J}(\mathbf{r}') \frac{jk(2l+1)(l-m)!}{4\pi(l+m)!} j_l(kr') P_l^m(\cos \theta') e^{-jm\phi'} dS'. \quad (4.14)$$

In Eqs. (4.13) and (4.14), (r, θ, ϕ) and (r', θ', ϕ') are spherical polar coordinates of the field and source points \mathbf{r} and \mathbf{r}' , respectively, relative to the distant coordinate system K_q . By truncating the summation over l in Eq. (4.13) after $(L + 1)$ terms, we are approximating the sources in panel q by a collection of M multipoles located at the center of this panel, where $M = \sum_{l=0}^L (2l + 1) = (L + 1)^2$. The magnetic field due to the sources in the distant panel q is obtained by taking the curl of the electric vector potential $\Delta \mathbf{A}_e^q(\mathbf{r})$. For sources in the neighboring panels, however, the multipole approximation cannot be used. Instead, the contributions from the nodes in the neighboring panels must be added individually.

If Eq. (4.13) were used to compute the distant-panel contributions to the scattered magnetic field at each of the N nodes of S_{obj} , the operation count would be proportional to $NMP \approx N(N/P)P = N^2$, since each node would require the evaluation of M multipole terms for each of approximately P distant panels. Here, we have used the fact that the number M of multipole terms needed to represent accurately the field in the far zone due to a given panel is on the order of the number of nodes in that panel, $M \approx N/P$. This would again be prohibitively expensive for large 3-D problems. Instead, we compute the distant-panel contributions by transforming the *distant* multipole expansion given by Eq. (4.13) into a *local* multipole expansion. This is accomplished by means of the appropriate addition theorem for spherical waves [39]. Let K_p be a coordinate system centered at the panel p over which we wish to evaluate the distant expansion Eq. (4.13). Without loss of generality, we assume that the axes of K_p are parallel to those of K_q . Suppose the spherical polar coordinates of the origin of the distant coordinate system K_q with respect to the local coordinate system K_p are (R_0, θ_0, ϕ_0) . Note that this is opposite to the convention used in [39]. Then, the addition theorem says that the spherical waves in the two coordinate systems are related by

$$h_n^{(1)}(k\tau) P_n^m(\cos \theta) e^{jm\phi} = \sum_{\nu=0}^{\infty} \sum_{\mu=-\nu}^{\nu} \sum_{p=|\nu-n|}^{\nu+n} j^{-n+\nu+p+2\mu} (-1)^p (2\nu + 1) a(-\mu, m|p, \nu, n) \\ \times h_p^{(1)}(kR_0) P_p^{m-\mu}(\cos \theta_0) e^{j(m-\mu)\phi_0} j_\nu(k\tau_1) P_\nu^\mu(\cos \theta_1) e^{j\mu\phi_1}, \quad (4.15)$$

where (r_1, θ_1, ϕ_1) are spherical coordinates of the field point with respect to the local system K_p , and the coefficients $a(-\mu, m|p, \nu, n)$ are defined through the relationship

$$P_\nu^\mu(\cos \theta) P_n^m(\cos \theta) = \sum_{p=|\nu-n|}^{\nu+n} a(\mu, m|p, \nu, n) P_p^{m+\mu}(\cos \theta). \quad (4.16)$$

The computation of the coefficients $a(m, -\mu|p, n, \nu)$ by means of recurrence relationship is discussed in Appendix I. Substituting Eq. (4.15) into Eq. (4.13) and renaming indices, we obtain the desired local expansion,

$$\Delta A_e^q(\mathbf{r}) = \sum_{l=0}^L \sum_{m=-l}^l c_{lm}^q j_l^{(1)}(kr_1) P_l^m(\cos \theta_1) e^{jm\phi_1}, \quad (4.17)$$

where the new multipole coefficients c_{lm}^q are related to the old coefficients \mathbf{b}_{lm}^q by

$$c_{\nu\mu}^q = \sum_{n=0}^L \sum_{m=-n}^n \sum_{p=|\nu-n|}^{\nu+n} j^{\nu-n+3p+2\mu} (2\nu+1) a(-\mu, m|p, \nu, n) h_p^{(1)}(kR_0) P_p^{m-\mu}(\cos \theta_0) \times e^{j(m-\mu)\phi_0} \mathbf{b}_{nm}^q. \quad (4.18)$$

In Eq. (4.17) we have truncated the summation over l after $(L+1)$ terms. This is valid because Eq. (4.17) is to be evaluated only over the local panel p , within which the field can be adequately approximated by the first M terms of the local expansion.

The summation over p in Eq. (4.18) can be computed in advance, since the terms depending on p in this equation, $h_p^{(1)}(kR_0)$ and $P_p^{m-\mu}(\cos \theta_0)$, involve only the fixed coordinates R_0 and θ_0 of panel q in the local system K_p . In each subsequent iteration step, according to Eq. (4.18), we still have to perform *two* summations, namely, those over n and m , for each pair of multipole indices (ν, μ) . This would result in an $O(N^2)$ algorithm as in ordinary matrix-vector multiplication. In order to obtain a faster algorithm, we need to develop a more efficient distant-to-local transformation procedure than the one represented by Eq. (4.18). The key to this development lies in the observation that Eq. (4.18) becomes simplified for translation along the $\pm z$ axis of the local coordinate system K_p . In that case, $\cos \theta_0 = \pm 1$ and the associated Legendre polynomial takes on the special value

$$P_p^{m-\mu}(\pm 1) = (\pm 1)^p \delta_{m,\mu}. \quad (4.19)$$

This means that the summation over m in Eq. (4.18) reduces to a single term $m = \mu$, and we are left with only one summation over n in each iteration step. The translation along the $\pm z$ axis can be achieved by performing the distant-to-local transformation in three steps:

1. Rotate the distant coordinate system K_q so that its z -axis becomes parallel to the radius vector \mathbf{R}_0 pointing from the origin of K_p to that of K_q .
2. Translate along the new z -axis of K_q in the negative direction until its origin coincides with that of K_p .
3. Rotate the translated system into the orientation of K_p .

The above three-step procedure corresponds to the successive computation of the following three sets of multipole coefficients:

$$\tilde{\mathbf{b}}_{nm}^q = \sum_{m'=-n}^n (-1)^{m-m'} \sqrt{\frac{(n-m)!(n+m')!}{(n+m)!(n-m')!}} \mathcal{D}_{mm'}^{(n)}(\phi_0, \theta_0, 0) \mathbf{b}_{nm'}^q, \quad (4.20)$$

$$\tilde{\mathbf{c}}_{\nu m}^q = \sum_{n=0}^L \sum_{p=|\nu-n|}^{\nu+n} j^{\nu-n+p+2(m+p)} (2\nu+1) a(-m, m|p, \nu, n) h_p^{(1)}(kR_0) \tilde{\mathbf{b}}_{nm}^q, \quad (4.21)$$

$$\mathbf{c}_{nm}^q = \sum_{m'=-n}^n (-1)^{m-m'} \sqrt{\frac{(n-m)!(n+m')!}{(n+m)!(n-m')!}} \mathcal{D}_{mm'}^{(n)}(0, -\theta_0, -\phi_0) \tilde{\mathbf{c}}_{nm'}^q, \quad (4.22)$$

where $\mathcal{D}_{mm'}^{(n)}(\alpha, \beta, \gamma)$ is the rotation matrix discussed in Appendix H. The use of Eqs. (4.20) to (4.22) for the distant-to-local transformation leads to an $O(N^{5/3})$ algorithm as shown in the next section.

For sources in the panel p containing the field point \mathbf{r} itself and sources in the panels adjacent to panel p , the multipole approximation cannot be used. Instead, the individual contributions from the sources in the local and neighboring panels must be computed directly.

What we actually need are the fields rather than the vector potential. Complete expressions for the magnetic and electric fields are given in Appendix J.

4.5 Operation Count

As in Section 3.11, we can estimate the number of floating-point operations required for each matrix-vector multiplication using the above FMM algorithm.

Step 1: The multipole coefficients of each panel are computed using Eq. (4.14). As in *Step 1* of Section 3.11, the total operation count for this step is c_1MN for some constant c_1 .

Step 2: For each pair of sufficiently separated panels, the multipole coefficients of the local expansion are computed from those of the distant expansion using Eqs. (4.20) to (4.22). To compute all M coefficients $\tilde{\mathbf{b}}_{nm}^q$ using Eq. (4.20) requires $O(M^{3/2})$ operations, as explained in *Step 2* of Section 3.11. The same is true of computing all M coefficients \mathbf{c}_{nm}^q using Eq. (4.22). Since the separation R_0 of each pair of panels is fixed, the summation over p in Eq. (4.21) can be computed in advance. Hence, to compute all M coefficients $\tilde{\mathbf{c}}_{nm}^q$ using Eq. (4.21) during each iteration requires only $O(ML) \sim O(M^{3/2})$ operations. Thus, the combined operation count of Eq. (4.20) to (4.22) is $O(M^{3/2})$ per pair of panels. Since there are approximately P^2 pairs of sufficiently separated panels, the total operation count for this step is $c_2M^{3/2}P^2$ for some constant c_2 .

Step 3: For each panel, the M multipole coefficients \mathbf{c}_{nm}^q are each summed over the index q of the distant panels. Since there are approximately P distant panel for each of the P panels, the total operation count for this step is c_3MP^2 for some constant c_3 .

Step 4: For each panel, the local expansion Eq. (4.17), with \mathbf{c}_{nm}^q replaced by its sum over the index q of the distant panels, is evaluated at all $\approx N/P$ nodes of that panel, using the formulas given in Section J.1 of Appendix J. The total operation count for this step is $c_4M(N/P)P = c_4MN$ for some constant c_4 .

Step 5: For each panel, the direct contribution to the vector potential at each of its $\approx N/P$ nodes due to all other nodes in the neighboring panels is computed, using the quadrature rule discussed in Section J.2 of Appendix J. Since each panel has only a small number of neighboring panels, there are on the order of N/P other

nodes in the neighboring panels. Hence, the total operation count for this step is $c_5(N/P)^2P = c_5N^2/P$ for some constant c_5 .

Adding the operation counts for the above five steps, the total operation count T for each computation of the matrix-vector product represented by the second term on the LHS of Eq. (4.8) is estimated to be

$$T = (c_1 + c_4)MN + c_2M^{3/2}P^2 + c_3MP^2 + c_5\frac{N^2}{P}. \quad (4.23)$$

Using the fact that the number M of multipoles is typically chosen to be of the order the number of nodes in each panel, $M \approx N/P$, Eq. (4.23) becomes

$$T = (c_1 + c_4 + c_5)\frac{N^2}{P} + c_2N^{3/2}\sqrt{P} + c_3NP. \quad (4.24)$$

We would like to choose P so that T is minimized. Differentiating Eq. (4.24) with respect to P and setting the result to zero, we obtain for the optimum value of P

$$0 = -(c_1 + c_4 + c_5)\frac{N^2}{P^2} + \frac{c_2N^{3/2}}{2\sqrt{P}} + c_3N. \quad (4.25)$$

Instead of solving Eq. (4.25) for P , we can always choose P to satisfy a simpler equation obtained from Eq. (4.25) by omitting the third term on the RHS. This simpler equation has the solution

$$P = [2(c_1 + c_4 + c_5)/c_2]^{2/3}N^{1/3}. \quad (4.26)$$

Substituting this value of P into Eq. (4.24) gives

$$T = \frac{3}{2}[2(c_1 + c_4 + c_5)c_2]^{1/3}N^{5/3} + c_3[2(c_1 + c_4 + c_5)/c_2]^{2/3}N^{4/3}. \quad (4.27)$$

This means that the optimum operation count of our FMM algorithm will be no worse than $O(N^{5/3})$ per iteration.

4.6 Use of Symmetry

The geometry of a typical scattering problem is shown in Fig. 4.2. A plane wave polarized in the x direction is incident in the y direction on a perfectly conducting

square plate whose broad faces are perpendicular to the incidence direction. Clearly, this problem has reflection symmetry in the x - y and y - z planes. Such symmetry can be exploited to reduce the number of unknowns in the problem fourfold. To do so, we need to know how the electric and magnetic fields transform under reflection in the x - y and y - z planes.

To determine how the fields transform under reflection in a coordinate plane, we write the Cartesian components of the Maxwell equation $\nabla \times \mathbf{H} = -j\omega\epsilon\mathbf{E}$ out in full,

$$\frac{\partial H_z}{\partial y} - \frac{\partial H_y}{\partial z} = -j\omega\epsilon E_x, \quad (4.28)$$

$$\frac{\partial H_x}{\partial z} - \frac{\partial H_z}{\partial x} = -j\omega\epsilon E_y, \quad (4.29)$$

$$\frac{\partial H_y}{\partial x} - \frac{\partial H_x}{\partial y} = -j\omega\epsilon E_z. \quad (4.30)$$

Let K' be a left-handed coordinate system obtained by inverting the z axis of the original right-handed coordinate system K of Fig. 4.2, that is, by reflecting about the x - y plane. The relationship between vector quantities in the two coordinate systems are

$$(x, y, z) = (x', y', -z'), \quad (4.31)$$

$$\begin{bmatrix} E_x(x, y, z) \\ E_y(x, y, z) \\ E_z(x, y, z) \end{bmatrix} = \begin{bmatrix} E'_x(x', y', z') \\ E'_y(x', y', z') \\ -E'_z(x', y', z') \end{bmatrix}, \quad (4.32)$$

$$\begin{bmatrix} H_x(x, y, z) \\ H_y(x, y, z) \\ H_z(x, y, z) \end{bmatrix} = \begin{bmatrix} H'_x(x', y', z') \\ H'_y(x', y', z') \\ -H'_z(x', y', z') \end{bmatrix}. \quad (4.33)$$

Substituting Eqs. (4.31) to (4.33) into Eqs. (4.28) to (4.30), we obtain

$$\frac{\partial(-H'_z)}{\partial y'} - \frac{\partial(-H'_y)}{\partial z'} = -j\omega\epsilon E'_x, \quad (4.34)$$

$$\frac{\partial(-H'_x)}{\partial z'} - \frac{\partial(-H'_z)}{\partial x'} = -j\omega\epsilon E'_y, \quad (4.35)$$

$$\frac{\partial(-H'_y)}{\partial x'} - \frac{\partial(-H'_x)}{\partial y'} = -j\omega\epsilon E'_z. \quad (4.36)$$

Eqs. (4.34) to (4.36) show that the set of functions (E'_x, E'_y, E'_z) and $[(-H'_x), (-H'_y), (-H'_z)]$ satisfy the Maxwell equation $\nabla \times \mathbf{H} = -j\omega\epsilon\mathbf{E}$ in the variables (x', y', z') .

Now, the incident fields in the original coordinate system K are $E_x^{\text{inc}} = E_0$ and $H_z^{\text{inc}} = -H_0$, the other components of the incident fields being zero. In the reflected coordinate system K' , the incident fields are $E_x^{\text{inc}'} = E_0$ and $(-H_z^{\text{inc}'}) = -H_0$. Thus, the incident excitation for (E_x, E_y, E_z) has the same form as that for (E'_x, E'_y, E'_z) , while the incident excitation for (H_x, H_y, H_z) has the same form as that for $[(-H'_x), (-H'_y), (-H'_z)]$. Because the Maxwell equations Eqs. (4.28) to (4.30) and (4.34) to (4.36) with the same boundary conditions and the same incident excitation must have the same solution, we conclude that the functions (E'_x, E'_y, E'_z) and $[(-H'_x), (-H'_y), (-H'_z)]$ are in fact identical to the functions (E_x, E_y, E_z) and (H_x, H_y, H_z) in the same variables:

$$E'_\mu(x, y, z) = E_\mu(x, y, z), \quad (4.37)$$

$$H'_\mu(x, y, z) = -H_\mu(x, y, z), \quad (4.38)$$

where $\mu = x, y$ or z . Eqs. (4.37) and (4.38) may be used to determine the fields in the half-space $z < 0$ from a knowledge of only the fields in the half-space $z > 0$. For example, suppose we know the fields $E_i(x, y, z)$ and $H_i(x, y, z)$ at a point (x, y, z) with $z > 0$. The image point reflected in the x - y plane has the coordinates $(x, y, -z)$ in the original system K and the coordinates $(x', y', z') = (x, y, +z)$ in the reflected system K' . Hence, Eqs. (4.32) to (4.33) can be rewritten for the image point as

$$\begin{bmatrix} E_x(x, y, -z) \\ E_y(x, y, -z) \\ E_z(x, y, -z) \end{bmatrix} = \begin{bmatrix} E'_x(x, y, z) \\ E'_y(x, y, z) \\ -E'_z(x, y, z) \end{bmatrix}, \quad (4.39)$$

$$\begin{bmatrix} H_x(x, y, -z) \\ H_y(x, y, -z) \\ H_z(x, y, -z) \end{bmatrix} = \begin{bmatrix} H'_x(x, y, z) \\ H'_y(x, y, z) \\ -H'_z(x, y, z) \end{bmatrix}. \quad (4.40)$$

Substituting Eqs. (4.37) and (4.38) into the RHS of Eqs. (4.39) and (4.40), respectively, we obtain the desired field components with respect to the *original* system K at the image point $(x, y, -z)$,

$$\begin{bmatrix} E_x(x, y, -z) \\ E_y(x, y, -z) \\ E_z(x, y, -z) \end{bmatrix} = \begin{bmatrix} E_x(x, y, z) \\ E_y(x, y, z) \\ -E_z(x, y, z) \end{bmatrix}, \quad (4.41)$$

$$\begin{bmatrix} H_x(x, y, -z) \\ H_y(x, y, -z) \\ H_z(x, y, -z) \end{bmatrix} = \begin{bmatrix} -H_x(x, y, z) \\ -H_y(x, y, z) \\ H_z(x, y, z) \end{bmatrix}. \quad (4.42)$$

By an exactly similar procedure, we can obtain the transformation of the field under reflection in the y - z plane,

$$\begin{bmatrix} E_x(-x, y, z) \\ E_y(-x, y, z) \\ E_z(-x, y, z) \end{bmatrix} = \begin{bmatrix} -E_x(x, y, z) \\ E_y(x, y, z) \\ -E_z(x, y, z) \end{bmatrix}, \quad (4.43)$$

$$\begin{bmatrix} H_x(-x, y, z) \\ H_y(-x, y, z) \\ H_z(-x, y, z) \end{bmatrix} = \begin{bmatrix} H_x(x, y, z) \\ -H_y(x, y, z) \\ H_z(x, y, z) \end{bmatrix}. \quad (4.44)$$

By successive application of the transformation equations (4.41) to (4.44), we can obtain the fields in the regions $(x > 0, z < 0)$, $(x < 0, z > 0)$ and $(x < 0, z < 0)$ from the fields in the region $(x > 0, z > 0)$. This way, the number of unknowns is reduced to one-fourth.

4.7 Scattering from Plates and Cubes

To illustrate the accuracy of the multipole approximation and the efficiency of the GMRES algorithm, we computed the radar cross sections (RCS) of perfectly conducting thick plates and cubes. The calculations were done on an IBM RS/6000 Model 530 workstation with 64 megabytes of storage. In order to conserve storage, we did not compute the summation over p in Eq. (4.21) in advance, nor did we compute the rotation matrices $\mathcal{D}_{mm}^{(n)}(\alpha, \beta, \gamma)$ in Eqs. (4.20) and (4.22) in advance. Hence, the CPU times given below are not the optimum values expected from the algorithm.

The plates used in our examples are square plates with a thickness of 0.0317λ . In order to sample accurately the sharp increase of induced currents near the edges, we used approximately 40 nodes per λ on the front and back faces and 60 nodes per λ on the side faces of the plates. For the cubes, we used approximately 40 nodes per λ on all the faces. Symmetry was used to reduce the number of unknowns to one-fourth. The number of multipole coefficients was chosen in all cases to be $M = 36 \approx 0.8$ times the average number of nodes per panel. Figs. 4.3 and 4.4 show the computed broadside

RCS of the plates and cubes, respectively, as functions of the side length W . Also shown in these figures are the measured results reported in the literature [44, 45]. It can be seen from these figures that our computed results are in good agreement with those of measurement. The number of iterations in the GMRES algorithm required to achieve an error tolerance of 10^{-4} and the CPU time per iteration are shown in Tables 4.1 and 4.2 as functions of the number of complex unknowns $n = 2N$. It can be seen that the number of iterations required, N_{iter} , increased rather slowly with problem size. For example, in the case of the plates, as n increased from 120 to 2624, N_{iter} increased only three times.

The speedup achieved with FMM is illustrated in Fig. 4.5, where the CPU time per iteration using FMM-GMRES is compared with that using standard GMRES. In the case of standard GMRES, the method discussed in Section J.2 of Appendix J for neighboring-panel contributions was used for both the distant- and neighboring-panel contributions to the scattered field. This is equivalent to ordinary matrix-vector multiplication whose CPU time per iteration is expected to scale as $O(N^2)$. This was indeed found to be the case, as can be seen from Fig. 4.5. On the other hand, the CPU time per iteration using FMM-GMRES is seen to follow roughly the $O(N^{5/3})$ curve, but rather erratically. This was because, in order to achieve the $O(N^{5/3})$ performance, the number of panels P would have to be chosen in accordance with the formula Eq. (4.26). For simplicity, however, we did not optimize P in this way in our examples. Still, Fig. 4.5 shows that our FMM-GMRES algorithm outperforms the standard GMRES algorithm for N greater than a few hundreds, with increasing speedup as N increases.

The storage cost of FMM-GMRES is compared in Fig. 4.6 with those of standard GMRES and the time-domain-finite-difference (TDFD) method. As stated near the beginning of Section 4.4, the matrix-vector product of the form $\mathcal{A}x$ required at each step of the GMRES algorithm represents the field scattered to each node m from all other nodes $n \neq m$. In standard GMRES, ordinary matrix-vector multiplication is used, in which both the matrix \mathcal{A} and the vector x must be supplied to the multiplica-

tion routine. Since \mathcal{A} is a $2N \times 2N$ dense matrix, the storage requirement for \mathcal{A} alone is $O(N^2)$. This is shown in Fig. 4.6, where the quantity $16n^2$ bytes is plotted against $n = 2N$, where n is the number of complex unknowns, each of which requires 16 bytes of storage in double precision. In FMM-GMRES, however, the scattered field itself, which is equivalent to the matrix-vector product, is computed. This eliminates the need to set up and store the matrix \mathcal{A} itself. Thus, the storage cost of FMM-GMRES scales as $O(N)$. In practice, as mentioned in Section 4.3, one usually stores as many basis vectors of the Krylov subspaces as are needed for convergence, in order to avoid restarting GMRES. Hence, the storage cost of FMM-GMRES is usually at least mn , where m is the number of iterations required for convergence. In all our examples discussed below, $m < 200$. Hence, in Fig. 4.6, we plot the quantity $16 \times 200n$ as being representative of the storage cost of FMM-GMRES. Lastly, in TDFD, one has to store all six components of the electric and magnetic fields at each node of the simulation volume. Furthermore, one has to store the field components at two successive times. Roughly speaking, the number of nodes in the simulation volume is $N^{3/2} = (n/2)^{3/2}$, where N is the number of nodes on a two-dimensional surface in the integral-equation method. Hence, in Fig. 4.6, we plot the quantity $8 \times 6 \times 2 \times (n/2)^{3/2}$ for TDFD, since 8 bytes are required for each *real* field component in double precision. From Fig. 4.6, it can be seen that FMM-GMRES outperforms standard GMRES in storage cost for n greater than a few hundreds, and that it outperforms TDFD for n greater than about 10^4 .

4.8 Problems with Guided Mode Excitation

The integral equation formulation discussed in Section 4.2 can be extended to treat problems with guided mode excitation, such as waveguide sections and horn antennas. Consider the horn model shown in Fig. 4.7. The horn is excited by a generator connected to a rectangular waveguide supporting only the lowest-order, or TE_{10} , mode. We assume that the generator is well shielded so that it radiates only into the rectangular waveguide. The problem is to compute the radiation pattern in the

external region V of Fig. 4.7 where the permittivity is ϵ . This external region is bounded by the surfaces S_0 to S_2 shown in Fig. 4.7 and the surface at infinity. Since there are no waves incident from infinity, the integral over the surface at infinity in the Kirchhoff-Huygens principle Eq. (3.4) gives zero. Hence, we are left with only the integral over the surfaces S_0 to S_2 . Since the generator is well-shielded, the only surface currents that exist on the exterior parts of these surfaces are those that pass out of the mouth of the horn and around the flange. These exterior surface currents are expected to be weaker the farther away they are from the mouth of the horn. Hence, for simplicity, we can discard the exterior part S_2 which is assumed to be sufficiently far from the mouth of the horn that the surface currents on S_2 are negligible. The integral in Eq. (3.4) is therefore confined to the surfaces S_0 and S_1 , where S_0 is a rectangular cross section of the waveguide, which we refer to as the input terminal, and S_1 consists of the inner walls of the waveguide and the inner and outer walls of the horn. We assume that the walls of the waveguide and horn are perfectly conducting. Hence, in the integral over S_1 , the terms involving $(\mathbf{n}' \times \mathbf{E}')$ are absent, and Eq. (3.4) becomes

$$\mathbf{H}(\mathbf{r}) = \mathbf{H}_{S_0}(\mathbf{r}) - \frac{1}{4\pi} \int_{S_1} (\mathbf{n}' \times \mathbf{H}') \times \nabla' \psi dS', \quad (4.45)$$

where $\mathbf{H}_{S_0}(\mathbf{r})$ represents the contribution from the input terminal S_0 ,

$$\mathbf{H}_{S_0}(\mathbf{r}) = \frac{1}{4\pi} \int_{S_0} \left[j\omega\epsilon(\mathbf{n}' \times \mathbf{E}')\psi + \frac{j}{\omega\mu}(\mathbf{n}' \times \mathbf{E}') \cdot \nabla'(\nabla'\psi) - (\mathbf{n}' \times \mathbf{H}') \times \nabla'\psi \right] dS'. \quad (4.46)$$

By letting the field point \mathbf{r} in Eq. (4.45) approach the perfectly conducting surface S_1 and taking the cross product with the outward surface normal \mathbf{n} at \mathbf{r} , we obtain the MFIE

$$\mathbf{n} \times \mathbf{H}(\mathbf{r}) = \mathbf{n} \times \mathbf{H}_{S_0}(\mathbf{r}) - \frac{1}{4\pi} \mathbf{n} \times \int_{S_1} (\mathbf{n}' \times \mathbf{H}') \times \nabla' \psi dS', \quad (4.47)$$

Since the integrand in Eq. (4.47) is singular at $\mathbf{r}' = \mathbf{r}$, we must integrate over the singularity analytically. Following the steps leading from Eq. (4.1) to Eq. (4.7), we

can remove the singular point from the integral by rewriting the MFIE as

$$\frac{1}{2} \mathbf{n} \times \mathbf{H}(\mathbf{r}) = \mathbf{n} \times \mathbf{H}_{S_0}(\mathbf{r}) - \frac{1}{4\pi} \mathbf{n} \times \int_{S_1}' (\mathbf{n}' \times \mathbf{H}') \times \nabla' \psi dS'. \quad (4.48)$$

In order to evaluate the quantity $\mathbf{H}_{S_0}(\mathbf{r})$ defined by Eq. (4.46), it is necessary to know the tangential fields $(\mathbf{n}' \times \mathbf{E}')$ and $(\mathbf{n}' \times \mathbf{H}')$ over the input terminal S_0 of the waveguide. In general, the waves inside the waveguide consist of an incident TE_{10} wave and a number of reflected waves belonging to various waveguide modes. Since the waveguide supports only the TE_{10} mode, we expect that the only reflected wave with significant amplitude at the input terminal is the TE_{10} reflected wave. This can be seen by considering the attenuation constants of the higher-order modes. The attenuation constant α of a cutoff mode in a rectangular waveguide is

$$\alpha = \sqrt{\left(\frac{m\pi}{a}\right)^2 + \left(\frac{n\pi}{b}\right)^2 - \left(\frac{2\pi}{\lambda}\right)^2}, \quad (4.49)$$

where a and b are the transverse dimensions of the waveguide, m and n are integers and λ is the free-space wavelength. In our example, $a = 3.485$ cm, $b = 1.58$ cm and $\lambda = 5$ cm. Hence, the cutoff waveguide mode with the *smallest* real value of α is the one with $m = 2$ and $n = 0$, for which $\alpha = 1.2928$ cm⁻¹. In propagating over the 15-cm distance between the waveguide-horn junction, where this cutoff mode could have been produced, and the input terminal S_0 , the amplitude of this cutoff mode would be attenuated by a factor of $e^{-\alpha \times 15 \text{ cm}} = 3.8 \times 10^{-9}$! Cutoff modes with larger values of α would, of course, be attenuated even more. This justifies neglecting the effects of all the reflected *cutoff* modes at the input terminal. The waves on the input terminal S_0 then consist of an incident TE_{10} wave with unit amplitude and a reflected TE_{10} wave with an unknown amplitude Γ . With respect to the coordinate system shown in Fig. 4.7, the tangential fields $\mathbf{H}' = \mathbf{H}(\mathbf{r}')$ and $\mathbf{E}' = \mathbf{E}(\mathbf{r}')$ on S_0 are thus given by [46]

$$H_y(z') = (1 + \Gamma) \cos \frac{\pi}{a} \left(z' + \frac{a}{2} \right), \quad (4.50)$$

$$H_z(z') = -j \frac{2a}{\lambda_g} (1 - \Gamma) \sin \frac{\pi}{a} \left(z' + \frac{a}{2} \right), \quad (4.51)$$

$$E_x(z') = j \frac{2a}{\lambda_g} Z_H (1 + \Gamma) \sin \frac{\pi}{a} \left(z' + \frac{a}{2} \right), \quad (4.52)$$

where

$$\lambda_g = \frac{\lambda}{\sqrt{1 - \left(\frac{\lambda}{2a}\right)^2}}, \quad (4.53)$$

$$Z_H = \frac{\sqrt{\mu/\epsilon}}{\sqrt{1 - \left(\frac{\lambda}{2a}\right)^2}}. \quad (4.54)$$

We may now evaluate the quantity $\mathbf{H}_{S_0}(\mathbf{r})$ by substituting Eqs. (4.50) to (4.52) into Eq. (4.46). The result may be written in the form

$$\mathbf{n} \times \mathbf{H}_{S_0}(\mathbf{r}) = \mathbf{n} \times \mathbf{H}_{TE_{10}}^{(+)}(\mathbf{r}) + \Gamma \left[\mathbf{n} \times \mathbf{H}_{TE_{10}}^{(-)}(\mathbf{r}) \right], \quad (4.55)$$

where

$$\begin{aligned} \mathbf{H}_{TE_{10}}^{(\pm)}(\mathbf{r}) = & \frac{1}{4\pi} \int_{S_0} \left[j\omega\epsilon(\mathbf{n}' \times \mathbf{E}^{(0)})\psi \right. \\ & \left. + \frac{j}{\omega\mu}(\mathbf{n}' \times \mathbf{E}^{(0)}) \cdot \nabla'(\nabla'\psi) \mp (\mathbf{n}' \times \mathbf{H}^{(0)}) \times \nabla'\psi \right] dS', \end{aligned} \quad (4.56)$$

and

$$H_y^{(0)}(z') = \cos \frac{\pi}{a} \left(z' + \frac{a}{2} \right), \quad (4.57)$$

$$H_z^{(0)}(z') = -j \frac{2a}{\lambda_g} \sin \frac{\pi}{a} \left(z' + \frac{a}{2} \right), \quad (4.58)$$

$$E_x^{(0)}(z') = j \frac{2a}{\lambda_g} Z_H \sin \frac{\pi}{a} \left(z' + \frac{a}{2} \right). \quad (4.59)$$

When Eq. (4.55) is substituted into the RHS of Eq. (4.48), we obtain the MFIE for the tangential magnetic field $\mathbf{n} \times \mathbf{H}(\mathbf{r})$ on the perfectly conducting surface S_1 and for the reflection coefficient Γ . It should be pointed out, from the steps leading from Eq. (4.46) to Eq. (4.48), that Eq. (4.48) is valid only when the field point \mathbf{r} approaches S_1 , rather than S_0 . To solve Eq. (4.48), we discretize S_1 into N surface elements, or nodes, over each of which the tangential magnetic field has a constant, unknown value $(\mathbf{n} \times \mathbf{H})_m$ for the m th node. By letting \mathbf{r} range over all the nodes on S_1 (point collocation), we obtain as many equations as there are unknown field values $(\mathbf{n} \times \mathbf{H})_m$ on S_1 . However, we need one more equation because we have an extra unknown Γ .

This extra equation may be obtained by letting \mathbf{r} in Eq. (4.47) approach the center \mathbf{r}_0 of the input terminal S_0 , rather than S_1 ,

$$\mathbf{n} \times \mathbf{H}(\mathbf{r}_0) = \mathbf{n} \times \mathbf{H}_{S_0}(\mathbf{r}_0) - \frac{1}{4\pi} \mathbf{n} \times \int_{S_1} (\mathbf{n}' \times \mathbf{H}') \times \nabla' \psi|_{\mathbf{r}=\mathbf{r}_0} dS'. \quad (4.60)$$

The quantity $\mathbf{H}(\mathbf{r}_0)$ on the LHS of Eq. (4.60) is the magnetic field on S_0 . From Eqs. (4.50) and (4.51), $\mathbf{H}(\mathbf{r}_0)$ has only the y and z components. Also, in the coordinate system of Fig. 4.7, the outward unit normal on S_0 is $\mathbf{n} = -\mathbf{y}$. Hence, the LHS of Eq. (4.60) is

$$\begin{aligned} \mathbf{n} \times \mathbf{H}(\mathbf{r}_0) &= -(\mathbf{y} \times \mathbf{z})H_z(0) \\ &= -x(1 - \Gamma)H_z^{(0)}(0), \end{aligned} \quad (4.61)$$

where we have used Eqs. (4.51) and (4.58). In the integral over S_1 in Eq. (4.60), the integrand has no singularity, since \mathbf{r}_0 is at the center of S_0 while \mathbf{r}' lies on S_1 , so that the denominator $|\mathbf{r}_0 - \mathbf{r}'|$ in ψ never vanishes. However, the integral over S_0 occurring in $\mathbf{H}_{S_0}(\mathbf{r}_0)$ now includes the point \mathbf{r}_0 on S_0 where the integrand is singular. Hence, the evaluation of the term $\mathbf{n} \times \mathbf{H}_{S_0}(\mathbf{r}_0)$ on the RHS of Eq. (4.60) must be done carefully. This is discussed in Appendix K. When Eq. (K.13) of Appendix K and Eq. (4.61) are substituted into Eq. (4.60) and the x component of the resulting equation is taken, we obtain the extra equation needed to solve for the unknown reflection coefficient Γ .

4.8.1 Shorted Waveguide

The accuracy of the formulation discussed above was tested on the trivial example of a shorted waveguide section, for which closed-form solution is available. The phase constant of the TE_{10} mode of the rectangular waveguide used in the horn problem of Fig. 4.7 is

$$\beta = \frac{2\pi}{\lambda} \sqrt{1 - \left(\frac{\lambda}{2a}\right)^2}. \quad (4.62)$$

The reflection coefficient at the input terminal S_0 for a waveguide section of length L shorted at the other end is given by

$$\Gamma = -e^{2j\beta L}. \quad (4.63)$$

In our example, $a = 3.485$ cm, $\lambda = 5$ cm and $L = 7.5$ or 15.0 cm. Hence,

$$\Gamma = \begin{cases} -0.84397 - 0.53640j, & L = 7.5 \text{ cm} \\ -0.42455 - 0.90540j, & L = 15.0 \text{ cm} \end{cases} \quad (4.64)$$

The computed reflection coefficients using FMM-GMRES were

$$\Gamma_{\text{computed}} = \begin{cases} -0.81598 - 0.51777j, & L = 7.5 \text{ cm} \\ -0.41672 - 0.85894j, & L = 15.0 \text{ cm} \end{cases} \quad (4.65)$$

The density of nodes used in the above calculations was approximately 30 nodes per wavelength. The number of GMRES iterations required to achieve an error tolerance of 10^{-4} was 28 for $L = 7.5$ cm and 41 for $L = 15.0$ cm. The agreement between the computed and theoretical reflection coefficients is seen to be quite good. The small discrepancies observed are believed to be due to (i) an insufficient density of nodes near the sharp edges, (ii) inaccuracy of the four-point Gaussian quadrature method used to compute neighboring-panel contributions, and (iii) inaccuracy of the rectangular rule used in the same-cell integration method discussed in Appendix K.

4.8.2 Horn Antenna

The horn geometry is shown in Fig. 4.8, which is similar to the geometry of the C36 horn antenna studied by Ratajczak et al. [47] except for the detailed shape of the flange. In our calculation, the density of nodes used was approximately 10 nodes per wavelength in regions of low current level and 15 nodes per wavelength in regions of high current level and near the sharp edges. Symmetry was used to reduce the number of unknowns to one-fourth. Thus, although the total number of nodes in all four quadrants of the horn was 10,240, the total number of complex unknowns was only $[(10,240/4) \times 2 + 1] = 5121$, since there are two tangential field components at each node and one extra unknown Γ . The total number of panels in all four quadrants was $P = 236$ and the number of multipole coefficients was $M = 36$. This calculation required 175 GMRES iterations to achieve an error tolerance of 10^{-4} , and the total CPU time was 6.0 hours. Of the 6 hours of CPU time, it was found that approximately 1.4 hours were spent in computing the rotation matrices in Eqs.

(4.20) and (4.22), and 0.2 hour in computing the summation over p in Eq. (4.21). Thus, for problems of the present size, whether the latter summation is computed in advance or not has little impact on CPU time. Had FMM not been used, the CPU time for this calculation would have been 14 hours. Our computed reflection coefficient of $\Gamma = -0.0697 + 0.0614j$ is in reasonable agreement with the measured results of [47], $\Gamma_{\text{measured}} \approx -0.049 + 0.049j$. Our computed radiation patterns shown in Fig. 4.9 are also in reasonable agreement with the measured results of [47]. The small discrepancies observed in the H plane results of this figure are believed to be due to the use of an insufficient density of nodes near the sharp edges.

4.9 The Long-Wavelength Limit

The examples we used in Section 4.7 to illustrate the efficiency of our FMM-GMRES algorithm are those in which the size of the scatterer is of the order of a wavelength or larger. Besides problems such as these in the intermediate-wavelength (resonance) to short-wavelength region of the electromagnetic spectrum, there is also much current interest in applying FMM to long-wavelength problems such as the modeling of parasitics in high-speed integrated circuits. The size of a typical scatterer within a high-speed integrated circuit may be of the order of $\Delta l = 10\mu\text{m}$ or less, while the frequency components of the voltage waveforms may range from $f = 500$ MHz to $f = 5$ GHz. Thus, the quantity kR_0 appearing in the argument of the spherical Hankel function in the distant-to-local transformation Eq. (4.18) may range from $(2\pi f/c)\Delta l = 0.0001$ to 0.001 radian. In this long-wavelength limit, we expect Eq. (4.18) to reduce to the transformation formula for multipoles in *electrostatics*. Indeed, from the small-argument limit of the spherical Hankel function,

$$\lim_{z \rightarrow 0} h_p^{(1)}(z) = -j \frac{(2p-1)!!}{z^{p+1}}, \quad (4.66)$$

we see that, as kR_0 becomes very small, successive terms in the summation over p in Eq. (4.18) grow as $1/(kR_0)^{p+1}$, so that in the long-wavelength limit, we may ignore all the terms in the summation over p except the one with $p = \nu + n$. Then,

using Eq. (4.66) and Eq. (I.11) with μ replaced by $-\mu$, Eq. (4.18) becomes in the long-wavelength limit

$$\begin{aligned} \mathbf{c}_{\nu\mu}^q &= \sum_{n=0}^L \sum_{m=-n}^n (-1)^{n+\mu} (2\nu+1) \frac{(2n-1)!!(2\nu-1)!!(n+\nu-m+\mu)!}{(2n+2\nu-1)!!(n-m)!(\nu+\mu)!} \\ &\quad \times (-j) \frac{(2n+2\nu-1)!!}{(kR_0)^{n+\nu+1}} P_{n+\nu}^{m-\mu}(\cos\theta_0) e^{j(m-\mu)\phi_0} \mathbf{b}_{nm}^q. \end{aligned} \quad (4.67)$$

Using Eq. (4.66) and the small-argument limit of the spherical bessel function,

$$\lim_{z \rightarrow 0} j_n(z) = \frac{z^n}{(2n+1)!!}, \quad (4.68)$$

we can rewrite the distant and local multipole expansions Eqs. (4.13) and (4.17) as

$$\Delta \mathbf{A}_e^q(\mathbf{r}) = \sum_{l=0}^L \sum_{m=-l}^l \frac{\mathbf{f}_{lm}^q}{r^{l+1}} \sqrt{\frac{4\pi}{2l+1}} Y_l^m(\theta, \phi), \quad (4.69)$$

$$\Delta \mathbf{A}_e^q(\mathbf{r}) = \sum_{l=0}^L \sum_{m=-l}^l \mathbf{g}_{lm}^q r^l \sqrt{\frac{4\pi}{2l+1}} Y_l^m(\theta_1, \phi_1), \quad (4.70)$$

where the spherical harmonics $Y_l^m(\theta, \phi)$ are defined in terms of the associated Legendre polynomials by

$$Y_l^m(\theta, \phi) = (-1)^m \sqrt{\frac{2l+1}{4\pi} \frac{(l-m)!}{(l+m)!}} P_l^m(\cos\theta) e^{jm\phi}, \quad (4.71)$$

and the new multipole coefficients \mathbf{f}_{lm}^q and \mathbf{g}_{lm}^q are related to the old coefficients \mathbf{b}_{lm}^q and \mathbf{c}_{lm}^q by

$$\mathbf{f}_{lm}^q = -j(-1)^m \frac{(2l-1)!!}{k^{l+1}} \sqrt{\frac{(l+m)!}{(l-m)!}} \mathbf{b}_{lm}^q, \quad (4.72)$$

$$\mathbf{g}_{lm}^q = (-1)^m \frac{k^l}{(2l+1)!!} \sqrt{\frac{(l+m)!}{(l-m)!}} \mathbf{c}_{lm}^q. \quad (4.73)$$

Substituting Eqs. (4.71) to (4.73) into Eq. (4.67), we obtain the transformation equation for the new multipole coefficients,

$$\begin{aligned} \mathbf{g}_{\nu\mu}^q &= \sum_{n=0}^L \sum_{m=-n}^n (-1)^{n+\mu} \sqrt{\frac{(n+\nu+m-\mu)!(n+\nu-m+\mu)!}{(n+m)!(n-m)!(\nu+\mu)!(\nu-\mu)!}} \\ &\quad \times \sqrt{\frac{4\pi}{2l+1}} Y_{n+\nu}^{m-\mu}(\theta_0, \phi_0) \frac{\mathbf{f}_{nm}^q}{R_0^{n+\nu+1}}. \end{aligned} \quad (4.74)$$

Eq. (4.74) is precisely the distant-to-local transformation formula in the electrostatics limit [48, 49]. This shows that the FMM formalism discussed in Section 4.4 is numerically stable in the long-wavelength limit, in that it goes over smoothly into the electrostatics result as the wavelength is increased. As such, our FMM formalism is suitable for application to on-chip interconnect and other long-wavelength problems.

4.10 Comparison with the Standard FMM

Recently, Coifman, Rokhlin and Wandzura [15] developed a three-dimensional FMM for the EFIE of electromagnetic scattering. We shall refer to their algorithm as the standard FMM algorithm. The operation count of the standard FMM algorithm is $O(N^{3/2})$ per iteration, which is more efficient than our $O(N^{5/3})$ algorithm discussed in Section 4.4. The question arises as to what advantage our FMM algorithm has over the standard FMM algorithm. The answer is that our FMM algorithm is numerically stable in the long-wavelength limit, as shown in the last section, whereas the standard algorithm is not. To see this, we first review the latter algorithm.

In our FMM algorithm discussed in Section 4.4, the radiation field in the far zone due to the current sources in a panel q is represented by a sum of *multipole waves* of the form Eq. (4.13). In the standard FMM algorithm, however, the same radiation field is represented by a sum of *plane waves* propagating in various directions. This is made possible by using an alternative series expansion for the Green function ψ equivalent to Eq. (3.49). Let \mathbf{X}_{pq} be the displacement vector from the origin of a distant coordinate system K_q to the origin of the coordinate system K_p centered at the field panel p . Then, we write $\mathbf{r} - \mathbf{r}' = \mathbf{X}_{pq} + \mathbf{d}$, where \mathbf{r} and \mathbf{r}' lie on panels p and q , respectively. This defines a vector \mathbf{d} as

$$\mathbf{d} = \mathbf{r} - \mathbf{r}' - \mathbf{X}_{pq}. \quad (4.75)$$

Noting that $d < X_{pq}$ for well separated panels p and q , the series expansion for the Green function is given by

$$\frac{e^{jk|\mathbf{X}_{pq}+\mathbf{d}|}}{|\mathbf{X}_{pq}+\mathbf{d}|} = \sum_{l=0}^{\infty} jk(-1)^l(2l+1)j_l(kd)h_l^{(1)}(kX_{pq})P_l[\cos \angle(\mathbf{d}, \mathbf{X}_{pq})]. \quad (4.76)$$

Eq. (4.76) is a series of multipole waves of the type $j_l(kd)P_l[\cos \angle(\mathbf{d}, \mathbf{X}_{pq})]$. These multipole waves can be transformed into plane waves by means of the following relationship [39],

$$j_l(kd)P_l[\cos \angle(\mathbf{d}, \mathbf{X}_{pq})] = \frac{1}{4\pi j^l} \int d\Omega_k e^{j\mathbf{k}\cdot\mathbf{d}} P_l[\cos \angle(\mathbf{k}, \mathbf{X}_{pq})], \quad (4.77)$$

where $d\Omega_k$ is an element of solid angle traced out by the vector \mathbf{k} of constant length k , and the integral is over all directions of \mathbf{k} . Substituting Eq. (4.77) into Eq. (4.76), we obtain

$$\frac{e^{jk|\mathbf{X}_{pq}+\mathbf{d}|}}{|\mathbf{X}_{pq}+\mathbf{d}|} = \frac{jk}{4\pi} \int d\Omega_k e^{j\mathbf{k}\cdot\mathbf{d}} \sum_{l=0}^L j^l (2l+1) h_l^{(1)}(kX_{pq}) P_l[\cos \angle(\mathbf{k}, \mathbf{X}_{pq})], \quad (4.78)$$

where we have truncated the summation over l to $(L+1)$ terms and have interchanged the order of summation and integration, even though it is mathematically illegitimate to do so. Defining a quantity $\mathcal{T}_{pq}(\mathbf{k})$ as

$$\mathcal{T}_{pq}(\mathbf{k}) = \frac{k}{(4\pi)^2} \sum_{l=0}^L j^l (2l+1) h_l^{(1)}(kX_{pq}) P_l[\cos \angle(\mathbf{k}, \mathbf{X}_{pq})], \quad (4.79)$$

Eq. (4.78) may be rewritten as

$$\frac{e^{jk|\mathbf{X}_{pq}+\mathbf{d}|}}{4\pi|\mathbf{X}_{pq}+\mathbf{d}|} = j \int d\Omega_k e^{j\mathbf{k}\cdot\mathbf{d}} \mathcal{T}_{pq}(\mathbf{k}). \quad (4.80)$$

Now, the vector potential due to the electric current sources in panel q is given by

$$\Delta \mathbf{A}_e^q(\mathbf{r}) = \int_{\Delta S_q} \mathbf{J}(\mathbf{r}') \frac{e^{jk|\mathbf{r}-\mathbf{r}'|}}{4\pi|\mathbf{r}-\mathbf{r}'|} dS', \quad (4.81)$$

in analogy with Eq. (3.47). Substituting Eq. (4.75) into Eq. (4.80) and then the resulting expression into Eq. (4.81), we obtain the desired *plane-wave representation* of the field in the far zone due to the sources in panel q ,

$$\Delta \mathbf{A}_e^q(\mathbf{r}) = \int d\Omega_k e^{j\mathbf{k}\cdot\mathbf{r}} \mathbf{U}_q(\mathbf{k}), \quad (4.82)$$

where

$$\mathbf{U}_q(\mathbf{k}) = j e^{-j\mathbf{k}\cdot\mathbf{X}_{pq}} \mathcal{T}_{pq}(\mathbf{k}) \int_{\Delta S_q} \mathbf{J}(\mathbf{r}') e^{-j\mathbf{k}\cdot\mathbf{r}'} dS'. \quad (4.83)$$

Note that the quantity $U_q(\mathbf{k})$ is independent of the field point \mathbf{r} . Hence, in summing the contributions from all the distant panels q , we can carry out the summation over q in Eq. (4.82) prior to evaluating the integral over all directions of \mathbf{k} for different field points \mathbf{r} in panel p . This leads to an $O(N^{3/2})$ FMM algorithm as discussed in [15].

The standard FMM algorithm discussed above is suitable for intermediate- and short-wavelength problems. This is because, as pointed out in [15], the quantity $\mathcal{T}_{pq}(\mathbf{k})$ defined by Eq. (4.79) diverges in the limit $L \rightarrow \infty$. For intermediate- and short-wavelength problems, where the argument kX_{pq} of the spherical Hankel function is of the order of unity or larger, the difficulty associated with the divergence of the sum over l in Eq. (4.79) does not become apparent until L is much larger than what one normally needs to obtain good accuracy. However, for long-wavelength problems, where kX_{pq} is much smaller than unity, the series in Eq. (4.79) diverges so rapidly that numerical instability sets in even for small values of L . This can be seen in more detail as follows. If Eq. (4.79) is substituted into Eq. (4.80) and the integration over the solid angle is performed, we expect to get back Eq. (4.76) but with the sum over l truncated to $(L+1)$ terms. To check this, we employ the following series expansion of a plane wave $e^{j\mathbf{k}\cdot\mathbf{r}}$ [39]:

$$e^{j\mathbf{k}\cdot\mathbf{d}} = \sum_{n=0}^{\infty} j^n (2n+1) j_n(kd) P_n[\cos \angle(\mathbf{k}, \mathbf{d})]. \quad (4.84)$$

Substituting Eqs. (4.84) and (4.79) into the RHS of Eq. (4.80), we obtain

$$\begin{aligned} 4\pi j \int d\Omega_k e^{j\mathbf{k}\cdot\mathbf{d}} \mathcal{T}_{pq}(\mathbf{k}) &= j \frac{k}{4\pi} \sum_{l=0}^L j^l (2l+1) h_l^{(1)}(kX_{pq}) \sum_{n=0}^{\infty} j^n (2n+1) j_n(kd) \\ &\quad \times \int d\Omega_k P_n[\cos \angle(\mathbf{k}, \mathbf{d})] P_l[\cos \angle(\mathbf{k}, \mathbf{X}_{pq})]. \end{aligned} \quad (4.85)$$

In exact arithmetic, we have the following orthogonality property of the Legendre polynomials,

$$\int d\Omega_k P_n[\cos \angle(\mathbf{k}, \mathbf{d})] P_l[\cos \angle(\mathbf{k}, \mathbf{X}_{pq})] = \frac{4\pi}{2l+1} \delta_{nl} P_l[\cos \angle(\mathbf{d}, \mathbf{X}_{pq})]. \quad (4.86)$$

In this case, Eq. (4.85) is seen indeed to reduce to Eq. (4.76). In numerical integration, however, orthogonality of the Legendre polynomials is only approximately true. Thus,

instead of Eq. (4.86), we have

$$\int d\Omega_k P_n[\cos \angle(\mathbf{k}, \mathbf{d})] P_l[\cos \angle(\mathbf{k}, \mathbf{X}_{pq})] = \frac{4\pi}{2l+1} \delta_{nl} P_l[\cos \angle(\mathbf{d}, \mathbf{X}_{pq})] + \varepsilon_{nl}, \quad (4.87)$$

where ε_{nl} is some small quantity which depends on the machine precision as well as on the accuracy of the numerical quadrature routine. Substituting Eq. (4.87) into Eq. (4.85), we see that the error ε_{nl} in the integration over the solid angle leads to an error $\Delta\psi$ in the computed Green function of amount

$$\Delta\psi = \sum_{l=0}^L \sum_{n=0}^{\infty} \frac{k}{4\pi} j^{l+n+1} (2l+1)(2n+1) j_n(kd) h_l^{(1)}(kX_{pq}) \varepsilon_{nl}. \quad (4.88)$$

In the long-wavelength, both kd and kX_{pq} are much smaller than unity, with $d < X_{pq}$. Thus, we may use the small-argument limit of the spherical Bessel and Hankel functions,

$$j_n(kd) h_l^{(1)}(kX_{pq}) \approx -j \frac{(2l-1)!!}{(2n+1)!!} \frac{(kd)^n}{(kX_{pq})^{l+1}}. \quad (4.89)$$

Since both kd and kX_{pq} are much smaller than unity, the RHS of Eq. (4.89) is largest for the smallest possible value of n and the largest possible value of l , namely, $n=0$ and $l=L$. Keeping only this largest term in Eq. (4.88), we obtain an estimate of the error in the computed Green function,

$$\Delta\psi \approx \frac{k}{4\pi} j^L (2L+1)!! \frac{\varepsilon_{0L}}{(kX_{pq})^{L+1}}. \quad (4.90)$$

On the other hand, ψ itself is of the order of $\frac{1}{|\mathbf{X}_{pq} + \mathbf{d}|} \approx \frac{1}{X_{pq}}$. Hence, the relative error in the computed Green function is estimated to be

$$\left| \frac{\Delta\psi}{\psi} \right| \approx \frac{(2L+1)!!}{4\pi} \frac{\varepsilon_{0L}}{(kX_{pq})^L}. \quad (4.91)$$

Let us apply this result to the parasitics-modeling problem mentioned at the beginning of Section 4.9, where kX_{pq} ranges from 0.0001 to 0.001. Suppose our numerical quadrature routine is exact, so that ε_{0L} is of the order of the machine epsilon. Then, for double precision arithmetic, $\varepsilon_{0L} \approx 10^{-15}$. Furthermore, if we

desire the relative error in the computed Green function to be one percent or less, Eq. (4.91) gives

$$\frac{(2L+1)!!}{4\pi} \frac{10^{-15}}{(kX_{pq})^L} < 0.01. \quad (4.92)$$

The inequality Eq. (4.92) has the solution $L \leq 3$ for $kX_{pq} = 0.0001$ to 0.001 . Thus, in this parasitics-modeling problem, we are limited by numerical instability of the standard FMM algorithm to four multipole terms, even in double precision arithmetic. The situation is, of course, worse if our numerical quadrature routine is inexact, or if we use single precision arithmetic.

Actually, Coifman et al. [15] gave a criterion for the applicability of the standard FMM which is more pessimistic than our above estimate. According to these authors, the upper limit L of the summation in Eq. (4.79) should be chosen according to the following rule:

$$L = \begin{cases} kD + 5 \ln(kD + \pi), & \text{single precision} \\ kD + 10 \ln(kD + \pi), & \text{double precision} \end{cases}, \quad (4.93)$$

where D is the diameter of the smallest sphere enclosing the largest panel. Furthermore, these authors state that, in order to avoid numerical instability, the standard FMM should only be used on sufficiently separated panel pairs (p, q) such that $kX_{pq} > L$. Applying these results to the above parasitics-modeling problem, we have $kD = 0.0001$ to 0.001 , so that $L \approx 6$ in single precision. Hence, in order to apply the standard FMM, the panel pairs (p, q) should be separated by a distance $X_{pq} > L/k = Lc/(2\pi f) \geq 6$ cm. Since a typical chip is not much larger than $2 \text{ cm} \times 2 \text{ cm}$, this would mean that the standard FMM should *not* be used anywhere inside a chip! Of course, this estimate of [15] is too pessimistic. On the contrary, the estimate we gave in the last paragraph indicates that one *can* still apply the standard FMM inside a chip, but with loss of accuracy in the computed Green function and in the multipole approximation, in which one is limited to $L = 3$.

Concerning the speed of the standard FMM algorithm, we find in the literature [50] that the total CPU time required to achieve an error tolerance of 10^{-4} in the solution of the RCS problem for a square metallic plate involving approximately

2000 unknowns was about 2000 seconds. The calculation was performed on a SUN-SPARC-2 workstation with 64 megabytes of storage. This may be compared with our results shown in Table 4.1, where it can be seen that the RCS problem for a thick square plate involving approximately 2000 unknowns required a total CPU time of $34 \times 21.0 = 714$ seconds on an IBM RS/6000 Model 530 workstation with the same amount of storage. Assuming that the SUN-SPARC-2 workstation in question was a 40 MHz variety with a benchmark of approximately 4 MFlops, while the benchmark of our IBM RS/6000 workstation was approximately 11 MFlops, we find that the performance of the standard FMM algorithm is actually about the same as that of our FMM algorithm, after adjusting for processor speed, for problems of the present size.

4.11 Conclusions

In this chapter, we have discussed a 3-D FMM formalism which differs from the standard FMM formalism in that the radiation field due to the sources in a *distant* panel is represented by a sum of multipole waves, rather than by a sum of plane waves. The accuracy of our algorithm was demonstrated by excellent agreement between our computed results and the published data on radar cross sections of perfectly conducting thick plates and cubes. We have also extended the boundary conditions to deal with problems with guided mode excitation. The accuracy of these extended boundary conditions was demonstrated by good agreement with published data on the radiation patterns of a pyramidal horn antenna.

The CPU cost of our FMM algorithm is $O(N^{5/3})$, compared with $O(N^{3/2})$ for the standard FMM algorithm. However, for problem size of a few thousand unknowns, our benchmark indicated that the two FMM algorithms are approximately equally fast. This shows that the overhead burden due to the use of more complicate transformation formulas in our FMM algorithm is quite insignificant for problems of the above size. More significant is the fact that the standard FMM algorithm is numerically unstable in the long-wavelength limit, whereas ours is numerically stable in this limit. Thus,

our algorithm is more suitable for application to long-wavelength problems such as the modeling of parasitics inside a chip.

Although the discussion in this chapter has been limited to perfectly conducting objects, it can be generalized to the case of dielectric objects by introducing a second vector potential to treat the fields radiated by equivalent *magnetic* surface currents. Also, the algorithm discussed in this chapter is based on a one-level grouping of the surface nodes into panels. More sophisticated, multi-level grouping schemes can be developed to reduce the CPU cost to $O(N \log N)$ in the limit of very large N . One such scheme developed for the standard FMM algorithm was recently proposed by Dembart and Yip [51].

Table 4.1: Computed Results for RCS of Perfectly Conducting Plates of Thickness 0.0317λ

Side length (λ)	No. of complex unknowns	No. of iterations (err = 10^{-4})	CPU per iteration (seconds)	RCS (λ^2)
0.1	48	10	0.2	0.000698
0.2	120	12	0.4	0.0344
0.3	224	15	0.9	0.410
0.4	368	16	1.0	1.43
0.5	544	18	4.4	2.47
0.6	736	19	5.6	3.59
0.7	976	22	7.4	5.06
0.8	1116	26	14.5	6.90
0.9	1536	30	17.6	9.16
1.0	2052	34	21.0	12.0
1.1	2624	37	42.1	17.3

Table 4.2: Computed Results for RCS of Perfectly Conducting Cubes

Side length (λ)	No. of complex unknowns	No. of iterations (err = 10^{-4})	CPU per iteration (seconds)	RCS (λ^2)
0.1	48	9	0.2	0.00335
0.2	192	11	0.8	0.151
0.3	432	13	2.5	0.268
0.4	736	14	5.5	0.0877
0.5	1200	15	17.3	2.23
0.6	1728	16	19.8	3.86
0.7	2464	24	27.2	3.34
0.8	2700	22	79.4	4.27
0.9	3888	22	83.4	7.63

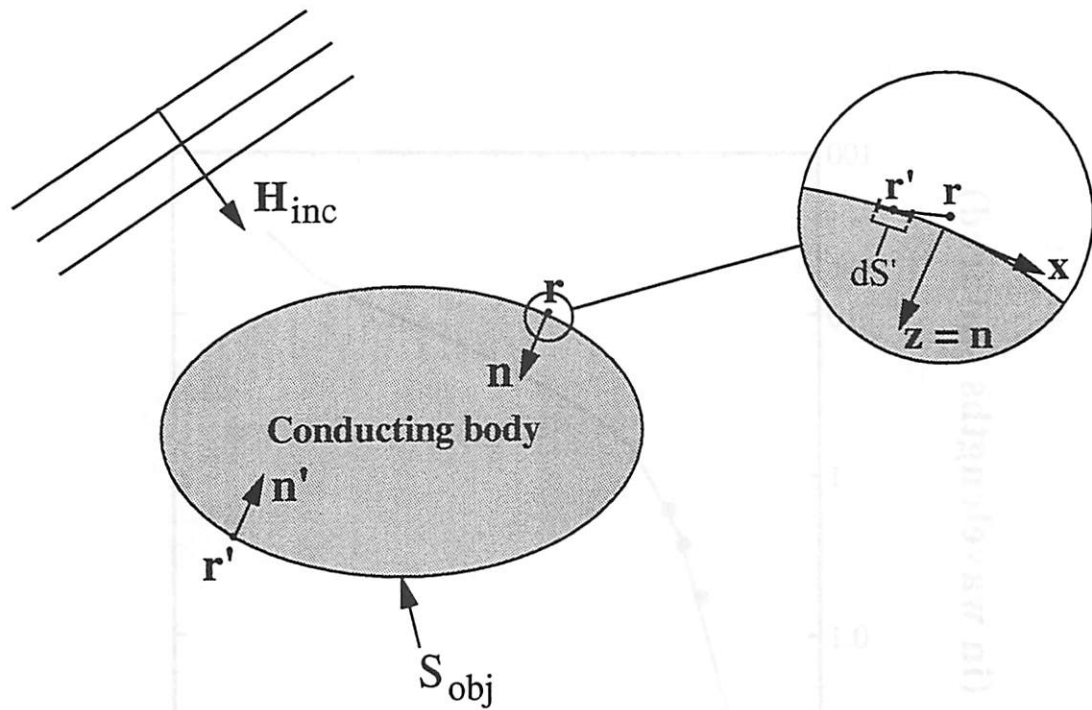


Figure 4.1: Electromagnetic scattering from a perfectly conducting object.

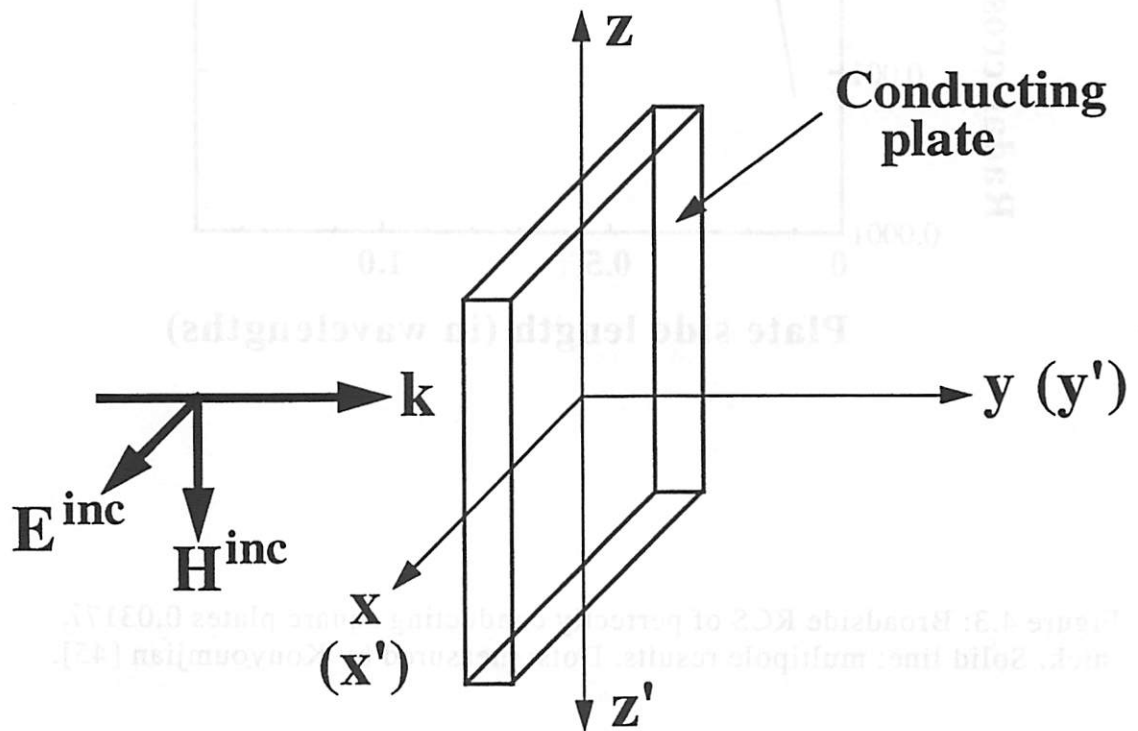


Figure 4.2: A scattering problem with symmetry in the x - y and y - z planes.

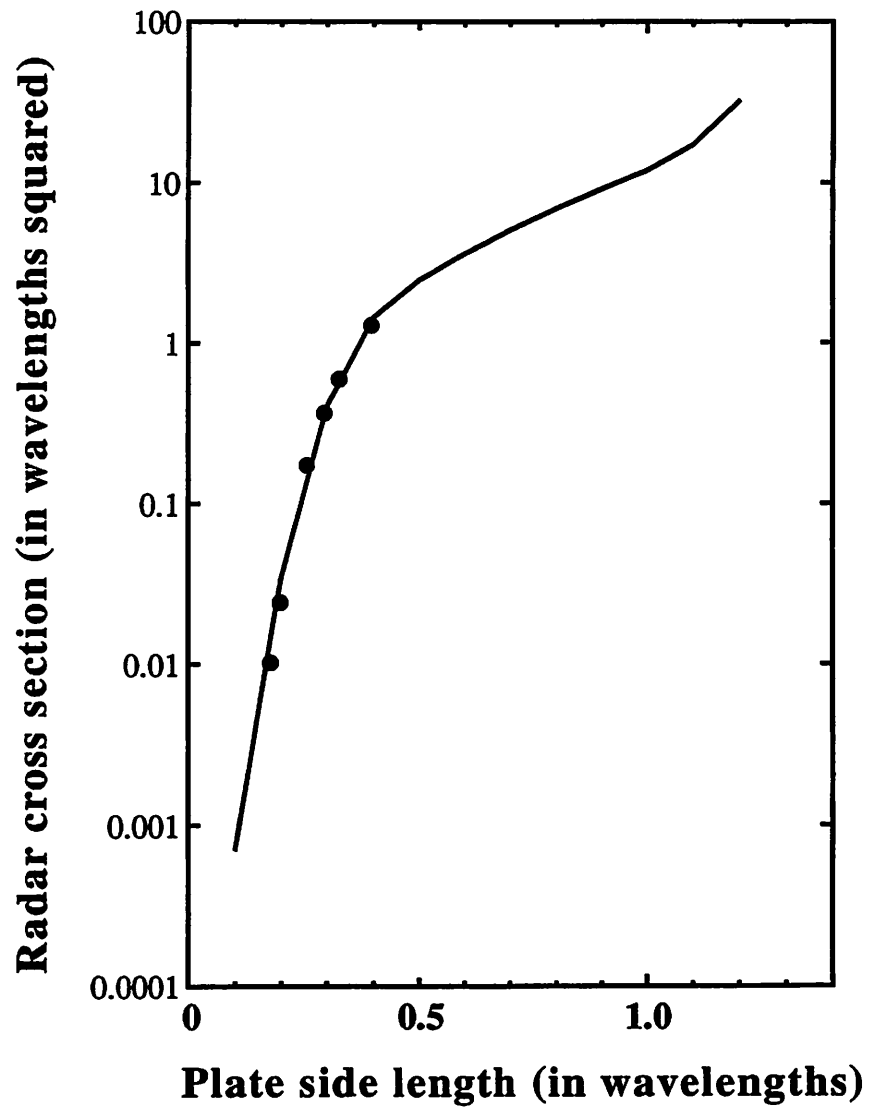


Figure 4.3: Broadside RCS of perfectly conducting square plates 0.0317λ thick. Solid line: multipole results. Dots: measured by Kouyoumjian [45].

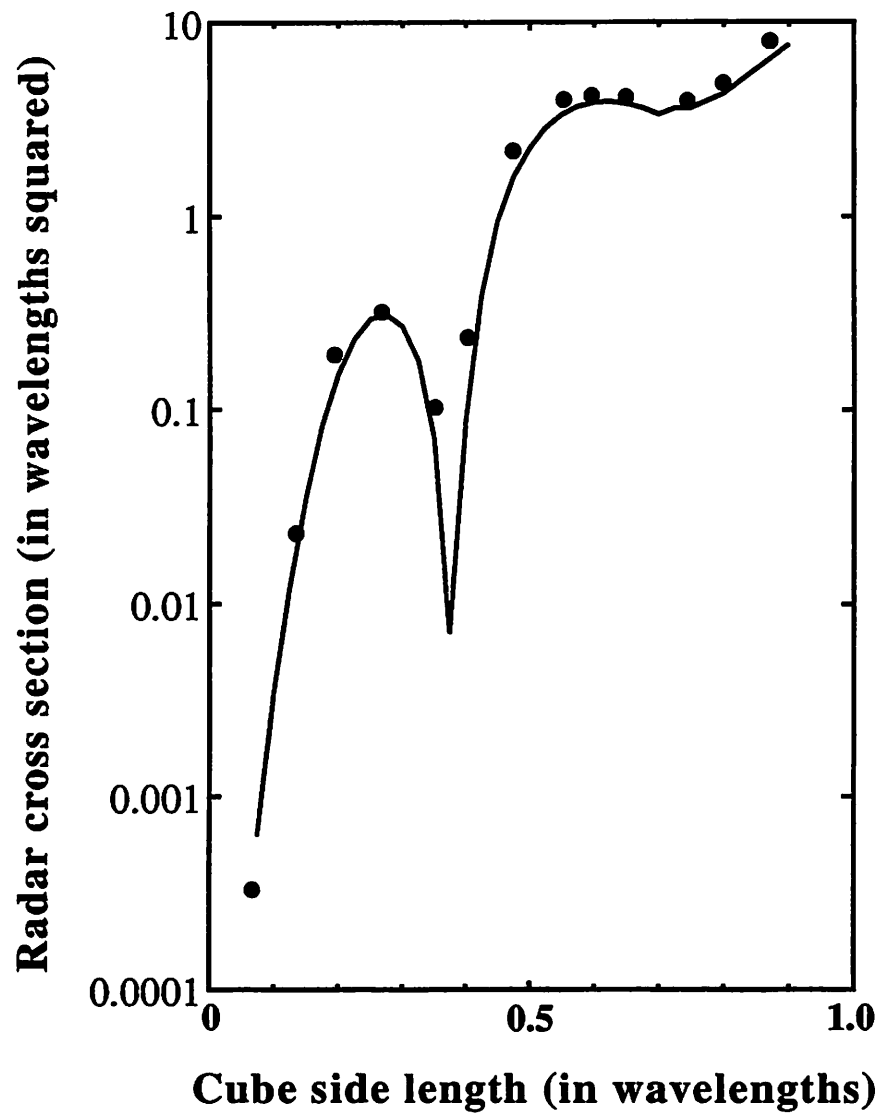


Figure 4.4: Broadside RCS of perfectly conducting cubes. Solid line: multipole results. Dots: measured by Ryan [44].

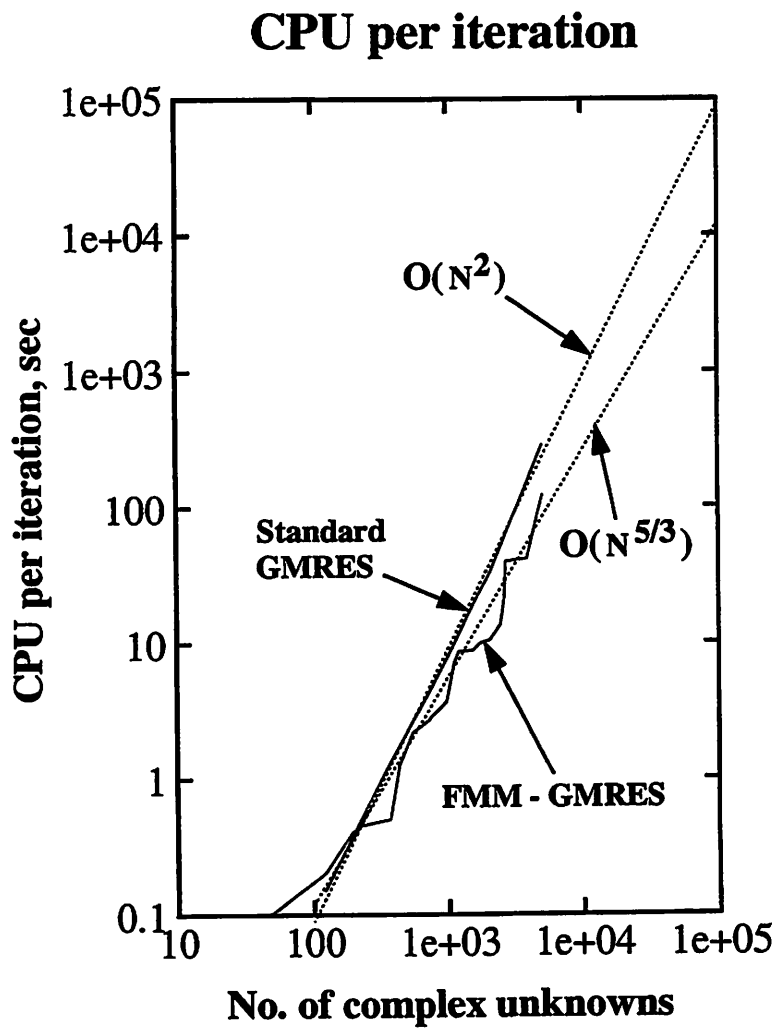


Figure 4.5: CPU cost per iteration.

Storage, double precision

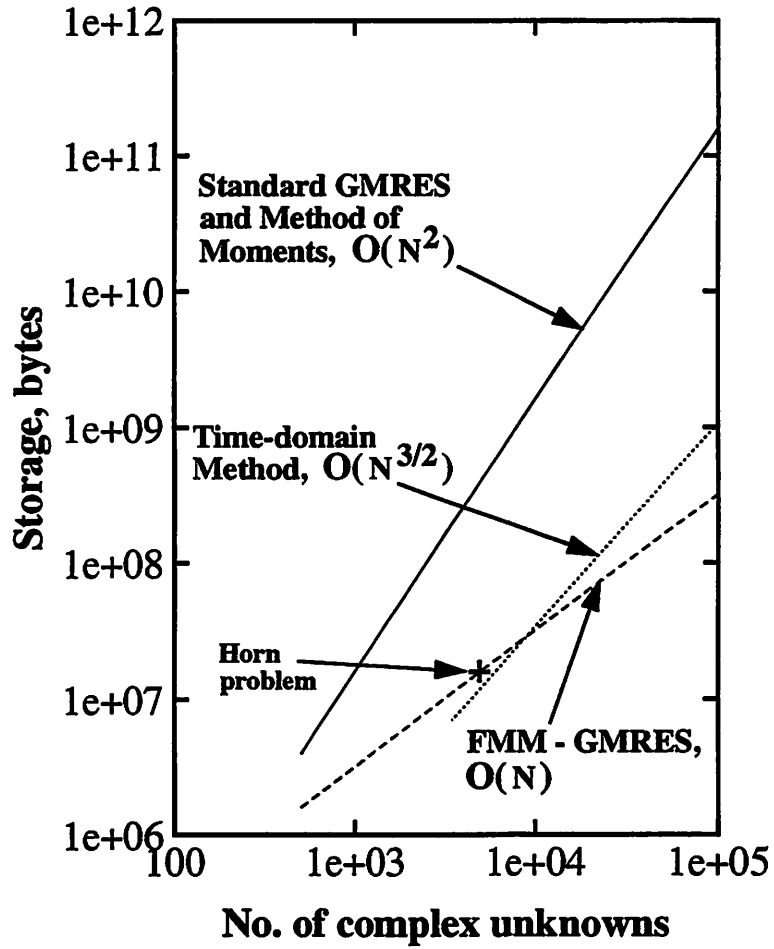


Figure 4.6: Storage cost for double precision.

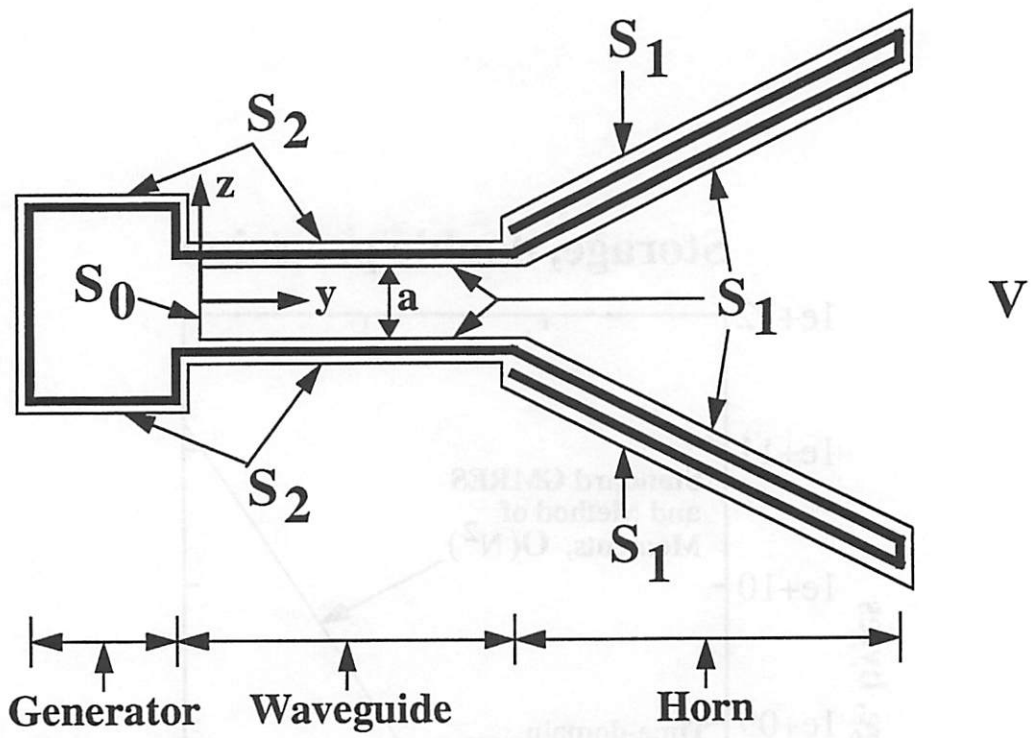


Figure 4.7: Horn model.

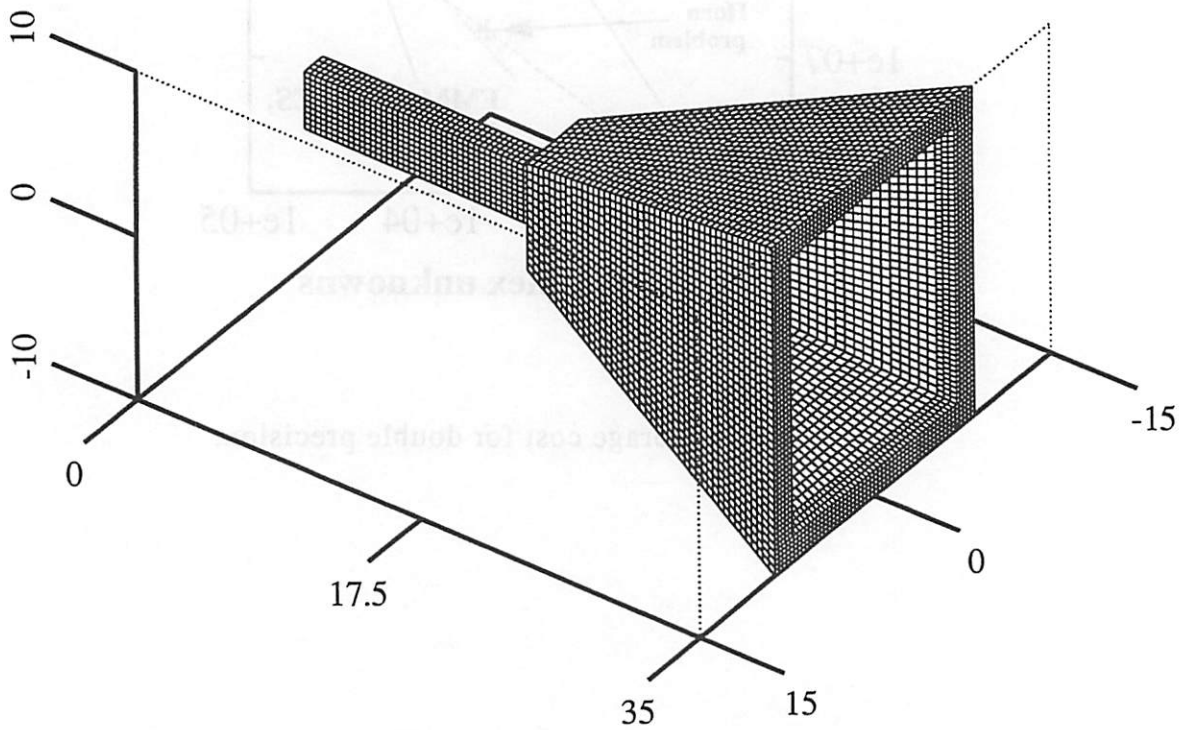
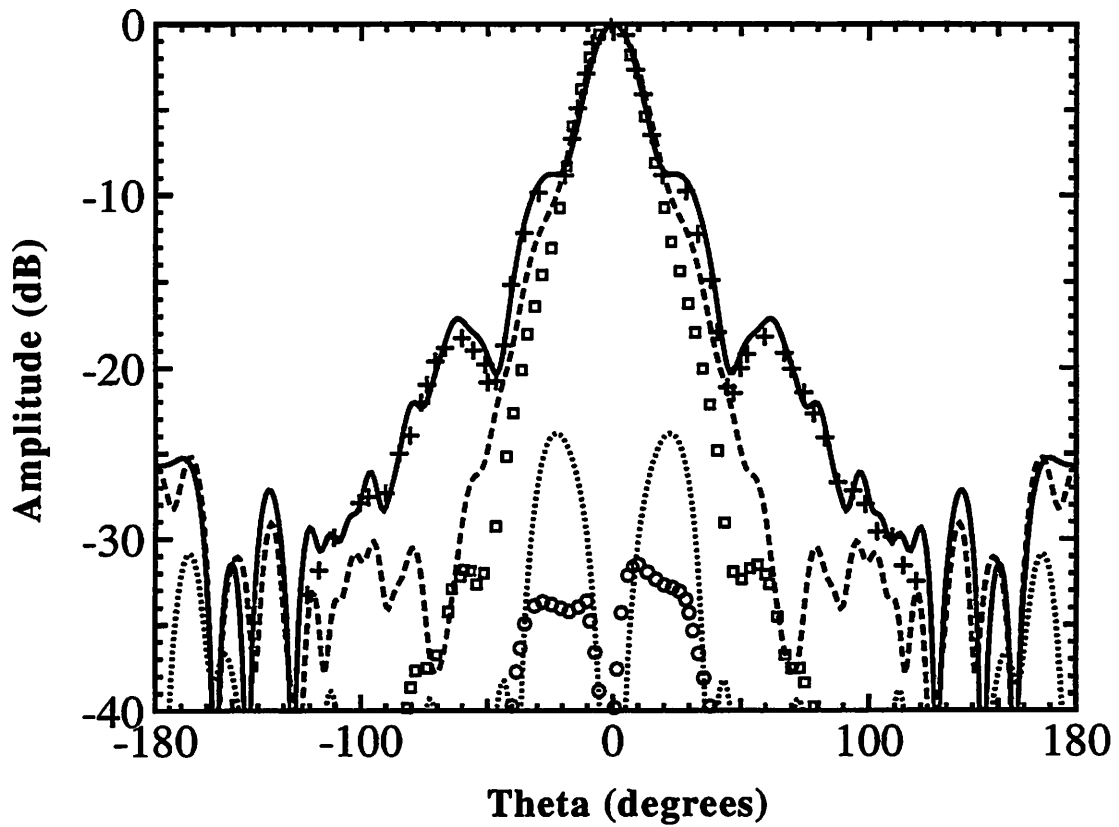


Figure 4.8: A pyramidal horn antenna. Distances are in cm.



Computed: ——— E plane - - - - H plane ······ 45 deg plane (cross)
 Measured by [47]: +++++ E plane □□□□ H plane ○○○○ 45 deg plane (cross)

Figure 4.9: Radiation patterns of the horn antenna.

Chapter 5

Conclusions

Two specific problems on the interaction of the electromagnetic field with material media have been discussed in this thesis. In Chapter 2, the rate of spontaneous emission by an excited atom near a lossy mirror was calculated from an exact solution of a microscopic Hamiltonian model, which included the effects of dispersion, local field correction and instantaneous Coulomb interaction near the surface. Numerical results for the total decay rate were found to be in excellent agreement with those based on classical electromagnetic theory and to reduce to the well-known result for the rate of nonradiative energy transfer in the limit of very small distance from the surface. Since our calculation was based on a fully canonical quantum theory, it provided the first fundamental demonstration of the validity of the classical electromagnetic theory of the rate of spontaneous emission near a lossy mirror.

Having thus established the validity of classical electromagnetic theory in a specialized situation of current interest in quantum optics, we proceeded to develop numerical techniques to solve the equations of electromagnetic theory in practical situations of interest to integrated-circuit process simulation. In Chapter 3, an approximate technique based on the physical-optics method was presented. This technique is suitable for the multilayer, piecewise-linear topography often encountered in 3-D photolithography simulation. The formalism of generalized Sommerfeld integrals was used to treat multiple scattering within a given surface in the physical-optics approximation. To speed up the computation of the physical-optics multiply scattered fields in 3-D,

we used the technique of multipole acceleration which resulted in an $O(N^{3/2})$ algorithm, where N is the number of surface unknowns. A complete photoresist-exposure simulation program based on this multipole accelerated physical-optics technique was written. It has enabled us to perform reflective-notching simulation of large 3-D structures on a workstation in reasonable CPU time.

In order to overcome the limitations of the approximate physical-optics method, we presented a rigorous technique based on FMM in Chapter 4. The present implementation of this technique is suitable for arbitrary, perfectly conducting objects. Our FMM algorithm differs from the standard FMM algorithm of [15] in that we use multipole waves rather than plane waves to represent the radiation field due to the sources in a distant panel. As a result, our distant-to-local transformation formulas are more complicated than those of the standard FMM algorithm. A three-step transformation procedure consisting of a rotation, a translation and another rotation was developed to achieve an $O(N^{5/3})$ algorithm, which is still somewhat slower than the standard FMM algorithm which is $O(N^{3/2})$. Nevertheless, our benchmarks have indicated that the difference in speed between the two algorithms is insignificant for problem size of a few thousand unknowns. Our FMM algorithm does have one important advantage over the standard FMM algorithm, namely, that our algorithm is numerically stable in the long-wavelength limit, whereas the standard algorithm is not. As such, our algorithm is more suitable for application to low-frequency problems such as on-chip interconnect modeling.

Compared with the time-domain finite-difference method (TDFD), the FMM algorithm presented in Section 4.4, as well as the standard FMM algorithm of [15], is more advantageous with respect to storage cost for 3-D problems involving more than 10^4 surface unknowns. This is because FMM uses a surface, rather than a volume, representation of the unknowns and because no matrix storage is needed in FMM. Furthermore, the storage advantage of FMM increases with problem size. For example, a 3-D problem involving 10^5 surface unknowns would require approximately 256 megabytes of storage with FMM and approximately one gigabytes with TDFD.

Thus, FMM will be far superior to TDFD in terms of storage cost for *very* large 3-D problems such as the simulation of photoresist exposure over magnetic disk heads.

Besides generalizing our FMM algorithm to the case of dielectric objects and to periodic topography, future work is needed to extend the guided-mode boundary conditions discussed in Section 4.8 for metallic waveguides to the case of dielectric waveguides. This will make FMM applicable to a wider class of problems such as the simulation of optical proximity probes. Also, research is needed to develop multi-level grouping schemes for our FMM algorithm in order to reduce its CPU cost to $O(N \log N)$. One such grouping scheme has recently been proposed by others for the standard FMM algorithm [51].

Appendix A

Expansion Coefficients for B_ω

In this appendix, the system of equations Eqs. (2.42) to (2.45) are solved to obtain the coefficients $\alpha_0(\omega)$, $\beta_0(\omega)$, $\alpha_1(\omega, \omega')$ and $\beta_1(\omega, \omega')$. Our discussion follows closely that of Huttner et al. [7] but contains more algebraic details.

From Eqs. (2.42) and (2.43) we obtain

$$\beta_0(\omega) = \frac{\omega - \tilde{\omega}_0}{\omega + \tilde{\omega}_0} \alpha_0(\omega). \quad (\text{A.1})$$

Substituting this into Eq. (2.45) we obtain

$$\beta_1(\omega, \omega') = \left[\frac{1}{\omega + \omega'} \right] \frac{\tilde{\omega}_0}{\omega + \tilde{\omega}_0} V(\omega') \alpha_0(\omega). \quad (\text{A.2})$$

For Eq. (2.44) we have to be more careful, since the quantity $1/(\omega - \omega')$ is singular at $\omega = \omega'$. We write this singularity as $\left[\frac{1}{\omega - \omega' - i\epsilon} + x(\omega)\delta(\omega - \omega') \right]$. Hence, Eqs. (A.1) and (2.44) give

$$\alpha_1(\omega, \omega') = \left[\frac{1}{\omega - \omega' - i\epsilon} + x(\omega)\delta(\omega - \omega') \right] \frac{\tilde{\omega}_0}{\omega + \tilde{\omega}_0} V(\omega') \alpha_0(\omega). \quad (\text{A.3})$$

To obtain the function $x(\omega)$, we substitute Eqs. (A.2) and (A.3) into Eq. (2.42),

$$\omega - \tilde{\omega}_0 = \int_0^\infty d\omega' \frac{\tilde{\omega}_0 V^2(\omega')}{2(\omega + \tilde{\omega}_0)} \left[\frac{1}{\omega - \omega' - i\epsilon} + x(\omega)\delta(\omega - \omega') - \frac{1}{\omega + \omega'} \right]. \quad (\text{A.4})$$

From the definition $V(\omega) = \frac{v(\omega)}{\rho} \sqrt{\omega/\tilde{\omega}_0}$, we see that $V^2(\omega)$ is an odd function of ω . Hence, the first and third terms inside the brackets in Eq. (A.4) can be combined into a single integral from $-\infty$ to ∞ ,

$$\omega - \tilde{\omega}_0 = \frac{\tilde{\omega}_0 V^2(\omega)}{2(\omega + \tilde{\omega}_0)} x(\omega) + \frac{\tilde{\omega}_0}{2(\omega + \tilde{\omega}_0)} \int_{-\infty}^\infty d\omega' \frac{V^2(\omega')}{\omega - \omega' - i\epsilon},$$

from which we may solve for $x(\omega)$,

$$x(\omega) = \frac{2(\omega^2 - \tilde{\omega}_0^2)}{\tilde{\omega}_0 V^2(\omega)} - \frac{1}{V^2(\omega)} \int_{-\infty}^{\infty} d\omega' \frac{V^2(\omega')}{\omega - \omega' - i\epsilon}. \quad (\text{A.5})$$

To solve for $\alpha_0(\omega)$, we substitute Eq. (2.38) into Eq. (2.40) and evaluate the commutator with the help of Eqs. (2.35) and (2.36). This gives

$$\begin{aligned} \delta(\omega - \omega') &= \alpha_0(\omega)\alpha_0^*(\omega') - \beta_0(\omega)\beta_0^*(\omega') \\ &+ \int_0^{\infty} d\nu [\alpha_1(\omega, \nu)\alpha_1^*(\omega', \nu) - \beta_1(\omega, \nu)\beta_1^*(\omega', \nu)]. \end{aligned} \quad (\text{A.6})$$

Substituting Eqs. (A.1) to (A.3) into Eq. (A.6) we obtain

$$\begin{aligned} \delta(\omega - \omega') &= \alpha_0(\omega)\alpha_0^*(\omega') \left\{ 1 - \left(\frac{\omega - \tilde{\omega}_0}{\omega + \tilde{\omega}_0} \right) \left(\frac{\omega' - \tilde{\omega}_0}{\omega' + \tilde{\omega}_0} \right) \right. \\ &+ \frac{\tilde{\omega}_0^2}{(\omega + \tilde{\omega}_0)(\omega' + \tilde{\omega}_0)} \int_0^{\infty} d\nu V^2(\nu) \left[x(\omega)x^*(\omega')\delta(\omega - \nu)\delta(\omega' - \nu) \right. \\ &+ \frac{x(\omega)\delta(\omega - \nu)}{\omega' - \nu + i\epsilon} + \frac{x^*(\omega')\delta(\omega' - \nu)}{\omega - \nu - i\epsilon} \\ &\left. \left. + \left(\frac{1}{\omega' - \nu + i\epsilon} \right) \left(\frac{1}{\omega - \nu - i\epsilon} \right) - \left(\frac{1}{\omega' + \nu} \right) \left(\frac{1}{\omega + \nu} \right) \right] \right\}. \end{aligned} \quad (\text{A.7})$$

Using the fact that $V^2(\omega)$ is an odd function of ω , the last two terms inside the brackets in Eq. (A.7) can be combined into a single integral from $-\infty$ to ∞ . Also, the integral of the first three terms inside the brackets in Eq. (A.7) can be evaluated.

After rearranging terms, we obtain

$$\begin{aligned} \delta(\omega - \omega') &= \frac{\alpha_0(\omega)\alpha_0^*(\omega')}{(\omega + \tilde{\omega}_0)(\omega' + \tilde{\omega}_0)} \left[2\tilde{\omega}_0(\omega + \omega') + \int_{-\infty}^{\infty} d\nu \frac{\tilde{\omega}_0^2 V^2(\nu)}{(\omega - \nu - i\epsilon)(\omega' - \nu + i\epsilon)} \right. \\ &+ \tilde{\omega}_0^2 V(\omega)V(\omega')x(\omega)x^*(\omega')\delta(\omega - \omega') \\ &\left. + \frac{\tilde{\omega}_0^2 V^2(\omega)x(\omega)}{\omega' - \omega + i\epsilon} + \frac{\tilde{\omega}_0^2 V^2(\omega')x^*(\omega')}{\omega - \omega' - i\epsilon} \right]. \end{aligned} \quad (\text{A.8})$$

The last two terms inside the brackets in Eq. (A.8) can be rewritten using Eq. (A.5),

$$\begin{aligned} \frac{\tilde{\omega}_0^2 V^2(\omega)x(\omega)}{\omega' - \omega + i\epsilon} + \frac{\tilde{\omega}_0^2 V^2(\omega')x^*(\omega')}{\omega - \omega' - i\epsilon} &= \frac{2\tilde{\omega}_0(\omega^2 - \omega'^2)}{\omega' - \omega + i\epsilon} \\ &+ \frac{\tilde{\omega}_0^2}{\omega' - \omega + i\epsilon} \int_{-\infty}^{\infty} d\nu \left[\frac{V^2(\nu)}{\nu - \omega + i\epsilon} - \frac{V^2(\nu)}{\nu - \omega' - i\epsilon} \right] \\ &= -2\tilde{\omega}_0(\omega + \omega') - \int_{-\infty}^{\infty} d\nu \frac{\tilde{\omega}_0^2 V^2(\nu)}{(\omega - \nu - i\epsilon)(\omega' - \nu + i\epsilon)} \end{aligned}$$

which is seen to cancel the first two terms inside the brackets in Eq. (A.8). Hence, Eq. (A.8) becomes

$$\begin{aligned}\delta(\omega - \omega') &= \frac{\alpha_0(\omega)\alpha_0^*(\omega')}{(\omega + \tilde{\omega}_0)(\omega' + \tilde{\omega}_0)} \tilde{\omega}_0^2 V(\omega)V(\omega')x(\omega)x^*(\omega')\delta(\omega - \omega') \\ &= \left| \frac{\alpha_0(\omega)\tilde{\omega}_0 V(\omega)x(\omega)}{\omega + \tilde{\omega}_0} \right|^2 \delta(\omega - \omega'),\end{aligned}\quad (\text{A.9})$$

The solution of Eq. (A.9) is, up to a phase factor,

$$\alpha_0(\omega) = \frac{\omega + \tilde{\omega}_0}{\tilde{\omega}_0 V(\omega)x(\omega)}.\quad (\text{A.10})$$

This may be rewritten using Eq. (A.5) as

$$\alpha_0(\omega) = \left(\frac{\omega + \tilde{\omega}_0}{2} \right) \frac{V(\omega)}{\omega^2 - \tilde{\omega}_0^2 z(\omega)},\quad (\text{A.11})$$

where $z(\omega)$ is defined by

$$z(\omega) = 1 - \frac{1}{2\tilde{\omega}_0} \int_{-\infty}^{\infty} d\omega' \frac{V^2(\omega')}{\omega' - \omega + i\epsilon}.\quad (\text{A.12})$$

Substituting Eq. (A.11) into Eqs. (A.1) and (A.2) we obtain

$$\beta_0(\omega) = \left(\frac{\omega - \tilde{\omega}_0}{2} \right) \frac{V(\omega)}{\omega^2 - \tilde{\omega}_0^2 z(\omega)},\quad (\text{A.13})$$

$$\beta_1(\omega, \omega') = \frac{\tilde{\omega}_0}{2} \left(\frac{V(\omega')}{\omega + \omega'} \right) \frac{V(\omega)}{\omega^2 - \tilde{\omega}_0^2 z(\omega)}.\quad (\text{A.14})$$

Finally, substituting Eqs. (A.5) and (A.10) into Eq. (A.3) we obtain

$$\alpha_1(\omega, \omega') = \delta(\omega - \omega') + \frac{\tilde{\omega}_0}{2} \left(\frac{V(\omega')}{\omega - \omega' - i\epsilon} \right) \frac{V(\omega)}{\omega^2 - \tilde{\omega}_0^2 z(\omega)}.\quad (\text{A.15})$$

Appendix B

Derivation of Eq. (2.101)

In this appendix the integral over τ in Eq. (2.99) is performed explicitly to give Eq. (2.101).

Consider the first term of the integral in Eq. (2.99),

$$F_1(\omega) = \int_0^\infty d\tau e^{i\omega\tau} \mathcal{D}_{[j][j]}(\mathbf{r}_a, \mathbf{r}_a; \tau). \quad (\text{B.1})$$

Let $\{|\Phi_s\rangle, s = 0, 1, \dots\}$ be a complete set of eigenstates of the system described by the the Hamiltonian density \mathcal{H} of Eq. (2.16), with eigenvalues E_s . From the definition of the photon Green function Eq. (2.74), we have, for $\tau > 0$,

$$\begin{aligned} \mathcal{D}_{[j][j]}(\mathbf{r}_a, \mathbf{r}_a; \tau) &= -\frac{i}{\hbar} \langle A_{[j]}(\mathbf{r}_a, \tau) A_{[j]}(\mathbf{r}_a, 0) \rangle \\ &= -\frac{i}{\hbar} \langle e^{\frac{i}{\hbar} H \tau} A_{[j]}(\mathbf{r}_a, 0) e^{-\frac{i}{\hbar} H \tau} A_{[j]}(\mathbf{r}_a, 0) \rangle \\ &= -\frac{i}{\hbar} \sum_s \langle e^{\frac{i}{\hbar} H \tau} A_{[j]}(\mathbf{r}_a, 0) e^{-\frac{i}{\hbar} H \tau} |\Phi_s\rangle \langle \Phi_s| A_{[j]}(\mathbf{r}_a, 0) \rangle \\ &= -\frac{i}{\hbar} \sum_s |A_{[j],0s}|^2 e^{-i\Omega_s \tau}, \text{ for } \tau > 0. \end{aligned} \quad (\text{B.2})$$

where $A_{[j],0s} = A_{[j],s0}^*$ is the matrix element of $A_{[j]}(\mathbf{r}_a, 0)$ between the eigenstates 0 and s , H is the Hamiltonian corresponding to the Hamiltonian density \mathcal{H} , and $\Omega_s = (E_s - E_0)/\hbar$. Note that $\Omega_s \geq 0$. Similarly, for $\tau < 0$, we have

$$\mathcal{D}_{[j][j]}(\mathbf{r}_a, \mathbf{r}_a; \tau) = -\frac{i}{\hbar} \sum_s |A_{[j],0s}|^2 e^{i\Omega_s \tau}, \text{ for } \tau < 0. \quad (\text{B.3})$$

Substituting Eqs. (B.2) into Eq. (B.1) and performing the integration over τ for

$\tau > 0$, we obtain

$$F_1(\omega) = \frac{1}{\hbar} \sum_s \frac{|A_{[j],0s}|^2}{\omega - \Omega_s + i\epsilon}. \quad (\text{B.4})$$

When we take the imaginary part of Eq. (B.4) as in Eq. (2.99), we obtain

$$\text{Im } F_1(\omega)|_{\omega=\omega_a} = -\frac{\pi}{\hbar} \sum_s |A_{[j],0s}|^2 \delta(\omega_a - \Omega_s), \quad (\text{B.5})$$

where ω_a , the atomic transition frequency, is positive.

On the other hand, the Fourier transform with respect to τ of $\mathcal{D}_{[j][j]}$ is given by

$$F_1^\omega = \int_{-\infty}^{\infty} d\tau e^{i\omega\tau} \mathcal{D}_{[j][j]}(\mathbf{r}_a, \mathbf{r}_a; \tau), \quad (\text{B.6})$$

which differs from Eq. (B.1) only in the lower limit of the integration. Substituting Eqs. (B.2) and (B.3) for $\tau >$ and $\tau < 0$, respectively, into Eq. (B.6) and performing the integration, we obtain a result similar to Eq. (B.4),

$$F_1^\omega = \frac{1}{\hbar} \sum_s |A_{[j],0s}|^2 \left[\frac{1}{\omega - \Omega_s + i\epsilon} - \frac{1}{\omega + \Omega_s - i\epsilon} \right]. \quad (\text{B.7})$$

When we take the imaginary part of Eq. (B.7) and evaluate it at $\omega = \omega_a > 0$, we obtain

$$\text{Im } F_1^\omega|_{\omega=\omega_a} = -\frac{\pi}{\hbar} \sum_s |A_{[j],0s}|^2 [\delta(\omega_a - \Omega_s) + \delta(\omega_a + \Omega_s)]. \quad (\text{B.8})$$

The second delta function in Eq. (B.8) does not contribute, since its argument ($\omega_a + \Omega_s$) is always positive. Hence we have

$$\text{Im } F_1^\omega|_{\omega=\omega_a} = -\frac{\pi}{\hbar} \sum_s |A_{[j],0s}|^2 \delta(\omega_a - \Omega_s), \quad (\text{B.9})$$

which is exactly the same as Eq. (B.5). Thus, we conclude that the imaginary part of the integral over τ of the first term in Eq. (2.99) is equal to the imaginary part of the Fourier transform of $\mathcal{D}_{[j][j]}$ evaluated at $\omega = \omega_a$. This establishes the first term in Eq. (2.101).

Next, consider the second term of the integral in Eq. (2.99),

$$F_2(\omega) = \int_0^{\infty} d\tau e^{i\omega\tau} M(\tau), \quad (\text{B.10})$$

where

$$M(\tau) = \frac{1}{e^2 \omega_a^2} \int_{z < 0} \int_{z' < 0} d^3 r d^3 r' F_{[j]m}(\mathbf{r}_a - \mathbf{r}) \mathcal{G}_{mn}(\mathbf{r}, \mathbf{r}'; \tau) F_{n[j]}(\mathbf{r}' - \mathbf{r}_a). \quad (\text{B.11})$$

Using Eq. (2.87) and following the steps leading from Eq. (B.1) to Eq. (B.2), we have, for $\tau > 0$,

$$M(\tau) = -\frac{i}{\hbar} \left(\frac{1}{e^2 \omega_a^2} \right) \int_{z < 0} \int_{z' < 0} d^3 r d^3 r' F_{[j]m}(\mathbf{r}_a - \mathbf{r}) F_{n[j]}(\mathbf{r}' - \mathbf{r}_a) \times \sum_s \langle X_m(\mathbf{r}, 0) | \Phi_s \rangle \langle \Phi_s | X_n(\mathbf{r}', 0) \rangle e^{-i\Omega_s \tau}, \text{ for } \tau > 0. \quad (\text{B.12})$$

From Eq. (2.24), we see that $F_{ij}(\mathbf{r}_1 - \mathbf{r}_2) = F_{ji}(\mathbf{r}_2 - \mathbf{r}_1)$. Also, \mathbf{X} is Hermitian. Hence, Eq. (B.12) may be rewritten as

$$M(\tau) = -\frac{i}{\hbar} \sum_s |Y_{[j],0s}|^2 e^{-i\Omega_s \tau}, \text{ for } \tau > 0, \quad (\text{B.13})$$

where

$$Y_{[j],0s} = \frac{1}{e \omega_a} \int_{z < 0} d^3 r F_{[j]m}(\mathbf{r}_a - \mathbf{r}) \langle X_m(\mathbf{r}, 0) | \Phi_s \rangle. \quad (\text{B.14})$$

Similarly, for $\tau < 0$, we have

$$M(\tau) = -\frac{i}{\hbar} \sum_s |Y_{[j],0s}|^2 e^{i\Omega_s \tau}, \text{ for } \tau < 0. \quad (\text{B.15})$$

Substituting Eq. (B.13) into Eq. (B.10), we obtain

$$F_2(\omega) = \frac{1}{\hbar} \sum_s \frac{|Y_{[j],0s}|^2}{\omega - \Omega_s + i\epsilon}. \quad (\text{B.16})$$

On the other hand, using Eqs. (B.13) and (B.15), the Fourier transform with respect to τ of $M(\tau)$ is

$$\begin{aligned} F_2^\omega &= \int_{-\infty}^{\infty} d\tau e^{i\omega\tau} M(\tau) \\ &= \frac{1}{\hbar} \sum_s |Y_{[j],0s}|^2 \left[\frac{1}{\omega - \Omega_s + i\epsilon} - \frac{1}{\omega + \Omega_s - i\epsilon} \right]. \end{aligned} \quad (\text{B.17})$$

Eqs. (B.16) and (B.17) differ from Eq. (B.4) and (B.7) only in interchanging $A_{[j],0s}$ and $Y_{[j],0s}$. Hence, exactly the same type of argument as the above leads us to conclude that the imaginary part of the integral over τ of the second term in Eq. (2.99) is equal

to the imaginary part of the Fourier transform of $M(\tau)$ evaluated at $\omega = \omega_a$. This establishes the second term in Eq. (2.101).

Lastly, consider the third term of the integral in Eq. (2.99),

$$F_3(\omega) = \int_0^\infty d\tau e^{i\omega\tau} N(\tau), \quad (\text{B.18})$$

where

$$N(\tau) = \frac{1}{e\omega_a} \int_{z<0} d^3r F_{[j]m}(\mathbf{r}_a - \mathbf{r}) C_{m[j]}(\mathbf{r}, \mathbf{r}_a; \tau). \quad (\text{B.19})$$

Using Eq. (2.100) and following the steps leading from Eq. (B.1) to Eq. (B.2), we have, for $\tau > 0$,

$$N(\tau) = \frac{1}{\hbar} \left(\frac{1}{e\omega_a} \right) \int_{z<0} d^3r F_{[j]m}(\mathbf{r}_a - \mathbf{r}) \sum_s \left[\langle X_m(\mathbf{r}, 0) | \Phi_s \rangle \langle \Phi_s | A_{[j]}(\mathbf{r}_a, 0) \rangle - \langle A_{[j]}(\mathbf{r}_a, 0) | \Phi_s \rangle \langle \Phi_s | X_m(\mathbf{r}, 0) \rangle \right] e^{-i\Omega_s \tau}, \text{ for } \tau > 0. \quad (\text{B.20})$$

The second term inside the brackets in Eq. (B.20) is seen to be the complex conjugate of the first term,

$$N(\tau) = -\frac{i}{\hbar} \sum_s B_{0s} e^{-i\Omega_s \tau}, \text{ for } \tau > 0, \quad (\text{B.21})$$

where

$$B_{0s} = \frac{2}{e\omega_a} \text{Im} \left[\langle A_{[j]}(\mathbf{r}_a, 0) | \Phi_s \rangle \langle \Phi_s | X_m(\mathbf{r}, 0) \rangle \right], \quad (\text{B.22})$$

is a *real* quantity. Similarly, for $\tau < 0$, we have

$$N(\tau) = -\frac{i}{\hbar} \sum_s B_{0s} e^{i\Omega_s \tau}, \text{ for } \tau < 0. \quad (\text{B.23})$$

Substituting Eq. (B.21) into Eq. (B.18), we obtain

$$F_3(\omega) = \frac{1}{\hbar} \sum_s \frac{B_{0s}}{\omega - \Omega_s + i\epsilon}. \quad (\text{B.24})$$

On the other hand, using Eqs. (B.21) and (B.23), the Fourier transform with respect to τ of $N(\tau)$ is

$$\begin{aligned} F_3^\omega &= \int_{-\infty}^\infty d\tau e^{i\omega\tau} N(\tau) \\ &= \frac{1}{\hbar} \sum_s B_{0s} \left[\frac{1}{\omega - \Omega_s + i\epsilon} - \frac{1}{\omega + \Omega_s - i\epsilon} \right]. \end{aligned} \quad (\text{B.25})$$

The similarity of Eqs. (B.24) and (B.25) to Eqs. (B.4) and (B.7) allows us to conclude, using exactly the same type of argument as before, that the imaginary part of the integral over τ of the third term in Eq. (2.99) is equal to the imaginary part of the Fourier transform of $N(\tau)$ evaluated at $\omega = \omega_a$. This establishes the third term in Eq. (2.101).

Appendix C

Green Function for the Matter Field

In this appendix, the Dyson equation Eq. (2.131) for the matter Green function $\mathcal{G}_{ij}^{(0)\omega}$ for the system described by the Hamiltonian density of Eq. (2.103) is solved exactly using an extension of the Wiener-Hopf technique. Before solving Eq. (2.131) for the dielectric half-space, we first consider the case of an *infinite* dielectric. In that case, the Dyson equation Eq. (2.131) is modified to read

$$\mathcal{G}_{ij}^{(\infty)\omega}(\mathbf{r}_1, \mathbf{r}_2) = -\frac{\epsilon_0[\epsilon(|\omega|) - 1]}{e^2} \left[\delta_{ij} \delta(\mathbf{r}_1 - \mathbf{r}_2) + \int_{\infty} d^3 r_3 F_{im}(\mathbf{r}_1 - \mathbf{r}_3) \mathcal{G}_{mj}^{(\infty)\omega}(\mathbf{r}_3, \mathbf{r}_2) \right], \quad (\text{C.1})$$

where the integral on the RHS ranges over all of space. As such, this integral is a convolution whose Fourier transform is a product of Fourier transforms. Taking the three-dimensional Fourier transform of Eq. (C.1) with respect to \mathbf{r}_1 , we obtain

$$G_{ij}^{(\infty)}(\mathbf{k}) = -[\epsilon(|\omega|) - 1] \left[\frac{\epsilon_0}{e^2} \delta_{ij} e^{-i\mathbf{k}\cdot\mathbf{r}_2} + \left(\frac{k_i k_m}{k^2} - \frac{1}{3} \delta_{im} \right) G_{mj}^{(\infty)}(\mathbf{k}) \right], \quad (\text{C.2})$$

where we have used the fact that the Fourier transform of the quantity $F_{ij}(\mathbf{r}_1 - \mathbf{r}_3)$ given by Eq. (2.24) is

$$\int d^3 r_1 F_{ij}(\mathbf{r}_1 - \mathbf{r}_3) e^{-i\mathbf{k}\cdot(\mathbf{r}_1 - \mathbf{r}_3)} = \frac{e^2}{\epsilon_0} \left[\frac{k_i k_j}{k^2} - \frac{1}{3} \delta_{ij} \right]. \quad (\text{C.3})$$

Rearranging terms in Eq. (C.2), we obtain

$$\left[\delta_{im} \left(1 - \frac{1}{3}[\epsilon(|\omega|) - 1] \right) + [\epsilon(|\omega|) - 1] \frac{k_i k_m}{k^2} \right] G_{mj}^{(\infty)}(\mathbf{k}) = -\frac{\epsilon_0[\epsilon(|\omega|) - 1]}{e^2} \delta_{ij} e^{-i\mathbf{k} \cdot \mathbf{r}_2}, \quad (\text{C.4})$$

which can be rewritten as

$$\left(\delta_{im} + B \frac{k_i k_m}{k^2} \right) G_{mj}^{(\infty)}(\mathbf{k}) = -\frac{\epsilon_0}{e^2} B \delta_{ij} e^{-i\mathbf{k} \cdot \mathbf{r}_2}, \quad (\text{C.5})$$

where

$$\begin{aligned} B &= \frac{\epsilon(|\omega|) - 1}{1 - \frac{1}{3}[\epsilon(|\omega|) - 1]} \\ &= \epsilon_L(|\omega|) - 1, \end{aligned} \quad (\text{C.6})$$

where we have used Eq. (2.133). Now, the inverse of $\left(\delta_{im} + B \frac{k_i k_m}{k^2} \right)$ is $\left(\delta_{im} - \frac{B}{1+B} \frac{k_i k_m}{k^2} \right)$ as can be verified by direct multiplication. Hence we can solve Eq. (C.5) for $G_{ij}^{(\infty)}(\mathbf{k})$,

$$G_{ij}^{(\infty)}(\mathbf{k}) = -\frac{\epsilon_0}{e^2} B \left(\delta_{ij} - \frac{B}{1+B} \frac{k_i k_j}{k^2} \right) e^{-i\mathbf{k} \cdot \mathbf{r}_2}. \quad (\text{C.7})$$

The inverse Fourier transform of Eq. (C.7) is

$$\begin{aligned} \mathcal{G}_{ij}^{(\infty)\omega}(\mathbf{r}_1, \mathbf{r}_2) &= -\frac{\epsilon_0[\epsilon_L(|\omega|) - 1]}{e^2} \delta_{ij} \delta(\mathbf{r}_1 - \mathbf{r}_2) \\ &\quad + \frac{\epsilon_0[\epsilon_L(|\omega|) - 1]^2}{4\pi\epsilon_L(|\omega|)e^2} \frac{\partial^2}{\partial x_{1i} \partial x_{2j}} \left(\frac{1}{|\mathbf{r}_1 - \mathbf{r}_2|} \right), \end{aligned} \quad (\text{C.8})$$

where we have used Eq. (C.6).

Next, we proceed to solve Eq. (2.131) for the dielectric half-space. Inspection of this equation shows that the second argument \mathbf{r}_2 of the Green function is fixed throughout the equation. Hence, we may fix \mathbf{r}_2 and regard $\mathcal{G}_{ij}^{(0)\omega}$ as a function of only one coordinate vector \mathbf{r}_1 . Since the dielectric half-space is translationally invariant in the x and y directions, we may further eliminate the x_1 and y_1 variables by taking the Fourier transform of Eq. (2.131) with respect to these two variables,

$$\begin{aligned} \tilde{G}_{ij}(z_1) &= -\frac{\epsilon_0[\epsilon(|\omega|) - 1]}{e^2} \left[\delta_{ij} e^{-i(k_x x_2 + k_y y_2)} \delta(z_1 - z_2) \right. \\ &\quad \left. + \int_{z_3 < 0} dz_3 \tilde{F}_{im}(z_1 - z_3) \tilde{G}_{mj}(z_3) \right], \end{aligned} \quad (\text{C.9})$$

where a tilde denotes Fourier transform with respect to x_1 and y_1 and we have suppressed the dependence of the Fourier transforms on the transverse momentum (k_x, k_y) for simplicity. The two-dimensional Fourier transform \tilde{F}_{ij} can be found by taking the inverse Fourier transform of Eq. (C.3) with respect to k_z ,

$$\tilde{F}_{ij}(z_1 - z_3) = \int \frac{dk_z}{2\pi} \frac{e^2}{\epsilon_0} \left[\frac{k_i k_j}{k^2} - \frac{1}{3} \delta_{ij} \right] e^{ik_z(z_1 - z_3)}. \quad (\text{C.10})$$

The integral over k_z can be evaluated by contour integration, by noting that the integrand has poles at $k_z = \pm iK$, where $K = \sqrt{k_x^2 + k_y^2}$. The result is

$$\tilde{F}_{ij}(z_1 - z_3) = \frac{e^2}{\epsilon_0} \times \begin{cases} \frac{r_i r_j}{2K} e^{-K(z_1 - z_3)} - \frac{1}{3} \delta_{ij} \delta(z_1 - z_3), & \text{for } z_1 > z_3, \\ \frac{r'_i r'_j}{2K} e^{K(z_1 - z_3)} - \frac{1}{3} \delta_{ij} \delta(z_1 - z_3), & \text{for } z_1 < z_3, \end{cases} \quad (\text{C.11})$$

where \mathbf{r} and \mathbf{r}' are vectors with the components

$$r_i = (k_x, k_y, iK), \quad (\text{C.12})$$

$$r'_i = (k_x, k_y, -iK). \quad (\text{C.13})$$

To solve Eq. (C.9) using the Wiener-Hopf technique, we write $\tilde{G}_{ij}(z_1)$ as a sum of two functions $\tilde{G}_{ij}^{(+)}(z_1)$ and $\tilde{G}_{ij}^{(-)}(z_1)$, the first of which vanishes for $z_1 > 0$ and the second of which vanishes for $z_1 < 0$. Substituting this into Eq. (C.9), we obtain

$$\tilde{G}_{ij}^{(+)}(z_1) + \tilde{G}_{ij}^{(-)}(z_1) = -\frac{\epsilon_0[\epsilon(|\omega|) - 1]}{e^2} \left[\delta_{ij} e^{-i(k_x x_2 + k_y y_2)} \delta(z_1 - z_2) + \int_{-\infty}^{\infty} dz_3 \tilde{F}_{im}(z_1 - z_3) \tilde{G}_{mj}^{(+)}(z_3) \right], \quad (\text{C.14})$$

where the integral is now along the entire z_3 -axis. As such, this integral is a convolution, whose Fourier transform is a product of Fourier transforms. Taking the Fourier transform of Eq. (C.14) with respect to z_1 , we obtain

$$G_{ij}^{(+)}(k_z) + G_{ij}^{(-)}(k_z) = -[\epsilon(|\omega|) - 1] \left[\frac{\epsilon_0}{e^2} \delta_{ij} e^{-i\mathbf{k} \cdot \mathbf{r}_2} + \left(\frac{k_i k_m}{k^2} - \frac{1}{3} \delta_{im} \right) G_{mj}^{(+)}(k_z) \right], \quad (\text{C.15})$$

where we have used Eq. (C.3).

It is necessary to identify the regions of analyticity of $G_{ij}^{(+)}(k_z)$ and $G_{ij}^{(-)}(k_z)$ in the complex k_z -plane. Taking the limit $z_1 \rightarrow +\infty$ of both sides of Eq. (C.14) and using Eq. (C.11), we have

$$\lim_{z_1 \rightarrow +\infty} \tilde{G}_{ij}^{(-)}(z_1) = -[\epsilon(|\omega|) - 1] \left[\frac{r_i r_m}{2K} e^{-Kz_1} \int_{-\infty}^0 dz_3 e^{Kz_3} \tilde{G}_{mj}^{(+)}(z_3) \right], \quad (\text{C.16})$$

using the fact that $\tilde{G}_{ij}^{(+)}(z_1)$ vanishes for $z_1 > 0$. Eq. (C.16) shows that the asymptotic behavior of $\tilde{G}_{ij}^{(-)}(z_1)$ as $z_1 \rightarrow +\infty$ is $\tilde{G}_{ij}^{(-)}(z_1) \sim e^{-Kz_1}$, up to a multiplicative factor. Now, by definition, $G_{ij}^{(-)}(k_z) = \int_0^\infty dz_1 e^{-ik_z z_1} \tilde{G}_{ij}^{(-)}(z_1)$. Since the behavior of the integrand at large, positive z_1 is $e^{-ik_z z_1 - Kz_1}$, this integral converges whenever $\text{Im } k_z < K$. Thus, we conclude that $G_{ij}^{(-)}(k_z)$ is analytic everywhere in the complex half-plane $\Sigma_- = \{k_z \mid \text{Im } k_z < K\}$.

Next, we assume that the asymptotic behavior of $\tilde{G}_{ij}^{(+)}(z_1)$ as $z_1 \rightarrow -\infty$ is $e^{\mu z_1}$, where $\mu \geq 0$ in order that $\tilde{G}_{ij}^{(+)}(z_1)$ remains finite as $z_1 \rightarrow -\infty$. By definition, $G_{ij}^{(+)}(k_z) = \int_{-\infty}^0 dz_1 e^{-ik_z z_1} \tilde{G}_{ij}^{(+)}(z_1)$. Since the behavior of the integrand at large, negative z_1 is $e^{-ik_z z_1 + \mu z_1}$, this integral converges whenever $\text{Im } k_z > -\mu$. Thus, we conclude that $G_{ij}^{(+)}(k_z)$ is analytic everywhere in the complex half-plane $\Sigma'_+ = \{k_z \mid \text{Im } k_z > -\mu\}$.

Lastly, we determine the region of analyticity of the first term on the RHS of Eq. (C.15), considered as a function of k_z . This term is proportional to $e^{-ik_z z_2}$. We are primarily interested in the solution for $z_2 < 0$. In this case, the first term on the RHS of Eq. (C.15) is analytic everywhere in the upper half of the complex k_z -plane, $\Sigma_+ = \{k_z \mid \text{Im } k_z > 0\}$. Since $\Sigma_+ \subseteq \Sigma'_+$, we see that $G_{ij}^{(+)}(k_z)$ is also analytic in Σ_+ . Also, because $\Sigma_+ \cap \Sigma_- \neq \emptyset$, there is a common domain of analyticity of the three functions $G_{ij}^{(+)}(k_z)$, $G_{ij}^{(-)}(k_z)$, and $e^{-ik_z z_2}$.

Rearranging terms in Eq. (C.15), we obtain

$$\left[\delta_{im} \left(1 - \frac{1}{3} [\epsilon(|\omega|) - 1] \right) + [\epsilon(|\omega|) - 1] \frac{k_i k_m}{k^2} \right] G_{mj}^{(+)}(k_z) + G_{ij}^{(-)}(k_z) = -\frac{\epsilon_0 [\epsilon(|\omega|) - 1]}{e^2} \delta_{ij} e^{-ik \cdot r_2}, \quad (\text{C.17})$$

which can be rewritten as

$$\left(\delta_{im} + B \frac{k_i k_m}{k^2} \right) G_{mj}^{(+)}(k_z) + C G_{ij}^{(-)}(k_z) = -\frac{\epsilon_0}{e^2} B \delta_{ij} e^{-ik \cdot r_2}, \quad (\text{C.18})$$

where B is given by Eq. (C.6) and

$$C = \frac{1}{1 - \frac{1}{3}[\epsilon(|\omega|) - 1]}. \quad (\text{C.19})$$

To apply the Wiener-Hopf technique, we must write each side of Eq. (C.18) as a sum of two terms, one of which is analytic in Σ_+ and the other of which is analytic in Σ_- . Although $G_{ij}^{(+)}(k_z)$ is analytic in Σ_+ , the first term on the LHS of Eq. (C.18) is not, because the quantity $1/k^2$ has poles at $k = \pm iK$. Hence, it is necessary to subtract the pole of this term at $k = +iK$ from both sides of the equation,

$$\begin{aligned} \left(\delta_{im} + B \frac{k_i k_m}{k^2} \right) \left[G_{mj}^{(+)}(k_z) - G_{mj}^{(+)}(iK) \right] + C G_{ij}^{(-)}(k_z) &= -\frac{\epsilon_0}{e^2} B \delta_{ij} e^{-i\mathbf{k} \cdot \mathbf{r}_2} \\ &- \left(\delta_{im} + B \frac{k_i k_m}{k^2} \right) G_{mj}^{(+)}(iK). \end{aligned} \quad (\text{C.20})$$

The first term on the LHS of Eq. (C.20) is now analytic in Σ_+ while the second term is analytic in Σ_- . Next, we decompose the RHS of this equation into a sum of two terms $Q_{ij}^{(+)}(k_z)$ and $Q_{ij}^{(-)}(k_z)$ which are analytic in Σ_+ and Σ_- , respectively. This is accomplished by using the identity

$$\frac{1}{k^2} = \frac{1}{(k_z - iK)(k_z + iK)} = \left(\frac{1}{k_z - iK} - \frac{1}{k_z + iK} \right) \frac{1}{2iK}. \quad (\text{C.21})$$

Thus,

$$\text{RHS of Eq. (C.20)} = Q_{ij}^{(+)}(k_z) + Q_{ij}^{(-)}(k_z), \quad (\text{C.22})$$

where

$$Q_{ij}^{(+)}(k_z) = -\frac{\epsilon_0}{e^2} B \delta_{ij} e^{-i\mathbf{k} \cdot \mathbf{r}_2} + \frac{B}{2iK} \frac{k_i k_m}{k_z + iK} G_{mj}^{(+)}(iK), \quad (\text{C.23})$$

$$Q_{ij}^{(-)}(k_z) = -\left(\delta_{im} + \frac{B}{2iK} \frac{k_i k_m}{k_z - iK} \right) G_{mj}^{(+)}(iK). \quad (\text{C.24})$$

Substituting Eq. (C.22) into Eq. (C.20) and rearranging terms, we obtain

$$\left(\delta_{im} + B \frac{k_i k_m}{k^2} \right) \left[G_{mj}^{(+)}(k_z) - G_{mj}^{(+)}(iK) \right] - Q_{ij}^{(+)}(k_z) = -C G_{ij}^{(-)}(k_z) + Q_{ij}^{(-)}(k_z). \quad (\text{C.25})$$

The LHS of Eq. (C.25) is analytic in Σ_+ and the RHS in Σ_- . Because $\Sigma_+ \cap \Sigma_- \neq \emptyset$, we conclude, based on a theorem in complex analysis [23], that both sides of Eq. (C.25) must be an entire function, which we denote by $P_{ij}(k_z)$. Setting each side of Eq. (C.25) equal to $P_{ij}(k_z)$, we obtain

$$G_{ij}^{(+)}(k_z) = G_{ij}^{(+)}(iK) + \left(\delta_{im} - \frac{B}{1+B} \frac{k_i k_m}{k^2} \right) [Q_{mj}^{(+)}(k_z) + P_{mj}(k_z)] , \quad (\text{C.26})$$

$$G_{ij}^{(-)}(k_z) = \frac{1}{C} [Q_{ij}^{(-)}(k_z) - P_{ij}(k_z)] . \quad (\text{C.27})$$

Substituting Eqs. (C.23) and (C.24) into Eqs. (C.26) and (C.27), we obtain the formal solution

$$G_{ij}^{(+)}(k_z) = G_{ij}^{(\infty)}(\mathbf{k}) + \left[\delta_{im} + \frac{B}{2iK(1+B)} \frac{k_i k_m}{k_z + iK} \right] G_{mj}^{(+)}(iK) + \left(\delta_{im} - \frac{B}{1+B} \frac{k_i k_m}{k^2} \right) P_{mj}(k_z) , \quad (\text{C.28})$$

$$G_{ij}^{(-)}(k_z) = -\frac{1}{C} \left[\left(\delta_{im} + \frac{B}{2iK} \frac{k_i k_m}{k_z - iK} \right) G_{mj}^{(+)}(iK) + P_{ij}(k_z) \right] , \quad (\text{C.29})$$

where we have used Eq. (C.7).

Eqs. (C.28) and (C.29) still contain the unknown quantities $G_{mj}^{(+)}(iK)$ and $P_{mj}(k_z)$. To solve for these quantities, we first recall that $G_{ij}^{(+)}(k_z)$ must be analytic in Σ_+ , whereas there appears to be a pole at $k = +iK \in \Sigma_+$ due to the factor $1/k^2$ in the first and third terms on the RHS of Eq. (C.28). The resolution of this paradox lies in demanding that the residue of the RHS of Eq. (C.28) at the pole $k = iK$ must be zero. Substituting Eq. (C.7) into Eq. (C.28) and extracting the residue of the pole at $k = iK$, we obtain the condition

$$0 = \frac{\epsilon_0}{e^2} \frac{B^2}{1+B} \frac{r_i r_j}{2iK} e^{-i\mathbf{r} \cdot \mathbf{r}_2} - \frac{B}{1+B} \frac{r_i r_m}{2iK} P_{mj}(iK) . \quad (\text{C.30})$$

Canceling common factors, we obtain

$$r_m P_{mj}(iK) = \frac{\epsilon_0}{e^2} B r_j e^{-i\mathbf{r} \cdot \mathbf{r}_2} . \quad (\text{C.31})$$

Next, we use the fact that the Green function $G_{ij}^{(0)}(\mathbf{r}_1, \mathbf{r}_2)$ represents a polarization wave originating from a point \mathbf{r}_2 , where $z_2 < 0$. This function is expected to have

a singularity at $\mathbf{r}_1 = \mathbf{r}_2$, but not on the surface of the dielectric $z_1 = 0$. For this to be true, the inverse Fourier transforms of Eqs. (C.28) and (C.29) evaluated at $z_1 = 0$ must be finite. Since $\tilde{G}_{ij}^{(\pm)}(z_1) = \int \frac{dk_z}{2\pi} e^{ik_z z_1} G_{ij}^{(\pm)}(k_z)$, its value at $z_1 = 0$ is $\int \frac{dk_z}{2\pi} G_{ij}^{(\pm)}(k_z)$, and this must be finite. This is so if $G_{ij}^{(\pm)}(k_z) \rightarrow 0$ as $k_z \rightarrow \pm\infty$, or if $G_{ij}^{(\pm)}(k_z)$ approaches an exponential phase factor $\sim e^{-ik_z z_2}$ as $k_z \rightarrow \pm\infty$. Examination of Eq. (C.28) shows that, in the limit $k_z \rightarrow \pm\infty$, the first term, which is given by Eq. (C.7), approaches an exponential phase factor $\sim e^{-ik_z z_2}$. The remaining terms in Eq. (C.28), therefore, must approach zero as $k_z \rightarrow \pm\infty$,

$$\lim_{k_z \rightarrow \pm\infty} \left\{ \left[\delta_{im} + \frac{B}{2iK(1+B)} \frac{k_i k_m}{k_z} \right] G_{mj}^{(+)}(iK) + \left(\delta_{im} - \frac{B}{1+B} \frac{k_i k_m}{k_z^2} \right) P_{mj}(k_z) \right\} = 0. \quad (\text{C.32})$$

Similarly, the RHS of Eq. (C.29) must approach zero as $k_z \rightarrow \pm\infty$,

$$\lim_{k_z \rightarrow \pm\infty} P_{ij}(k_z) = \lim_{k_z \rightarrow \pm\infty} - \left(\delta_{im} + \frac{B}{2iK} \frac{k_i k_m}{k_z - iK} \right) G_{mj}^{(+)}(iK). \quad (\text{C.33})$$

We define a matrix $a_{ij} = \lim_{k_z \rightarrow \pm\infty} \frac{k_i k_j}{k_z}$ which appears in Eqs. (C.32) and (C.33).

The elements of this matrix are

$$a_{ij} = \lim_{k_z \rightarrow \pm\infty} \frac{k_i k_j}{k_z} = \begin{pmatrix} 0 & 0 & k_x \\ 0 & 0 & k_y \\ k_x & k_y & k_z \end{pmatrix}, \quad (\text{C.34})$$

where we have neglected terms of order $(1/k_z)$. From Eq. (C.34) we obtain

$$\begin{aligned} \lim_{k_z \rightarrow \pm\infty} \frac{a_{ij}}{k_z} &= \begin{pmatrix} 0 & 0 & 0 \\ 0 & 0 & 0 \\ 0 & 0 & 1 \end{pmatrix}, \quad (\text{C.35}) \\ \lim_{k_z \rightarrow \pm\infty} \frac{(a^2)_{ij}}{k_z} &= \lim_{k_z \rightarrow \pm\infty} \frac{1}{k_z} \begin{pmatrix} k_x k_x & k_x k_y & k_x k_z \\ k_y k_x & k_y k_y & k_y k_z \\ k_z k_x & k_z k_y & k_z^2 \end{pmatrix} \\ &= \begin{pmatrix} 0 & 0 & k_x \\ 0 & 0 & k_y \\ k_x & k_y & k_z \end{pmatrix} = a_{ij}. \quad (\text{C.36}) \end{aligned}$$

Using Eq. (C.34), we may rewrite Eq. (C.33) as

$$P_{ij}(k_z) = - \left(\delta_{im} + \frac{B}{2iK} a_{im} \right) G_{mj}^{(+)}(iK) + O\left(\frac{1}{k_z}\right). \quad (\text{C.37})$$

Since $P_{ij}(k_z)$ is an entire function, it must be a polynomial in k_z . Eq. (C.34) shows that a_{im} is a polynomial of the first degree in k_z , but the $O(1/k_z)$ term in Eq. (C.37) is not a polynomial. Hence the latter must be zero and we obtain the solution

$$P_{ij}(k_z) = - \left(\delta_{im} + \frac{B}{2iK} a_{im} \right) G_{mj}^{(+)}(iK) \quad (\text{C.38})$$

which is valid for all k_z . When we substitute Eq. (C.38) into Eq. (C.32), the second term on the LHS of the latter equation becomes

$$\begin{aligned} \lim_{k_z \rightarrow \pm\infty} \left(\delta_{im} - \frac{B}{1+B} \frac{k_i k_m}{k_z^2} \right) P_{mj}(k_z) &= - \left(\delta_{im} + \frac{B}{2iK} a_{im} \right) G_{mj}^{(+)}(iK) \\ &+ \lim_{k_z \rightarrow \pm\infty} \left[\frac{a_{im}}{k_z} + \frac{B}{2iK} \frac{(a^2)_{im}}{k_z} \right] \left(\frac{B}{1+B} \right) G_{mj}^{(+)}(iK) \\ &= - \left[\delta_{im} + \frac{B}{2iK(1+B)} a_{im} \right] G_{mj}^{(+)}(iK) + \left(\frac{B}{1+B} \right) \delta_{i3} G_{3j}^{(+)}(iK), \end{aligned} \quad (\text{C.39})$$

where we have used Eqs. (C.35) and (C.36). When Eq. (C.39) is substituted into Eq. (C.32), the first term on the RHS of the former equation cancels the first term on the LHS of the latter equation. Thus, we are left with the condition

$$G_{3j}^{(+)}(iK) = 0. \quad (\text{C.40})$$

To solve for the remaining components of $G_{ij}^{(+)}(iK)$, we substitute Eq. (C.38) into Eq. (C.31),

$$\frac{\epsilon_0}{e^2} B r_j e^{-i\mathbf{r} \cdot \mathbf{r}_2} = - \left(r_m + \frac{B}{2iK} r_i a_{im} \right) \Big|_{k_z=iK} G_{mj}^{(+)}(iK). \quad (\text{C.41})$$

The quantity $r_i a_{im}|_{k_z=iK} = b_m$ is a vector with the components

$$\begin{pmatrix} b_1 \\ b_2 \\ b_3 \end{pmatrix} = \begin{pmatrix} k_x & k_y & iK \end{pmatrix} \begin{pmatrix} 0 & 0 & k_x \\ 0 & 0 & k_y \\ k_x & k_y & iK \end{pmatrix} = \begin{pmatrix} iK k_x \\ iK k_y \\ 0 \end{pmatrix}, \quad (\text{C.42})$$

where we have used Eqs. (C.12) and (C.34). Substituting Eq. (C.42) into Eq. (C.41) and using Eq. (C.40), we obtain

$$\frac{\epsilon_0}{e^2} B r_j e^{-i\mathbf{r} \cdot \mathbf{r}_2} = - \left(1 + \frac{B}{2} \right) \left[r_1 G_{1j}^{(+)}(iK) + r_2 G_{2j}^{(+)}(iK) \right]. \quad (\text{C.43})$$

Since the dielectric half-space has no preferred direction in the x - y plane we expect $G_{11}^{(+)}(iK) = G_{22}^{(+)}(iK)$. Hence, we obtain one possible solution to Eq. (C.43),

$$\begin{aligned}
G_{11}^{(+)}(iK) &= G_{22}^{(+)}(iK) = -\frac{\epsilon_0 B}{e^2(1+B/2)} e^{-i\mathbf{r}\cdot\mathbf{r}_2} \\
G_{12}^{(+)}(iK) &= G_{21}^{(+)}(iK) = 0 \\
G_{13}^{(+)}(iK) &= -\frac{i r_1}{K} \frac{\epsilon_0 B}{e^2(1+B/2)} e^{-i\mathbf{r}\cdot\mathbf{r}_2} \\
G_{23}^{(+)}(iK) &= -\frac{i r_2}{K} \frac{\epsilon_0 B}{e^2(1+B/2)} e^{-i\mathbf{r}\cdot\mathbf{r}_2}.
\end{aligned} \tag{C.44}$$

Eqs. (C.40) and (C.44) may be combined into a single equation,

$$G_{ij}^{(+)}(iK) = -\left(\delta_{ij} - \frac{r_i \delta_{3j}}{iK}\right) \frac{\epsilon_0 B}{e^2(1+B/2)} e^{-i\mathbf{r}\cdot\mathbf{r}_2}. \tag{C.45}$$

We now have all the quantities we need in the solutions Eqs. (C.28) and (C.29). Since we are primarily interested in the solution for z_1 and z_2 both < 0 , as shown in Eq. (2.162), we only need to compute the inverse Fourier transform of Eq. (C.28). Substituting Eq. (C.38) into the latter equation, we obtain

$$\begin{aligned}
G_{ij}^{(+)}(k_z) &= G_{ij}^{(\infty)}(\mathbf{k}) + \frac{B}{2iK(1+B)} \frac{k_i k_m}{k_z - iK} G_{mj}^{(+)}(iK) \\
&\quad - \frac{B}{2iK} \left(a_{im} - \frac{B}{1+B} \frac{k_i k_l}{k^2} a_{lm} \right) G_{mj}^{(+)}(iK).
\end{aligned} \tag{C.46}$$

The inverse Fourier transform of the first term on the RHS of Eq. (C.46) is given by Eq. (C.8). For the remaining terms in Eq. (C.46), we first find the inverse Fourier transform with respect to k_z ,

$$\tilde{G}_{ij}^{(+)}(z_1) - \tilde{G}_{ij}^{(\infty)}(z_1) = \int_{-\infty}^{\infty} \frac{dk_z}{2\pi} e^{ik_z z_1} [G_{ij}^{(+)}(k_z) - G_{ij}^{(\infty)}(\mathbf{k})], \tag{C.47}$$

where $z_1 < 0$. Since the quantity in brackets in Eq. (C.47) approaches zero as $|k_z| \rightarrow \infty$, as expressed by Eq. (C.32), we may close the contour in the lower half of the complex k_z -plane. In doing so, only the pole at $k_z = -iK$ due to the $1/k^2$ term on the second line of Eq. (C.46) contributes. The result is

$$\tilde{G}_{ij}^{(+)}(z_1) - \tilde{G}_{ij}^{(\infty)}(z_1) = \frac{B^2}{2iK(1+B)} \frac{r'_i r'_l}{2K} a'_{lm} e^{Kz_1} G_{mj}^{(+)}(iK), \tag{C.48}$$

where a'_{lm} is the matrix a_{lm} of Eq. (C.34) evaluated at $k_z = -iK$. Using Eqs. (C.34) and (C.40), the summation over m in Eq. (C.48) is seen to range over 1 and 2 only, and the summation over l reduces to $l = 3$. Hence,

$$\tilde{G}_{ij}^{(+)}(z_1) - \tilde{G}_{ij}^{(\infty)}(z_1) = \frac{B^2}{2iK(1+B)} \frac{r'_i(-iK)}{2K} \left[a'_{31} G_{1j}^{(+)}(iK) + a'_{32} G_{2j}^{(+)}(iK) \right] e^{Kz_1}. \quad (\text{C.49})$$

The quantity in brackets in Eq. (C.49) can be computed using Eqs. (C.34) and (C.45),

$$\begin{aligned} \left[a'_{31} G_{1j}^{(+)}(iK) + a'_{32} G_{2j}^{(+)}(iK) \right] &= -\frac{\epsilon_0 B}{e^2(1+B/2)} e^{-i\mathbf{r}\cdot\mathbf{r}_2} \times \begin{pmatrix} k_x \\ k_y \\ iK \end{pmatrix} \\ &= -\frac{\epsilon_0 B}{e^2(1+B/2)} e^{-i\mathbf{r}\cdot\mathbf{r}_2} r_j. \end{aligned} \quad (\text{C.50})$$

Substituting Eq. (C.50) into (C.49), we obtain

$$\tilde{G}_{ij}^{(+)}(z_1) - \tilde{G}_{ij}^{(\infty)}(z_1) = \frac{\epsilon_0 B^3}{2e^2(1+B)(1+B/2)} e^{-i(k_x x_2 + k_y y_2)} \left[\frac{r'_i r_j}{2K} e^{K(z_1+z_2)} \right]. \quad (\text{C.51})$$

The quantity in brackets in Eq. (C.51) can be written as

$$\frac{r'_i r_j}{2K} e^{K(z_1+z_2)} = \int_{-\infty}^{\infty} \frac{dk_z}{2\pi} e^{ik_z(z_1+z_2)} \frac{k_i k'_j}{k^2}, \quad (\text{C.52})$$

where $k'_j = (k_x, k_y, -k_z)$ is the image of the vector $k_j = (k_x, k_y, k_z)$ in the plane $z = 0$. Eq. (C.52) can be verified by closing the contour of integration in the lower half of the k_z -plane, since $(z_1 + z_2) < 0$, and noting that only the pole at $k_z = -iK$ contributes.

The Green function $\mathcal{G}_{ij}^{(0)\omega}(\mathbf{r}_1, \mathbf{r}_2)$ is obtained by taking the inverse Fourier transform of Eq. (C.51) with respect to k_x and k_y . Using Eq. (C.52), we obtain

$$\begin{aligned} \mathcal{G}_{ij}^{(0)\omega}(\mathbf{r}_1, \mathbf{r}_2) - \mathcal{G}_{ij}^{(\infty)\omega}(\mathbf{r}_1, \mathbf{r}_2) &= \frac{\epsilon_0 B^3}{2e^2(1+B)(1+B/2)} \\ &\quad \times \int \frac{d^3 k}{(2\pi)^3} e^{ik_x(x_1-x_2) + ik_y(y_1-y_2) + ik_z(z_1+z_2)} \frac{k_i k'_j}{k^2} \\ &= \frac{\epsilon_0 B^3}{2e^2(1+B)(1+B/2)} \left[\frac{\partial^2}{\partial x_{1i} \partial x_{2j}} \int \frac{d^3 k}{(2\pi)^3} e^{ik_x(x_1-x_2) + ik_y(y_1-y_2) + ik_z(z_1+z_2)} \frac{1}{k^2} \right] \\ &= \frac{\epsilon_0 B^3}{2e^2(1+B)(1+B/2)} \left[\frac{\partial^2}{\partial x_{1i} \partial x_{2j}} \int \frac{d^3 k}{(2\pi)^3} e^{i\mathbf{k}\cdot(\mathbf{r}_1 - \bar{\mathbf{r}}_2)} \frac{1}{k^2} \right], \end{aligned} \quad (\text{C.53})$$

where $\tilde{\mathbf{r}}_2 = (x_2, y_2, -z_2)$ is the image of $\mathbf{r}_2 = (x_2, y_2, z_2)$ in the plane $z = 0$. Using the fact that the three-dimensional inverse Fourier transform of $1/k^2$ evaluated at \mathbf{r} is $1/4\pi|\mathbf{r}|$, we obtain

$$\mathcal{G}_{ij}^{(0)\omega}(\mathbf{r}_1, \mathbf{r}_2) - \mathcal{G}_{ij}^{(\infty)\omega}(\mathbf{r}_1, \mathbf{r}_2) = \frac{\epsilon_0[\epsilon_L(|\omega|) - 1]^3}{4\pi e^2 \epsilon_L(|\omega|)[\epsilon_L(|\omega|) + 1]} \left[\frac{\partial^2}{\partial x_{1i} \partial x_{2j}} \left(\frac{1}{|\mathbf{r}_1 - \tilde{\mathbf{r}}_2|} \right) \right], \quad (\text{C.54})$$

where we have used Eq. (C.6). Finally, when Eq. (C.8) is substituted into Eq. (C.54), we obtain Eq. (2.132).

Appendix D

Integral of $\xi(\omega)$

In this appendix, the integral I defined by

$$\begin{aligned} I &= \int_0^\infty d\omega \xi(\omega) \\ &= \int_0^\infty d\omega \frac{\tilde{\omega}_0 \omega V^2(\omega)}{|\omega^2 - \tilde{\omega}_0^2 z(\omega)|^2} \end{aligned} \quad (\text{D.1})$$

is shown to be unity. Our discussion follows closely that of Huttner et al. [7] but contains more algebraic details.

We start with the equality

$$\frac{1}{\omega^2 - \tilde{\omega}_0^2 z(\omega)} - \frac{1}{\omega^2 - \tilde{\omega}_0^2 z^*(\omega)} = \frac{\tilde{\omega}_0^2 [z(\omega) - z^*(\omega)]}{|\omega^2 - \tilde{\omega}_0^2 z(\omega)|^2}. \quad (\text{D.2})$$

From Eq. (A.12) we find

$$\begin{aligned} z(\omega) - z^*(\omega) &= -\frac{1}{2\tilde{\omega}_0} \int_{-\infty}^\infty d\omega' V^2(\omega') \left[\frac{1}{\omega' - \omega + i\epsilon} - \frac{1}{\omega' - \omega - i\epsilon} \right] \\ &= -\frac{1}{2\tilde{\omega}_0} \int_{-\infty}^\infty d\omega' V^2(\omega') [-2\pi i \delta(\omega' - \omega)] \\ &= \frac{\pi i}{\tilde{\omega}_0} V^2(\omega). \end{aligned} \quad (\text{D.3})$$

Substituting Eq. (D.3) into Eq. (D.2), we see that Eq. (D.1) may be written as

$$I = \frac{1}{\pi i} \int_0^\infty d\omega \omega \left[\frac{1}{\omega^2 - \tilde{\omega}_0^2 z(\omega)} - \frac{1}{\omega^2 - \tilde{\omega}_0^2 z^*(\omega)} \right]. \quad (\text{D.4})$$

Using the fact that $V^2(\omega)$ is an odd function of ω , it can be seen from Eq. (A.12) that $z^*(\omega) = z(-\omega)$. Hence, the two terms in Eq. (D.4) may be combined,

$$I = \frac{1}{\pi i} \int_{-\infty}^\infty d\omega \frac{\omega}{\omega^2 - \tilde{\omega}_0^2 z(\omega)}. \quad (\text{D.5})$$

The integrand in Eq. (D.5) can be shown to be analytic in the lower half of the complex ω plane [7]. Hence, the integration path can be deformed into a semicircle in the lower half plane with radius $R \rightarrow \infty$,

$$I = \frac{1}{\pi i} \int_{\theta=\pi}^{\theta=2\pi} d\Omega \frac{\Omega}{\Omega^2 - \tilde{\omega}_0^2 z(\Omega)}, \quad (\text{D.6})$$

where $\Omega = Re^{i\theta}$. In the limit $R \rightarrow \infty$, we find

$$\begin{aligned} I &= \frac{1}{\pi i} \int_{\theta=\pi}^{\theta=2\pi} iRe^{i\theta} d\theta \frac{Re^{i\theta}}{R^2 e^{2i\theta}} \\ &= 1. \end{aligned} \quad (\text{D.7})$$

Appendix E

Green Function for the Transverse Photons

In this appendix, the Dyson equation Eq. (2.164) for the photon Green function \mathcal{D}_{ij}^ω for the dielectric half-space described by the Hamiltonian density \mathcal{H} of Eq. (2.102) is solved exactly using an extension of the Wiener-Hopf technique. Our approach is similar to that used in Appendix C, but the algebra here is considerably more complicated. As in Appendix C, we fix \mathbf{r}_2 in Eq. (2.164) and regard \mathcal{D}_{ij}^ω as a function of only one coordinate vector \mathbf{r}_1 . Then we eliminate the x_1 and y_1 variables by taking the Fourier transform of Eq. (2.164) with respect to $(x_1 - x_2)$ and $(y_1 - y_2)$,

$$\begin{aligned} \tilde{D}_{ij}^\omega(z_1) &= \tilde{D}_{ij}^{(0)\omega}(z_1) - \omega^2 \epsilon_0 [\epsilon_L(|\omega|) - 1] \int_{z_3 < 0} dz_3 \tilde{D}_{im}^{(0)\omega}(z_1 - z_3 + z_2) \tilde{D}_{mj}^\omega(z_3) \\ &\quad + \frac{\omega^2 \epsilon_0 [\epsilon_L(|\omega|) - 1]^2}{[\epsilon_L(|\omega|) + 1]} \tilde{D}_{i3}^{(0)\omega}(z_1 + z_2) \frac{1}{K} \tilde{D}_{3j}^\omega(0), \end{aligned} \quad (\text{E.1})$$

where $\tilde{D}_{ij}^{(0)\omega}(z_1)$ is the two-dimensional Fourier transform of the free-space photon Green function Eq. (2.112) with respect to $(x_1 - x_2)$ and $(y_1 - y_2)$,

$$\tilde{D}_{ij}^{(0)\omega}(z_1) = \frac{1}{\epsilon_0} \int \frac{dk_z}{2\pi} \frac{\left(\delta_{ij} - \frac{k_i k_j}{k^2}\right)}{\omega^2 - k^2 c^2 + i\epsilon} e^{ik_z(z_1 - z_2)}. \quad (\text{E.2})$$

In Eq. (E.1) and (E.2) we have omitted writing the dependence of the Fourier transforms $\tilde{D}_{ij}^\omega(z_1)$ and $\tilde{D}_{ij}^{(0)\omega}(z_1)$ on z_2 , k_x and k_y . The integral over k_z in Eq. (E.2) can be evaluated by contour integration, by noting that the integrand has poles at $k_z = \pm iK$ and $k_z = \pm iS/c$, where

$$S = S(K) = \sqrt{K^2 c^2 - \omega^2 - i\epsilon}. \quad (\text{E.3})$$

The branch of the square root in Eq. (E.3) is chosen so that the real part of S is always positive. Thus, Eq. (E.2) becomes

$$\bar{D}_{ij}^{(0)\omega}(z_1) = \frac{1}{\epsilon_0} \times \begin{cases} -\frac{\left(\delta_{ij} - \frac{q'_i q'_j}{q^2}\right)}{2Sc} e^{-S(z_1-z_2)/c} - \frac{r_i r_j}{2K(\omega^2 + i\epsilon)} e^{-K(z_1-z_2)}, & z_1 > z_2, \\ -\frac{\left(\delta_{ij} - \frac{q_i q_j}{q^2}\right)}{2Sc} e^{S(z_1-z_2)/c} - \frac{r'_i r'_j}{2K(\omega^2 + i\epsilon)} e^{K(z_1-z_2)}, & z_1 < z_2. \end{cases} \quad (\text{E.4})$$

where r_i and r'_i are given by Eqs. (C.12) and (C.13), and

$$q_i = \left(k_x, k_y, -\frac{iS}{c}\right), \quad (\text{E.5})$$

$$q'_i = \left(k_x, k_y, \frac{iS}{c}\right). \quad (\text{E.6})$$

To solve Eq. (E.1) using the Wiener-Hopf technique, we write $\bar{D}_{ij}^\omega(z_1)$ as a sum of two functions $\bar{D}_{ij}^{(+)}(z_1)$ and $\bar{D}_{ij}^{(-)}(z_1)$, the first of which vanishes for $z_1 > 0$ and the second of which vanishes for $z_1 < 0$. Eq. (E.1) then becomes

$$\begin{aligned} \bar{D}_{ij}^{(+)}(z_1) + \bar{D}_{ij}^{(-)}(z_1) &= \bar{D}_{ij}^{(0)\omega}(z_1) - \omega^2 \epsilon_0 [\epsilon_L(|\omega|) - 1] \int_{-\infty}^{\infty} dz_3 \bar{D}_{im}^{(0)\omega}(z_1 - z_3 + z_2) \\ &\quad \times \bar{D}_{mj}^{(+)}(z_3) + \frac{\omega^2 \epsilon_0 [\epsilon_L(|\omega|) - 1]^2}{[\epsilon_L(|\omega|) + 1]} \bar{D}_{i3}^{(0)\omega}(z_1 + z_2) \frac{1}{K} \bar{D}_{3j}^\omega(0), \end{aligned} \quad (\text{E.7})$$

where the integral is now over the entire z_3 -axis. As such, this integral is a convolution. Taking the Fourier transform of Eq. (E.7) with respect to z_1 , we obtain

$$\begin{aligned} D_{ij}^{(+)}(k_z) + D_{ij}^{(-)}(k_z) &= D_{ij}^{(0)\omega}(k_z) - \omega^2 \epsilon_0 [\epsilon_L(|\omega|) - 1] D_{im}^{(0)\omega}(k_z) e^{ik_z z_2} D_{mj}^{(+)}(k_z) \\ &\quad + \frac{\omega^2 \epsilon_0 [\epsilon_L(|\omega|) - 1]^2}{[\epsilon_L(|\omega|) + 1]} D_{i3}^{(0)\omega}(k_z) e^{ik_z z_2} \frac{1}{K} \bar{D}_{3j}^\omega(0), \end{aligned} \quad (\text{E.8})$$

where the Fourier transform with $D_{ij}^{(0)\omega}(k_z)$ with respect to z_1 can be obtained from Eq. (E.2),

$$D_{ij}^{(0)\omega}(k_z) = \frac{1}{\epsilon_0} \frac{\left(\delta_{ij} - \frac{k_i k_j}{k^2}\right)}{\omega^2 - k^2 c^2 + i\epsilon} e^{-ik_z z_2}. \quad (\text{E.9})$$

To determine the regions of analyticity of $D_{ij}^{(\pm)}(k_z)$, we proceed as in Eq. (C.16) and take the limit $z_1 \rightarrow +\infty$ of both sides of Eq. (E.7). The LHS of this equation

then becomes $\lim_{z_1 \rightarrow +\infty} \tilde{D}_{ij}^{(-)}(z_1)$. When Eq. (E.4) for $z_1 > z_2$ is substituted into the RHS of Eq. (E.7), we see that, because of the $\tilde{D}_{ij}^{(0)\omega}$ factor in each of the terms on the RHS of Eq. (E.7), the latter RHS can be written as a sum of a term proportional to $e^{-S z_1/c}$ and a term proportional to $e^{-K z_1}$. Examination of Eq. (E.3) shows that, for $K \neq 0$, the real part of S/c is always smaller than K . Hence, in the limit $z_1 \rightarrow +\infty$, $e^{-S z_1/c} \gg e^{-K z_1}$. The asymptotic behavior of $\tilde{D}_{ij}^{(-)}(z_1)$ as $z_1 \rightarrow +\infty$ is therefore $\tilde{D}_{ij}^{(-)}(z_1) \sim e^{-S z_1/c}$, up to a multiplicative factor. By definition, $D_{ij}^{(-)}(k_z) = \int_0^\infty dz_1 e^{-i k_z z_1} \tilde{D}_{ij}^{(-)}(z_1)$. Since the behavior of the integrand at large, positive z_1 is $\sim e^{-i k_z z_1 - S z_1/c}$, this integral converges whenever $\text{Im } k_z < \text{Re } S/c$. Thus, we conclude that $D_{ij}^{(-)}(k_z)$ is analytic everywhere in the complex half-plane $\Sigma^{(-)} = \{k_z \mid \text{Im } k_z < \text{Re } S/c\}$.

Next, we assume that the asymptotic behavior of $\tilde{D}_{ij}^{(+)}(z_1)$ as $z_1 \rightarrow -\infty$ is $\sim e^{\mu_1 z_1}$, where $\mu_1 \geq 0$ in order that $\tilde{D}_{ij}^{(+)}(z_1)$ remains finite at $z_1 \rightarrow -\infty$. By definition, $D_{ij}^{(+)}(k_z) = \int_{-\infty}^0 dz_1 e^{-i k_z z_1} \tilde{D}_{ij}^{(+)}(z_1)$. Since the behavior of the integrand at large, negative z_1 is $\sim e^{-i k_z z_1 + \mu_1 z_1}$, this integral converges whenever $\text{Im } k_z > -\mu_1$. Thus, we conclude that $D_{ij}^{(+)}(k_z)$ is analytic everywhere in the complex half-plane $\Sigma^{(+)} = \{k_z \mid \text{Im } k_z > -\mu_1\}$.

From Eq. (E.9), the first term on the RHS of Eq. (E.8), $D_{ij}^{(0)\omega}(k_z)$, has poles at $k_z = \pm iK$ and $k_z = \pm iS/c$, since the denominator $(\omega^2 - k^2 c^2 + i\varepsilon) = (iS + k_z c)(iS - k_z c)$. Hence, this quantity is analytic in the strip $\Lambda = \{k_z \mid -\text{Re } S/c < \text{Im } k_z < \text{Re } S/c\}$. Since $\Sigma^{(+)} \cap \Sigma^{(-)} \cap \Lambda \neq \emptyset$, we conclude that there is a common domain of analyticity of the three functions $D_{ij}^{(+)}(k_z)$, $D_{ij}^{(-)}(k_z)$ and $D_{ij}^{(0)\omega}(k_z)$.

We now proceed to solve Eq. (E.8). Rearranging terms in this equation, we obtain

$$\left\{ [\omega^2 - \Pi(\omega) - k^2 c^2 + i\varepsilon] \delta_{im} + \Pi(\omega) \frac{k_i k_m}{k^2} \right\} \frac{D_{mj}^{(+)}(k_z)}{\omega^2 - k^2 c^2 + i\varepsilon} + D_{ij}^{(-)}(k_z) = D_{ij}^{(0)\omega}(k_z) + \Sigma(\omega, K) \frac{(\delta_{i3} - \frac{k_i k_z}{k^2})}{\omega^2 - k^2 c^2 + i\varepsilon} \tilde{D}_{3j}^\omega(0), \quad (\text{E.10})$$

where $\Pi(\omega)$ and $\Sigma(\omega, K)$ are the bulk and surface photon self-energies divided by ϵ_0 ,

$$\Pi(\omega) = -\omega^2 [\epsilon_L(|\omega|) - 1], \quad (\text{E.11})$$

$$\Sigma(\omega, K) = \frac{\omega^2[\epsilon_L(|\omega|) - 1]^2}{K[\epsilon_L(|\omega|) + 1]}. \quad (\text{E.12})$$

Ideally, we would like to factorize the 3×3 matrix in braces on the LHS of Eq. (E.10) into a product $\mathcal{M}_{il}^{(-)}\mathcal{M}_{im}^{(+)}$ such that $\mathcal{M}_{ij}^{(+)}$ is analytic in $\Sigma^{(+)}$ and the *inverse* of $\mathcal{M}_{ij}^{(-)}$ is analytic in $\Sigma^{(-)}$. However, this was found to be difficult. Instead, we factorize the 3×3 matrix in braces into the following factors,

$$\mathcal{M}_{ij}^{(-)} = (iL - k_z c)\delta_{ij} + i(S - L)\frac{k_i k_j}{k^2}, \quad (\text{E.13})$$

$$\mathcal{M}_{ij}^{(+)} = (iL + k_z c)\delta_{ij} + i(S - L)\frac{k_i k_j}{k^2}, \quad (\text{E.14})$$

where S is given by Eq. (E.3) and

$$L = L(K) = \sqrt{K^2 c^2 + \Pi(\omega) - \omega^2 - i\epsilon}. \quad (\text{E.15})$$

The branch of the square root in Eq. (E.15) is chosen so that the real part of L is always positive. The inverse matrices are

$$\mathcal{M}_{ij}^{(-)-1} = \frac{1}{iL - k_z c} \left[\delta_{ij} - \frac{i(S - L)}{iS - k_z c} \frac{k_i k_j}{k^2} \right], \quad (\text{E.16})$$

$$\mathcal{M}_{ij}^{(+)-1} = \frac{1}{iL + k_z c} \left[\delta_{ij} - \frac{i(S - L)}{iS + k_z c} \frac{k_i k_j}{k^2} \right]. \quad (\text{E.17})$$

Eq. (E.14) shows that $\mathcal{M}_{ij}^{(+)}$ is analytic in $\Sigma^{(+)}$ *except* for a pole at $k_z = +iK$. Similarly, Eq. (E.16) shows that $\mathcal{M}_{ij}^{(-)-1}$ is analytic in $\Sigma^{(-)}$ *except* for a pole at $k_z = -iK$. As a result of these unwanted poles at $k_z = \pm iK$, the standard Wiener-Hopf technique must be extended to deal with these singularities. This consists of subtracting the unwanted poles from Eq. (E.10). After multiplying this equation throughout by $(iS - k_z c)\mathcal{M}^{(-)-1}$ and rearranging terms, we obtain

$$\begin{aligned} \mathcal{M}_{im}^{(+)} \left[\frac{D_{mj}^{(+)}(k_z)}{iS + k_z c} - A_{mj}^{(+)} \right] + \mathcal{M}_{im}^{(-)-1} \left[D_{mj}^{(-)}(k_z)(iS - k_z c) - A_{mj}^{(-)} \right] \\ = \mathcal{M}_{im}^{(-)-1} \left[D_{mj}^{(0)}(k_z) + \Sigma(\omega, K) \frac{(\delta_{m3} - \frac{k_m k_z}{k^2})}{\omega^2 - k^2 c^2 + i\epsilon} \bar{D}_{3j}^{\omega}(0) \right] (iS - k_z c) \\ - \mathcal{M}_{im}^{(+)} A_{mj}^{(+)} - \mathcal{M}_{im}^{(-)-1} A_{mj}^{(-)}, \end{aligned} \quad (\text{E.18})$$

where we have subtracted quantities $\mathcal{M}_{im}^{(+)} A_{mj}^{(+)}$ and $\mathcal{M}_{im}^{(-)-1} A_{mj}^{(-)}$ from both sides of the equation so as to make the residues of the poles at $k_z = iK$ and $k_z = -iK$ due to $\mathcal{M}_{im}^{(+)}$ and $\mathcal{M}_{im}^{(-)-1}$ in the first and second terms, respectively, on the LHS of Eq. (E.18) vanish. As a result, the first and second terms on the LHS of this equation are analytic in $\Sigma^{(+)}$ and $\Sigma^{(-)}$, respectively.

The RHS of Eq. (E.18) can be simplified by using the fact that $k_m \left(\delta_{mj} - \frac{k_m k_j}{k^2} \right) = 0$. Using Eqs. (E.9) and (E.16), the RHS of Eq. (E.18) is simplified to:

$$\begin{aligned} \text{RHS of (E.18)} = & \frac{\left(\delta_{im} - \frac{k_i k_m}{k^2} \right)}{(iL - k_z c)(iS + k_z c)} \left[\frac{1}{\epsilon_0} e^{-ik_z z_2} \delta_{mj} + \Sigma(\omega, K) \delta_{m3} \tilde{D}_{3j}^\omega(0) \right] \\ & - \mathcal{M}_{im}^{(+)} A_{mj}^{(+)} - \mathcal{M}_{im}^{(-)-1} A_{mj}^{(-)}. \end{aligned} \quad (\text{E.19})$$

We now have to decompose the expression Eq. (E.19) into a sum of two terms $P_{ij}^{(+)}(k_z)$ and $P_{ij}^{(-)}(k_z)$ analytic in $\Sigma^{(+)}$ and $\Sigma^{(-)}$, respectively.

Consider the first term inside the brackets in Eq. (E.19) proportional to $e^{-ik_z z_2}$. Depending on whether z_2 is positive or negative, this term has an essential singularity at $\text{Im } k_z \rightarrow +\infty$ or $\text{Im } k_z \rightarrow -\infty$, respectively. We are primarily interested in the solution for $z_2 \geq 0$. Hence, we assume in the following that $z_2 \geq 0$. In that case, the quantity in brackets in Eq. (E.19) must be associated with $P_{ij}^{(-)}(k_z)$, since it has an essential singularity in $\Sigma^{(+)}$. However, the factor in front of the quantity in brackets in Eq. (E.19) has poles in $\Sigma^{(-)}$ at $k_z = -iS/c$ and $k_z = -iK$. Hence, before we may assign the first term on the LHS of Eq. (E.19) to $P_{ij}^{(-)}(k_z)$, we must subtract these unwanted poles in $\Sigma^{(-)}$ from this term. The subtracted poles, since they are in $\Sigma^{(-)}$, can then be added back as part of $P_{ij}^{(+)}(k_z)$. For the unwanted pole at $k_z = -iS/c$, the quantity $F_{ij}^{(1)}(k_z)$ that must be subtracted is $1/(iS + k_z c)$ times the residue of the first term on the RHS of Eq. (E.19) at this pole,

$$F_{ij}^{(1)}(k_z) = -\frac{i \left(\delta_{im} - \frac{q_i q_m}{q^2} \right)}{(L + S)(iS + k_z c)} \left[\frac{1}{\epsilon_0} e^{-S z_2 / c} \delta_{mj} + \Sigma(\omega, K) \delta_{m3} \tilde{D}_{3j}^\omega(0) \right]. \quad (\text{E.20})$$

Similarly, for the unwanted pole at $k_z = -iK$, the quantity $F_{ij}^{(2)}(k_z)$ that must be subtracted is $1/(iK + k_z)$ times the residue of the first term on the RHS of Eq. (E.19)

at this pole,

$$F_{ij}^{(2)}(k_z) = \frac{i r'_i r'_m}{2K(L+Kc)(S-Kc)(iK+k_z)} \left[\frac{1}{\epsilon_0} e^{-Kz_2} \delta_{mj} + \Sigma(\omega, K) \delta_{m3} \bar{D}_{3j}^\omega(0) \right]. \quad (\text{E.21})$$

Next, we have to decide whether the last two terms on the RHS of Eq. (E.19) should be assigned to $\Sigma^{(+)}$ or $\Sigma^{(-)}$. Examination of Eq. (E.16) shows that the inverse matrix $\mathcal{M}_{ij}^{(-)-1}$ has three poles in $\Sigma^{(+)}$, namely, $k_z = iL/c$, $k_z = iS/c$ and $k_z = iK$, but only one in $\Sigma^{(-)}$ at $k_z = -iK$. Hence, it is simplest to assign the term $[-\mathcal{M}_{im}^{(-)-1} A_{mj}^{(-)}]$ in Eq. (E.19) to $P_{ij}^{(-)}(k_z)$ and to remove the unwanted pole at $k_z = -iK$ from this term, by subtracting the quantity $F_{ij}^{(3)}(k_z)$ from it,

$$F_{ij}^{(3)}(k_z) = \frac{(S-L)r'_i r'_m A_{mj}^{(-)}}{2K(L+Kc)(S+Kc)(iK+k_z)}. \quad (\text{E.22})$$

The remaining term $[-\mathcal{M}_{im}^{(+)} A_{mj}^{(+)}]$ in Eq. (E.19) can be assigned to $P_{ij}^{(+)}(k_z)$, after we have removed the unwanted pole at $k_z = +iK$ from it by subtracting the quantity $F_{ij}^{(4)}(k_z)$ from it,

$$F_{ij}^{(4)}(k_z) = -\frac{(S-L)r_i r_m A_{mj}^{(+)}}{2K(k_z - iK)}. \quad (\text{E.23})$$

Summarizing, we have decomposed the RHS of Eq. (E.18) into a sum of two terms $P_{ij}^{(+)}(k_z)$ and $P_{ij}^{(-)}(k_z)$,

$$P_{ij}^{(-)}(k_z) = \frac{(\delta_{im} - \frac{k_i k_m}{k^2})}{(iL - k_z c)(iS + k_z c)} \left[\frac{1}{\epsilon_0} e^{-ik_z z_2} \delta_{mj} + \Sigma(\omega, K) \delta_{m3} \bar{D}_{3j}^\omega(0) \right] - \mathcal{M}_{im}^{(-)-1} A_{mj}^{(-)} - F_{ij}^{(1)}(k_z) - F_{ij}^{(2)}(k_z) - F_{ij}^{(3)}(k_z) + F_{ij}^{(4)}(k_z), \quad (\text{E.24})$$

$$P_{ij}^{(+)}(k_z) = -\mathcal{M}_{im}^{(+)} A_{mj}^{(+)} + F_{ij}^{(1)}(k_z) + F_{ij}^{(2)}(k_z) + F_{ij}^{(3)}(k_z) - F_{ij}^{(4)}(k_z), \quad (\text{E.25})$$

where $F_{ij}^{(1)}(k_z)$ to $F_{ij}^{(4)}(k_z)$ are given by Eqs. (E.20) to (E.23).

Replacing the RHS of Eq. (E.18) by $P_{ij}^{(+)}(k_z) + P_{ij}^{(-)}(k_z)$ and rearranging terms, we obtain

$$\mathcal{M}_{im}^{(+)} \left[\frac{D_{mj}^{(+)}(k_z)}{iS + k_z c} - A_{mj}^{(+)} \right] - P_{ij}^{(+)}(k_z) = -\mathcal{M}_{im}^{(-)-1} \left[D_{mj}^{(-)}(k_z)(iS - k_z c) - A_{mj}^{(-)} \right] + P_{ij}^{(-)}(k_z). \quad (\text{E.26})$$

The LHS of Eq. (E.26) is analytic in $\Sigma^{(+)}$ and the RHS in $\Sigma^{(-)}$. Because $\Sigma^{(+)} \cap \Sigma^{(-)} \neq \emptyset$, we conclude that both sides of Eq. (E.26) must be an entire function, which we denote by $R_{ij}(k_z)$. Setting each side of Eq. (E.26) equal to $R_{ij}(k_z)$, we obtain

$$D_{ij}^{(+)}(k_z) = (iS + k_z c) \left\{ A_{ij}^{(+)} + \mathcal{M}_{im}^{(+)-1} \left[P_{mj}^{(+)}(k_z) + R_{mj}(k_z) \right] \right\}, \quad (\text{E.27})$$

$$D_{ij}^{(-)}(k_z) = \frac{1}{iS - k_z c} \left\{ A_{ij}^{(-)} + \mathcal{M}_{im}^{(-)} \left[P_{mj}^{(-)}(k_z) - R_{mj}(k_z) \right] \right\}. \quad (\text{E.28})$$

Substituting Eqs. (E.24) and (E.25) into Eqs. (E.27) and (E.28), we obtain the formal solution

$$D_{ij}^{(+)}(k_z) = (iS + k_z c) \mathcal{M}_{im}^{(+)-1} \left[F_{mj}^{(1)}(k_z) + F_{mj}^{(2)}(k_z) + F_{mj}^{(3)}(k_z) - F_{mj}^{(4)}(k_z) + R_{mj}(k_z) \right], \quad (\text{E.29})$$

$$\begin{aligned} D_{ij}^{(-)}(k_z) &= \frac{\left(\delta_{im} - \frac{k_i k_m}{k^2} \right)}{(iS - k_z c)(iS + k_z c)} \left[\frac{1}{\epsilon_0} e^{-ik_z z_2} \delta_{mj} + \Sigma(\omega, K) \delta_{m3} \tilde{D}_{3j}^\omega(0) \right] \\ &\quad - \frac{1}{iS - k_z c} \mathcal{M}_{im}^{(-)} \left[F_{mj}^{(1)}(k_z) + F_{mj}^{(2)}(k_z) + F_{mj}^{(3)}(k_z) - F_{mj}^{(4)}(k_z) + R_{mj}(k_z) \right] \\ &= D_{ij}^{(0)\omega}(k_z) + \frac{\left(\delta_{i3} - \frac{k_i k_z}{k^2} \right)}{\omega^2 - k^2 c^2 + i\epsilon} \Sigma(\omega, K) \tilde{D}_{3j}^\omega(0) \\ &\quad - \frac{1}{iS - k_z c} \mathcal{M}_{im}^{(-)} \left[F_{mj}^{(1)}(k_z) + F_{mj}^{(2)}(k_z) + F_{mj}^{(3)}(k_z) - F_{mj}^{(4)}(k_z) + R_{mj}(k_z) \right], \quad (\text{E.30}) \end{aligned}$$

where we have used Eqs. (E.13), (E.9) and the fact that $k_m \left(\delta_{mj} - \frac{k_m k_j}{k^2} \right) = 0$ in Eq. (E.30).

Eqs. (E.29) and (E.30) still contain the unknown quantities $r_m A_{mj}^{(+)}$, $r'_m A_{mj}^{(-)}$, $R_{ij}(k_z)$ and $\tilde{D}_{3j}^\omega(0)$. To solve for these quantities, we first use the fact that the photon Green function $\mathcal{D}_{ij}^\omega(\mathbf{r}_1, \mathbf{r}_2)$ represents the radiation field due to a point source at \mathbf{r}_2 . For a point source in air, $z_2 > 0$, this Green function is expected to have the same singularity at $\mathbf{r}_1 = \mathbf{r}_2$ as the free-space photon Green function $\mathcal{D}_{ij}^{(0)\omega}(\mathbf{r}_1 - \mathbf{r}_2)$. Hence, we expect $\tilde{D}_{ij}^{(+)}(z_1)$ and $[\tilde{D}_{ij}^{(-)}(z_1) - \tilde{D}_{ij}^{(0)\omega}(z_1)]$ to be finite at $z_1 = 0$. Now, $\tilde{D}_{ij}^{(+)}(z_1)|_{z_1=0} = \int \frac{dk_z}{2\pi} D_{ij}^{(+)}(k_z)$ and $[\tilde{D}_{ij}^{(-)}(z_1) - \tilde{D}_{ij}^{(0)\omega}(z_1)]|_{z_1=0} = \int \frac{dk_z}{2\pi} [D_{ij}^{(-)}(k_z) - D_{ij}^{(0)\omega}(k_z)]$. These quantities are finite if

$$\lim_{k_z \rightarrow \pm\infty} D_{ij}^{(+)}(k_z) = 0, \quad (\text{E.31})$$

$$\lim_{k_z \rightarrow \pm\infty} [D_{ij}^{(\pm)}(k_z) - D_{ij}^{(0)\omega}(k_z)] = 0. \quad (\text{E.32})$$

Examination of Eqs. (E.17) and (E.13) shows that $\lim_{k_z \rightarrow \pm\infty} (iS + k_z c) \mathcal{M}_{im}^{(+)-1} = \lim_{k_z \rightarrow \pm\infty} \frac{\mathcal{M}_{im}^{(-)}}{iS - k_z c} = \delta_{im}$. Also, examination of Eqs. (E.20) to (E.23) shows that $\lim_{k_z \rightarrow \pm\infty} F_{ij}^{(n)}(k_z) = 0$ for $n = 1$ to 4. Using these results in Eqs. (E.29) and (E.30), we obtain

$$\lim_{k_z \rightarrow \pm\infty} D_{ij}^{(+)}(k_z) = \lim_{k_z \rightarrow \pm\infty} R_{ij}(k_z), \quad (\text{E.33})$$

$$\lim_{k_z \rightarrow \pm\infty} [D_{ij}^{(\pm)}(k_z) - D_{ij}^{(0)\omega}(k_z)] = \lim_{k_z \rightarrow \pm\infty} -R_{ij}(k_z). \quad (\text{E.34})$$

Substituting Eqs. (E.33) and (E.34) into Eqs. (E.31) and (E.32), we conclude that

$$R_{ij}(k_z) = 0. \quad (\text{E.35})$$

Next, we use the fact that $D_{ij}^{(\pm)}(k_z)$ must be analytic in $\Sigma^{(\pm)}$, respectively. However, Eqs. (E.27) and (E.28) show that $D_{ij}^{(\pm)}(k_z)$ contain terms proportional to $1/k^2$ due to the matrices $\mathcal{M}_{im}^{(+)-1}$ and $\mathcal{M}_{im}^{(-)}$. The resolution of this paradox lies in demanding that the residues of the RHS of Eqs. (E.27) and (E.28) at the poles $k_z = \pm iK$, respectively, must be zero. The latter poles come from the terms proportional to $\frac{k_i k_m}{k^2} P_{mj}^{(\pm)}(k_z)$ in Eqs. (E.27) and (E.28), respectively, since $R_{mj}(k_z) = 0$. Canceling common factors, we obtain the conditions

$$r_m P_{mj}^{(+)}(iK) = 0, \quad (\text{E.36})$$

$$r'_m P_{mj}^{(-)}(-iK) = 0. \quad (\text{E.37})$$

According to Eq. (E.36), we have to evaluate $P_{mj}^{(+)}(k_z)$ given by Eq. (E.25) at $k_z = iK$. Evaluating $F_{ij}^{(1)}(k_z)$ to $F_{ij}^{(3)}(k_z)$ at $k_z = iK$ is straightforward, since these functions are finite at $k_z = iK$ according to Eqs. (E.20) to (E.22). However, Eq. (E.23) shows that $F_{ij}^{(4)}(k_z)$ is singular at $k_z = iK$. In fact, this singularity was chosen to cancel a similar singularity in the first term of Eq. (E.25). Hence, we should take the limit of the latter term and $F_{ij}^{(4)}(k_z)$ together,

$$\begin{aligned} \lim_{k_z \rightarrow iK} [-\mathcal{M}_{im}^{(+)} A_{mj}^{(+)} - F_{ij}^{(4)}(k_z)] &= -i(L + Kc) A_{ij}^{(+)} \\ &- \lim_{k_z \rightarrow iK} \frac{i(S - L)}{k_z - iK} \left[\frac{k_i k_m}{k_z + iK} - \frac{r_i r_m}{2iK} \right] A_{mj}^{(+)}, \end{aligned} \quad (\text{E.38})$$

where we have used Eqs. (E.14) and (E.23). The quantity in brackets in Eq. (E.38) can be expanded in a Taylor series about $k_z = iK$. The zeroth order term vanishes, as expected for the above-mentioned cancellation of singularities. The first order term leads to a finite result, and we have

$$\begin{aligned} \lim_{k_z \rightarrow iK} \left[-\mathcal{M}_{im}^{(+)} A_{mj}^{(+)} - F_{ij}^{(4)}(k_z) \right] &= -i(L + Kc)A_{ij}^{(+)} \\ &\quad -i(S - L) \frac{\partial}{\partial k_z} \left(\frac{k_i k_m}{k_z + iK} \right) \Big|_{k_z=iK} A_{mj}^{(+)} \\ &= -i(L + Kc)A_{ij}^{(+)} - i(S - L) \left[\frac{\delta_{i3} k_m}{k_z + iK} + k_i \frac{\partial}{\partial k_z} \left(\frac{k_m}{k_z + iK} \right) \right] \Big|_{k_z=iK} A_{mj}^{(+)}. \end{aligned} \quad (\text{E.39})$$

When we multiply both sides of Eq. (E.39) by r_i and sum over i as in Eq. (E.36), the second term inside the brackets in Eq. (E.39) is seen to be proportional to $r_i k_i|_{k_z=iK} = r_i r_i = 0$, by Eq. (C.12). Hence, using the fact that $\left(\frac{r_3}{k_z + iK} \right) \Big|_{k_z=iK} = 1/2$, we obtain

$$\lim_{k_z \rightarrow iK} r_i \left[-\mathcal{M}_{im}^{(+)} A_{mj}^{(+)} - F_{ij}^{(4)}(k_z) \right] = -i \left[L + Kc + \frac{1}{2}(S - L) \right] r_m A_{mj}^{(+)}. \quad (\text{E.40})$$

Substituting Eq. (E.40) in Eq. (E.36) and using Eqs. (E.20) to (E.22), we obtain the condition

$$\begin{aligned} 0 &= -\frac{i}{2}(L + S + 2Kc)r_m A_{mj}^{(+)} - \frac{i(S - L)}{2(L + Kc)(S + Kc)} r'_m A_{mj}^{(-)} \\ &\quad - \frac{r_i \left(\delta_{im} - \frac{q_i q_m}{q^2} \right)}{(L + S)(S + Kc)} \left[\frac{1}{\epsilon_0} e^{-S z_2/c} \delta_{mj} + \Sigma(\omega, K) \delta_{m3} \tilde{D}_{3j}^\omega(0) \right] \\ &\quad + \frac{r'_m}{2(L + Kc)(S - Kc)} \left[\frac{1}{\epsilon_0} e^{-K z_2} \delta_{mj} + \Sigma(\omega, K) \delta_{m3} \tilde{D}_{3j}^\omega(0) \right], \end{aligned} \quad (\text{E.41})$$

where we have used the fact that $r_i r'_i = 2K^2$. Eq. (E.41) is the first of two algebraic equations for the unknowns $r_m A_{mj}^{(+)}$ and $r'_m A_{mj}^{(-)}$.

Next, according to the second condition Eq. (E.37), we have to evaluate $P_{mj}^{(-)}(k_z)$ given by Eq. (E.24) at $k_z = -iK$. According to the discussion preceding Eq. (E.21), the term $-F_{ij}^{(2)}(k_z)$ in Eq. (E.24) is used to cancel the singularity at $k_z = -iK$ in the first term of this equation. Hence, we must take the limit of these two terms together,

$$\begin{aligned}
& \lim_{k_z \rightarrow -iK} \left\{ \frac{(\delta_{im} - \frac{k_i k_m}{k^2})}{(iL - k_z c)(iS + k_z c)} \left[\frac{e^{-ik_z z_2}}{\epsilon_0} \delta_{mj} + \Sigma(\omega, K) \delta_{m3} \tilde{D}_{3j}^\omega(0) \right] - F_{ij}^{(2)}(k_z) \right\} \\
& \quad = -\frac{1}{(L + Kc)(S - Kc)} \left[\frac{1}{\epsilon_0} e^{-Kz_2} \delta_{ij} + \Sigma(\omega, K) \delta_{i3} \tilde{D}_{3j}^\omega(0) \right] \\
& - \frac{\partial}{\partial k_z} \left\{ \frac{k_i k_m}{(iL - k_z c)(iS + k_z c)(k_z - iK)} \left[\frac{1}{\epsilon_0} e^{-ik_z z_2} \delta_{mj} + \Sigma(\omega, K) \delta_{m3} \tilde{D}_{3j}^\omega(0) \right] \right\} \Big|_{k_z = -iK}, \tag{E.42}
\end{aligned}$$

by expanding $(k_z + iK)$ times the first term on the RHS of Eq. (E.24) in a Taylor series about $k_z = -iK$. When the partial derivative in Eq. (E.42) is expanded, it can be written as the sum of a term proportional to δ_{i3} and one proportional to k_i , as in Eq. (E.39). When we multiply both sides of Eq. (E.42) by r'_i and sum over i as in Eq. (E.37), the term proportional to k_i evaluates to zero, since $r'_i k_i|_{k_z = -iK} = r'_i r'_i = 0$ by Eq. (C.13). Hence, Eq. (E.42) gives

$$\begin{aligned}
& \lim_{k_z \rightarrow -iK} r'_i \left\{ \frac{(\delta_{im} - \frac{k_i k_m}{k^2})}{(iL - k_z c)(iS + k_z c)} \left[\frac{e^{-ik_z z_2}}{\epsilon_0} \delta_{mj} + \Sigma(\omega, K) \delta_{m3} \tilde{D}_{3j}^\omega(0) \right] - F_{ij}^{(2)}(k_z) \right\} \\
& \quad = -\frac{r'_m}{(L + Kc)(S - Kc)} \left[\frac{1}{\epsilon_0} e^{-Kz_2} \delta_{mj} + \Sigma(\omega, K) \delta_{m3} \tilde{D}_{3j}^\omega(0) \right] \\
& \quad \quad + \frac{(-iK)r'_m}{(L + Kc)(S - Kc)(-2iK)} \left[\frac{1}{\epsilon_0} e^{-Kz_2} \delta_{mj} + \Sigma(\omega, K) \delta_{m3} \tilde{D}_{3j}^\omega(0) \right] \\
& \quad = -\frac{r'_m}{2(L + Kc)(S - Kc)} \left[\frac{1}{\epsilon_0} e^{-Kz_2} \delta_{mj} + \Sigma(\omega, K) \delta_{m3} \tilde{D}_{3j}^\omega(0) \right]. \tag{E.43}
\end{aligned}$$

Next, according to the discussion preceding Eq. (E.22), the term $-F_{ij}^{(3)}(k_z)$ in Eq. (E.24) is used to cancel the singularity at $k_z = -iK$ in the second term of this equation. Hence, we must take the limit of these two terms together,

$$\begin{aligned}
& \lim_{k_z \rightarrow -iK} \left[-\mathcal{M}_{im}^{(-) -1} A_{mj}^{(-)} - F_{ij}^{(3)}(k_z) \right] = \frac{iA_{ij}^{(-)}}{L + Kc} \\
& \quad + \frac{\partial}{\partial k_z} \left[\frac{i(S - L)k_i k_m A_{mj}^{(-)}}{(iL - k_z c)(iS - k_z c)(k_z - iK)} \right] \Big|_{k_z = -iK}, \tag{E.44}
\end{aligned}$$

by expanding $(k_z + iK)$ times the second term on the RHS of Eq. (E.24) in a Taylor series about $k_z = -iK$. As before, when we multiply both sides of Eq. (E.44) by

r'_i and sum over i , only the term proportional to δ_{i3} in the expansion of the partial derivative in Eq. (E.44) contributes,

$$\begin{aligned} \lim_{k_z \rightarrow -iK} r'_i \left[-\mathcal{M}_{im}^{(-)-1} A_{mj}^{(-)} - F_{ij}^{(3)}(k_z) \right] &= \frac{i r'_m A_{mj}^{(-)}}{L + Kc} - \frac{i(S-L)(-iK) r'_m A_{mj}^{(-)}}{(L+Kc)(S+Kc)(-2iK)} \\ &= i \frac{L+S+2Kc}{2(L+Kc)(S+Kc)} r'_m A_{mj}^{(-)}. \end{aligned} \quad (\text{E.45})$$

The remaining terms $-F_{ij}^{(1)}(k_z)$ and $F_{ij}^{(4)}(k_z)$ in Eq. (E.24) are finite at $k_z = -iK$. Substituting Eqs. (E.43) and (E.45) into Eq. (E.37) and using Eqs. (E.20) and (E.23), we obtain the second condition

$$\begin{aligned} 0 &= -\frac{r'_m}{2(L+Kc)(S-Kc)} \left[\frac{1}{\epsilon_0} e^{-Kz_2} \delta_{mj} + \Sigma(\omega, K) \delta_{m3} \tilde{D}_{3j}^\omega(0) \right] \\ &\quad + i \frac{L+S+2Kc}{2(L+Kc)(S+Kc)} r'_m A_{mj}^{(-)} - \frac{i(S-L)}{2} r'_m A_{mj}^{(+)} \\ &\quad + \frac{r'_i \left(\delta_{im} - \frac{q_i q_m}{q^2} \right)}{(L+S)(S-Kc)} \left[\frac{1}{\epsilon_0} e^{-Sz_2/c} \delta_{mj} + \Sigma(\omega, K) \delta_{m3} \tilde{D}_{3j}^\omega(0) \right]. \end{aligned} \quad (\text{E.46})$$

Eqs. (E.41) and (E.46) are two algebraic equations for the two unknowns $r'_m A_{mj}^{(+)}$ and $r'_m A_{mj}^{(-)}$. The solution can be obtained by applying Cramer's rule,

$$\begin{aligned} r'_m A_{mj}^{(-)} &= \frac{2i}{\Delta_0} \left\{ \frac{L+Kc}{S-L} r'_i + \frac{(S+Kc)(L+Kc)(L+S+2Kc)}{(S-L)^2(S-Kc)} r'_i \right\} \\ &\quad \times \frac{\left(\delta_{im} - \frac{q_i q_m}{q^2} \right)}{L+S} \left[\frac{1}{\epsilon_0} e^{-Sz_2/c} \delta_{mj} + \Sigma(\omega, K) \delta_{m3} \tilde{D}_{3j}^\omega(0) \right] \\ &\quad - \frac{2i(S+Kc)^2}{\Delta_0(S-L)^2(S-Kc)} r'_m \left[\frac{1}{\epsilon_0} e^{-Kz_2} \delta_{mj} + \Sigma(\omega, K) \delta_{m3} \tilde{D}_{3j}^\omega(0) \right], \end{aligned} \quad (\text{E.47})$$

$$\begin{aligned} r'_m A_{mj}^{(+)} &= -\frac{2i}{\Delta_0} \left\{ \frac{1}{(S-L)(S-Kc)} r'_i - \frac{L+S+2Kc}{(S-L)^2(S+Kc)} r'_i \right\} \\ &\quad \times \frac{\left(\delta_{im} - \frac{q_i q_m}{q^2} \right)}{L+S} \left[\frac{1}{\epsilon_0} e^{-Sz_2/c} \delta_{mj} + \Sigma(\omega, K) \delta_{m3} \tilde{D}_{3j}^\omega(0) \right] \\ &\quad - \frac{2i}{\Delta_0(S-L)^2(S-Kc)} r'_m \left[\frac{1}{\epsilon_0} e^{-Kz_2} \delta_{mj} + \Sigma(\omega, K) \delta_{m3} \tilde{D}_{3j}^\omega(0) \right], \end{aligned} \quad (\text{E.48})$$

where

$$\Delta_0 = 1 + \left[\frac{L+S+2Kc}{S-L} \right]^2. \quad (\text{E.49})$$

The solutions Eqs. (E.47) and (E.48) still contain the unknown $\tilde{D}_{3j}^\omega(0)$, which, as pointed out at the beginning of this Appendix, is the Fourier transform of the photon Green function \mathcal{D}_{3j}^ω with respect to $(x_1 - x_2)$ and $(y_1 - y_2)$ *evaluated at* $z_1 = 0$. To solve for $\tilde{D}_{3j}^\omega(0)$, we must substitute Eqs. (E.47) and (E.48) into Eqs. (E.22) and (E.23) and the latter two equations into Eq. (E.30). Then we take the inverse Fourier transform of Eq. (E.30) with respect to k_z to obtain $\tilde{D}_{ij}^\omega(z_1)$ and set $i = 3$ and $z_1 = 0$. This will yield an algebraic equation for the unknown $\tilde{D}_{3j}^\omega(0)$.

The inverse Fourier transform of Eq. (E.30) with respect to k_z is defined by,

$$\tilde{D}_{ij}^\omega(z_1) = \int_{-\infty}^{\infty} \frac{dk_z}{2\pi} e^{ik_z z_1} D_{ij}^{(-)}(k_z). \quad (\text{E.50})$$

When $z_1 < 0$, the contour of integration is closed in the lower half of the k_z -plane. The result is zero, since $D_{ij}^{(-)}(k_z)$ is analytic in $\Sigma^{(-)}$. Hence, we only need to consider the case $z_1 > 0$. In that case, the contour of integration is closed in the upper half plane. We consider each of the terms in Eq. (E.30) separately.

The inverse Fourier transform of the first term $D_{ij}^{(0)\omega}(k_z)$ is $\tilde{D}_{ij}^{(0)\omega}(z_1)$ given by Eq. (E.4). Since we assumed in the above discussion that $z_2 > 0$ and are going to take the limit $z_1 \rightarrow 0$, we should use the formula for $z_1 < z_2$ in Eq. (E.4).

The second term on the RHS of Eq. (E.30) contains the denominator $(\omega^2 - k^2 c^2 + i\epsilon) = (iS + k_z c)(iS - k_z c)$. Hence, there is a pole at $k_z = iS/c$ in the upper half plane due to this denominator, as well as a pole at $k_z = iK$ due to the $\frac{k_i k_x}{k^2}$ term in the numerator. Thus, the inverse Fourier transform of the second term in Eq. (E.30) for $z_1 > 0$ is

$$\int_{-\infty}^{\infty} \frac{dk_z}{2\pi} e^{ik_z z_1} \frac{(\delta_{i3} - \frac{k_i k_x}{k^2})}{\omega^2 - k^2 c^2 + i\epsilon} \Sigma(\omega, K) \tilde{D}_{3j}^\omega(0) = \left[-\frac{1}{2Sc} \left(\delta_{i3} - \frac{q'_i q'_3}{q^2} \right) e^{-S z_1 / c} + \frac{r_i r_3}{2K(S + Kc)(S - Kc)} e^{-K z_1} \right] \Sigma(\omega, K) \tilde{D}_{3j}^\omega(0). \quad (\text{E.51})$$

Eqs. (E.20) to (E.22) show that $F_{ij}^{(1)}(k_z)$ to $F_{ij}^{(3)}(k_z)$ are analytic in the upper half plane. Hence, the terms involving $F_{ij}^{(1)}(k_z)$ to $F_{ij}^{(3)}(k_z)$ on the RHS of Eq. (E.30) have simple poles at $k_z = iS/c$ and $k_z = iK$ in the upper half plane due to the denominator

$(iS - k_z c)$ and the $\frac{k_i k_z}{k^2}$ term in $\mathcal{M}_{im}^{(-)}$. Thus, the inverse Fourier transform of the $F_{ij}^{(1)}(k_z)$ to $F_{ij}^{(3)}(k_z)$ terms in Eq. (E.30) for $z_1 > 0$ is

$$\begin{aligned} & \int_{-\infty}^{\infty} \frac{dk_z}{2\pi} e^{ik_z z_1} \left(\frac{-1}{iS - k_z c} \right) \mathcal{M}_{im}^{(-)} [F_{mj}^{(1)}(k_z) + F_{mj}^{(2)}(k_z) + F_{mj}^{(3)}(k_z)] \\ &= \frac{(S - L)}{c} \left(\delta_{im} - \frac{q'_i q'_m}{q^2} \right) e^{-S z_1 / c} [F_{mj}^{(1)}(iS/c) + F_{mj}^{(2)}(iS/c) + F_{mj}^{(3)}(iS/c)] \\ & \quad - \frac{(S - L)}{2K(S - Kc)} r_i r_m e^{-K z_1} [F_{mj}^{(1)}(iK) + F_{mj}^{(2)}(iK) + F_{mj}^{(3)}(iK)]. \end{aligned} \quad (\text{E.52})$$

Eq. (E.23) shows that $F_{ij}^{(4)}(k_z)$ has a pole at $k_z = iK$ in the upper half plane. Hence, the term involving $F_{ij}^{(4)}(k_z)$ on the RHS of Eq. (E.30) has an additional *double pole* at $k_z = iK$ due to an extra $1/(k_z - iK)$ factor from the $\frac{k_i k_z}{k^2}$ term in $\mathcal{M}_{im}^{(-)}$. Thus, the inverse Fourier transform of the $F_{ij}^{(4)}(k_z)$ term in Eq. (E.30) for $z_1 > 0$ is

$$\begin{aligned} \int_{-\infty}^{\infty} \frac{dk_z}{2\pi} e^{ik_z z_1} \frac{\mathcal{M}_{im}^{(-)} F_{mj}^{(4)}(k_z)}{iS - k_z c} &= -\frac{(S - L)}{c} \left(\delta_{im} - \frac{q'_i q'_m}{q^2} \right) e^{-S z_1 / c} F_{mj}^{(4)}(iS/c) \\ & \quad - \frac{i(L - Kc)(S - L)}{2K(S - Kc)} e^{-K z_1} r_i r_m A_{mj}^{(+)} \\ & \quad + \frac{\partial}{\partial k_z} \left\{ \frac{(S - L)^2 e^{ik_z z_1} k_i k_l}{2K(iS - k_z c)(k_z + iK)} r_l r_m A_{mj}^{(+)} \right\} \Big|_{k_z = iK}. \end{aligned} \quad (\text{E.53})$$

In expanding the partial derivative in Eq. (E.53), only the term involving $\frac{\partial k_l}{\partial k_z} = \delta_{l3}$ contributes, since otherwise the factor $(k_l r_l)|_{k_z = iK} = r_l r_l = 0$. Hence, Eq. (E.53) becomes

$$\begin{aligned} \int_{-\infty}^{\infty} \frac{dk_z}{2\pi} e^{ik_z z_1} \frac{\mathcal{M}_{im}^{(-)} F_{mj}^{(4)}(k_z)}{iS - k_z c} &= -\frac{(S - L)}{c} \left(\delta_{im} - \frac{q'_i q'_m}{q^2} \right) e^{-S z_1 / c} F_{mj}^{(4)}(iS/c) \\ & \quad - \frac{i(L - Kc)(S - L)}{2K(S - Kc)} e^{-K z_1} r_i r_m A_{mj}^{(+)} - \frac{i(S - L)^2}{4K(S - Kc)} e^{-K z_1} r_i r_m A_{mj}^{(+)} \\ &= -\frac{(S - L)}{c} \left(\delta_{im} - \frac{q'_i q'_m}{q^2} \right) e^{-S z_1 / c} F_{mj}^{(4)}(iS/c) \\ & \quad - \frac{i(S + L - 2Kc)(S - L)}{4K(S - Kc)} e^{-K z_1} r_i r_m A_{mj}^{(+)}. \end{aligned} \quad (\text{E.54})$$

The inverse Fourier transform $\tilde{D}_{ij}^{\omega}(z_1)$ of Eq. (E.50) for $z_1 > 0$ is now given by the sum of Eqs. (E.4), (E.51), (E.52) and (E.54). Using Eqs. (E.20) to (E.23), we obtain, for $z_1 > 0$,

$$\begin{aligned}
\tilde{D}_{ij}^\omega(z_1) &= \tilde{D}_{ij}^{(0)\omega}(z_1) - \left[\frac{1}{2Sc} \left(\delta_{i3} - \frac{q'_i q'_3}{q^2} \right) e^{-S z_1/c} + \frac{r_i r_3}{2K \omega^2} e^{-K z_1} \right] \Sigma(\omega, K) \tilde{D}_{3j}^\omega(0) \\
&- \frac{S-L}{2Sc(L+S)} \left(\delta_{il} - \frac{q'_i q'_l}{q^2} \right) \left(\delta_{lm} - \frac{q_l q_m}{q^2} \right) e^{-S z_1/c} \left[\frac{1}{\epsilon_0} e^{-S z_2/c} \delta_{mj} + \Sigma(\omega, K) \delta_{m3} \tilde{D}_{3j}^\omega(0) \right] \\
&- \frac{S-L}{2K(L+Kc)\omega^2} \left(\delta_{il} - \frac{q'_i q'_l}{q^2} \right) r'_i r'_m e^{-S z_1} \left[\frac{1}{\epsilon_0} e^{-K z_2} \delta_{mj} + \Sigma(\omega, K) \delta_{m3} \tilde{D}_{3j}^\omega(0) \right] \\
&- \frac{S-L}{2K(L+S)\omega^2} r_i r_l \left(\delta_{lm} - \frac{q_l q_m}{q^2} \right) e^{-K z_1} \left[\frac{1}{\epsilon_0} e^{-S z_2/c} \delta_{mj} + \Sigma(\omega, K) \delta_{m3} \tilde{D}_{3j}^\omega(0) \right] \\
&- \frac{S-L}{4K(L+Kc)(S-Kc)^2} r_i r'_m e^{-K z_1} \left[\frac{1}{\epsilon_0} e^{-K z_2} \delta_{mj} + \Sigma(\omega, K) \delta_{m3} \tilde{D}_{3j}^\omega(0) \right] \\
&+ \frac{i(S-L)^2}{2K(L+Kc)(S+Kc)^2} \left\{ \frac{S+Kc}{2(S-Kc)} e^{-K z_1} r_i - \left[r'_i - \frac{q'_i K(K + \frac{S}{c})}{q^2} \right] e^{-S z_1/c} \right\} r'_m A_{mj}^{(-)} \\
&- \frac{i(S-L)^2}{2K(S-Kc)} \left\{ \frac{S+L-2Kc}{2(S-L)} e^{-K z_1} r_i + \left[r_i - \frac{q'_i K(K - \frac{S}{c})}{q^2} \right] e^{-S z_1/c} \right\} r_m A_{mj}^{(+)}, \quad (\text{E.55})
\end{aligned}$$

where we have used the fact that $(S+Kc)(S-Kc) = -\omega^2$.

The RHS of Eq. (E.55) still contains the unknown $\tilde{D}_{3j}^\omega(0)$. To obtain an algebraic equation for this unknown, we set $i = 3$ and $z_1 = 0$ on both sides of Eq. (E.55). Since the unknown $\tilde{D}_{3j}^\omega(0)$ appears also in the quantities $r'_m A_{mj}^{(-)}$ and $r_m A_{mj}^{(+)}$ on the RHS of Eq. (E.55), we rewrite the latter quantities by separating out the terms containing $\tilde{D}_{3j}^\omega(0)$,

$$r'_m A_{mj}^{(-)} = a_j^{(-)} + V_1 \tilde{D}_{3j}^\omega(0), \quad (\text{E.56})$$

$$r_m A_{mj}^{(+)} = a_j^{(+)} + W_1 \tilde{D}_{3j}^\omega(0), \quad (\text{E.57})$$

From Eqs. (E.47) and (E.48), we obtain

$$\begin{aligned}
V_1 &= \frac{2i}{\Delta_0} \left\{ \frac{L+Kc}{S-L} r_i + \frac{(S+Kc)(L+Kc)(L+S+2Kc)}{(S-L)^2(S-Kc)} r'_i \right\} \\
&\quad \times \frac{\left(\delta_{i3} - \frac{q_i q_3}{q^2} \right)}{L+S} \Sigma(\omega, K) - \frac{2K(S+Kc)^2}{\Delta_0(S-L)^2(S-Kc)} \Sigma(\omega, K), \quad (\text{E.58})
\end{aligned}$$

$$\begin{aligned}
W_1 &= -\frac{2i}{\Delta_0} \left\{ \frac{1}{(S-L)(S-Kc)} r'_i - \frac{L+S+2Kc}{(S-L)^2(S+Kc)} r_i \right\} \\
&\quad \times \frac{\left(\delta_{i3} - \frac{q_i q_3}{q^2} \right)}{L+S} \Sigma(\omega, K) - \frac{2K}{\Delta_0(S-L)^2(S-Kc)} \Sigma(\omega, K). \quad (\text{E.59})
\end{aligned}$$

Also, $a_j^{(-)}$ and $a_j^{(+)}$ are obtained from Eqs. (E.47) and (E.48), respectively, by setting $\tilde{D}_{3j}^\omega(0)$ in these equations to zero. The resulting quantities can be written in the form

$$\begin{aligned} a_j^{(-)} &= \beta_1 r_i \left(\delta_{ij} - \frac{q_i q_j}{q^2} \right) + \beta_2 r'_i \left(\delta_{ij} - \frac{q_i q_j}{q^2} \right) + \beta_3 r'_j \\ &= \beta_1 \left[r_j - \frac{K(K+S/c)q_j}{q^2} \right] + \beta_2 \left[r'_j - \frac{K(K-S/c)q_j}{q^2} \right] + \beta_3 r'_j, \end{aligned} \quad (\text{E.60})$$

$$\begin{aligned} a_j^{(+)} &= \alpha_1 r'_i \left(\delta_{ij} - \frac{q_i q_j}{q^2} \right) + \alpha_2 r_i \left(\delta_{ij} - \frac{q_i q_j}{q^2} \right) + \alpha_3 r'_j \\ &= \alpha_1 \left[r'_j - \frac{K(K-S/c)q_j}{q^2} \right] + \alpha_2 \left[r_j - \frac{K(K+S/c)q_j}{q^2} \right] + \alpha_3 r'_j, \end{aligned} \quad (\text{E.61})$$

where

$$\beta_1 = \frac{2i(L+Kc)}{\Delta_0(S-L)(L+S)} \frac{1}{\epsilon_0} e^{-S z_2/c}, \quad (\text{E.62})$$

$$\beta_2 = \frac{2i(S+Kc)(L+Kc)(L+S+2Kc)}{\Delta_0(S-L)^2(S-Kc)(L+S)} \frac{1}{\epsilon_0} e^{-S z_2/c}, \quad (\text{E.63})$$

$$\beta_3 = -\frac{2i(S+Kc)^2}{\Delta_0(S-L)^2(S-Kc)} \frac{1}{\epsilon_0} e^{-K z_2} \quad (\text{E.64})$$

$$\alpha_1 = -\frac{2i}{\Delta_0(S-L)(S-Kc)(L+S)} \frac{1}{\epsilon_0} e^{-S z_2/c}, \quad (\text{E.65})$$

$$\alpha_2 = \frac{2i(L+S+2Kc)}{\Delta_0(S-L)^2(S+Kc)(L+S)} \frac{1}{\epsilon_0} e^{-S z_2/c}, \quad (\text{E.66})$$

$$\alpha_3 = -\frac{2i}{\Delta_0(S-L)^2(S-Kc)} \frac{1}{\epsilon_0} e^{-K z_2}. \quad (\text{E.67})$$

Setting $i = 3$ and $z_1 = 0$ on both sides of Eq. (E.55) and using Eqs. (E.56), (E.57), (E.60) and (E.61), we obtain an algebraic equation for $\tilde{D}_{3j}^\omega(0)$,

$$\begin{aligned} \tilde{D}_{3j}^\omega(0) &= \tilde{D}_{3j}^{(0)\omega}(0) - (\sigma_1 W_1 + \sigma_2 V_1 - U_1) \tilde{D}_{3j}^\omega(0) \\ &\quad - \frac{S-L}{2Sc(L+S)} \left(\delta_{3l} - \frac{q'_3 q'_l}{q^2} \right) \left(\delta_{lj} - \frac{q_l q_j}{q^2} \right) \frac{1}{\epsilon_0} e^{-S z_2/c} \\ &\quad - \frac{S-L}{2K(L+Kc)\omega^2} \left(\delta_{3l} - \frac{q'_3 q'_l}{q^2} \right) r'_l r'_j \frac{1}{\epsilon_0} e^{-K z_2} \\ &\quad - \frac{S-L}{2K(L+S)\omega^2} r_3 r_l \left(\delta_{lj} - \frac{q_l q_j}{q^2} \right) \frac{1}{\epsilon_0} e^{-S z_2/c} \\ &\quad - \frac{S-L}{4K(L+Kc)(S-Kc)^2} r_3 r'_j \frac{1}{\epsilon_0} e^{-K z_2} - \sigma_1 a_j^{(+)} - \sigma_2 a_j^{(-)}, \end{aligned} \quad (\text{E.68})$$

where

$$\sigma_1 = -\frac{(S-L)^2}{2(S-Kc)} \left\{ \frac{S+L-2Kc}{2(S-L)} + \left[1 - \frac{S(K-\frac{S}{c})}{q^2c} \right] \right\}, \quad (\text{E.69})$$

$$\sigma_2 = \frac{(S-L)^2}{2(L+Kc)(S+Kc)^2} \left\{ \frac{S+Kc}{2(S-Kc)} + \left[1 + \frac{S(K+\frac{S}{c})}{q^2c} \right] \right\}, \quad (\text{E.70})$$

$$\begin{aligned} U_1 = & -\frac{1}{2Sc} \left(1 + \frac{S^2}{q^2c^2} \right) + \frac{K}{2\omega^2} \\ & -\frac{S-L}{2Sc(L+S)} \left[1 + \frac{2S^2}{q^2c^2} + \frac{S^2(K^2 + \frac{S^2}{c^2})}{q^4c^2} \right] + \frac{(S-L)K}{2(L+Kc)\omega^2} \left[1 + \frac{S(K+\frac{S}{c})}{q^2c} \right] \\ & + \frac{(S-L)K}{2(L+S)\omega^2} \left[1 + \frac{S(K+\frac{S}{c})}{q^2c} \right] - \frac{(S-L)K}{4(L+Kc)(S-Kc)^2}. \end{aligned} \quad (\text{E.71})$$

Expanding out the products in Eq. (E.68), we obtain

$$\begin{aligned} (1 + \sigma_1 W_1 + \sigma_2 V_1 - U_1) \tilde{D}_{3j}^\omega(0) = & \tilde{D}_{3j}^{(0)\omega}(0) \\ & -\frac{S-L}{2Sc(L+S)} \left[\delta_{3j} - \frac{iS(q'_j - q_j)}{q^2c} + \frac{iS(K^2 + \frac{S^2}{c^2})q_j}{q^4c} \right] \frac{1}{\epsilon_0} e^{-Sz_2/c} \\ & + \frac{i(S-L)}{2(L+Kc)\omega^2} \left[1 + \frac{S(K+\frac{S}{c})}{q^2c} \right] r'_j \frac{1}{\epsilon_0} e^{-Kz_2} \\ & -\frac{i(S-L)}{2(L+S)\omega^2} \left[r_j - \frac{K(K+\frac{S}{c})q_j}{q^2} \right] \frac{1}{\epsilon_0} e^{-Sz_2/c} \\ & -\frac{i(S-L)}{4(L+Kc)(S-Kc)^2} r'_j \frac{1}{\epsilon_0} e^{-Kz_2} - \sigma_1 a_j^{(+)} - \sigma_2 a_j^{(-)}. \end{aligned} \quad (\text{E.72})$$

When Eqs. (E.4), (E.60) and (E.61) are substituted into Eq. (E.72) and the fact that $(q'_j - q_j) = (2iS/c)\delta_{3j}$ is used, we obtain the solution $\tilde{D}_{3j}^\omega(0)$ which can be written in the form

$$\tilde{D}_{3j}^\omega(0) = \gamma_1 \delta_{3j} + \gamma_2 r'_j + \gamma_3 r_j + \gamma_4 q_j, \quad (\text{E.73})$$

where

$$\gamma_1 = \frac{1}{\Delta_1} \left[-\frac{1}{2Sc} - \frac{S-L}{2Sc(L+S)} \left(1 + \frac{2S^2}{q^2c^2} \right) \right] \frac{1}{\epsilon_0} e^{-Sz_2/c}, \quad (\text{E.74})$$

$$\begin{aligned} \gamma_2 = & \frac{1}{\Delta_1} \left(\left\{ \frac{i}{2\omega^2} + \frac{i(S-L)}{2(L+Kc)\omega^2} \left[1 + \frac{S(K+\frac{S}{c})}{q^2c} \right] \right. \right. \\ & \left. \left. - \frac{i(S-L)}{4(L+Kc)(S-Kc)^2} \right\} \frac{1}{\epsilon_0} e^{-Kz_2} - \sigma_1(\alpha_1 + \alpha_3) - \sigma_2(\beta_2 + \beta_3) \right), \end{aligned} \quad (\text{E.75})$$

$$\gamma_3 = \frac{1}{\Delta_1} \left[-\frac{i(S-L)}{2(L+S)\omega^2} \frac{1}{\epsilon_0} e^{-S z_2/c} - \sigma_1 \alpha_2 - \sigma_2 \beta_1 \right], \quad (\text{E.76})$$

$$\begin{aligned} \gamma_4 = \frac{1}{\Delta_1} \left\{ \left[-\frac{i}{2q^2 c^2} - \frac{i(S-L)(K^2 + \frac{S^2}{c^2})}{2(L+S)q^4 c^2} + \frac{i(S-L)K(K + \frac{S}{c})}{2(L+S)\omega^2 q^2} \right] \frac{1}{\epsilon_0} e^{-S z_2/c} \right. \\ \left. + \sigma_1 \frac{K}{q^2} \left[\alpha_1 \left(K - \frac{S}{c} \right) + \alpha_2 \left(K + \frac{S}{c} \right) \right] + \sigma_2 \frac{K}{q^2} \left[\beta_1 \left(K + \frac{S}{c} \right) + \beta_2 \left(K - \frac{S}{c} \right) \right] \right\}, \end{aligned} \quad (\text{E.77})$$

and $\Delta_1 = (1 + \sigma_1 W_1 + \sigma_2 V_1 - U_1)$.

This completes our determination of all the unknown parameters in the quantity $\tilde{D}_{ij}^\omega(z_1)$ given by Eq. (E.55). Finally, the photon Green function $\mathcal{D}_{ij}^\omega(\mathbf{r}_1, \mathbf{r}_2)$ is calculated by evaluating the inverse Fourier transform of $\tilde{D}_{ij}^\omega(z_1)$ with respect to k_x and k_y numerically,

$$\mathcal{D}_{ij}^\omega(\mathbf{r}_1, \mathbf{r}_2) = \int \frac{dk_x dk_y}{(2\pi)^2} e^{ik_x(x_1-x_2)+ik_y(y_1-y_2)} \tilde{D}_{ij}^\omega(z_1). \quad (\text{E.78})$$

Appendix F

Derivation of Eq. (2.191)

In this Appendix, the integrals over \mathbf{r} and \mathbf{r}' in Eq. (2.190) are evaluated to give Eq. (2.191). First, we consider an integral of the form

$$I_{ij}(\mathbf{r}_1, \mathbf{r}_2) = \int_{z_3 < 0} d^3 r_3 \left(\frac{\partial^2}{\partial x_{1i} \partial x_{3m}} \frac{1}{|\mathbf{r}_1 - \mathbf{r}_3|} \right) \left(\frac{\partial^2}{\partial x_{3m} \partial x_{2j}} \frac{1}{|\mathbf{r}_3 - \mathbf{r}_2|} \right), \quad (\text{F.1})$$

where $z_2 > 0$. Integrating by parts and using the fact that the Laplacian of $1/r$ is $-4\pi\delta(\mathbf{r})$, we obtain

$$\begin{aligned} I_{ij}(\mathbf{r}_1, \mathbf{r}_2) &= \int d^2 s_3 \left[\left(\frac{\partial}{\partial x_{1i}} \frac{1}{|\mathbf{r}_1 - \mathbf{r}_3|} \right) \left(\frac{\partial^2}{\partial z_3 \partial x_{2j}} \frac{1}{|\mathbf{r}_3 - \mathbf{r}_2|} \right) \right] \Big|_{z_3=0} \\ &\quad + 4\pi \int_{z_3 < 0} d^3 r_3 \left(\frac{\partial}{\partial x_{1i}} \frac{1}{|\mathbf{r}_1 - \mathbf{r}_3|} \right) \frac{\partial}{\partial x_{2j}} \delta(\mathbf{r}_3 - \mathbf{r}_2), \end{aligned} \quad (\text{F.2})$$

where $d^2 s_3 = dx_3 dy_3$. Since $z_3 < 0$ and $z_2 > 0$, the delta function on the second line of Eq. (F.2) does not contribute. Hence,

$$\begin{aligned} I_{ij}(\mathbf{r}_1, \mathbf{r}_2) &= \frac{\partial^2}{\partial x_{1i} \partial x_{2j}} \int d^2 s_3 \left[\frac{1}{|\mathbf{r}_1 - \mathbf{r}_3|} \left(\frac{\partial}{\partial z_3} \frac{1}{|\mathbf{r}_3 - \mathbf{r}_2|} \right) \right] \Big|_{z_3=0} \\ &= \frac{\partial^2}{\partial x_{1i} \partial x_{2j}} \left(-\frac{\partial}{\partial z_2} \int d^2 s_3 \frac{1}{|\mathbf{r}_1 - \mathbf{s}_3|} \frac{1}{|\mathbf{s}_3 - \mathbf{r}_2|} \right), \end{aligned} \quad (\text{F.3})$$

where \mathbf{s}_3 is an integration point on the plane $z = 0$.

We now have to consider the integral

$$\mathcal{I} = \int d^2 s_3 \frac{1}{|\mathbf{r}_1 - \mathbf{s}_3|} \frac{1}{|\mathbf{s}_3 - \mathbf{r}_2|}. \quad (\text{F.4})$$

Using the representation

$$\frac{1}{|\mathbf{r} - \mathbf{r}'|} = \int \frac{d^3 k}{(2\pi)^3} \frac{4\pi}{k^2} e^{i\mathbf{k} \cdot (\mathbf{r} - \mathbf{r}')}, \quad (\text{F.5})$$

Eq. (F.4) becomes

$$\begin{aligned}
\mathcal{I} &= \int \frac{d^3k}{(2\pi)^3} \int \frac{d^3k'}{(2\pi)^3} \int d^2s_3 \frac{(4\pi)^2}{k^2 k'^2} e^{i\mathbf{k}\cdot\mathbf{r}_1 - i\mathbf{k}'\cdot\mathbf{r}_2 - i(\mathbf{k}-\mathbf{k}')\cdot\mathbf{s}_3} \\
&= \int \frac{d^3k}{(2\pi)^3} \int \frac{d^3k'}{(2\pi)^3} \frac{(4\pi)^2}{k^2 k'^2} e^{i\mathbf{k}\cdot\mathbf{r}_1 - i\mathbf{k}'\cdot\mathbf{r}_2} (2\pi)^2 \delta(k_x - k'_x) \delta(k_y - k'_y) \\
&= 8\pi \int \frac{d^3k}{(2\pi)^3} \int dk'_z \frac{e^{ik_z z_1 - ik'_z z_2 + ik_x(x_1 - x_2) + ik_y(y_1 - y_2)}}{k^2(k_x^2 + k_y^2 + k_z'^2)}. \tag{F.6}
\end{aligned}$$

Since $z_2 > 0$, the contour of integration over k'_z may be closed in the lower half-plane, and we obtain a contribution from the pole at $k'_z = -iK$,

$$\mathcal{I} = \int \frac{d^3k}{(2\pi)^3} \frac{8\pi^2}{K k^2} e^{ik_z z_1 - K z_2 + ik_x(x_1 - x_2) + ik_y(y_1 - y_2)}. \tag{F.7}$$

The integral over k_z in Eq. (F.7) can be evaluated by closing the contour in the upper (lower) half-plane for $z_1 > 0$ ($z_1 < 0$),

$$\mathcal{I} = \int \frac{dk_x dk_y}{(2\pi)^2} \frac{4\pi^2}{K^2} e^{-K|z_1| - K z_2 + ik_x(x_1 - x_2) + ik_y(y_1 - y_2)}. \tag{F.8}$$

Thus,

$$\begin{aligned}
-\frac{\partial}{\partial z_2} \mathcal{I} &= \int \frac{dk_x dk_y}{(2\pi)^2} \frac{4\pi^2}{K} e^{-K|z_1| - K z_2 + ik_x(x_1 - x_2) + ik_y(y_1 - y_2)} \\
&= \int \frac{d^3k}{(2\pi)^3} \frac{8\pi^2}{k^2} e^{ik_x(x_1 - x_2) + ik_y(y_1 - y_2) + ik_z(|z_1| + z_2)}, \tag{F.9}
\end{aligned}$$

where we have used the fact that $\int \frac{dk_z}{2\pi} (1/k^2) e^{ik_z z} = e^{-K|z|}/(2K)$ and noting that $(|z_1| + z_2)$ is always positive. Comparing Eq. (F.9) with Eq. (F.5), we see that, when $z_1 > 0$,

$$-\frac{\partial}{\partial z_2} \mathcal{I} = \frac{2\pi}{|\mathbf{r}_1 - \bar{\mathbf{r}}_2|}, \quad z_1 > 0, \tag{F.10}$$

where $\bar{\mathbf{r}}_2$ is the image of \mathbf{r}_2 in the plane $z = 0$. When $z_1 < 0$, we have

$$-\frac{\partial}{\partial z_2} \mathcal{I} = \frac{2\pi}{|\mathbf{r}_1 - \mathbf{r}_2|}, \quad z_1 < 0. \tag{F.11}$$

Substituting Eqs. (F.10) and (F.11) into Eq. (F.3), we obtain, for $z_2 > 0$,

$$I_{ij}(\mathbf{r}_1, \mathbf{r}_2) = \frac{\partial^2}{\partial x_{1i} \partial x_{2j}} \begin{cases} \frac{2\pi}{|\mathbf{r}_1 - \bar{\mathbf{r}}_2|}, & z_1 > 0, \\ \frac{2\pi}{|\mathbf{r}_1 - \mathbf{r}_2|}, & z_1 < 0. \end{cases} \tag{F.12}$$

We are now ready to evaluate the integrals in Eq. (2.190). First, we perform the integration over \mathbf{r}' . The delta function term in $F_{n[j]}(\mathbf{r}' - \mathbf{r}_a)$ given by Eq. (2.24) does not contribute, since $z' < 0$ and $z_a > 0$. Hence, using Eqs. (2.132) and (2.24), we obtain

$$\begin{aligned} \int_{z' < 0} d^3 r' \mathcal{G}_{mn}^{(0)\omega}(\mathbf{r}, \mathbf{r}') F_{n[j]}(\mathbf{r}' - \mathbf{r}_a) &= -\frac{[\epsilon_L(|\omega|) - 1]}{4\pi} \frac{\partial^2}{\partial x_m \partial x_{a[j]}} \left(\frac{1}{|\mathbf{r} - \mathbf{r}_a|} \right) \\ &+ \frac{[\epsilon_L(|\omega|) - 1]^2}{(4\pi)^2 \epsilon_L(|\omega|)} \int_{z' < 0} d^3 r' \left[\frac{\partial^2}{\partial x_m \partial x'_n} \left(\frac{1}{|\mathbf{r} - \mathbf{r}'|} \right) \right. \\ &\left. + \frac{\epsilon_L(|\omega|) - 1}{\epsilon_L(|\omega|) + 1} \frac{\partial^2}{\partial x_m \partial x'_n} \left(\frac{1}{|\mathbf{r} - \tilde{\mathbf{r}}'|} \right) \right] \frac{\partial^2}{\partial x'_n \partial x_{a[j]}} \left(\frac{1}{|\mathbf{r}' - \mathbf{r}_a|} \right). \end{aligned} \quad (\text{F.13})$$

Using Eq. (F.1), Eq. (F.13) may be written as

$$\begin{aligned} \int_{z' < 0} d^3 r' \mathcal{G}_{mn}^{(0)\omega}(\mathbf{r}, \mathbf{r}') F_{n[j]}(\mathbf{r}' - \mathbf{r}_a) &= -\frac{[\epsilon_L(|\omega|) - 1]}{4\pi} \frac{\partial^2}{\partial x_m \partial x_{a[j]}} \left(\frac{1}{|\mathbf{r} - \mathbf{r}_a|} \right) \\ &+ \frac{[\epsilon_L(|\omega|) - 1]^2}{(4\pi)^2 \epsilon_L(|\omega|)} \left[I_{m[j]}(\mathbf{r}, \mathbf{r}_a) + \frac{\epsilon_L(|\omega|) - 1}{\epsilon_L(|\omega|) + 1} \tilde{I}_{m[j]}(\mathbf{r}, \mathbf{r}_a) \right], \end{aligned} \quad (\text{F.14})$$

where \tilde{I}_{ij} is similar to I_{ij} except for a tilde over the first \mathbf{r}_3 variable,

$$\tilde{I}_{ij}(\mathbf{r}_1, \mathbf{r}_2) = \int_{z_3 < 0} d^3 r_3 \left(\frac{\partial^2}{\partial x_{1i} \partial x_{3m}} \frac{1}{|\mathbf{r}_1 - \tilde{\mathbf{r}}_3|} \right) \left(\frac{\partial^2}{\partial x_{3m} \partial x_{2j}} \frac{1}{|\mathbf{r}_3 - \mathbf{r}_2|} \right). \quad (\text{F.15})$$

From the steps leading from Eq. (F.1) to (F.3), it is seen that, when z_3 is set equal to zero in the latter equation, the tilde over the first \mathbf{r}_3 variable has no effect. Hence,

$$\tilde{I}_{ij}(\mathbf{r}_1, \mathbf{r}_2) = I_{ij}(\mathbf{r}_1, \mathbf{r}_2). \quad (\text{F.16})$$

Substituting Eq. (F.16) and Eq. (F.12) for $z_1 < 0$ into Eq. (F.14), we obtain

$$\begin{aligned} \int_{z' < 0} d^3 r' \mathcal{G}_{mn}^{(0)\omega}(\mathbf{r}, \mathbf{r}') F_{n[j]}(\mathbf{r}' - \mathbf{r}_a) &= -\frac{[\epsilon_L(|\omega|) - 1]}{4\pi} \frac{\partial^2}{\partial x_m \partial x_{a[j]}} \left(\frac{1}{|\mathbf{r} - \mathbf{r}_a|} \right) \\ &+ \frac{[\epsilon_L(|\omega|) - 1]^2}{4\pi [\epsilon_L(|\omega|) + 1]} \frac{\partial^2}{\partial x_m \partial x_{a[j]}} \left(\frac{1}{|\mathbf{r} - \mathbf{r}_a|} \right) \\ &= -\frac{[\epsilon_L(|\omega|) - 1]}{2\pi [\epsilon_L(|\omega|) + 1]} \frac{\partial^2}{\partial x_m \partial x_{a[j]}} \left(\frac{1}{|\mathbf{r} - \mathbf{r}_a|} \right). \end{aligned} \quad (\text{F.17})$$

When Eq. (F.17) is multiplied by $F_{[j]m}(\mathbf{r}_a - \mathbf{r})$ and the resulting expression integrated over \mathbf{r} , we see that the delta function term in $F_{[j]m}(\mathbf{r}_a - \mathbf{r})$ again does not

contribute, since $z_a > 0$ and $z < 0$. Hence,

$$\begin{aligned}
& \int_{z < 0} \int_{z' < 0} d^3 r d^3 r' F_{[j]m}(\mathbf{r}_a - \mathbf{r}) \mathcal{G}_{mn}^{(0)\omega_a}(\mathbf{r}, \mathbf{r}') F_{n[j]}(\mathbf{r}' - \mathbf{r}_a) \\
&= - \frac{e^2 [\epsilon_L(|\omega|) - 1]}{8\pi^2 \epsilon_0 [\epsilon_L(|\omega|) + 1]} \Big|_{\omega = \omega_a} \int_{z < 0} d^3 r \left(\frac{\partial^2}{\partial x_{a[j]} \partial x_m} \frac{1}{|\mathbf{r}_a - \mathbf{r}|} \right) \left(\frac{\partial^2}{\partial x_m \partial x_{a[j]}} \frac{1}{|\mathbf{r} - \mathbf{r}_a|} \right) \\
&= - \frac{e^2 [\epsilon_L(\omega_a) - 1]}{8\pi^2 \epsilon_0 [\epsilon_L(\omega_a) + 1]} I_{[j][j]}(\mathbf{r}_a, \mathbf{r}_a). \tag{F.18}
\end{aligned}$$

This time, we have to substitute Eq. (F.12) for $z_1 > 0$ into Eq. (F.18). This leads at once to Eq. (2.191).

Appendix G

Physical-Optics Induced Fields

In this appendix, the complete expressions for the induced tangential fields in the physical-optics approximation are derived.

G.1 Distant-Panel Contributions

Consider first the magnetic vector potential $\mathbf{A}_m(\mathbf{r})$ due to the distant magnetic multipoles. According to Eqs. (3.12) and (3.13), the fields are given in terms of this vector potential by

$$\mathbf{E}(\mathbf{r}) = \nabla \times \mathbf{A}_m, \quad (\text{G.1})$$

$$\mathbf{H}(\mathbf{r}) = -\frac{j}{\omega\mu} \nabla \times \nabla \times \mathbf{A}_m. \quad (\text{G.2})$$

For the contribution due to all the distant *vertical* magnetic multipoles, $\mathbf{A}_m(\mathbf{r}) = \mathbf{A}^{(z)}(\mathbf{r}) = z_1 A^{(z)}(\mathbf{r})$, where $A^{(z)}(\mathbf{r})$ is given by Eq. (3.85). Since the latter equation is expressed in terms of cylindrical polar coordinates (ρ_1, z_1, ϕ_1) of the field point \mathbf{r} , it is convenient to evaluate Eqs. (G.1) and (G.2) in cylindrical polar coordinates and then transform the results into Cartesian components. We only need the tangential (ρ, ϕ) components,

$$E_\rho^{(z)}(\mathbf{r}) = \frac{1}{\rho_1} \frac{\partial A^{(z)}}{\partial \phi_1}, \quad (\text{G.3})$$

$$E_\phi^{(z)}(\mathbf{r}) = -\frac{\partial A^{(z)}}{\partial \rho_1}, \quad (\text{G.4})$$

$$j\omega\mu H_\rho^{(z)}(\mathbf{r}) = \frac{\partial^2 A^{(z)}}{\partial z_1 \partial \rho_1}, \quad (\text{G.5})$$

$$j\omega\mu H_\phi^{(z)}(\mathbf{r}) = \frac{1}{\rho_1} \frac{\partial^2 A^{(z)}}{\partial z_1 \partial \phi_1}. \quad (\text{G.6})$$

The Cartesian components are then obtained from the cylindrical components by

$$E_x^{(z)}(\mathbf{r}) = E_\rho^{(z)} \cos \phi_1 - E_\phi^{(z)} \sin \phi_1, \quad (\text{G.7})$$

$$E_y^{(z)}(\mathbf{r}) = E_\rho^{(z)} \sin \phi_1 + E_\phi^{(z)} \cos \phi_1, \quad (\text{G.8})$$

and similarly for the magnetic field components. Substituting Eq. (3.85) into Eqs. (G.3) and (G.4) and the latter into Eqs. (G.7) and (G.8), we obtain for the total induced tangential electric field on panel p due to distant vertically polarized magnetic multipoles

$$\begin{aligned} E_x^{(z)}(\mathbf{r})|_{z_1=0} &= \int_{\Gamma_a} d\lambda [1 + R_s(\lambda)] j\lambda \int_0^{2\pi} d\beta e^{j\lambda\rho_1 \cos(\beta-\phi_1)} \sin \beta I^{(z)}(\lambda, \beta) \\ &+ \int_{\Gamma_a+\Gamma_c} d\lambda [1 + R_s(\lambda)] j\lambda \sum_{i=1}^n e^{j\lambda\rho_1 \cos(\theta_i-\phi_1)} \sin \theta_i J_1^{(z)}(\lambda, i) \\ &- \int_{\Gamma_a+\Gamma_b} d\lambda [1 + R_s(\lambda)] j\lambda \sum_{i=1}^n e^{-j\lambda\rho_1 \cos(\theta_i-\phi_1)} \sin \theta_i J_2^{(z)}(\lambda, i), \end{aligned} \quad (\text{G.9})$$

$$\begin{aligned} E_y^{(z)}(\mathbf{r})|_{z_1=0} &= - \int_{\Gamma_a} d\lambda [1 + R_s(\lambda)] j\lambda \int_0^{2\pi} d\beta e^{j\lambda\rho_1 \cos(\beta-\phi_1)} \cos \beta I^{(z)}(\lambda, \beta) \\ &- \int_{\Gamma_a+\Gamma_c} d\lambda [1 + R_s(\lambda)] j\lambda \sum_{i=1}^n e^{j\lambda\rho_1 \cos(\theta_i-\phi_1)} \cos \theta_i J_1^{(z)}(\lambda, i) \\ &+ \int_{\Gamma_a+\Gamma_b} d\lambda [1 + R_s(\lambda)] j\lambda \sum_{i=1}^n e^{-j\lambda\rho_1 \cos(\theta_i-\phi_1)} \cos \theta_i J_2^{(z)}(\lambda, i). \end{aligned} \quad (\text{G.10})$$

The corresponding tangential magnetic field on panel p is

$$\begin{aligned} j\omega\mu H_x^{(z)}(\mathbf{r})|_{z_1=0} &= \int_{\Gamma_a} d\lambda [1 - R_s(\lambda)] \lambda \sqrt{k_1^2 - \lambda^2} \int_0^{2\pi} d\beta e^{j\lambda\rho_1 \cos(\beta-\phi_1)} \cos \beta I^{(z)}(\lambda, \beta) \\ &+ \int_{\Gamma_a+\Gamma_c} d\lambda [1 - R_s(\lambda)] \lambda \sqrt{k_1^2 - \lambda^2} \sum_{i=1}^n e^{j\lambda\rho_1 \cos(\theta_i-\phi_1)} \cos \theta_i J_1^{(z)}(\lambda, i) \\ &- \int_{\Gamma_a+\Gamma_b} d\lambda [1 - R_s(\lambda)] \lambda \sqrt{k_1^2 - \lambda^2} \sum_{i=1}^n e^{-j\lambda\rho_1 \cos(\theta_i-\phi_1)} \cos \theta_i J_2^{(z)}(\lambda, i), \end{aligned} \quad (\text{G.11})$$

$$\begin{aligned} j\omega\mu H_y^{(z)}(\mathbf{r})|_{z_1=0} &= \int_{\Gamma_a} d\lambda [1 - R_s(\lambda)] \lambda \sqrt{k_1^2 - \lambda^2} \int_0^{2\pi} d\beta e^{j\lambda\rho_1 \cos(\beta-\phi_1)} \sin \beta I^{(z)}(\lambda, \beta) \\ &+ \int_{\Gamma_a+\Gamma_c} d\lambda [1 - R_s(\lambda)] \lambda \sqrt{k_1^2 - \lambda^2} \sum_{i=1}^n e^{j\lambda\rho_1 \cos(\theta_i-\phi_1)} \sin \theta_i J_1^{(z)}(\lambda, i) \\ &- \int_{\Gamma_a+\Gamma_b} d\lambda [1 - R_s(\lambda)] \lambda \sqrt{k_1^2 - \lambda^2} \sum_{i=1}^n e^{-j\lambda\rho_1 \cos(\theta_i-\phi_1)} \sin \theta_i J_2^{(z)}(\lambda, i). \end{aligned} \quad (\text{G.12})$$

For the contribution due to all the distant *horizontal* magnetic multipoles, $\mathbf{A}_m(\mathbf{r}) = \mathbf{A}^{(\pm)}(\mathbf{r}) = (\mathbf{e}_{\rho_1} \pm j\mathbf{e}_{\phi_1})A_{\text{hor}}^{(\pm)}(\mathbf{r}) \pm jz_1A_{\text{ver}}^{(\pm)}(\mathbf{r})$, where $A_{\text{hor}}^{(\pm)}$ and $A_{\text{ver}}^{(\pm)}$ are given by Eqs. (3.88) and (3.89). Again, we only need the (ρ, ϕ) components. First, we consider the contribution due to the horizontal component $A_{\text{hor}}^{(\pm)}(\mathbf{r})$ of the magnetic vector potential,

$$E_{\text{hor},\rho}^{(\pm)}(\mathbf{r}) = \mp j \frac{\partial A_{\text{hor}}^{(\pm)}}{\partial z_1}, \quad (\text{G.13})$$

$$E_{\text{hor},\phi}^{(\pm)}(\mathbf{r}) = \frac{\partial A_{\text{hor}}^{(\pm)}}{\partial z_1}, \quad (\text{G.14})$$

$$E_{\text{hor},z}^{(\pm)}(\mathbf{r}) = \pm \frac{j}{\rho_1} \frac{\partial}{\partial \rho_1} (\rho_1 A_{\text{hor}}^{(\pm)}) - \frac{1}{\rho_1} \frac{\partial A_{\text{hor}}^{(\pm)}}{\partial \phi_1}, \quad (\text{G.15})$$

$$j\omega\mu H_{\text{hor},\rho}^{(\pm)}(\mathbf{r}) = \pm \frac{j}{\rho_1^2} \frac{\partial}{\partial \rho_1} \left(\rho_1 \frac{\partial A_{\text{hor}}^{(\pm)}}{\partial \phi_1} \right) - \frac{1}{\rho_1^2} \frac{\partial^2 A_{\text{hor}}^{(\pm)}}{\partial \phi_1^2} - \frac{\partial^2 A_{\text{hor}}^{(\pm)}}{\partial z_1^2}, \quad (\text{G.16})$$

$$j\omega\mu H_{\text{hor},\phi}^{(\pm)}(\mathbf{r}) = \mp j \frac{\partial^2 A_{\text{hor}}^{(\pm)}}{\partial z_1^2} \mp j \frac{\partial}{\partial \rho_1} \left[\frac{1}{\rho_1} \frac{\partial}{\partial \rho_1} (\rho_1 A_{\text{hor}}^{(\pm)}) \right] + \frac{\partial}{\partial \rho_1} \left(\frac{1}{\rho_1} \frac{\partial A_{\text{hor}}^{(\pm)}}{\partial \phi_1} \right). \quad (\text{G.17})$$

In deriving Eqs. (G.16) and (G.17), we have used the fact that $A_{\text{hor}}^{(\pm)}(\mathbf{r})e^{\mp j\phi_1}$, rather than $A_{\text{hor}}^{(\pm)}(\mathbf{r})$ itself, satisfies the scalar wave equation. This is because the *Cartesian* components of the vector potential $\mathbf{A}^{(\pm)}(\mathbf{r})$, rather than the cylindrical components, satisfy the scalar wave equation. From Eqs. (3.86) and (3.87), the Cartesian components of $\mathbf{A}^{(\pm)}(\mathbf{r})$ are

$$\mathbf{A}^{(\pm)}(\mathbf{r}) = (\mathbf{x}_1 \pm jy_1)A_{\text{hor}}^{(\pm)}(\mathbf{r})e^{\mp j\phi_1} \pm jz_1A_{\text{ver}}^{(\pm)}(\mathbf{r}). \quad (\text{G.18})$$

$A_{\text{hor}}^{(\pm)}(\mathbf{r})$ itself satisfies a different equation,

$$\frac{1}{\rho_1} \frac{\partial}{\partial \rho_1} \left(\rho_1 \frac{\partial A_{\text{hor}}^{(\pm)}}{\partial \rho_1} \right) + \frac{1}{\rho_1^2} \left(\frac{\partial^2 A_{\text{hor}}^{(\pm)}}{\partial \phi_1^2} \mp 2j \frac{\partial A_{\text{hor}}^{(\pm)}}{\partial \phi_1} - A_{\text{hor}}^{(\pm)} \right) + \frac{\partial^2 A_{\text{hor}}^{(\pm)}}{\partial z_1^2} + k_1^2 A_{\text{hor}}^{(\pm)} = 0. \quad (\text{G.19})$$

Substituting Eq. (3.88) into Eqs. (G.13) and (G.14) and the latter into Eqs. (G.7) and (G.8), we obtain for the contribution to the induced tangential electric field on panel p due to the horizontal component $A_{\text{hor}}^{(\pm)}(\mathbf{r})$ of the magnetic vector potential

$$\begin{aligned}
E_{\text{hor},x}^{(\pm)}(\mathbf{r})\Big|_{z_1=0} &= \mp \int_{\Gamma_a} d\lambda [1 - R_p(\lambda)] \sqrt{k_1^2 - \lambda^2} \int_0^{2\pi} d\beta e^{j\lambda\rho_1 \cos(\beta - \phi_1)} I^{(\pm)}(\lambda, \beta) \\
&\mp \int_{\Gamma_a + \Gamma_c} d\lambda [1 - R_p(\lambda)] \sqrt{k_1^2 - \lambda^2} \sum_{i=1}^n e^{j\lambda\rho_1 \cos(\theta_i - \phi_1)} J_1^{(\pm)}(\lambda, i) \\
&\mp \int_{\Gamma_a + \Gamma_b} d\lambda [1 - R_p(\lambda)] \sqrt{k_1^2 - \lambda^2} \sum_{i=1}^n e^{-j\lambda\rho_1 \cos(\theta_i - \phi_1)} J_2^{(\pm)}(\lambda, i), \quad (\text{G.20})
\end{aligned}$$

$$E_{\text{hor},y}^{(\pm)}(\mathbf{r})\Big|_{z_1=0} = \pm j E_{\text{hor},x}^{(\pm)}(\mathbf{r})\Big|_{z_1=0}. \quad (\text{G.21})$$

The corresponding tangential magnetic field on panel p is

$$\begin{aligned}
j\omega\mu H_{\text{hor},x}^{(\pm)}(\mathbf{r})\Big|_{z_1=0} &= \int_{\Gamma_a} d\lambda [1 + R_p(\lambda)] \int_0^{2\pi} d\beta (k_1^2 - \lambda^2 \cos\beta e^{\pm j\beta}) e^{j\lambda\rho_1 \cos(\beta - \phi_1)} \\
&\times I^{(\pm)}(\lambda, \beta) + \int_{\Gamma_a + \Gamma_c} d\lambda [1 + R_p(\lambda)] \sum_{i=1}^n (k_1^2 - \lambda^2 \cos\theta_i e^{\pm j\theta_i}) e^{j\lambda\rho_1 \cos(\theta_i - \phi_1)} J_1^{(\pm)}(\lambda, i) \\
&+ \int_{\Gamma_a + \Gamma_b} d\lambda [1 + R_p(\lambda)] \sum_{i=1}^n (k_1^2 - \lambda^2 \cos\theta_i e^{\pm j\theta_i}) e^{-j\lambda\rho_1 \cos(\theta_i - \phi_1)} J_2^{(\pm)}(\lambda, i), \quad (\text{G.22})
\end{aligned}$$

$$\begin{aligned}
j\omega\mu H_{\text{hor},y}^{(\pm)}(\mathbf{r})\Big|_{z_1=0} &= \int_{\Gamma_a} d\lambda [1 + R_p(\lambda)] \int_0^{2\pi} d\beta (\pm j k_1^2 - \lambda^2 \sin\beta e^{\pm j\beta}) e^{j\lambda\rho_1 \cos(\beta - \phi_1)} \\
&\times I^{(\pm)}(\lambda, \beta) + \int_{\Gamma_a + \Gamma_c} d\lambda [1 + R_p(\lambda)] \sum_{i=1}^n (\pm j k_1^2 - \lambda^2 \sin\theta_i e^{\pm j\theta_i}) e^{j\lambda\rho_1 \cos(\theta_i - \phi_1)} J_1^{(\pm)}(\lambda, i) \\
&+ \int_{\Gamma_a + \Gamma_b} d\lambda [1 + R_p(\lambda)] \sum_{i=1}^n (\pm j k_1^2 - \lambda^2 \sin\theta_i e^{\pm j\theta_i}) e^{-j\lambda\rho_1 \cos(\theta_i - \phi_1)} J_2^{(\pm)}(\lambda, i). \quad (\text{G.23})
\end{aligned}$$

Next, we consider the contribution due to the vertical component $A_{\text{ver}}^{(\pm)}(\mathbf{r})$ of the magnetic vector potential,

$$E_{\text{ver},\rho}^{(\pm)}(\mathbf{r}) = \pm \frac{j}{\rho_1} \frac{\partial A_{\text{ver}}^{(\pm)}}{\partial \phi_1}, \quad (\text{G.24})$$

$$E_{\text{ver},\phi}^{(\pm)}(\mathbf{r}) = \mp j \frac{\partial A_{\text{ver}}^{(\pm)}}{\partial \rho_1}, \quad (\text{G.25})$$

$$j\omega\mu H_{\text{ver},\rho}^{(\pm)}(\mathbf{r}) = \pm j \frac{\partial^2 A_{\text{ver}}^{(\pm)}}{\partial \rho_1 \partial z_1}, \quad (\text{G.26})$$

$$j\omega\mu H_{\text{ver},\phi}^{(\pm)}(\mathbf{r}) = \pm \frac{j}{\rho_1} \frac{\partial^2 A_{\text{ver}}^{(\pm)}}{\partial \phi_1 \partial z_1}. \quad (\text{G.27})$$

Substituting Eq. (3.89) into Eqs. (G.24) and (G.25) and the latter into Eqs. (G.7) and (G.8), we obtain for the contribution to the induced tangential electric field on

panel p due to the vertical component $A_{\text{ver}}^{(\pm)}(\mathbf{r})$ of the magnetic vector potential

$$\begin{aligned}
E_{\text{ver},x}^{(\pm)}(\mathbf{r})\Big|_{z_1=0} &= j \int_{\Gamma_a} d\lambda S(\lambda) \sqrt{k_1^2 - \lambda^2} \int_0^{2\pi} d\beta e^{j\lambda\rho_1 \cos(\beta-\phi_1)} \sin \beta e^{\pm j\beta} I^{(\pm)}(\lambda, \beta) \\
&\quad + j \int_{\Gamma_a+\Gamma_c} d\lambda S(\lambda) \sqrt{k_1^2 - \lambda^2} \sum_{i=1}^n e^{j\lambda\rho_1 \cos(\theta_i-\phi_1)} \sin \theta_i e^{\pm j\theta_i} J_1^{(\pm)}(\lambda, i) \\
&\quad + j \int_{\Gamma_a+\Gamma_b} d\lambda S(\lambda) \sqrt{k_1^2 - \lambda^2} \sum_{i=1}^n e^{-j\lambda\rho_1 \cos(\theta_i-\phi_1)} \sin \theta_i e^{\pm j\theta_i} J_2^{(\pm)}(\lambda, i), \quad (\text{G.28})
\end{aligned}$$

$$\begin{aligned}
E_{\text{ver},y}^{(\pm)}(\mathbf{r})\Big|_{z_1=0} &= -j \int_{\Gamma_a} d\lambda S(\lambda) \sqrt{k_1^2 - \lambda^2} \int_0^{2\pi} d\beta e^{j\lambda\rho_1 \cos(\beta-\phi_1)} \cos \beta e^{\pm j\beta} I^{(\pm)}(\lambda, \beta) \\
&\quad - j \int_{\Gamma_a+\Gamma_c} d\lambda S(\lambda) \sqrt{k_1^2 - \lambda^2} \sum_{i=1}^n e^{j\lambda\rho_1 \cos(\theta_i-\phi_1)} \cos \theta_i e^{\pm j\theta_i} J_1^{(\pm)}(\lambda, i) \\
&\quad - j \int_{\Gamma_a+\Gamma_b} d\lambda S(\lambda) \sqrt{k_1^2 - \lambda^2} \sum_{i=1}^n e^{-j\lambda\rho_1 \cos(\theta_i-\phi_1)} \cos \theta_i e^{\pm j\theta_i} J_2^{(\pm)}(\lambda, i). \quad (\text{G.29})
\end{aligned}$$

The corresponding tangential magnetic field on panel p is

$$\begin{aligned}
j\omega\mu H_{\text{ver},x}^{(\pm)}(\mathbf{r})\Big|_{z_1=0} &= - \int_{\Gamma_a} d\lambda S(\lambda) (k_1^2 - \lambda^2) \int_0^{2\pi} d\beta e^{j\lambda\rho_1 \cos(\beta-\phi_1)} \cos \beta e^{\pm j\beta} I^{(\pm)}(\lambda, \beta) \\
&\quad - \int_{\Gamma_a+\Gamma_c} d\lambda S(\lambda) (k_1^2 - \lambda^2) \sum_{i=1}^n e^{j\lambda\rho_1 \cos(\theta_i-\phi_1)} \cos \theta_i e^{\pm j\theta_i} J_1^{(\pm)}(\lambda, i) \\
&\quad - \int_{\Gamma_a+\Gamma_b} d\lambda S(\lambda) (k_1^2 - \lambda^2) \sum_{i=1}^n e^{-j\lambda\rho_1 \cos(\theta_i-\phi_1)} \cos \theta_i e^{\pm j\theta_i} J_2^{(\pm)}(\lambda, i), \quad (\text{G.30})
\end{aligned}$$

$$\begin{aligned}
j\omega\mu H_{\text{ver},y}^{(\pm)}(\mathbf{r})\Big|_{z_1=0} &= - \int_{\Gamma_a} d\lambda S(\lambda) (k_1^2 - \lambda^2) \int_0^{2\pi} d\beta e^{j\lambda\rho_1 \cos(\beta-\phi_1)} \sin \beta e^{\pm j\beta} I^{(\pm)}(\lambda, \beta) \\
&\quad - \int_{\Gamma_a+\Gamma_c} d\lambda S(\lambda) (k_1^2 - \lambda^2) \sum_{i=1}^n e^{j\lambda\rho_1 \cos(\theta_i-\phi_1)} \sin \theta_i e^{\pm j\theta_i} J_1^{(\pm)}(\lambda, i) \\
&\quad - \int_{\Gamma_a+\Gamma_b} d\lambda S(\lambda) (k_1^2 - \lambda^2) \sum_{i=1}^n e^{-j\lambda\rho_1 \cos(\theta_i-\phi_1)} \sin \theta_i e^{\pm j\theta_i} J_2^{(\pm)}(\lambda, i). \quad (\text{G.31})
\end{aligned}$$

We have now given the complete expressions for the tangential field components on panel p induced by all the distant *magnetic* multipoles of arbitrary polarization. The corresponding expressions for the distant *electric* multipoles can be obtained by duality. According to Eqs. (3.12) and (3.13), the fields are given in terms of the electric vector potential $\mathbf{A}_e(\mathbf{r})$ by

$$\mathbf{E}(\mathbf{r}) = \frac{j}{\omega\epsilon_1} \nabla \times \nabla \times \mathbf{A}_e, \quad (\text{G.32})$$

$$\mathbf{H}(\mathbf{r}) = \nabla \times \mathbf{A}_e. \quad (\text{G.33})$$

Comparing Eqs. (G.32) and (G.33) with Eqs. (G.1) and (G.2), we see that the new field expressions can be obtained from the old field expressions given in the above paragraphs by: (i) replacing \mathbf{A}_m by \mathbf{A}_e , (ii) replacing μ by ϵ_1 , (iii) replacing the old \mathbf{E} by \mathbf{H} , and (iv) replacing the old \mathbf{H} by $-\mathbf{E}$. Furthermore, step (i) amounts to replacing the magnetic multipole coefficients a_{lm}^q by the electric multipole coefficients b_{lm}^q in Eqs. (3.80) to (3.82) and corresponding expressions for $J_1^{(\pm)}(\lambda, i)$, $J_2^{(\pm)}(\lambda, i)$ and $I^{(\pm)}(\lambda, \beta)$.

G.2 Neighboring-Panel Contributions

The expressions for the tangential fields on panel p induced by each *neighboring* surface element dS' are derived from the vector potentials given in Eqs. (3.39), (3.40), (3.44) and (3.45). Here, there is no advantage to transforming from cylindrical coordinates (ρ_2, ϕ_2, z_2) centered at the neighboring dipole, in the coordinate system shown in Fig. 3.3, to cylindrical coordinates (ρ_1, ϕ_1, z_1) centered at the field panel p . Thus, the tangential fields contributed by *each* neighboring surface element are expressed in the coordinates (ρ_2, ϕ_2, z_2) centered at *that* element. The final results can be obtained from those given above for the distant-panel contributions by making the following changes:

1. Change (ρ_1, ϕ_1) to (ρ_2, ϕ_2) on the RHS of the above field expressions, namely, Eqs. (G.9) to (G.12), (G.20) to (G.23) and (G.28) to (G.31). Also, change the subscript $z_1 = 0$ on the LHS of these expressions to $z_2 = -d$.
2. Set θ_i on the RHS of the above field expressions equal to $\phi_2 (= \phi_1)$. Then, omit the summation over the index i in the resulting field expressions.
3. Replace $I^{(z)}(\lambda, \beta)$, $J_1^{(z)}(\lambda, i)$ and $J_2^{(z)}(\lambda, i)$ in the above field expressions by the quantities $I_{\text{near}}^{(z)}(\lambda)$, $J_{\text{near},1}^{(z)}(\lambda)$ and $J_{\text{near},2}^{(z)}(\lambda)$, respectively,

$$J_{\text{near},1}^{(z)}(\lambda) = \sqrt{\frac{1}{2\pi\lambda\rho_2}} e^{-j\frac{\pi}{4} + j\sqrt{k_1^2 - \lambda^2}d} (a_{00})_z f_{0,0}(\lambda), \quad (\text{G.34})$$

$$J_{\text{near},2}^{(z)}(\lambda) = \sqrt{\frac{1}{2\pi\lambda\rho_2}} e^{j\frac{\pi}{4} + j\sqrt{k_1^2 - \lambda^2}d} (a_{00})_z f_{0,0}(\lambda), \quad (\text{G.35})$$

$$I_{\text{near}}^{(z)}(\lambda) = \frac{1}{2\pi} e^{j\sqrt{k_1^2 - \lambda^2}d} (a_{00})_z f_{0,0}(\lambda), \quad (\text{G.36})$$

where $\mathbf{a}_{00} = -jk_1(\mathbf{n}' \times \mathbf{E}') \frac{dS'}{4\pi}$ [or $-jk_1(\mathbf{n}' \times \mathbf{H}') \frac{dS'}{4\pi}$], for tangential fields ($\mathbf{n}' \times \mathbf{E}'$) [or ($\mathbf{n}' \times \mathbf{H}'$)] existing on the source element dS' .

4. Change the paths of integration on the RHS of the field expressions given in the last section as follows:

$$\int_{\Gamma_a} \rightarrow \int_0^{\lambda_{\text{near}}}, \quad (\text{G.37})$$

$$\int_{\Gamma_a + \Gamma_c} \text{ and } \int_{\Gamma_a + \Gamma_b} \rightarrow \int_{\lambda_{\text{near}}}^{\lambda_{\text{max}}}. \quad (\text{G.38})$$

Here, λ_{near} is determined by the requirement that the asymptotic approximation

$$\frac{1}{2\pi} \int_0^{2\pi} d\beta e^{j\lambda\rho_2 \cos(\beta - \phi_2)} \approx \sqrt{\frac{1}{2\pi\lambda\rho_2}} \left[e^{j(\lambda\rho_2 - \frac{\pi}{4})} + e^{-j(\lambda\rho_2 - \frac{\pi}{4})} \right] \quad (\text{G.39})$$

be valid for $\lambda > \lambda_{\text{near}}$. This is the case when $\lambda_{\text{near}}\rho_2 \gg 1$. In practice, a value of $\lambda_{\text{near}} \approx 10/\rho_2$ was found to be adequate. Also, the upper limit λ_{max} of the λ integral on the RHS of Eq. (G.38) is chosen so that the factor $e^{j\sqrt{k_1^2 - \lambda^2}d} \rightarrow e^{-\lambda d}$ in Eqs. (G.34) to (G.36) becomes small enough to guarantee convergence of the integral. Now, from the discussion at the end of Section 3.5, there is a minimum $d = d_{\text{min}}$ for interacting pairs of neighboring elements, where d_{min} is determined by the discretization of the surface S_j . In the photolithography simulation problems we have studied, $k_1 d_{\text{min}} \geq 0.15$. In such case, a value of $\lambda_{\text{max}} = 40k_1$, for which $e^{-\lambda_{\text{max}}d_{\text{min}}} = e^{-40 \times 0.15} = 2.5 \times 10^{-3}$, was found to be adequate.

Appendix H

Rotation Matrices

In this appendix, the numerical evaluation of the matrix elements $\mathcal{D}_{mm'}^{(l)}(\alpha, \beta, \gamma)$ of the irreducible representations of the rotation group is discussed. The theory of group representations was developed by Wigner [41] in connection with the symmetry properties of atomic wave functions under coordinate rotations. A concise but rather advanced treatment of the theory is given in the monograph by Edmonds [40], whose notation is used in the following discussion.

The matrix elements $\mathcal{D}_{mm'}^{(l)}(\alpha, \beta, \gamma)$ relate the spherical harmonics $Y_{lm}(\theta, \phi)$ in one coordinate system K to the spherical harmonics $Y_{lm}(\theta', \phi')$ in another coordinate system K' obtained by rotating the axes of K through the Euler angles (α, β, γ) , as defined in Fig. H.1. Using the defining relationship between the spherical harmonics and associated Legendre polynomials,

$$Y_{lm}(\theta, \phi) = (-1)^m \sqrt{\frac{2l+1}{4\pi} \frac{(l-m)!}{(l+m)!}} P_l^m(\cos \theta) e^{jm\phi}, \quad (\text{H.1})$$

we can write the transformation of the latter polynomials under coordinate rotation as

$$P_l^m(\cos \theta) e^{jm\phi} = \sum_{m'=-l}^l (-1)^{m'-m} P_l^{m'}(\cos \theta') e^{jm'\phi'} \mathcal{D}_{m'm}^{(l)}(\alpha, \beta, \gamma) \sqrt{\frac{(l-m')!(l+m)!}{(l+m')!(l-m)!}}. \quad (\text{H.2})$$

Substituting Eq. (H.2) into Eq. (3.47), we obtain

$$\begin{aligned}
\Delta \mathbf{A}_m^q(\mathbf{r}) &\approx \sum_{l=0}^L \sum_{m=-l}^l \mathbf{a}_{lm}^q h_l^{(1)}(k_1 r) P_l^m(\cos \theta) e^{jm\phi} \\
&= \sum_{l=0}^L \sum_{m=-l}^l \tilde{\mathbf{a}}_{lm}^q h_l^{(1)}(k_1 r') P_l^m(\cos \theta') e^{jm\phi'} , \tag{H.3}
\end{aligned}$$

where $\tilde{\mathbf{a}}_{lm}^q$ is given by Eq. (3.71) and we have used the fact that $r' = r$ under coordinate rotation.

The matrix $\mathcal{D}_{mm'}^{(l)}(\alpha, \beta, \gamma)$, which represents the successive rotations by the Euler angles α, β and γ with respect to the z, y and z axes, respectively, of a coordinate system *carried along by the rotations*, is equal to the product of the matrices representing the individual rotations written in the order from right to left. In the usual convention, the matrix representing a rotation by an angle Θ about the z axis is just $e^{jm\Theta}$ times the unit matrix. Hence,

$$\mathcal{D}_{mm'}^{(l)}(\alpha, \beta, \gamma) = e^{jm\gamma} d_{mm'}^{(l)}(\beta) e^{jm'\alpha} , \tag{H.4}$$

where $d_{mm'}^{(l)}(\beta)$ is the matrix representing a rotation by angle β about the y axis. A closed-form expression exists for computing the latter matrix elements [40],

$$\begin{aligned}
d_{mm'}^{(l)}(\beta) &= \sqrt{\frac{(l+m)!(l-m)!}{(l+m')!(l-m')!}} \sum_{\sigma} (-1)^{l-m-\sigma} \begin{pmatrix} l+m' \\ l-m-\sigma \end{pmatrix} \begin{pmatrix} l-m' \\ \sigma \end{pmatrix} \\
&\quad \times \left(\cos \frac{\beta}{2} \right)^{2\sigma+m+m'} \left(\sin \frac{\beta}{2} \right)^{2l-2\sigma-m-m'} . \tag{H.5}
\end{aligned}$$

Instead of computing $d_{mm'}^{(l)}(\beta)$ for the different values of β encountered in a problem, it is sufficient to compute this quantity for $\beta = \frac{\pi}{2}$ only. This is because the result for a general value of β can be expressed in terms of the result for $\beta = \frac{\pi}{2}$ by means of a similarity transformation. Indeed, a rotation of the axes of a coordinate system by β about the y axis is equivalent to the following sequence of five successive rotations: (1) rotation about the z axis by $\frac{\pi}{2}$, (2) rotation about the new y axis by $\frac{\pi}{2}$, (3) rotation about the new z axis by β , (4) rotation about the new y axis by $-\frac{\pi}{2}$, and (5) rotation about the new z axis by $-\frac{\pi}{2}$. Multiplication of the corresponding

matrices written in the order from right to left then gives

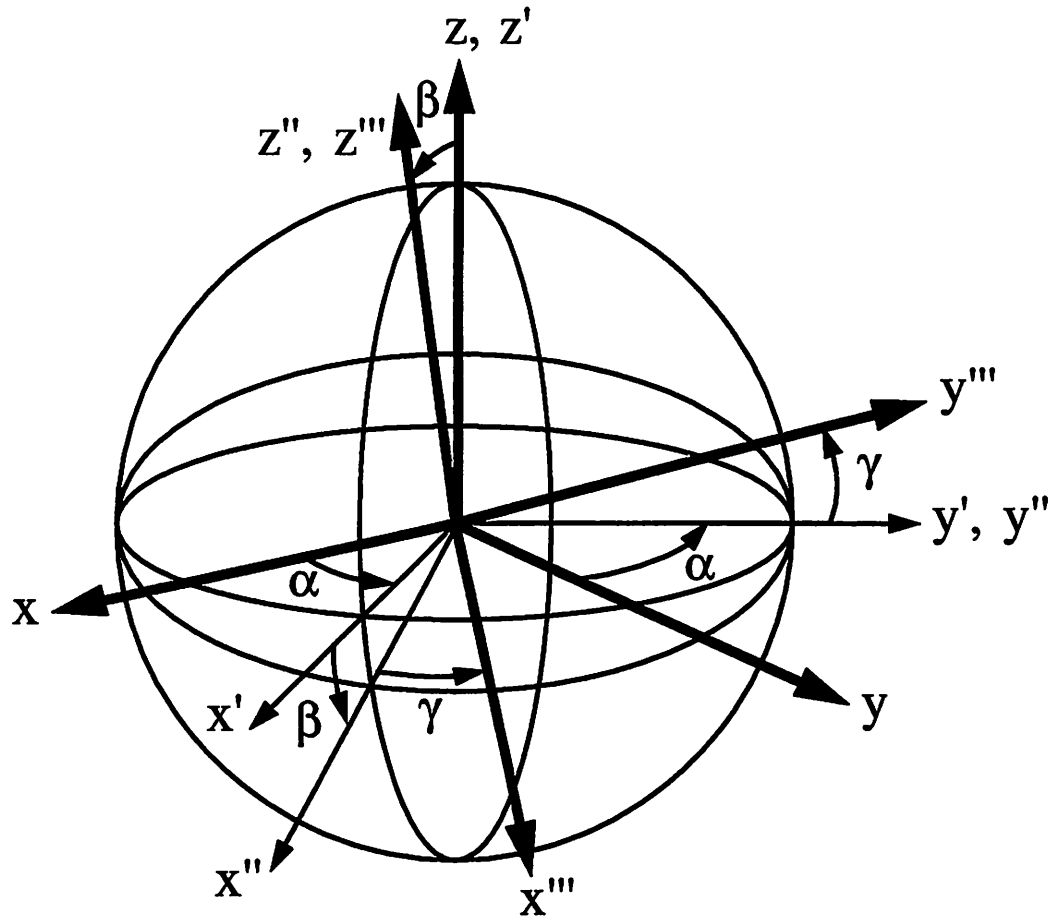
$$d_{mm'}^{(l)}(\beta) = \sum_{m''} e^{-jm''\frac{\pi}{2}} \Delta_{m''m}^{(l)} e^{jm''\beta} \Delta_{m''m'}^{(l)} e^{jm'\frac{\pi}{2}}, \quad (\text{H.6})$$

where $\Delta_{m''m'}^{(l)} = d_{m''m'}^{(l)}(\frac{\pi}{2})$ and we have used the fact that $d_{m'm}^{(l)}(-\beta) = d_{mm'}^{(l)}(\beta)$. Thus, we only need to compute the quantities $\Delta_{m''m}^{(l)}$ and then use Eq. (H.6) to compute $d_{mm'}^{(l)}(\beta)$ for general values of β .

The quantities $\Delta_{m''m}^{(l)}$ may be computed directly by using Eq. (H.5) specialized to $\beta = \frac{\pi}{2}$, or recursively by means of a recurrence relationship for $d_{m''m}^{(l)}(\beta)$. Edmonds [40] gave such a recurrence relationship which, however, is incorrect. This can be seen by setting $j = \frac{1}{2}$ in his Eq. (4.4.1) and showing that the resulting matrix elements disagree with those given in his Eq. (4.1.13), taking into account $d_{00}^{(0)}(\beta) = 1$. Instead, the correct recurrence relationship is

$$\begin{aligned} d_{m'm}^{(l)}(\beta) = & \frac{1}{2j} \left(\cos \frac{\beta}{2} \right) (-1)^{2l-m'-m} \left[d_{-m'-\frac{1}{2}, -m-\frac{1}{2}}^{(l-\frac{1}{2})}(\beta) \sqrt{(l-m')(l-m)} \right. \\ & \left. + d_{-m'+\frac{1}{2}, -m+\frac{1}{2}}^{(l-\frac{1}{2})}(\beta) \sqrt{(l+m')(l+m)} \right] \\ & + \frac{1}{2j} \left(\sin \frac{\beta}{2} \right) (-1)^{m'-m} \left[d_{-m'-\frac{1}{2}, -m+\frac{1}{2}}^{(l-\frac{1}{2})}(\beta) \sqrt{(l-m')(l+m)} \right. \\ & \left. - d_{-m'+\frac{1}{2}, -m-\frac{1}{2}}^{(l-\frac{1}{2})}(\beta) \sqrt{(l+m')(l-m)} \right]. \quad (\text{H.7}) \end{aligned}$$

Eq. (H.7) gives the matrix elements $d_{m'm}^{(l)}(\beta)$ of the l -th representation in terms of those of the $(l - \frac{1}{2})$ -th representation. Thus, starting with the $l = 0$ representation, $d_{00}^{(0)}(\beta) = 1$, we can compute the matrix elements of all the higher dimensional representations $d_{m'm}^{(l)}(\beta)$ by repeated use of Eq. (H.7).



- 1) A rotation α about the z -axis brings the frame of axes S into S' .
- 2) A rotation β about the y' -axis brings the frame of axes S' into S'' .
- 3) A rotation γ about the z'' -axis brings the frame of axes S'' into S''' .

Figure H.1: Euler angles

Appendix I

Translation Coefficients

In this appendix, the computation of the coefficients $a(\mu, m|p, \nu, n)$ used in the translation addition theorem Eq. (4.15) is discussed. These coefficients are defined through a reduction formula for the product of two rotation matrices of the type $\mathcal{D}_{m'm}^{(l)}(\alpha, \beta, \gamma)$. Specifically, $\mathcal{D}_{m'm}^{(l)}(\alpha, \beta, \gamma)$ is the matrix element of the rotation operator $\hat{D}(\alpha, \beta, \gamma)$ between angular momentum eigenstates $|lm\rangle$ and $|lm'\rangle$ [40],

$$\mathcal{D}_{m'm}^{(l)}(\alpha, \beta, \gamma) = \langle lm' | \hat{D}(\alpha, \beta, \gamma) | lm \rangle, \quad (\text{I.1})$$

while the product of two such quantities *with the same Euler angles* is the matrix element of the rotation operator between *product* eigenstates $|l_1 m_1\rangle |l_2 m_2\rangle$ and $|l_1 m'_1\rangle |l_2 m'_2\rangle$,

$$\mathcal{D}_{m'_1 m_1}^{(l_1)}(\alpha, \beta, \gamma) \mathcal{D}_{m'_2 m_2}^{(l_2)}(\alpha, \beta, \gamma) = \langle l_1 m'_1 | \langle l_2 m'_2 | \hat{D}(\alpha, \beta, \gamma) | l_1 m_1 \rangle | l_2 m_2 \rangle. \quad (\text{I.2})$$

From the theory of the coupling of angular momenta, we have the following reduction formula for the product of two angular momentum eigenstates,

$$|l_1 m_1\rangle |l_2 m_2\rangle = \sum_l (l_1 l_2 l, m_1 + m_2 | l_1 m_1 l_2 m_2) |l, m_1 + m_2\rangle, \quad (\text{I.3})$$

where $(l_1 l_2 l, m_1 + m_2 | l_1 m_1 l_2 m_2)$ are the Clebsch-Gordon coefficients, which are related to the Wigner 3- j symbols $\begin{pmatrix} l_1 & l_2 & l \\ m_1 & m_2 & m \end{pmatrix}$ by

$$(l_1 l_2 l, m_1 + m_2 | l_1 m_1 l_2 m_2) = (-1)^{l_1 - l_2 + m_1 + m_2} \sqrt{2l + 1} \begin{pmatrix} l_1 & l_2 & l \\ m_1 & m_2 & -m_1 - m_2 \end{pmatrix}. \quad (\text{I.4})$$

The summation in Eq. (I.3) ranges from $l = |l_1 - l_2|$ to $l = l_1 + l_2$. Substituting Eq. (I.3) into Eq. (I.2) and using the orthonormality property of the angular momentum eigenstates, we obtain

$$\begin{aligned} \mathcal{D}_{m'_1 m_1}^{(l_1)}(\alpha, \beta, \gamma) \mathcal{D}_{m'_2 m_2}^{(l_2)}(\alpha, \beta, \gamma) &= \sum_l (-1)^{-m'_1 - m'_2 + m_1 + m_2} \mathcal{D}_{m'_1 + m'_2, m_1 + m_2}^{(l)}(\alpha, \beta, \gamma) \\ &\times (2l + 1) \begin{pmatrix} l_1 & l_2 & l \\ m'_1 & m'_2 & -m'_1 - m'_2 \end{pmatrix} \begin{pmatrix} l_1 & l_2 & l \\ m_1 & m_2 & -m_1 - m_2 \end{pmatrix}. \end{aligned} \quad (\text{I.5})$$

Setting $m'_1 = m'_2 = 0$ in Eq. (I.5) and using the fact that

$$\mathcal{D}_{0m}^{(l)}(\alpha, \beta, \gamma) = (-1)^m \sqrt{\frac{(l-m)!}{(l+m)!}} P_l^m(\beta) e^{jm\gamma}, \quad (\text{I.6})$$

we obtain the following reduction formula for the product of two associated Legendre polynomials,

$$\begin{aligned} P_{l_1}^{m_1}(\beta) P_{l_2}^{m_2}(\beta) &= \sum_l (-1)^{m_1 + m_2} (2l + 1) \sqrt{\frac{(l_1 + m_1)!(l_2 + m_2)!(l - m_1 - m_2)!}{(l_1 - m_1)!(l_2 - m_2)!(l + m_1 + m_2)!}} \\ &\times \begin{pmatrix} l_1 & l_2 & l \\ 0 & 0 & 0 \end{pmatrix} \begin{pmatrix} l_1 & l_2 & l \\ m_1 & m_2 & -m_1 - m_2 \end{pmatrix} P_l^{m_1 + m_2}(\beta). \end{aligned} \quad (\text{I.7})$$

Comparing Eq. (I.7) with Eq. (4.16), we obtained the desired result for the coefficients $a(\mu, m|p, \nu, n)$ in terms of Wigner 3- j symbols,

$$\begin{aligned} a(\mu, m|p, \nu, n) &= (-1)^{m+\mu} (2p + 1) \sqrt{\frac{(n+m)!(\nu+\mu)!(p-m-\mu)!}{(n-m)!(\nu-\mu)!(p+m+\mu)!}} \\ &\times \begin{pmatrix} n & \nu & p \\ 0 & 0 & 0 \end{pmatrix} \begin{pmatrix} n & \nu & p \\ m & \mu & -m-\mu \end{pmatrix}. \end{aligned} \quad (\text{I.8})$$

Direct computation of the coefficients $a(\mu, m|p, \nu, n)$ using Eq. (I.8) is cumbersome owing to the fact that the Wigner 3- j symbols needed in this expression are quite difficult to compute. Instead, it is more efficient to compute these coefficients by recurrence relationships. Furthermore, it is desirable to have a recurrence relationship in which only one of the indices in $a(\mu, m|p, \nu, n)$ changes. Since in FMM the summation over p in Eq. (4.16) is to be computed in advance, it is convenient that only the index p cycles in the desired recurrence relationship. Cruzan [52] listed a number of recurrence relationships for the $a(\mu, m|p, \nu, n)$ s. However, these recurrence

relationships all involve the simultaneous cycling of two or more indices. Bruning and Lo [53] later succeeded in reducing the recurrence relationships of Cruzan, by a tedious process of algebraic elimination, to a *pair* of three-term recurrence relationships in the two indices ν and p . However, one of their equations contains a sign error. Hence, it is appropriate for us to list the correct recurrence relationships here:

$$\begin{aligned}
0 = & (2p+1)(2p-3)(\nu-\mu+1)[(m-\mu)p(p-1) - m_3(n-\nu)(n+\nu+1)] \\
& \times a(\mu, m|p-1, \nu+1, n) \\
& + (2p+1)(p-m_3-1)(-n+\nu+p-1)(n+\nu+p)[\mu(p-\nu-1) - m(\nu+1)] \\
& \times a(\mu, m|p-2, \nu, n) \\
& + (2p-3)(p+m_3)(n+\nu-p+1)(n-\nu+p)[\mu(p+\nu) + m(\nu+1)] \\
& \times a(\mu, m|p, \nu, n), \quad (I.9)
\end{aligned}$$

$$\begin{aligned}
0 = & (2p+1)(2p-3)(\nu+\mu)[(m-\mu)p(p-1) - m_3(n-\nu)(n+\nu+1)] \\
& \times a(\mu, m|p-1, \nu-1, n) \\
& + (2p+1)(p-m_3-1)(n+\nu-p+2)(n-\nu+p-1)[\mu(p+\nu) + m\nu] \\
& \times a(\mu, m|p-2, \nu, n) \\
& + (2p-3)(p+m_3)(n+\nu+p+1)(-n+\nu+p)[\mu(p-\nu-1) - m\nu] \\
& \times a(\mu, m|p, \nu, n), \quad (I.10)
\end{aligned}$$

where $m_3 = m + \mu$. Eqs. (I.9) and (I.10) can be further reduced to a single three-term recurrence relationship in the index p alone. To start the calculations, it is necessary to know the values of $a(\mu, m|p, \nu, n)$ for $p = n + \nu$ and $p = n + \nu - 2$. These starting values can be found in [53]. Again, one of their formulas is in error and so we give here the correct starting values of the coefficients:

$$a_{n+\nu} = \frac{(2n-1)!!(2\nu-1)!!}{(2n+2\nu-1)!!} \frac{(n+\nu-m_3)!}{(n-m)!(\nu-\mu)!}, \quad (I.11)$$

$$\begin{aligned}
a_{n+\nu-2} = & \frac{(2n+2\nu-3)}{(2n-1)(2\nu-1)(n+\nu-m_3)(n+\nu-m_3-1)} \{(n+\nu-1) \\
& \times [n\nu + m\mu(2n+2\nu-1)] - m_3[\nu m(2\nu-1) + n\mu(2n-1)]\} a_{n+\nu}, \quad (I.12)
\end{aligned}$$

where $a_q = a(\mu, m|q, \nu, n)$.

For translation along the $\pm z$ -axis, Eq. (4.21), we only need the $a(\mu, m|p, \nu, n)$ s for $\mu = -m$. In this case, Eqs. (I.9) and (I.10) can be readily combined to give a single three-term recurrence relationship [54]:

$$\alpha_{p-3}a_{p-4} - (\alpha_{p-2} + \alpha_{p-1} - 4m^2)a_{p-2} + \alpha_p a_p = 0, \quad (\text{I.13})$$

where $a_q = a(-m, m|q, \nu, n)$ and

$$\alpha_p = \frac{[(n + \nu + 1)^2 - p^2][p^2 - (n - \nu)^2]}{4p^2 - 1}. \quad (\text{I.14})$$

The starting values are

$$a_{n+\nu} = \frac{(2n-1)!!(2\nu-1)!!}{(2n+2\nu-1)!!} \frac{(n+\nu)!}{(n-m)!(\nu+m)!}, \quad (\text{I.15})$$

$$a_{n+\nu-2} = \frac{(2n+2\nu-3)}{(2n-1)(2\nu-1)(n+\nu)} [\nu n - m^2(2n+2\nu-1)] a_{n+\nu}. \quad (\text{I.16})$$

Appendix J

Fields of the Multipole Waves

In this appendix, complete expressions for the electric and magnetic fields due to the distant and neighboring panels are given.

J.1 Distant-Panel Contributions

The local expansion for the electric vector potential in a panel p due to all the distant panels is given by the sum over the distant-panel index q of Eq. (4.17). Consider the (l, m) th term of this local expansion which has the form

$$\mathbf{A}_e(\mathbf{r}) = c_{lm} j_l^{(1)}(kr) P_l^m(\cos \theta) e^{jm\phi}, \quad (\text{J.1})$$

where for simplicity we have written (r, θ, ϕ) instead of (r_1, θ_1, ϕ_1) for the spherical polar coordinates in the *local* system K_p . It is convenient to resolve the polarization vector c_{lm} in Eq. (J.1) into a vertical component and two circularly polarized components in the horizontal plane,

$$c_{lm} = c_{lm,z} \mathbf{z} + c_{lm}^{(+)} (\mathbf{x} + j\mathbf{y}) + c_{lm}^{(-)} (\mathbf{x} - j\mathbf{y}), \quad (\text{J.2})$$

where (x, y, z) , rather than (x_1, y_1, z_1) , are the Cartesian coordinates in the local system K_p , and

$$c_{lm}^{(\pm)} = \frac{1}{2} [c_{lm,x} \mp j c_{lm,y}]. \quad (\text{J.3})$$

Although in MFIE we only need to compute the magnetic field, both the magnetic and electric fields would be needed in a combined-field-integral-equation (CFIE)

formulation for dielectric bodies. For completeness, therefore, we give below the expressions for both the magnetic and electric fields. We refer to the modes associated with the *electric* vector potential as the *TM* modes. The fields of these modes are given by

$$\mathbf{H}(\mathbf{r}) = \nabla \times \mathbf{A}_e, \quad (\text{J.4})$$

$$\mathbf{E}(\mathbf{r}) = \frac{j}{\omega\epsilon} \nabla \times \nabla \times \mathbf{A}_e, \quad (\text{J.5})$$

where ϵ is the permittivity of the medium outside the perfectly conducting body.

J.1.1 Vertically Polarized *TM* Mode

The electric vector potential for this mode is

$$\mathbf{A}_e^{(z)}(\mathbf{r}) = \mathbf{z}\Psi(r, \theta, \phi), \quad (\text{J.6})$$

where

$$\Psi(r, \theta, \phi) = j_l^{(1)}(kr)P_l^m(\cos\theta)e^{jm\phi}. \quad (\text{J.7})$$

The fields of this mode were derived by Chang [38]. We include them here for completeness. First, we express the unit vector \mathbf{z} in terms of the spherical unit vectors \mathbf{e}_r and \mathbf{e}_θ ,

$$\mathbf{z} = \mathbf{e}_r \cos\theta - \mathbf{e}_\theta \sin\theta. \quad (\text{J.8})$$

Then we substitute Eq. (J.6) into Eqs. (J.4) and (J.5) to obtain the spherical polar components of the fields:

$$H_r^{(z)} = \frac{jm}{r} \Psi, \quad (\text{J.9})$$

$$H_\theta^{(z)} = \frac{jm}{r} \left(\frac{\cos\theta}{\sin\theta} \right) \Psi, \quad (\text{J.10})$$

$$H_\phi^{(z)} = \sin\theta \left(-\frac{\partial}{\partial r} + \frac{\cos\theta}{r} \frac{\partial}{\partial \cos\theta} \right) \Psi, \quad (\text{J.11})$$

$$-j\omega\epsilon E_r^{(z)} = \cos\theta \left[-\frac{2}{r} \frac{\partial}{\partial r} + \frac{l(l+1)}{r^2} \right] \Psi + \sin^2\theta \left(\frac{1}{r} \frac{\partial}{\partial r} - \frac{1}{r^2} \right) \frac{\partial \Psi}{\partial \cos\theta}, \quad (\text{J.12})$$

$$-j\omega\epsilon E_\theta^{(z)} = \sin\theta \left[-k^2 + \frac{l(l+1)}{r^2} - \frac{1}{r} \frac{\partial}{\partial r} \right] \Psi - \frac{m^2}{r^2 \sin\theta} \Psi - \frac{\cos\theta \sin\theta}{r} \frac{\partial^2 \Psi}{\partial r \partial \cos\theta}, \quad (\text{J.13})$$

$$-j\omega\epsilon E_\phi^{(z)} = \frac{jm}{r} \left(\frac{\cos\theta}{\sin\theta} \right) \frac{\partial \Psi}{\partial r} + \frac{jm}{r^2} \sin\theta \frac{\partial \Psi}{\partial \cos\theta}. \quad (\text{J.14})$$

The tangential field components can be computed from the above spherical components by taking the vector dot product of each of two tangential unit vectors $\mathbf{e}_\mu, \mu = 1, 2$, with the above magnetic or electric field.

J.1.2 Horizontally Polarized *TM* Modes

The electric vector potential for these modes are

$$\begin{aligned} \mathbf{A}_e^{(\pm)}(\mathbf{r}) &= (\mathbf{x} \pm jy)\Psi(r, \theta, \phi) \\ &= (\mathbf{e}_\rho \pm j\mathbf{e}_\phi)\Phi(r, \theta, \phi), \end{aligned} \quad (\text{J.15})$$

where

$$\Phi(r, \theta, \phi) = e^{\pm j\phi} \Psi(r, \theta, \phi), \quad (\text{J.16})$$

and \mathbf{e}_ρ and \mathbf{e}_ϕ are cylindrical unit vectors in the local system K_p . Eq. (J.15) is similar to the horizontally rotating, or *RTM*, modes introduced by Chang and Mei [12],

$$\mathbf{A}_{(\pm m)}^{RTM}(\mathbf{r}) = (\mathbf{x} \pm jy)h_{m-1}^{(1)}(kr)P_{m-1}^{m-1}(\cos\theta)e^{\pm j(m-1)\phi}. \quad (\text{J.17})$$

The fields derived from these *RTM* vector potentials turn out to be exactly the same as the well-known spherical vector wave functions [55] with $l = m$, up to a factor $k/[(2m-1)m]$. The latter wave functions are derived from the vector potential

$$\mathbf{A}_{ml}^{(r)}(\mathbf{r}) = r h_l^{(1)}(kr) P_l^m(\cos\theta) e^{jm\phi}, \quad (\text{J.18})$$

where \mathbf{r} is the radius vector from the origin of K_p to the field point \mathbf{r} . This is because the vector potentials Eqs. (J.17) and (J.18) are in fact related by a gauge transformation, up to a factor $k/[(2m-1)m]$:

$$\mathbf{A}_{(m)}^{RTM}(\mathbf{r}) - \frac{k}{(2m-1)m} \mathbf{A}_{mm}^{(r)}(\mathbf{r}) = \frac{1}{m} \nabla \left[r \sin\theta h_{m-1}^{(1)}(kr) P_{m-1}^{m-1}(\cos\theta) e^{jm\phi} \right], \quad (\text{J.19})$$

as can be verified by direct calculation. It is a well-known fact that the electric and magnetic fields are invariant under a gauge transformation.

For general values of l and m , the field expressions derived from the vector potential $\mathbf{A}_e^{(\pm)}(\mathbf{r})$ given by Eq. (J.15) differ from the spherical vector wave functions. First, we express the cylindrical unit vectors \mathbf{e}_ρ and \mathbf{e}_ϕ in terms of the spherical unit vectors \mathbf{e}_r , \mathbf{e}_θ and \mathbf{e}_ϕ ,

$$\mathbf{e}_\rho \pm j\mathbf{e}_\phi = \mathbf{e}_r \sin \theta + \mathbf{e}_\theta \cos \theta \pm j\mathbf{e}_\phi, \quad (\text{J.20})$$

Then, we substitute Eq. (J.15) into Eqs. (J.4) and (J.5) to obtain the spherical polar components of the fields:

$$H_r^{(\pm)} = \mp \frac{j \sin \theta}{r} \frac{\partial \Phi}{\partial \cos \theta} - \frac{j m}{r} \left(\frac{\cos \theta}{\sin \theta} \right) \Phi, \quad (\text{J.21})$$

$$H_\theta^{(\pm)} = \left(\mp j \frac{\partial}{\partial r} + \frac{j m}{r} \right) \Phi, \quad (\text{J.22})$$

$$H_\phi^{(\pm)} = \left(\cos \theta \frac{\partial}{\partial r} + \frac{\sin^2 \theta}{r} \frac{\partial}{\partial \cos \theta} \right) \Phi, \quad (\text{J.23})$$

$$\begin{aligned} -j\omega\epsilon E_r^{(\pm)} &= \frac{\sin \theta}{r^2} \left[\cos \theta \frac{\partial}{\partial \cos \theta} \pm \frac{m}{\sin^2 \theta} + l(l+1) \right] \Phi \\ &\quad + \frac{\sin \theta}{r} \left(\mp \frac{m}{\sin^2 \theta} - 2 - \cos \theta \frac{\partial}{\partial \cos \theta} \right) \frac{\partial \Phi}{\partial r}, \end{aligned} \quad (\text{J.24})$$

$$\begin{aligned} -j\omega\epsilon E_\theta^{(\pm)} &= \frac{1}{r^2} \left\{ \pm(m \pm 1) \frac{\partial}{\partial \cos \theta} + \frac{m(m \pm 1) \cos \theta}{\sin^2 \theta} + [k^2 r^2 - l(l+1)] \cos \theta \right\} \Phi \\ &\quad + \frac{1}{r} \left(\cos \theta - \sin^2 \theta \frac{\partial}{\partial \cos \theta} \right) \frac{\partial \Phi}{\partial r}, \end{aligned} \quad (\text{J.25})$$

$$\begin{aligned} -j\omega\epsilon E_\phi^{(\pm)} &= \frac{1}{r^2} \left[\pm j k^2 r^2 \mp \frac{j m(m \pm 1)}{\sin^2 \theta} - j(m \pm 1) \cos \theta \frac{\partial}{\partial \cos \theta} \right] \Phi + \frac{j(m \pm 1)}{r} \frac{\partial \Phi}{\partial r}. \end{aligned} \quad (\text{J.26})$$

Again, the tangential field components can be computed from the above spherical components by taking the vector dot product of each of two tangential unit vectors \mathbf{e}_μ , $\mu = 1, 2$, with the above magnetic or electric field.

We have now given the complete expressions for the fields of the *TM* modes associated with the *electric* vector potentials. Corresponding expressions for the *TE*

modes associated with the *magnetic* vector potentials can be obtained from Eqs. (J.9) to (J.14) and Eqs. (J.21) to (J.26) by duality: (i) replace ϵ by μ , (ii) replace the old \mathbf{E} by $-\mathbf{H}$, and (iii) replace the old \mathbf{H} by \mathbf{E} .

J.2 Neighboring-Panel Contributions

For sources in the neighboring panels, the multipole approximation cannot be used. Instead, the contributions from such sources must be computed individually. The magnetic field scattered from a neighboring surface element $\delta S''$ centered at \mathbf{r}'' to the field point at \mathbf{r} is obtained from the second term on the RHS of Eq. (4.7) by restricting the integration to the surface element $\delta S''$,

$$\begin{aligned}\delta\mathbf{H}(\mathbf{r}) &= \nabla \times \int_{\delta S''} \mathbf{J}(\mathbf{r}') \frac{e^{jk|\mathbf{r}-\mathbf{r}'|}}{4\pi|\mathbf{r}-\mathbf{r}'|} dS' \\ &= \int_{\delta S''} \mathbf{J}(\mathbf{r}') \times \nabla' \psi \frac{dS'}{4\pi},\end{aligned}\quad (\text{J.27})$$

where we have used the fact that $\nabla = -\nabla'$ when acting on $\psi = \frac{e^{jk|\mathbf{r}-\mathbf{r}'|}}{|\mathbf{r}-\mathbf{r}'|}$. When $|\mathbf{r}-\mathbf{r}'|$ is large, the rectangular rule may be used for the integration in Eq. (J.27),

$$\delta\mathbf{H}(\mathbf{r}) \approx \mathbf{J}(\mathbf{r}'') \times (\nabla' \psi)|_{\mathbf{r}'=\mathbf{r}''} \frac{\delta S''}{4\pi}.\quad (\text{J.28})$$

When $|\mathbf{r}-\mathbf{r}'|$ is small, however, $\nabla' \psi$ is nearly singular and the rectangular rule is inaccurate. In that case, four-point or higher-order Gaussian quadrature rule must be used. In all the examples discussed in Chapter 4, we used four-point Gaussian quadrature when $|\mathbf{r}-\mathbf{r}'|$ is less than approximately twice the linear dimension of a typical surface element $\delta S''$.

J.2.1 Gaussian Quadrature

The examples we tested all used quadrilateral, planar surface elements. Consider a typical element $\delta S''$ lying on the $x'-y'$ plane of a local coordinate system. The coordinates of its four corners are (x_i, y_i) , $i = 1$ to 4, numbered clockwise. It may be considered as the result of an *isoparametric* mapping from a *master* element in a ξ - η

plane, as shown in Fig. J.1. This mapping is described mathematically by

$$x'(\xi, \eta) = \sum_{i=1}^4 x_i N_i^e(\xi, \eta), \quad (\text{J.29})$$

$$y'(\xi, \eta) = \sum_{i=1}^4 y_i N_i^e(\xi, \eta), \quad (\text{J.30})$$

where $N_i^e(\xi, \eta)$ are the finite-element interpolation functions for a four-node linear element,

$$N_1^e(\xi, \eta) = \frac{1}{4}(1 - \xi)(1 - \eta), \quad (\text{J.31})$$

$$N_2^e(\xi, \eta) = \frac{1}{4}(1 - \xi)(1 + \eta), \quad (\text{J.32})$$

$$N_3^e(\xi, \eta) = \frac{1}{4}(1 + \xi)(1 + \eta), \quad (\text{J.33})$$

$$N_4^e(\xi, \eta) = \frac{1}{4}(1 + \xi)(1 - \eta). \quad (\text{J.34})$$

The four-point Gaussian quadrature rule provides us with four integration points (ξ_i, η_i) , $i = 1$ to 4, and the associated weights w_i . An integral of some function $F(x', y')$ over the element $\delta S''$ in the $x'-y'$ plane is then approximated by a summation over the four Gauss points (ξ_i, η_i) within the master element, weighed by the weights w_i and the Jacobian of the mapping,

$$\int_{\delta S''} F(x', y') dx' dy' \approx \sum_{i=1}^4 F[x'(\xi_i, \eta_i), y'(\xi_i, \eta_i)] w_i \left. \frac{\partial(x', y')}{\partial(\xi, \eta)} \right|_{\xi_i, \eta_i}, \quad (\text{J.35})$$

where $\partial(x', y')/\partial(\xi, \eta)$ is the Jacobian,

$$\frac{\partial(x', y')}{\partial(\xi, \eta)} = \det \begin{bmatrix} \frac{\partial x'}{\partial \xi} & \frac{\partial y'}{\partial \xi} \\ \frac{\partial x'}{\partial \eta} & \frac{\partial y'}{\partial \eta} \end{bmatrix}. \quad (\text{J.36})$$

Substituting Eqs. (J.29) to (J.34) into Eq. (J.36), we obtain

$$\frac{\partial(x', y')}{\partial(\xi, \eta)} = \frac{1}{16}[(D + F\xi)(A + E\eta) - (B + E\xi)(C + F\eta)], \quad (\text{J.37})$$

where

$$A = -x_1 - x_2 + x_3 + x_4, \quad (\text{J.38})$$

$$B = -x_1 + x_2 + x_3 - x_4, \quad (\text{J.39})$$

$$C = -y_1 - y_2 + y_3 + y_4, \quad (\text{J.40})$$

$$D = -y_1 + y_2 + y_3 - y_4, \quad (\text{J.41})$$

$$E = x_1 - x_2 + x_3 - x_4, \quad (\text{J.42})$$

$$F = y_1 - y_2 + y_3 - y_4. \quad (\text{J.43})$$

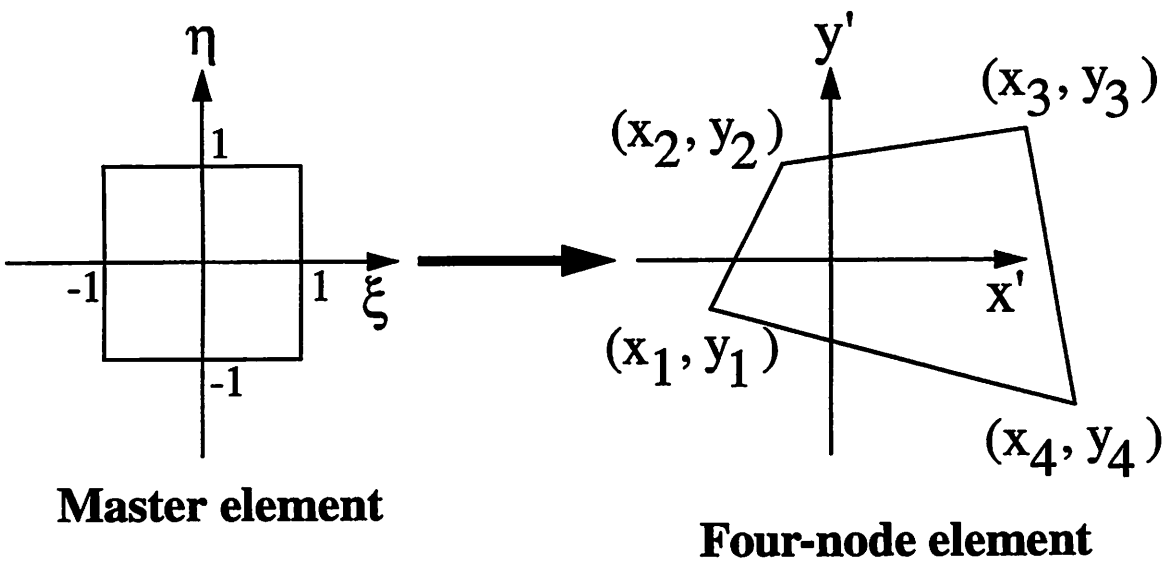


Figure J.1: Isoparametric mapping.

Appendix K

Integration over Singularities

In this appendix, the evaluation of the quantity $\mathbf{n} \times \mathbf{H}_{S_0}(\mathbf{r}_0)$ on the RHS of Eq. (4.60) is discussed. Substituting Eq. (4.56) into Eq. (4.55) and setting $\mathbf{r} = \mathbf{r}_0$, we obtain

$$\begin{aligned} \mathbf{n} \times \mathbf{H}_{S_0}(\mathbf{r}_0) &= (1 + \Gamma) \frac{1}{4\pi} \mathbf{n} \times \int_{S_0} \left[j\omega\epsilon(\mathbf{n}' \times \mathbf{E}^{(0)})\psi + \frac{j}{\omega\mu}(\mathbf{n}' \times \mathbf{E}^{(0)}) \cdot \nabla'(\nabla'\psi) \right] dS' \\ &\quad - (1 - \Gamma) \frac{1}{4\pi} \mathbf{n} \times \int_{S_0} (\mathbf{n}' \times \mathbf{H}^{(0)}) \times \nabla'\psi dS', \end{aligned} \quad (\text{K.1})$$

where $\psi = \frac{e^{jk|\mathbf{r}_0 - \mathbf{r}'|}}{|\mathbf{r}_0 - \mathbf{r}'|}$. We first consider the term depending on $\mathbf{H}^{(0)}$ on the RHS of Eq. (K.1). This has the same form as the second term on the RHS of Eq. (4.1). From the discussion leading to Eq. (4.3), we conclude that, since S_0 is planar, each element of area dS' on S_0 contributes an amount proportional to the solid angle $d\Omega'$ subtended by that area element at the center \mathbf{r}_0 of S_0 . Since S_0 is planar, $d\Omega'$ is zero when dS' does not contain \mathbf{r}_0 and $d\Omega' = 2\pi$ when dS' does contain \mathbf{r}_0 . Hence, following the discussion leading to Eq. (4.4), the term depending on $\mathbf{H}^{(0)}$ on the RHS of Eq. (K.1) evaluates to:

$$\begin{aligned} \mathbf{I}_1 &= -(1 - \Gamma) \frac{1}{4\pi} \mathbf{n} \times \int_{S_0} (\mathbf{n}' \times \mathbf{H}^{(0)}) \times \nabla'\psi dS' \\ &= \frac{1}{2}(1 - \Gamma) \mathbf{n} \times \mathbf{H}^{(0)}(\mathbf{r}_0) \\ &= -\mathbf{x} \frac{1}{2}(1 - \Gamma) H_z^{(0)}(0), \end{aligned} \quad (\text{K.2})$$

where we have used the fact that $\mathbf{n} = -\mathbf{y}$ on S_0 , in the coordinate system shown in Fig. 4.7.

Next, we consider the first term depending on $\mathbf{E}^{(0)}$ on the RHS of Eq. (K.1). Since S_0 is planar, $\mathbf{n}' = \mathbf{n} = -\mathbf{y}$. Also, from Eq. (4.59), $\mathbf{E}^{(0)}$ has only an x component. Hence, $\mathbf{n} \times [\mathbf{n}' \times \mathbf{E}^{(0)}] = -\mathbf{x}E_x^{(0)}(z')$. Hence, the first term on the RHS of Eq. (K.1) is

$$\begin{aligned} \mathbf{I}_2 &= (1 + \Gamma) \frac{1}{4\pi} \mathbf{n} \times \int_{S_0} j\omega\epsilon(\mathbf{n}' \times \mathbf{E}^{(0)})\psi dS' \\ &= -\mathbf{x}(1 + \Gamma) \frac{1}{4\pi} \int_{S_0} j\omega\epsilon E_x^{(0)}(z')\psi dS'. \end{aligned} \quad (\text{K.3})$$

The integral over S_0 in Eq. (K.3) must be evaluated numerically. The rectangular cross section S_0 lying on the x - z plane is divided into a number of rectangular area elements. For area elements *not* containing the center \mathbf{r}_0 of S_0 , the rectangular rule is used to compute the contributions of these area elements to \mathbf{I}_2 . As for the area element $\Delta x \Delta z$ containing \mathbf{r}_0 , the integral of ψ over this area element is computed by using the Fourier expansion of ψ :

$$\begin{aligned} \frac{e^{jk|\mathbf{r}_0 - \mathbf{r}'|}}{|\mathbf{r}_0 - \mathbf{r}'|} \Big|_{y_0 - y' = 0^+} &= 4\pi \int \frac{d^3q}{(2\pi)^3} \frac{e^{j\mathbf{q} \cdot (\mathbf{r}_0 - \mathbf{r}')}}{q^2 - k^2 - i\epsilon} \\ &= \frac{j}{2\pi} \int_{-\infty}^{\infty} \int_{-\infty}^{\infty} dq_x dq_z \frac{e^{jq_x(x_0 - x') + jq_z(z_0 - z')}}{\sqrt{k^2 - q_x^2 - q_z^2}}, \end{aligned} \quad (\text{K.4})$$

where the second line is obtained from the first by performing the integral over q_y using the technique of contour integration. The integral of ψ over the area element $\Delta x \Delta z$ containing \mathbf{r}_0 can then be computed:

$$\begin{aligned} &\int_{x_0 - \Delta x/2}^{x_0 + \Delta x/2} dx' \int_{z_0 - \Delta z/2}^{z_0 + \Delta z/2} dz' \frac{e^{jk|\mathbf{r}_0 - \mathbf{r}'|}}{|\mathbf{r}_0 - \mathbf{r}'|} \Big|_{y_0 - y' = 0^+} \\ &= \frac{2j}{\pi} \int_{-\infty}^{\infty} \int_{-\infty}^{\infty} \frac{dq_x dq_z}{\sqrt{k^2 - q_x^2 - q_z^2}} \frac{\sin\left(\frac{q_x \Delta x}{2}\right)}{q_x} \frac{\sin\left(\frac{q_z \Delta z}{2}\right)}{q_z} \\ &= \frac{j\Delta x \Delta z}{2\pi} \int_0^{2\pi} d\phi \int_0^{\infty} \frac{q dq}{\sqrt{k^2 - q^2}} \text{sinc}\left(\frac{q\Delta x}{2} \cos\phi\right) \text{sinc}\left(\frac{q\Delta z}{2} \sin\phi\right), \end{aligned} \quad (\text{K.5})$$

where $\text{sinc } x = \sin x/x$. The integrand in Eq. (K.5) is still singular at $q^2 = k^2$. This singularity can be avoided by changing the variable of integration from q to ν :

$$\nu = -j\sqrt{k^2 - q^2}, \quad \text{Re } \nu \geq 0. \quad (\text{K.6})$$

In the complex ν -plane, there is no longer any singularity at $q^2 = k^2$, since

$$\frac{q dq}{\sqrt{k^2 - q^2}} = -j d\nu. \quad (\text{K.7})$$

The integrals over ϕ and q in Eq. (K.5) can then be performed using the rectangular rule by substituting Eq. (K.7) into the integrand in Eq. (K.5). The upper limit of the q -integration must, of course, be approximated by some finite value.

Lastly, we consider the second term depending on $\mathbf{E}^{(0)}$ on the RHS of Eq. (K.1),

$$\begin{aligned} \mathbf{I}_3 &= (1 + \Gamma) \frac{1}{4\pi} \mathbf{n} \times \int_{S_0} \frac{j}{\omega\mu} (\mathbf{n}' \times \mathbf{E}^{(0)}) \cdot \nabla' (\nabla' \psi) dS' \\ &= (1 + \Gamma) \frac{1}{4\pi} \frac{j}{\omega\mu} \mathbf{n} \times \int_{S_0} \mathbf{n}' \cdot (\mathbf{E}^{(0)} \times \nabla') (\nabla' \psi) dS'. \end{aligned} \quad (\text{K.8})$$

Consider the j th component of the integral over S_0 ,

$$\begin{aligned} \int_{S_0} \mathbf{n}' \cdot (\mathbf{E}^{(0)} \times \nabla') \frac{\partial \psi}{\partial x'_j} dS' &= - \int_{S_0} \mathbf{n}' \cdot \left[\nabla' \times \left(\mathbf{E}^{(0)} \frac{\partial \psi}{\partial x'_j} \right) \right] dS' \\ &\quad + \int_{S_0} [\mathbf{n}' \cdot (\nabla' \times \mathbf{E}^{(0)})] \frac{\partial \psi}{\partial x'_j} dS' \\ &= \int_{\Gamma_0} \left(\mathbf{E}^{(0)} \frac{\partial \psi}{\partial x'_j} \right) \cdot d\mathbf{l} + \int_{S_0} \mathbf{n}' \cdot (j\omega\mu \mathbf{H}^{(0)}) \frac{\partial \psi}{\partial x'_j} dS', \end{aligned} \quad (\text{K.9})$$

where Γ_0 is the boundary of the surface S_0 and $d\mathbf{l}$ is the line element along this boundary. The direction of $d\mathbf{l}$ is taken to be counterclockwise when the surface S_0 is viewed *from* the side facing the horn. Now, since S_0 is bounded by the perfectly conducting walls of the waveguide, the quantity $\mathbf{E}^{(0)} \cdot d\mathbf{l}$ in the integrand of the first term on the RHS of Eq. (K.9) is proportional to the component of the electric field $\mathbf{E}^{(0)}$ of the TE_{10} mode *tangential* to the perfectly conducting walls, which must be zero. Hence, the first term on the RHS of Eq. (K.9) is zero. Substituting the resulting Eq. (K.9) into Eq. (K.8), we obtain

$$\mathbf{I}_3 = -(1 + \Gamma) \frac{1}{4\pi} \mathbf{n} \times \int_{S_0} (\mathbf{n}' \cdot \mathbf{H}^{(0)}) \nabla' \psi dS'. \quad (\text{K.10})$$

Using the fact that $\mathbf{n} = \mathbf{n}' = -\mathbf{y}$ on S_0 , Eq. (K.10) becomes

$$\mathbf{I}_3 = -(1 + \Gamma) \frac{1}{4\pi} \int_{S_0} H_y^{(0)}(z') \left(\mathbf{x} \frac{\partial \psi}{\partial z'} - \mathbf{z} \frac{\partial \psi}{\partial x'} \right) dS'. \quad (\text{K.11})$$

Examination of Eq. (4.57) shows that $H_y^{(0)}(-z') = -H_y^{(0)}(z')$. Hence, $H_y^{(0)}(z')$ is an odd function of z' . Also, since ψ is evaluated at the center \mathbf{r}_0 of S_0 , which coincides with the origin of the coordinate system shown in Fig. 4.7, $\partial\psi/\partial z'$ is an odd function

of z' while $\partial\psi/\partial x'$ is an even function of z' . Hence, the second term in the integrand of Eq. (K.11), which is a product of an odd and an even function of z' , integrates to zero, and we are left with

$$\begin{aligned}
\mathbf{I}_3 &= -\mathbf{x}(1 + \Gamma) \frac{1}{4\pi} \int_{S_0} H_y^{(0)}(z') \frac{\partial\psi}{\partial z'} dS' \\
&= -\mathbf{x}(1 + \Gamma) \frac{1}{4\pi} \int_{S_0} \left\{ \frac{\partial}{\partial z'} [H_y^{(0)}(z')\psi] - \psi \frac{\partial H_y^{(0)}(z')}{\partial z'} \right\} dS' \\
&= -\mathbf{x}(1 + \Gamma) \frac{1}{4\pi} \left\{ \int_{\Gamma_0} [H_y^{(0)}(z')\psi] dl_x - \int_{S_0} \psi \frac{\partial H_y^{(0)}(z')}{\partial z'} dS' \right\}. \quad (\text{K.12})
\end{aligned}$$

In the integral over the boundary Γ_0 in the first term on the RHS of Eq. (K.12), $\mathbf{r} = \mathbf{r}_0$ is at the center of S_0 while \mathbf{r}' is on the boundary of S_0 . Hence, ψ in this integral is never singular and the rectangular rule suffices. In the integral over S_0 in Eq. (K.12), however, ψ is singular at the point $\mathbf{r}' = \mathbf{r}_0$. Fortunately, this integral is of the same form as that in Eq. (K.3) and so can be evaluated by exactly the same method used to evaluate the latter integral.

Summarizing,

$$\mathbf{n} \times \mathbf{H}_{S_0}(\mathbf{r}_0) = \mathbf{I}_1 + \mathbf{I}_2 + \mathbf{I}_3, \quad (\text{K.13})$$

where \mathbf{I}_1 , \mathbf{I}_2 and \mathbf{I}_3 are given by Eqs. (K.2), (K.3) and (K.12), respectively.

Bibliography

- [1] K. H. Drexhage, in *Progress in Optics XII*, edited by E. Wolf (North-Holland, Amsterdam, 1974).
- [2] F. De Martini, M. Marrocco, P. Mataloni and D. Murra, "Spontaneous and simulated emission in the thresholdless microlaser", *J. Opt. Soc. Am. B*, Vol. 10, pp. 360-381 (1993).
- [3] E. A. Hinds and V. Sandoghdar, "Cavity QED level shifts of simple atoms", *Phys. Rev. A*, Vol. 43, pp. 398-403 (1991).
- [4] R. R. Chance, A. Prock and R. Silbey, "Lifetime of an emitting molecule near a partially reflecting surface", *J. Chem. Phys.*, Vol 60, pp. 2744-2748 (1974).
- [5] F. De Martini, M. Marrocco, P. Mataloni, L. Crescentini and R. Loudon, "Spontaneous emission in the optical microscopic cavity", *Phys. Rev. A*, Vol. 43, pp. 2480-2497 (1991).
- [6] C. K. Carniglia and L. Mandel, "Quantization of evanescent electromagnetic waves", *Phys. Rev. D*, Vol. 3, pp.280-296 (1971).
- [7] B. Huttner and S. M. Barnett, "Quantization of the electromagnetic field in dielectrics", *Phys. Rev. A*, Vol. 46, pp. 4306-4322 (1992).
- [8] S. M. Barnett, B. Huttner and R. Loudon, "Spontaneous emission in absorbing dielectric media", *Phys. Rev. Lett.*, Vol. 68, pp. 3698-3701 (1992).
- [9] J. Bischoff, U. Glaubitz and N. Haase, "New method of topography simulation in photolithography", *Proc. SPIE*, Vol. 1674, pp. 423-434 (1992).

- [10] M. S. Yeung and A. R. Neureuther, "Improvement of the physical-optics approximation for topography simulation in optical lithography", *Proc. SPIE*, Vol. 1927, pp. 833-846 (1993).
- [11] V. Rokhlin, "Rapid solution of integral equations of scattering theory in two dimensions", *J. Comput. Phys.*, Vol. 86, pp. 414-439 (1990).
- [12] S. K. Chang and K. K. Mei, "Generalized Sommerfeld integrals and field expansions in two-medium half-spaces", *IEEE Trans. Antennas Propagat.*, Vol. AP-28, pp. 504-512 (1980).
- [13] D. M. Pai and K. A. Awada, "Analysis of dielectric gratings of arbitrary profiles and thicknesses", *J. Opt. Soc. Am. A*, Vol. 8, pp. 755-762 (1991).
- [14] N. Engheta, W. D. Murphy, V. Rokhlin and M. S. Vassiliou, "The fast multipole method (FMM) for electromagnetic scattering problems", *IEEE Trans. Antennas Propagat.*, Vol. AP-40, pp. 634-641 (1992).
- [15] R. Coifman, V. Rokhlin and S. Wandzura, "The Fast Multipole Method for the wave equation: A pedestrian prescription", *IEEE Antennas and Propagation Magazine*, Vol. 35, pp. 7-12 (1993).
- [16] R. R. Chance, A. Prock and R. Silbey, "Comments on the classical theory of energy transfer", *J. Chem. Phys.*, Vol. 62, pp. 2245-2253 (1975).
- [17] H. Kuhn, "Classical aspects of energy transfer in molecular systems", *J. Chem. Phys.*, Vol. 53, pp. 101-108 (1970).
- [18] H. Khosravi and R. Loudon, "Vacuum field fluctuations and spontaneous emission in the vicinity of a dielectric surface", *Proc. R. Soc. London Ser. A*, Vol. 433, 337-352 (1991).
- [19] A. A. Abrikosov, L. P. Gorkov and I. E. Dzyaloshinski, *Methods of Quantum Field Theory in Statistical Physics* (Dover, New York, 1963).

- [20] G. D. Mahan, *Many-Particle Physics*, 2nd ed. (Plenum, New York, 1990).
- [21] Z. Huang, C. C. Lin and D. G. Deppe, "Spontaneous lifetime and quantum efficiency in light emitting diodes affected by a close metal mirror", *IEEE J. Quantum Electronics*, Vol. 29, pp. 2940-2949 (1993).
- [22] D. G. Boulware, L. S. Brown and T. Lee, "Apparatus-dependent contributions to $g - 2$?", *Phys. Rev. D*, Vol. 32, pp. 729-735 (1985).
- [23] P. M. Morse and H. Feshbach, *Methods of Theoretical Physics*, Part 1, Chapter 8 (McGraw-Hill, New York, 1953).
- [24] J. Gamelin, "Simulation of topography scattering for optical lithography with the Connection Machine", *M. S. Thesis*, Memorandum No. UCB/ERL M89/71, University of California, Berkeley (1989).
- [25] R. Guerrieri, K. H. Tadros, J. Gamelin and A. Neureuther, "Massively parallel algorithms for scattering in optical lithography", *IEEE Trans. CAD*, Vol. CAD-10, pp. 1091-1100 (1991).
- [26] K. Tadros, A. Neureuther, J. Gamelin and R. Guerrieri, "Investigation of reflective notching with massively parallel simulation", *Proc. SPIE*, Vol. 1264, pp. 322-332 (1990).
- [27] A. K. Wong, "Two-dimensional electromagnetic simulation of topography scattering and diffraction in optical lithography", *M. S. Thesis*, Memorandum No. UCB/ERL M92/115, University of California, Berkeley (1992).
- [28] C. M. Yuan and A. J. Strojwas, "Modeling optical microscope images of integrated-circuit structures", *J. Opt. Soc. Am A*, Vol. 8, pp. 778-790 (1991).
- [29] M. S. Yeung, "Photolithography simulation on non-planar substrates", *Proc. SPIE*, Vol. 1264, pp. 309-321 (1990).

- [30] T. Matzusawa, A. Moniwa, N. Hasegawa and H. Sunami, "Two-dimensional simulation of photolithography on reflective stepped substrate", *IEEE Trans. CAD*, Vol. CAD-6, pp. 446-451 (1987).
- [31] H. P. Urbach and D. Bernard, "Modeling latent-image formation in photolithography using the Helmholtz equation", *J. Opt. Soc. Am. A*, Vol. 6, pp. 1343-1356 (1989).
- [32] E. Barouch, B. Bradie, U. Hollerbach, G. Karniadakis and S. Orszag, "Comprehensive 3-D notching simulator with non-planar substrates", *Proc. SPIE*, Vol. 1264, pp. 334-342 (1990).
- [33] S. Silver, *Microwave Antenna Theory and Design* (Peter Peregrinus Ltd., London, UK, 1986), p. 160.
- [34] J. Stratton, *Electromagnetic Theory* (McGraw-Hill, New York, 1941), Sec. 8.14.
- [35] P. Beckmann and A. Spizzichino, *The Scattering of Electromagnetic Waves from Rough Surfaces* (Pergamon, New York, 1963).
- [36] J. Stratton, *ibid*, p.30.
- [37] A. Sommerfeld, *Partial Differential Equations in Physics* (Academic Press, New York, 1964).
- [38] S. K. Chang, "On Electromagnetic Wave Scattering by Buried Obstacles", *Ph. D. Thesis*, University of California, Berkeley (1977).
- [39] B. Friedman and J. Russek, "Addition theorems for spherical waves", *Quart. Appl. Math.*, Vol. 12, pp. 13-23 (1954).
- [40] A. R. Edmonds, "Angular Momentum in Quantum Mechanics" (Princeton Univ. Press, Princeton, New Jersey, 1957).
- [41] E. P. Wigner, *Group Theory and its Application to the Quantum Mechanics of Atomic Spectra* (Academic Press, New York, 1959).

- [42] Y. Saad and M. H. Schultz, "GMRES: A generalized minimal residual algorithm for solving nonsymmetric linear systems", *SIAM J. Sci. Stat. Comput.*, Vol. 7, pp. 856-869 (1986).
- [43] *SLAP Version 2.0*, User Systems Division, Lawrence Livermore National Laboratory, Livermore, California 94550 (1989).
- [44] L. L. Tsai, D. G. Dudley and D. R. Wilton, "Electromagnetic scattering by a three-dimensional conducting rectangular box", *J. Appl. Phys.*, Vol. 45, pp. 4393-4400 (1974).
- [45] G. T. Ruck, D. E. Barrik, W. D. Stuart and C. K. Krichbaum, *Radar Cross Section Handbook*, Vol. 2 (Plenum Press, New York, 1970).
- [46] S. Ramo, J. R. Whinnery and T. Van Duzer, *Fields and Waves in Communication Electronics* (John Wiley and Sons, New York, 1984) Sec. 8.8.
- [47] P. Ratajczak, P. Brachat and J.-L. Guiraud, "Rigorous analysis of three-dimensional structures incorporating dielectrics", *IEEE Trans. Antennas Propagat.*, Vol. AP-42, pp. 1077-1088 (1994).
- [48] L. Greengard, *The Rapid Evaluation of Potential Fields in Particle Systems* (M. I. T. Press, Cambridge, MA, 1988).
- [49] K. Nabors and J. White, "FastCap: A multipole accelerated 3-D Capacitance Extraction Program", *IEEE Trans. Computer-Aided Design*, Vol. 10, pp. 1447-1459 (1991).
- [50] J. M. Song and W. C. Chew, "Fast Multipole Method solution using parametric geometry", *Micro. Opt. Tech. Lett.*, Vol. 7, pp. 760-765 (1994).
- [51] B. Dembart and E. Yip, "A 3-D Fast Multipole Method for electromagnetics with multiple level", *11th Annual Review of Progress in Applied Computational Electromagnetics*, Vol. 1, pp. 621-628 (Applied Computational Electromagnetics Society, Monterey, California, 1995).

- [52] O. R. Cruzan, "Translational addition theorems for spherical vector wave functions", *Quart. Appl. Math.*, Vol. 20, pp. 33-40 (1962).
- [53] J. H. Bruning and Y. T. Lo, *Multiple Scattering by Spheres*, Antenna Lab., Univ. Illinois, Urbana, Tech. Rep. 69-5 (1969).
- [54] J. H. Bruning and Y. T. Lo, "Multiple scattering of EM waves by spheres part I - Multipole expansion and ray-optical solutions", *IEEE Trans. Antennas Propagat.*, AP-19, 378-390 (1971).
- [55] W. W. Hansen, "A new type of expansion in radiation problems", *Phys. Rev*, Vol. 47, pp. 139-143 (1935).